

Dissertation zur Erlangung des Doktorgrades
der Fakultät für Chemie und Pharmazie
der Ludwig-Maximilians-Universität München

**Screening of Oxime Libraries Derived from 5-Membered
Cyclic Amino Acids by Means of MS Binding Assays for
mGAT1 Inhibitors**

Simone Katharina Huber, geb. Schmidt

aus

Gräfelfing, Deutschland

2019

Erklärung

Diese Dissertation wurde im Sinne von § 7 der Promotionsordnung vom 28. November 2011 von Herrn Professor Dr. Klaus T. Wanner betreut.

Eidesstattliche Versicherung

Diese Dissertation wurde eigenständig und ohne unerlaubte Hilfe erarbeitet.

München, den 06.05.2019

Simone Huber

Dissertation eingereicht am 11.12.2018

- 1. Gutachter: Professor Dr. Klaus T. Wanner
- 2. Gutachter: Professor Dr. Franz Paintner

Mündliche Prüfung am 15.01.2019

Die vorliegende Arbeit entstand in der Zeit von Oktober 2013 bis Januar 2019
am Department Pharmazie – Zentrum für Pharmaforschung – der
Ludwig-Maximilians-Universität München auf Anregung und unter Leitung von

Herrn Prof. Dr. Klaus T. Wanner

Für die hervorragende und sehr engagierte Betreuung und Förderung meiner Arbeit sowie
die ausgezeichneten Forschungsbedingungen danke ich Herrn Prof. Dr. Klaus T. Wanner
sehr herzlich.

Herrn Prof. Dr. Franz Paintner danke ich herzlich
für die Übernahme des Koreferats.

The cumulative thesis is based on the following original publications

Reprint with permission,

Cover article

Simone K. Schmidt, Georg Höfner, and Klaus T. Wanner, *Chirality* **2017**, 29, 48–56.

“Determination of enantiomeric excess of nipecotic acid as 1-(7-nitrobenzo[c][1,2,5]oxadiazol-4-yl) derivatives”

Cover article

Simone K. Huber, Georg Höfner, and Klaus T. Wanner, *ChemMedChem* **2018**, 13, 2488–2503.

“Identification of Pyrrolidine-3-acetic Acid Derived Oximes as Potent Inhibitors of γ -Aminobutyric Acid Transporter 1 through Library Screening with MS Binding Assays”

Simone K. Huber, Georg Höfner, and Klaus T. Wanner, *Bioorg. Med. Chem.* **2019**, submitted.

“Application of the Concept of Oxime Library Screening by Mass Spectrometry (MS) Binding Assays to Pyrrolidine-3-carboxylic Acid Derivatives as Potential Inhibitors of γ -Aminobutyric Acid Transporter 1 (GAT1)”

Copyright of the publications belong to the publishers.

Parts of this thesis have also been presented at international conferences

Poster presentation at the “Annual Meeting of the German Pharmaceutical Society – DPhG” 2016, Munich.

Simone K. Schmidt, Georg Höfner, and Klaus T. Wanner

“Determination of the Enantiomeric Purity of Nipectic Acid as 1-(7-Nitrobenzo[c][1,2,5]oxadiazol-4-yl) Derivatives”

Danksagung

Mein großer Dank gilt allen Mitarbeitern des Arbeitskreises für die tolle Zusammenarbeit und die schönen gemeinsamen Momente, die ich während meiner Zeit hier erleben durfte.

Besonderer Dank geht an die Oberassistenten, die mich bei jedem kleinen oder großen Problem tatkräftig unterstützt haben.

Bei Dr. Lars Allmendinger möchte ich mich bedanken, dass er immer Zeit für mich hatte, für jede Frage eine Antwort parat hatte (wirklich jede!) und mir jeden NMR-Wunsch von den Augen abgelesen hat. Lars, vielen Dank für die schöne Zeit mit interessanten Diskussionen über Gott und die Welt (und manchmal auch mehr), für das gute Essen, das du mir gekocht hast und für das viele viele Korrekturlesen meiner Arbeit. Dr. Georg Höfner danke ich für die Unterstützung bei der Entstehung der ersten Publikation, bei Fragen rund um HPLC Methodenentwicklung und Validierung und für die prompte Hilfe bei Problemen mit der Masse. Auch an Dr. Jörg Pabel geht ein großes Dankeschön für die Hilfe bei den zahlreichen PC-Problemen, bei dem kreativen Brainstorming für die Coverbilder oder diversen graphical abstracts und natürlich bei der Lösung allerlei chemischer Probleme.

Den Mitarbeiterinnen der analytischen Abteilung Claudia Glas, Ursula Groß und Keum-Ja Pankau danke ich für die Aufnahme der unzähligen NMR-Spektren und vor allem der vielen NMR-Sonderwünsche. Auch ein großer Dank geht an die Mitarbeiterinnen der biologischen Prüfung Silke Duensing-Kropp und Miriam Sandner für die Bereitstellung der Membranpräparationen und für die Bestimmung der pK_i - und pIC_{50} -Werte meiner Substanzen.

Bei meinen Laborkollegen Michael Böck (Mickey-Maus) und Sebastian Rappenglück (Rappi-Maus) möchte ich mich für die sehr angenehme Laboratmosphäre bedanken. Es hat sehr viel Spaß gemacht mit euch in einem Labor zu arbeiten und die vielen Stunden wurden durch angeregte Diskussionen oder spontane Yogastunden mit Guru Lars versüßt.

Ich danke auch Lars, Mark, Jörg, Patrick, Heinrich und Tobi für die Rätsel-Sessions zum Mittagessen, die vielen Eiskugeln, die wir zusammen vernichtet haben und die lustigen Trash-TV Abende. Auch darf mein Dank an unsere Laufgruppe für die Motivation zum Joggen – egal bei welchem Wetter – nicht fehlen. Lars als Teamkapitän, Tobi, Janina, Patrick, Mark, Michi, Li und Adrian haben mir die „Freuden“ des Laufens nähergebracht.

Meinen Eltern und meinem Bruder Fabi danke ich von Herzen, dass sie mich auf diesem Weg begleitet und mich immer unterstützt haben. Vielen Dank für die schöne Zeit und die tollen Augenblicke – sei's in Garmisch beim obligatorischen guten Frühstück, beim Wandern oder Langlaufen oder in München bei euch im Garten bei einem guten Steak oder im Biergarten.

Doch mein allergrößter Dank gehört meinem Mann Stefan, der mich in schlechten Zeiten auffing und wiederaufbaute, sich so sehr für meine Arbeit begeisterte und mir mit Rat und Tat zur Seite stand. Du bist der Anker in meinem Leben und dafür bin ich dir unendlich dankbar. Ich liebe dich.

Table of Contents

1	Introduction	1
1.1	GABAergic Neurotransmission	1
1.2	Pathology and Therapy	3
1.3	GABA Transporters	4
1.3.1	SLC6 Family	4
1.3.2	Classification of GABA Transporters	4
1.3.3	Structure and Transport Mechanism of SLC6 Transporters	5
1.3.4	Selective Inhibitors of murine GABA Transporter Subtype 1 (mGAT1)	7
1.4	Drug Discovery	10
1.4.1	Ligand Binding Assays	10
1.4.2	Ligand Binding Experiments	11
2	Aims and Scope	14
3	Results and Discussion	17
3.1	First Publication	17
3.1.1	Summary of the Results	17
3.1.2	Declaration of Contribution	18
3.2	Second Publication	19
3.2.1	Summary of the Results	19
3.2.2	Declaration of Contribution	20
3.3	Third Publication	21
3.3.1	Summary of the Results	21
3.3.2	Declaration of Contribution	22
4	Further Experiments	23
4.1	Generation of Oxime Libraries – Kinetic Experiments	23
4.1.1	Kinetic Experiments using 2-(Pyrrolidin-3-yl)acetic acid derived Hydroxylamine	24
4.1.2	Kinetic Experiments using Pyrrolidine-3-carboxylic acid derived Hydroxylamine	37
4.2	Generated Libraries – Stability Experiments	43
4.2.1	Stability Experiments using 2-(Pyrrolidin-3-yl)acetic acid derived Oximes	44
4.2.2	Stability Experiments using Pyrrolidine-3-carboxylic acid derived Oximes	57
5	Summary of the Thesis	67
6	List of Abbreviations	70
7	References	72

1 Introduction

In 2006, the World Health Organization (WHO) drew attention to the importance of the burden of neurological diseases for the public health.¹ Hundreds of millions of people over the world suffer from neurological disorders like epilepsy, Alzheimer's disease or dementia, Parkinson's disease and depressions whereby more than 50 million people are affected by epilepsy globally.^{2,3} Epilepsy is defined as a chronic disorder of the brain and is characterized by having two or more unprovoked seizures over a period greater than 24 hours apart. Seizures are brief episodes of uncontrolled movement of part of the body or the entire body of a patient.⁴ 80 % of the epilepsy patient are living in low- or middle-income countries and 75 % do not receive necessary treatments.³ But also upon applying one of over 15 approved antiepileptic drugs (AEDs) more than 30 % of the patients continue to have seizures and up to the half of them are affected by psychiatric, cognitive and social side-effects.⁵ Hence, the development of more potent and lower-cost medications with minor side-effects are a huge field of interest for research.

One key structure as starting point for the research of the mentioned neurological disorders and for the identification of novel drugs for the treatment is γ -aminobutyric acid (GABA, **1**, Figure 1) as the major inhibitory neurotransmitter in the mammalian central nervous system (CNS).⁶

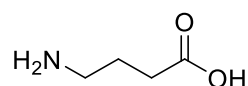


Figure 1: Structure of γ -aminobutyric acid (GABA, **1**).

1.1 GABAergic Neurotransmission

A summary of the neurotransmission of GABA in the mammalian brain is displayed in Figure 2.^{7,8} GABA is synthesized in the presynaptic neurons through enzymatic decarboxylation of glutamate (Glu) – a potent excitatory neurotransmitter – by glutamic acid decarboxylase (GAD) and is then stored in synaptic vesicles by vesicular neurotransmitter transporter (vGAT). Due to depolarization of the presynaptic neuron the neurotransmitter GABA is released in the synaptic cleft where it can bind to the GABA receptors GABA_A and GABA_B.⁷

The GABA_A receptors are chloride ion channels mainly located on the postsynaptic membrane which enable the influx of chloride ions in the postsynaptic neuron upon the binding of GABA. This results in the hyperpolarization of the neuron and thus leads to an inhibition of the neural transmission. In contrast, the GABA_B receptors are G-protein coupled receptors (GPCR) found on pre- and postsynaptic neurons which regulate the excitability of the cell in two location-dependent mechanisms. Binding of GABA to the presynaptic GABA_B receptors causes a

Introduction

reduced calcium influx and therefore a reduction of the release of GABA in the synaptic cleft. Differently, postsynaptic GABA_B receptors mediate a G-protein induced stimulation which causes the efflux of potassium through K⁺-ion channels and thus a hyperpolarization of the neuron. This leads to an inhibition of the GABAergic neurotransmission.⁹

The inhibitory neurotransmission mediated by GABA is terminated by the reuptake of the neurotransmitter from the synaptic cleft in the presynaptic neurons or the surrounding glial cells by membrane-bound GABA transport proteins (GATs) subtype 1 and 3.¹⁰ Thereafter, GABA is either restored again in synaptic vesicles in the presynaptic neurons or is enzymatically degraded in the glial cells by GABA transaminase (GABA-T) to succinic semialdehyde.⁸

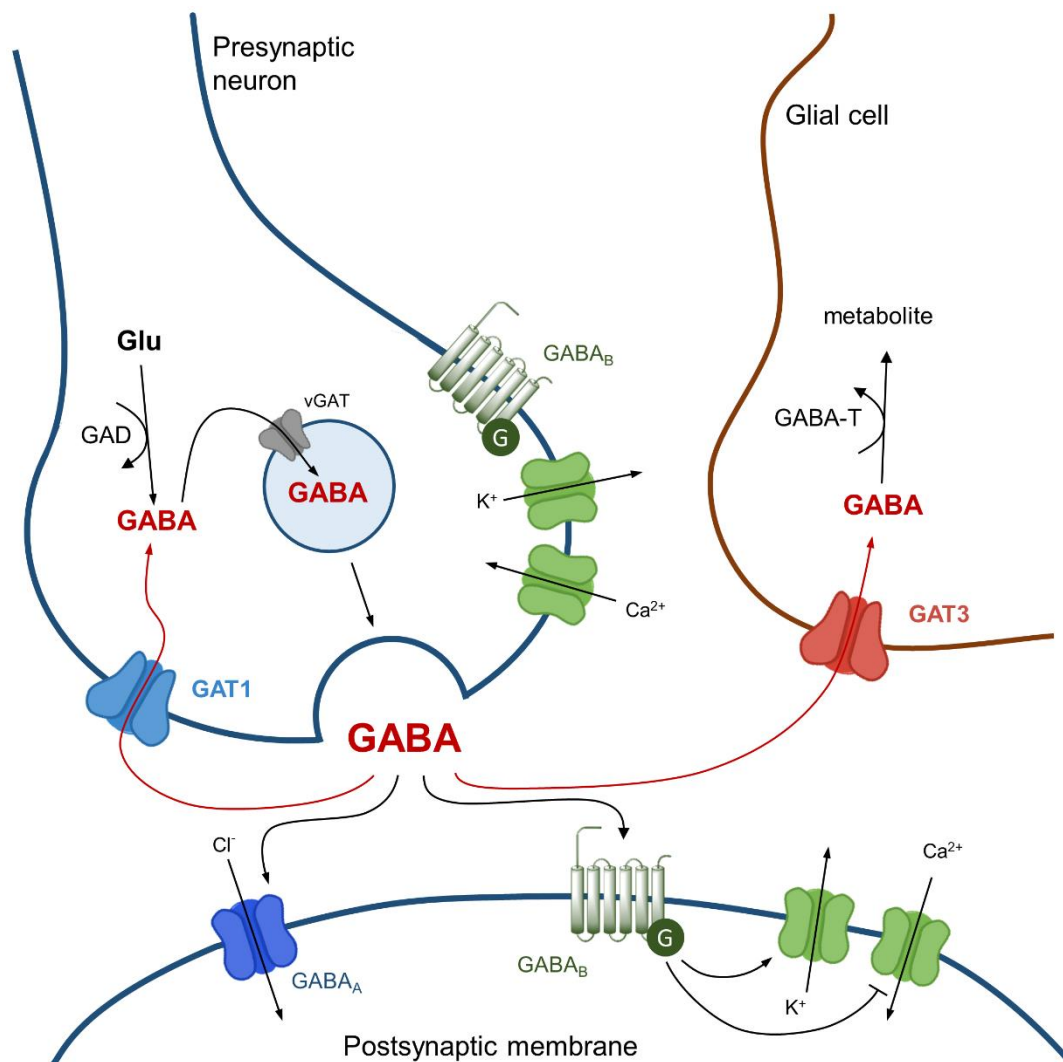


Figure 2: GABAergic neurotransmission according to literature.^{7,8} γ -Aminobutyric acid (GABA) is synthesized through enzymatic decarboxylation of glutamine (Glu) and stored in vesicles by vesicular GABA transporter (vGAT). After release in the synaptic cleft due to an action potential it can interact with the receptors GABA_A and GABA_B. Reuptake of GABA in the presynaptic neuron or glial cells is accomplished by GABA transporters (GATs) subtype 1 and 3.

1.2 Pathology and Therapy

An imbalance between inhibitory neurotransmission facilitated by GABA and glutamate mediated excitatory transmission caused by a reduced GABAergic neurotransmission⁸ are assumed to be associated with the development of neurological diseases like epilepsy¹¹, Alzheimer's disease or depression¹². To reset the balance, the enhancement of the GABAergic signaling is one possible approach with different targets to address as e.g. the GABA receptors, GABA transaminase (GABA-T) and the GABA transporters (see Figure 2).

Benzodiazepines are known positive allosteric modulators (PAMs) of the GABA_A receptor which are in clinical use as medications for many years. Binding of the PAM to the GABA_A receptor leads to a conformational change of the receptor. Thus, the required concentration of GABA is decreased for the opening of the ion-channel to enable the influx of chloride and therefore the inhibitory effect of GABA is increased. A prominent example of the benzodiazepine family is diazepam (Valium®, **2**, Figure 3).¹³

Furthermore, the GABA_B selective agonist baclofen (Lioresal®, **3**, Figure 3) enhances the GABAergic neurotransmission by activating GABA_B receptors and has been used for the treatment of spasticity for many years.⁸

Another possible approach to increase the extracellular GABA concentration is to block the degradation of GABA in the glial cells by irreversible inhibition of the GABA transaminase (GABA-T) using vigabatrin (Sabril®, **4**, Figure 3).¹⁴

By inhibition of the GABA transporters the reuptake of GABA from the synaptic cleft is suppressed and as a consequence the concentration of the neurotransmitter is increased. Tiagabine (Gabitril®, **5**, Figure 3) is known as a drug for the reuptake inhibition which is in clinic use for the treatment of epilepsy.¹⁵

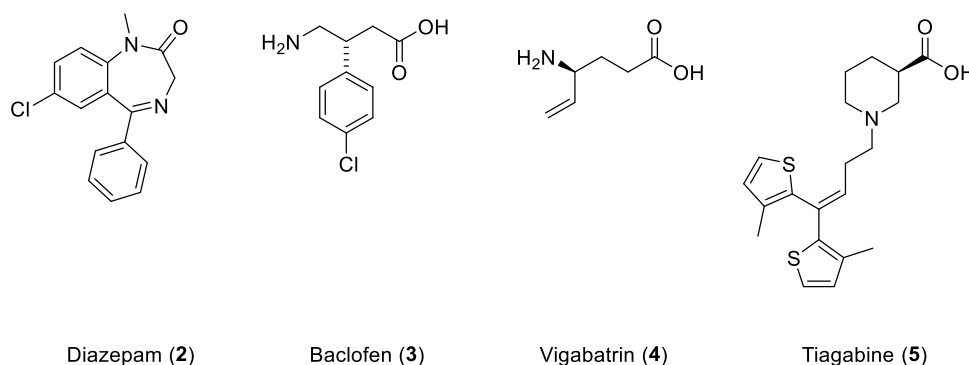


Figure 3: Medications addressing different target in the GABAergic neurotransmission.

However, all known therapeutics suffer from more or less severe side-effects like ataxia or dizziness so that the development of more potent and more selective antiepileptic drugs with lower side-effects is needed.⁸

1.3 GABA Transporters

1.3.1 SLC6 Family

The exchange of compounds which cannot permeate through membranes like ions, amino acids or signaling molecules between cells or cell compartments is realized by membrane proteins termed solute carriers or more general transporters. Many transport proteins are members of the solute carrier superfamily (SLCs) which is divided in 55 SLC families.¹⁶ These include the SLC6 gene family also known as neurotransmitter transporter (NTTs) of which 20 different transporters are identified so far distributed into four subtypes: transporters for monoamine neurotransmitter e.g. serotonin, dopamine and norepinephrine transporters, the GABA transporters and two different amino acid transporters e.g. glycine transporters.¹⁷ All NTTs are Na^+/Cl^- dependent transporters as their transport of solutes is coupled to the cotransport of sodium in the same direction as a driving force for substrate transport against its chemical gradient.¹⁸ Therefore, the neurotransmitter transporters are also termed neurotransmitter-sodium-symporters (NSS).¹⁹

1.3.2 Classification of GABA Transporters

Four different subtypes of GABA transporters are known which are termed GAT1, BGT1, GAT2 and GAT3 according to suggested nomenclature of the Human Genome Organization (HUGO).²⁰ But other different designation for GABA transporter were also established over the time depending on the origin of cloning, e.g. the human GATs are named hGAT-1, hBGT-1, hGAT-2 and hGAT-3 and GATs derived from rat are designated as rGAT-1, rBGT-1, rGAT-2 and rGAT-3, respectively. Differently, when cloned from mice the transporters are indicated as mGAT1 (=GAT1), mGAT2 (BGT1), mGAT3 (=GAT2) and mGAT4 (=GAT3).²¹ Since the GATs used in the following studies are cloned from mouse, the latter nomenclature for the GABA transporter subtypes of this species will be applied. All used designations are summarized in Table 1.

Table 1: Different nomenclature of the four GABA transporter subtypes.

Species	Designation of GABA transporters			
HUGO	GAT1	BGT1	GAT2	GAT3
human	hGAT-1	hBGT-1	hGAT-2	hGAT-3
rat	rGAT-1	rBGT-1	rGAT-2	rGAT-3
mouse	mGAT1	mGAT2	mGAT3	mGAT4

Both subtypes mGAT1 and mGAT4 are the only transporters present in the central nervous system in notable densities whereby mGAT1 is the most abundant transporter in the CNS mainly located on neurons and mGAT4 is predominantly responsible for the GABA uptake in glial cells.²² Consequently, these two subtypes are the key structures to address for an enhancement of the GABA concentration in the synaptic cleft. Besides, mGAT2 and mGAT3 are predominantly expressed in the kidney and liver and therefore are not involved in termination of GABA signaling in the CNS.^{22,23}

1.3.3 Structure and Transport Mechanism of SLC6 Transporters

The comprehension of the transport mechanism is dependent on the understanding of the molecular structures of the SLC6 transporter family. In the year 1990, the group around Guastella was able to clone the GABA transporter subtype 1 from rat brain tissue (rGAT-1) for the first time²⁴ followed by the cloning of the monoamine neurotransmitter transporter for serotonin²⁵, dopamine²⁶ and norepinephrine²⁷. By analysis of the amino acid sequences of the cloned transporters the claim was made that the transporters consist of 12 transmembrane helices²⁸, which was confirmed in 2005 by the successful crystallization and X-ray analysis of the leucine transporter LeuT_{Aa} from the bacteria *Aquifex aeolicus* in the presence of leucine as its substrate and two sodium ions accomplished by Yamashita et al.²⁹ As the amino acid sequence of LeuT_{Aa} responsible for the area of the substrate binding site is 55-67 % homologous compared to the other SLC6 family transporters³⁰, the crystal structure of LeuT_{Aa} serves as a valid source for the comprehension of molecular structure and also the function of all other neurotransmitter transporters of the SLC6 family.

LeuT_{Aa} consists of twelve transmembrane helices (TM1–TM12) with both N and C termini in the intracellular side. The first ten helices TM1–TM5 and TM6–TM10 are arranged in a C₂-pseudosymmetrical order which is also named the 5 + 5 inverted repeat fold. The binding site for the substrate leucine (yellow triangle) and two sodium ions (blue circles, Figure 4) is located within the antiparallel arranged helices TM1 and TM6 which are broken into two parts (a and b). Through this unfolding of the helices additional binding sites for hydrogen bridges or ionic bonds are available for the binding of the substrate (Figure 4).²⁹

Introduction

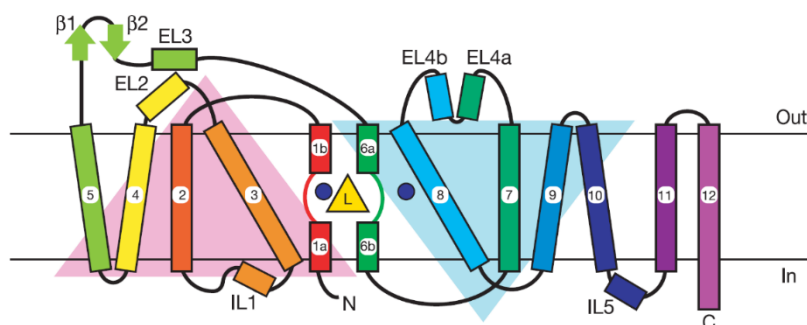


Figure 4: Schematic secondary structure of LeuT_{Aa} according to Yamashita et al. The substrate leucine is depicted as a yellow triangle and the sodium ions are pictured as blue circles.²⁹

Since the crystallization of the leucine transporter many crystallographic and computational studies supported the assumption of the transport mechanism according to the alternating access model which describes the transport through a combination of global and local structural changes (Figure 5).³¹

In the first step of one transport cycle, the transporter protein faces towards the extracellular side in an open conformation called outward-facing open state (O Fo) which enables the binding of the substrate and ions in the S1 binding pocket. Upon binding of the substrate (outward-facing open, with substrate = O Fo*) local changes of the conformation are initiated which leads to the closure of the extracellular gate (outward-facing closed, with substrate = O Fc*). Subsequently, global conformational changes of the protein results in the inward-facing closed state (with substrate = I Fc*) which opens to the intracellular media immediately (inward-facing open, with substrate = I Fo*). The bound substrate and ions are released into the cytoplasm and the inward-facing open state (without substrate = I Fo) is transformed to the outward-facing open state whereby a new transport cycle starts again.³²

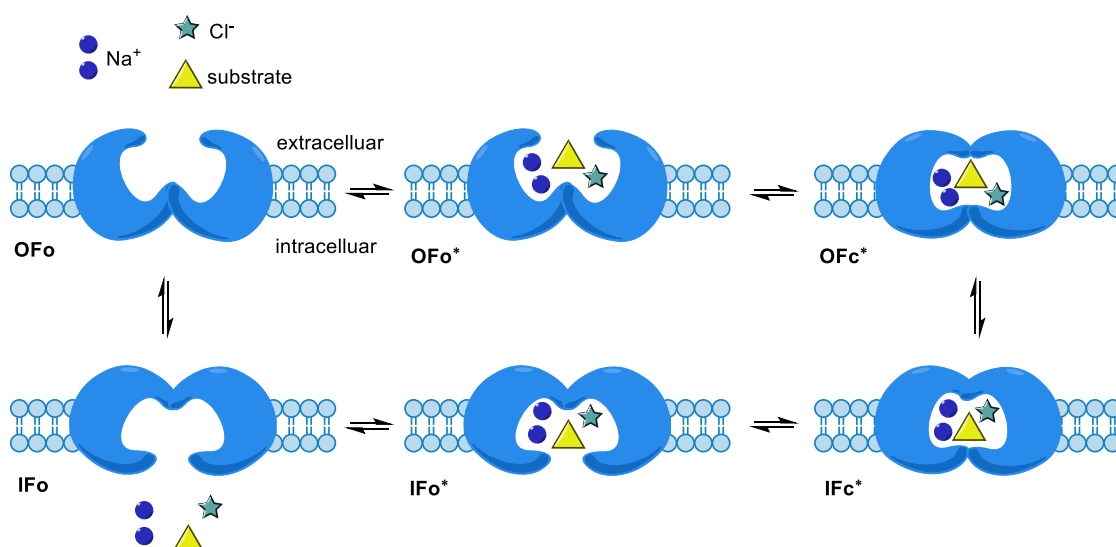


Figure 5: Postulated transport mechanism according to the „alternating access model“ by Yamashita et al.²⁹

The first successful crystallization of LeuT_{Aa} in the outward-facing closed state (OFc*) containing two sodium ions and one leucine as substrate was accomplished by Yamashita et al.²⁹ Shortly after the group of Gouaux had been able to crystalize the outward-facing open conformer (OFo*) in the presence of the competitive inhibitor tryptophan³³ and recently they presented the resolution of the inward-facing open state (IFo) and outward-facing open state (OFo) without substrate³⁴. These studies provided more detailed information of the different conformers for clarification of the molecular processes during the transport which finally confirmed the postulated transport mechanism of Yamashita et al.

Based on molecular dynamics simulations and other experimental data, Shi and co-workers were able to identify a second binding pocket designated S2 which is located above the extracellular gate of LeuT_{Aa}.³⁵ The existence of S2 was verified by many other studies regarding leucine transporter and other neurotransmitter transporter as e.g. dopamine transporter.³⁶ Additionally, Shi et al. claimed that the occupation of S2 is required for the allosteric release of the substrate of the central binding site (S1) in the cytoplasm³⁵, but this relevance of S2 for allosteric regulation is still questionable^{37,38}. Further studies indicated that S2 is a binding site for non-competitive inhibitors of LeuT that prevent conformational changes of the transporter and therefore inhibit the transport of the substrate.³⁷

Meanwhile, further crystal structures of neurotransmitter transporters were obtained that confirm the structure of LeuT as a reliable tool for the understanding of the other SLC6 family transporters. In 2013, Penmatsa et al. reported the crystal structure of the eukaryotic dopamine transporter as a complex together with the tricyclic antidepressant nortriptyline³⁹ and in a later publication the same group achieved the crystallization of the eukaryotic DAT with nisoxetine and reboxetine⁴⁰. In the year 2016, the human serotonin transporter SERT was successfully crystallized together with the antidepressants paroxetine and (S)-citalopram by Coleman et al.⁴¹ All published core structures were in good accordance with the crystal structure of the prokaryotic LeuT_{Aa}. Furthermore, in the structure of the human SERT an allosteric binding site located near the extracellular gate was identified which inhibit the release of the bound substrate from the central binding site.⁴¹

All in all, these recently published crystal structures support and extend the understanding of the function of neurotransmitter transporter.

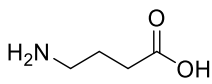
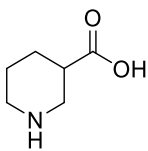
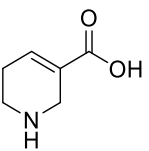
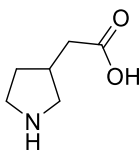
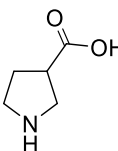
1.3.4 Selective Inhibitors of murine GABA Transporter Subtype 1 (mGAT1)

One possible way of treating neurological diseases like epilepsy caused by a disturbed regulation of GABA activity is the selective inhibition of the GABA transporter subtype 1 (GAT1) responsible for the reuptake of GABA in the presynaptic neurons.⁴²

Introduction

Since the late 1960, potent cyclic inhibitors for mGAT1 were discovered like (*R,S*)-nipecotic acid [(*R,S*)-**6**]⁴³, guvacine (**7**)⁴², (*R,S*)-2-(pyrrolidin-3-yl)acetic acid [(*R,S*)-**8**]⁴⁴ and (*R,S*)-pyrrolidine-3-carboxylic acid [(*R,S*)-**9**]⁴⁵. The determined pIC₅₀ values of the mentioned compounds are summarized in Table 2. For the sake of better comparability, the inhibitory potencies of all compounds were determined by [³H]GABA uptake assays in our group in every case employing the same test system unless otherwise stated. Compared to the substrate GABA with an pIC₅₀ values of 5.14 ± 0.09⁴⁶, these small amino acids reveal even slightly higher pIC₅₀ values in the case of (*R,S*)-2-(pyrrolidin-3-yl)acetic acid (pIC₅₀ = 5.39 ± 0.05, Table 2)⁴⁷ and almost equal pIC₅₀ values for (*R,S*)-nipecotic acid (pIC₅₀ = 4.88 ± 0.07, Table 2)⁴⁸ and guvacine (pIC₅₀ = 4.87 ± 0.06, Table 2)⁴⁹. In the case of (*R,S*)-pyrrolidine-3-carboxylic acid the inhibitory potency at mGAT1 is decreased by approximately one log unit (pIC₅₀ = 4.17 ± 0.06, Table 2)⁵⁰ compared to GABA itself. Except for mGAT2, these cyclic amino acids do not show selectivity for mGAT1 as the pIC₅₀ values are in the same range regarding the other subtypes mGAT3 and mGAT4 (see Table 2). This and their inability to cross the blood brain barrier limit their prospective application for pharmacological treatment.

Table 2: pIC₅₀ values of GABA and small cyclic amino acid as GAT inhibitors.

<div style="display: flex; justify-content: space-around; align-items: flex-end;"> <div style="text-align: center;">  <p>γ-aminobutyric acid (GABA, 1)</p> </div> <div style="text-align: center;">  <p>(<i>R,S</i>)-nipecotic acid [(<i>R,S</i>)-6]</p> </div> <div style="text-align: center;">  <p>guvacine (7)</p> </div> <div style="text-align: center;">  <p>(<i>R,S</i>)-pyrrolidine-3- acetic acid [(<i>R,S</i>)-8]</p> </div> <div style="text-align: center;">  <p>(<i>R,S</i>)-pyrrolidine-3- carboxylic acid [(<i>R,S</i>)-9]</p> </div> </div>				
compound	GABA uptake inhibition (pIC ₅₀ ± SEM) ^a			
	mGAT1	mGAT2	mGAT3	mGAT4
GABA (1)	5.14 ± 0.09	4.56 ± 0.06	4.94 ± 0.09	5.18 ± 0.13
(<i>R,S</i>)- 6	4.88 ± 0.07	3.10 ± 0.09	4.94 ± 0.07	4.70 ± 0.07
7	4.87 ± 0.06	3.31 ± 0.03	4.59 ± 0.05	4.59 ± 0.05
(<i>R,S</i>)- 8	5.39 ± 0.05	3.78 ± 0.08	5.21 ± 0.06	5.42 ± 0.07
(<i>R,S</i>)- 9	4.17 ± 0.06	3.50 ± 0.06	4.25 ± 0.04	4.21 ± 0.10

^apIC₅₀ values from [³H]GABA uptake assay performed with murine GABA transporters expressing HEK cells. The values represent the mean ± SEM of three independent experiments, each performed in triplicate.

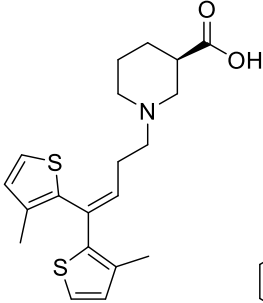
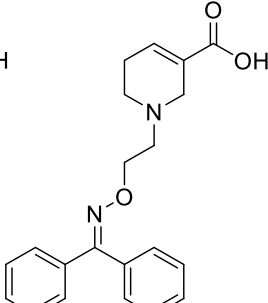
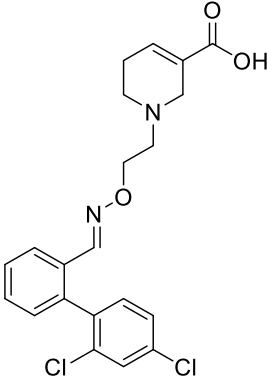
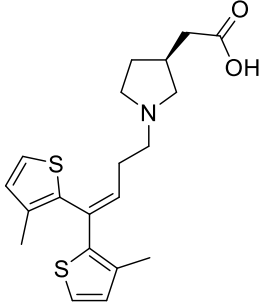
To enhance the ability for CNS penetration lipophilicity has been increased by attaching bulky aromatic residues via an alkyl chain bearing different functionalities to the nitrogen of the small amino acids. As a result, not only lipophilicity increased but also selectivity for mGAT1 with substantially enhanced inhibitory potential.

Introduction

The pIC_{50} of some mGAT1 selective inhibitors are presented in Table 3. Lots of lipophilic derivatives of nipecotic acid are described in literature whereas tiagabine (**5**) is the most famous representative with a pIC_{50} value of 6.88 ± 0.12 for mGAT1 (Table 3)^{15,49}. NO711 shows similar inhibitory potency at mGAT1 (**10**, $pIC_{50} = 6.83 \pm 0.06$, Table 3)⁵¹ but the compound DDPM-2571 reveals an pIC_{50} value almost 1.5 log units higher as tiagabine (**11**, $pIC_{50} = 8.27 \pm 0.03$, Table 3)⁵². Both examples are guvacine derivatives with an oxime functionality in the alkyl chain bearing different aromatic residues. (S)-**12** represents one example of only few reported substances with 2-(pyrrolidin-3-yl)acetic acid substructure as a tiagabine-like derivative with pIC_{50} value only slightly lower than the value of tiagabine itself [(S)-**12**, $pIC_{50} = 6.69 \pm 0.01$, Table 3].⁴⁹

Compared to the corresponding unsubstituted amino acids it is apparent that the subtype selectivity for mGAT1 improved significantly as the pIC_{50} values for mGAT1 increased by approximately one log unit or even more whereas the inhibitory potencies for mGAT2 remained or increased only slightly over 4 and pIC_{50} values for mGAT3 and mGAT4 even decreased. In the cases of **5** and (S)-**12**, the results for the affinity towards mGAT2-4 are given as the percentage values of the remaining [³H]GABA uptake of the radioligand assay at an applied concentration of 100 μ M of **10** and 10 μ M of (S)-**12**, respectively.

Table 3: pIC_{50} values of mGAT1 selective inhibitors.

<div style="display: flex; justify-content: space-around; align-items: flex-end;"> <div style="text-align: center;">  <p>tiagabine (5)</p> </div> <div style="text-align: center;">  <p>NO711 (10)</p> </div> <div style="text-align: center;">  <p>DDPM-2571 (11)</p> </div> <div style="text-align: center;">  <p>(S)-12</p> </div> </div>				
compound	GABA uptake inhibition ($pIC_{50} \pm SEM$) ^a			
	mGAT1	mGAT2	mGAT3	mGAT4
5	6.88 ± 0.12	50 %	64 %	73 %
10	6.83 ± 0.06	3.20 ± 0.09	3.63 ± 0.04	3.07 ± 0.06
11	8.27 ± 0.03	4.31	4.35	4.07
(S)- 12	6.69 ± 0.01	85 % ^b	89 % ^b	63 % ^b

^a pIC_{50} values from [³H]GABA uptake assay performed with murine GABA transporters expressing HEK cells. The values represent the mean \pm SEM of three independent experiments, each performed in

triplicate. Percentage values represent remaining [^3H]GABA uptake in present of 100 μM test compound.

^bPercentage values represent remaining [^3H]GABA uptake in present of 10 μM test compound.

As already mentioned the majority of selective and potent mGAT1 inhibitors with lipophilic residues contains nipecotic acid as amino acid motif next to some guvacine derivatives. But only a few publications are known concerning mGAT1 inhibitors derived from 2-(pyrrolidin-3-yl)acetic acid^{49,53} and no publication reported about pyrrolidine-3-carboxylic acid derivatives as potential mGAT1 inhibitors. So to say, tremendous amount of information about structure-activity-relationships (SARs) for mGAT1 regarding diverse aromatic residues with various substituents attached via different linker regarding length and functionalities to the nipecotic acid and guvacine are available but SARs concerning different other amino acid substructures are rare. As a consequence, the expansion of SARs on the 5-membered cyclic amino acids 2-(pyrrolidin-3-yl)acetic acid and pyrrolidine-3-carboxylic acid presents a huge step towards the identification of novel selective and potent inhibitors for the GABA transporter subtype 1.

1.4 Drug Discovery

In the beginning of the history of drug discovery, the identification of novel drugs was often only achieved by coincidence e.g. the discovery of penicillin, but nowadays target-oriented screening techniques are applied in the early stage of the drug discovery process in order to screen various substances to determine their affinity on a chosen target.⁵⁴ The requirement to observe this affinity is the binding of the studied compounds so called ligands to the target. One possibility is the measurement of the changes of the target caused by the binding of ligand which can be detected by NMR or X-Ray crystallography. The advantage of this technique is that more information about the binding interactions (i.e. kinetics, mechanism) can be received with regard to one single ligand but with limited throughput. The second possibility is the detection of the bound ligand in the screening process using various assays. Thereby affine ligands can be identified out of a mixture of numerous compounds with a high throughput but without providing information about binding mechanism.⁵⁵

1.4.1 Ligand Binding Assays

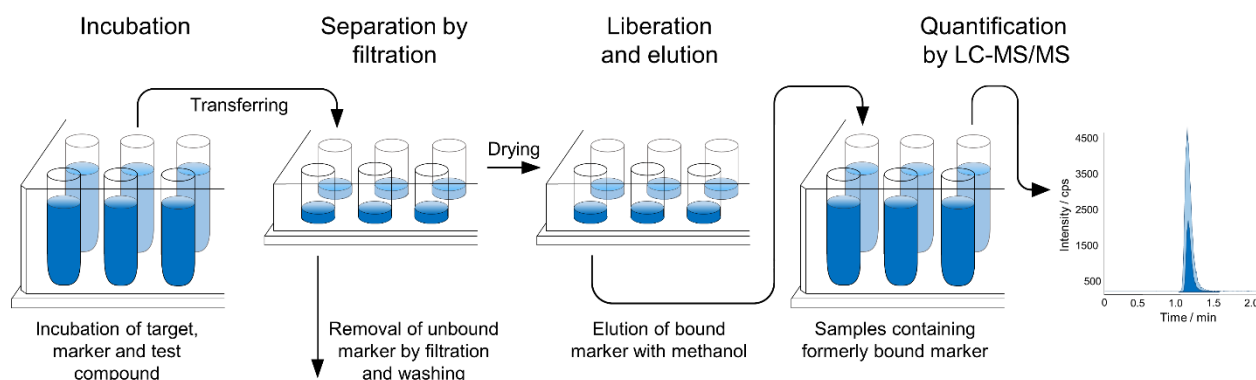
For the latter screening assays, the opportunities for the readout are manifold and can be done by optical sensors as in fluorescence-based assays or by mass spectrometry.⁵⁴ Another way is the use of radioactively labelled reporter ligands to analyze ligand-target binding by scintillation counting.⁵⁶ These so called radioligand binding assays have been developed in the 1970s and are still widely used for the screening in drug discovery processes.⁵⁷ In contrast to other ligand labels as fluorophores the effect of the insertion of a radioisotope as ^3H , ^{125}I or

^{32}P in the ligand has only insignificantly impact on the binding affinity towards the target. Additionally, the detection method via scintillation counting is highly selective for the labeled ligand and has a high sensitivity. On the other hand, due to the radioactivity high costs for the radioligands as well for the disposal of the contaminated waste and increased health hazards for the operators have to be considered.

Therefore, mass spectrometry (MS) Binding Assays have been developed for different targets as an alternative to radioligand binding assays.⁵⁸ The differences between these two assay methods are, that the quantification of the reporter ligand is achieved by liquid chromatography-tandem mass spectrometry (LC-MS/MS) for the MS Binding Assays and no labeling of the reporter ligand which is also called MS marker is necessary, so every compound with an appropriate affinity towards the desired target is suitable. Thus, the costs for non-labeled compounds is usually lower and there is no need for special disposal of the waste as necessary for radioactively labeled substances.

1.4.2 Ligand Binding Experiments

With either the radioligand as well as the MS binding assays, several experiments can be performed i.e. saturation, kinetic and competition experiments. Each of them based on the same simple and robust procedure which will be explained in the case of a competitive MS Binding Assay (Figure 6). Within these experiments the affinity of the competitor towards the target can be determined indirectly by the quantification of the marker bound to this target. This procedure offers the advantage to characterize various different test compounds with only one quantification method for one marker. The quantified amount of the marker represents the total-binding of the marker towards the target, which comprises the binding to the specific binding site of the target, termed specific binding and of the non-specific binding which is the binding of the marker to other binding sites e.g. lipid membranes in the protein preparation or filter materials used in the assay. The specific binding of the marker which is needed for the calculations of the affinity of the test compounds has to be determined by the subtraction of the non-specific binding from the total binding.⁵⁶



Introduction

Figure 6: Diagram of the procedure of MS Binding Assays. Marker and test compound are incubated with the target. After incubation unbound marker is separated from the marker-target complexes by filtration. Denaturation of the target upon drying is followed by elution of the formerly bound marker. Finally, the marker is quantified by LC-MS/MS.

In the first step a defined concentration of the MS marker and different concentration levels of the test compound as competitor are incubated with the target. Upon equilibration, target-ligand complexes are generated where the marker and the test compound are in competition for the binding site of the target. These complexes are then separated by filtration from the non-bound components of the incubation sample followed by the liberation of the bound marker by denaturation of the target protein by drying at elevated temperature and subsequent treatment with an organic solvent. After the elution of the formerly bound marker with methanol from the filter, the liberated marker is quantified by LC-MS/MS to determine the total binding. The higher the applied concentrations of the competitor the more the marker will be replaced from the target-ligand complexes and therefore the lower the amount of quantified marker will be. With the quantified amount of the marker competition curves in dependence of the applied concentrations of the competitor can be constructed as outlined in Figure 7.

The non-specific binding has to be determined separately by incubation of the target and different concentration of the marker with a high excess of a highly affine inhibitor of the specific binding site of the target. Another possibility is to denature the specific binding site by heat shock.

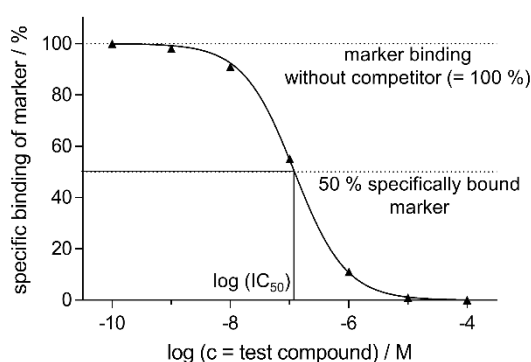


Figure 7: Schematic figure of typical competition curve in which specific binding of marker is plotted against applied concentrations of test compound. With increasing concentrations of competitor reduction of the specific binding of marker is observed. 100 % represents marker binding without competitor and $\log(\text{IC}_{50})$ is the concentration of the test compound which reduced the specific marker binding to 50 %.

The competition curve is fixed to 100 % which represents the marker binding without competitor. The IC_{50} value – defined as the concentration of test compound which reduces the

Introduction

specific binding of the marker to 50 % – describes the inhibitory potency of the corresponding test compound.

Using the equation of Cheng-Prusoff (1) the IC_{50} values can be transformed into the inhibition constant K_i to reveal the affinity of the test compound towards the target.⁵⁹

$$K_i = \frac{IC_{50}}{1 + \frac{[L]}{K_d}} \quad (1)$$

In this equation K_d is the equilibrium dissociation constant of the marker, which has to be known and $[L]$ represents the free concentration of the ligand also termed marker, which can be substituted by the nominal concentration of the marker if marker depletion is negligible (<10 %). Marker depletion occurs when significant amount of the marker is bound to the target (≥ 10 %) but can be avoided easily by applying target concentrations which do not exceed $0.1 \cdot K_d$ of the marker.⁶⁰

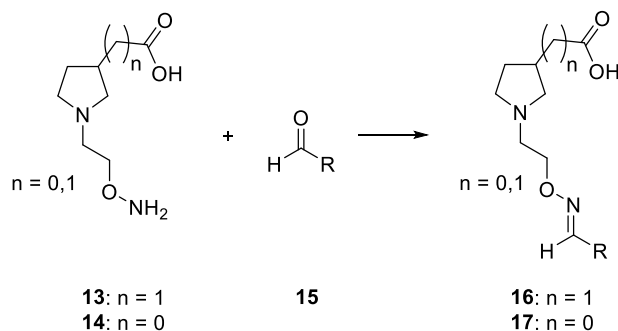
2 Aims and Scope

Binding assays are useful tools for the identification of novel highly affine ligands for a certain target. This technique is used in form of MS Binding Assays for the determination of potent and selective mGAT1 inhibitors with NO711 (**10**) as MS marker in our group.^{58a} This technique has been extended to the screening of substance libraries delineated from different amino acid key structures, whereby library generation and activity analysis are combined to a single step. This combinatorial screening concept is based on a simple condensation reaction known from dynamic combinatorial chemistry to obtain libraries with a broad range of structures with a vast variety of different functionalities. This was already published for pseudostatic hydrazone libraries with nipecotic acid substructure⁶¹ and stable oxime libraries with a guvacine motif⁵² by our group. In contrast to competitive MS Binding Assays in which the single test compounds are applied in different concentration levels to obtain a competition curve for those compounds, a set of different test compounds is employed in only one defined concentration. In the thus by means of MS Binding Assay performed library screening information about the potency of the whole library towards the target mGAT1 is obtained. The most potent libraries are then further subjected to so-called deconvolution experiments in which the individual compounds are screened once more at a single concentration level to identify the substance in the library responsible for the formerly observed potency at mGAT1. With this concept it is possible to quickly identify the most potent compounds out of a large set of different libraries.

The aim of the present study was to transfer this screening concept to 5-membered cyclic amino acid substructures such as 2-(pyrrolidin-3-yl)acetic acid (**8**) and pyrrolidine-3-carboxylic acid (**9**) to identify novel potent and selective inhibitors of mGAT1 and to expand the known information about structure-activity-relationships of mGAT1 to other amino acid motifs. The focus was set on libraries with an oxime functionality due to their higher hydrolytic stability compared to the hydrazone moiety.⁶² Moreover, the oxime functionality might also contribute to the affinity of the new mGAT1 inhibitors as some highly affine inhibitors containing this function are already known (e.g. NO711 and DDPM-2571).

Hence, stable oxime libraries should be examined within the MS Binding Assays which should be generated by the reaction of the respective amino acids **8** and **9** bearing a hydroxylamine functionality with different aldehydes **15** as outlined in Scheme 1.

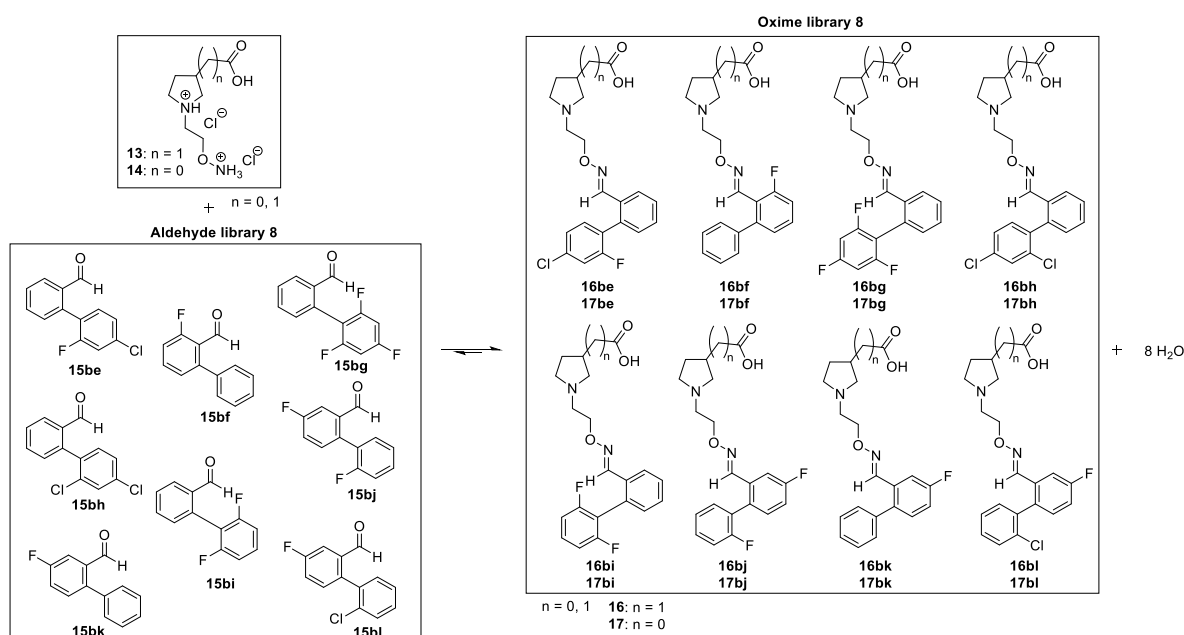
Aims and Scope



Scheme 1: Condensation reaction of hydroxylamine derivative **13** ($n = 1$) and **14** ($n = 0$) with various aldehydes **15** to yield the corresponding oximes **16** ($n = 1$) and **17** ($n = 0$).

In the case of hydrazone libraries⁶¹ it has been shown that the generation of the libraries can be performed in the presence of the target protein, mGAT1. However, oxime formation is known to be very slow under physiological conditions. Hence, library formation and determination of the activity of the library by MS Binding Assays the latter requiring the presence of the target protein should be performed in separate steps. The same approach has already been applied before to the screening of related oxime libraries in our group.⁵²

Contrary to aforementioned study, the number of aldehydes **15** in a single library should be increased from four to eight compounds, which would improve the efficiency of the present MS Binding Assay. Therefore, the actual approach was conducted as follows: Oxime libraries are pre-generated in absence of the target mGAT1 by reaction of 28 different aldehyde libraries each consisting of eight different components with either hydroxylamine **13** or **14** to give the corresponding oxime libraries **16** and **17** as exemplarily outlined in Scheme 2.



Scheme 2: Exemplary reaction of hydroxylamine **13** and **14** with aldehyde library 8 to yield corresponding oxime library 8.

Aims and Scope

As the increase of the number of aldehydes (4 x 1 mM to 8 x 1 mM of each aldehyde) with constant concentration of the hydroxylamine (40 mM) changes the ratio of the reactants for the oxime generation (from 10:1 to 5:1), the suitability of the experimental conditions has to be proven which should be accomplished by ^1H NMR studies.

After the pre-generation the formed oxime libraries has to be diluted to concentrations suitable for the MS Binding Assays (1 μM , 100 nM or 10 nM) and are subsequently incubated with the marker and the target protein mGAT1 for 4 hours. The stability of the diluted oxime libraries has to be examined over the subsequent incubation time. Due to the low concentration the measurements should be achieved by fluorescence detection.

The affinity of the libraries can be indirectly measured by the quantification of the marker. Hence, the protein-ligand complexes, which were formed during incubation, have to be separated from the unbound oximes and marker, denatured and eluted with organic solvent. Afterward, the formerly bound marker is quantified by LC-MS/MS. If a library is able to reduce the specific binding of the marker under a certain level, this particular library should then be tested in deconvolution experiments in which each single oxime is examined in order to identify which oxime is responsible for the affinity of the library.

After the deconvolution experiments the most potent oximes should be resynthesized to determine their binding affinities ($\text{p}K_i$ values) in full-scale competitive MS Binding Assays^{58a} as well as their inhibitory activities (pIC_{50} values) in [^3H]GABA uptake assays⁵¹. Finally, these compounds should be fully characterized regarding their subtype selectivity at all four murine GABA transporters.

In the course of this study also an HPLC method for the enantiomeric purity determination of nipecotic acid (**6**) should be developed and validated. Furthermore, it should be used for the characterization of both enantiomers of nipecotic acid. This method should then enable the determination of the enantiomeric excess for other cyclic amino acids including those utilized in this work.

3 Results and Discussion

3.1 First Publication

Determination of enantiomeric excess of nipecotic acid as 1-(7-nitrobenzo-[c][1,2,5]oxadiazol-4-yl) derivatives

3.1.1 Summary of the Results

Nipecotic acid (piperidine-3-carboxylic acid) is an important precursor for the synthesis of novel enantiopure inhibitors of γ -aminobutyric acid transporters (GATs), for the enantiomers of which frequently quite different biological activities are found.⁴² One well-known example is tiagabine – a selective and highly affine GABA reuptake inhibitor for the transporter subtype GAT1 – for which the (*R*)-enantiomer is known to be distinctly more potent than the (*S*)-enantiomer.⁴⁹ With the data of pharmacological testing being dependent on the enantiopurity of the studied samples, the knowledge of the enantiopurity of nipecotic acid serving as starting material for the synthesis of new GAT inhibitors is of fundamental importance.

Several methods have been reported in the literature⁶³ so far for enantiopurity determination of nipecotic acid but the only validated HPLC method was published in 1995 by Rustum et al. In that case, however, not the enantiopurity of the free amino acid but the ethyl ester using a Chiralcel-OG stationary phase (Daicel Corporation) with UV detection at 230 nm was analyzed.⁶⁴ Due to the low absorption coefficient of the carboxylic acid ester function, sensitivity and selectivity of this method appears to be low, its suitability for an exact determination of highly enantioenriched samples of nipecotic acid ethyl ester thus being limited. Moreover, for this method the resolution of both enantiomers was specified to be around 1.3 though only for a resolution of ≥ 1.5 , peaks with Gaussian shape can be assumed to be baseline separated. Hence, especially in higher concentration ranges and when tailing occurs the validity of % ee determination of the (*S*)-enantiomer in the presence of small amounts of (*R*)-enantiomer appears questionable.

Therefore, a reliable new HPLC method for the determination of the enantiopurity of both enantiomers of nipecotic acid should be developed and validated. To this end, *N*-substituted derivatives of nipecotic acid provided with a suitable chromophore should be generated prior to chromatography. Due to the presence of the chromophore high wavelengths for UV-Vis detection would be expected, that should ensure a selective determination of high ee values of the individual enantiomers of the analyte. Additionally, due to *N*-substitution of the nipecotic acid amphoteric properties of the analyte were eliminated which should facilitate the development and optimization of the chromatographic conditions.

4-Fluoro-7-nitrobenzo[c][1,2,5]oxadiazole⁶⁵ was used as a derivatization reagent as it enabled a detection wavelength of 490 nm. A Chiralpak ID-3 (250 x 4.6 mm, 3 μ m, Daicel) in combination with a polar mobile phase consisting of acetonitrile with 20 mM of formic acid and 20 mM of *N,N*-diisopropylethylamine was found suitable for enantioseparation after the chromatographic conditions such as flow rate, column temperature or injection volumes had been optimized. The final chromatographic conditions consisted of a flow rate of 1 mL/min, a column temperature of 40 °C and an injection volume of 10 μ L (samples dissolved in the mobile phase) and enabled a separation of the enantiomers with a resolution of 5.44.

The reliability of the optimized HPLC method was successfully demonstrated by validation of the parameters specificity, linearity, accuracy, precision and lower limit of quantification for both enantiomers. Due to the broad quantification range established for each enantiomer, enantiomeric excesses up to 99.87% ee for the (*R*)-enantiomer and 99.86% ee for the (*S*)-enantiomer could be determined.

In addition, by spiking of highly enantiopure samples of nipecotic acid derivatives with small amounts of racemic mixture, the newly developed method has been shown to even enable the detection of slight changes of ee values.

3.1.2 Declaration of Contribution

The idea of the publication was based on the bachelor thesis “*Development of an HPLC Method for Enantiopurity Determination of Cyclic β -Amino Acids*” by Marie Niedermeier prepared under my supervision. During this time, I derivatized racemic, (*S*)- and (*R*)-nipecotic acid using 4-fluoro-7-nitrobenzo[c][1,2,5]oxadiazole as derivatization reagent, which were used as analytes, respectively. Based on the preliminary experiments regarding stationary and mobile phase performed by Marie Niedermeier, I developed an HPLC method for the enantioseparation and the determination of the enantiomeric excesses of nipecotic acid as 1-(7-nitrobenzo[c][1,2,5]oxadiazol-4-yl) derivatives. Validation and the spiking experiments to verify the HPLC results were carried out by myself. I wrote the manuscript and generated all graphics and tables, assisted by Dr. Georg Höfner. The manuscript was corrected by Prof. Dr. Klaus T. Wanner. The cover image resulted in collaboration with Dr. Jörg Pabel.

REGULAR ARTICLE

Determination of enantiomeric excess of nipecotic acid as 1-(7-nitrobenzo[c][1,2,5]oxadiazol-4-yl) derivatives

Simone K. Schmidt | Georg Höfner | Klaus T. Wanner

Department of Pharmacy – Center of Drug Research, Ludwig-Maximilians-Universität München, Munich, Germany

Correspondence

K.T. Wanner, Department of Pharmacy – Center of Drug Research, Ludwig-Maximilians-Universität München, Butenandtstr. 5-13, 81377 Munich, Germany.

Email: klaus.wanner@cup.uni-muenchen.de

Abstract

For the enantiopure synthesis of novel chiral GABA uptake inhibitors, nipecotic acid (**1**) is an important key precursor. To characterize accurately the pharmacological activity of these interesting target compounds, the determination of the correct enantiomeric purity of nipecotic acid as the starting material is indispensable. In this report, a sensitive high-performance liquid chromatography (HPLC) based method for the separation and quantitation of both enantiomers of nipecotic acid as 1-(7-nitrobenzo[c][1,2,5]oxadiazol-4-yl) derivatives (**5**) on a Chiralpak ID-3 column (Daicel, Illkirch, France) was established. UV/Vis-detection at 490 nm was chosen to ensure a selective determination of even highly enantioenriched samples. Reliability was demonstrated by validation of specificity, linearity, lower limit of quantification (LLOQ), accuracy, and precision. By spiking highly enantiopure samples with small amounts of racemic *rac*-**5**, it was proven that the established HPLC method is able to detect even slight changes in enantiomeric excess (*ee*) values. Thus, accurate determination of *ee* values up to 99.87% *ee* for (*R*)-**5** and 99.86% *ee* for (*S*)-**5** over a linear concentration range of 1–1500 μ M for (*R*)-**5** and of 1–1455 μ M for (*S*)-**5** could be demonstrated.

KEYWORDS

amino acid, derivatization, enantiopurity, high performance liquid chromatography, NBD-F, validation

1 | INTRODUCTION

Nipecotic acid (*rac*-piperidine-3-carboxylic acid, **1**) is a nonnatural cyclic β -amino acid that is a key precursor for the synthesis of important inhibitors for γ -aminobutyric acid transporters (GATs¹).² For example, tiagabine [(*R*)-**2**] and SK&F-89976A (**3**) are reuptake inhibitors for the subtype GAT1 for which the (*R*)-enantiomers are known to be more potent than the (*S*)-enantiomer [(*S*)-**2**: pIC₅₀ = 6.20 \pm 0.13; (*R*)-**2**: pIC₅₀ = 6.88 \pm 0.12; (*S*)-**3**: pIC₅₀ = 4.97 \pm 0.10; (*R*)-**3**: pIC₅₀ = 5.49 \pm 0.09].^{3,4} In contrast, the (*S*)-enantiomer DDPM-1457 (**4**) is more active on the GABA transporter subtype mGAT4 than its (*R*)-enantiomer [(*S*)-**4**: pIC₅₀ = 5.87 \pm 0.08; (*R*)-**4**: pIC₅₀ = 4.33 \pm 0.05] (Figure 1).^{4,5}

As can be seen from these examples and in the case of even higher enantioselectivities, it is necessary to use only highly enantiopure samples for the determination of the

pharmacological data of novel chiral GABA reuptake inhibitors, as the false enantiomer will distort the resulting data the more it is present. Especially when characterizing the pharmacological activity of the distomer of a pair of biologically active enantiomers exhibiting high enantioselectivity, the presence of small amounts of the eutomer may significantly falsify the results. Thus, in the case of the preparation of novel target compounds derived from enantiopure nipecotic acid (**1**), a reliable and sensitive determination of the precise enantiomeric excess (*ee*) of nipecotic acid (**1**) is indispensable. As far as multistep syntheses are concerned, a determination of the enantiomeric purity of **1** may be sufficient, when a racemization during the synthetic process can be excluded which, e.g., can exemplarily be verified by chiral analysis of a final product.

Several different methods have been reported in the literature for the enantiopurity determination of nipecotic

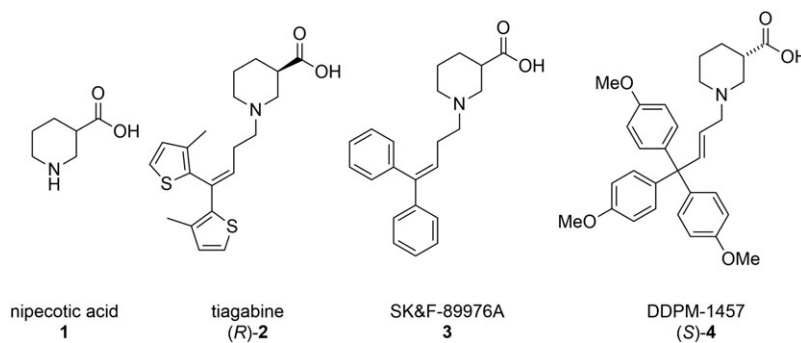


FIGURE 1 Nipecotic acid (**1**) as key precursor for the synthesis of novel GABA reuptake inhibitors and important derivatives: tiagabine [(*R*)-**2**],³ SK&F-89976A (**3**)³ and DDPM-1457 [(*S*)-**4**]⁵

acid (**1**). Besides an indirect method relying on separation of diastereomers generated by derivatization with an enantiopure isothiocyanate reagent on an RP column,⁶ several high-performance liquid chromatography (HPLC) methods in which the separation of both enantiomers of nipecotic acid (**1**) after derivatization with achiral reagents could be achieved on chiral stationary phases are known: methods accomplished by employing carboxylic acid esters,^{7–9} *N*-carbamoyl,¹⁰ and *N*-aminocarbonothioyl substituted nipecotic acid,^{11,12} and nipecotic acid derivatives with modifications at both functional groups.^{13,14}

A validated HPLC method for the enantioseparation of a nipecotic acid derivative has so far only been published for the ethyl ester of **1**, in 1995 by Rustum.⁹ This method is based on Chiralcel-OG stationary phase (Daicel, Tokyo, Japan) and utilizes UV detection at 230 nm.⁹ But this method was only validated for the quantification of (*S*)-enantiomer in the presence of (*R*)-enantiomer, but not vice versa. The concentration range was reported to be linear from 0.1 to 1.0 mg·mL^{−1} for a 10 µl injection volume with a linear regression coefficient of >0.999 indicating the highest possible quantification of 10% of the minor enantiomer in the presence of the major enantiomer. Because of the absorption wavelength of 230 nm resulting from the carboxylic acid ester function exhibiting a low absorption coefficient, the selectivity and sensitivity of this method is to be regarded as low and thus of limited suitability for the determination of highly enantioenriched samples of the ethyl ester of **1**. Moreover, the resolution of the two enantiomers was specified to be only around 1.3. Considering that only for a resolution of ≥1.5, Gaussian peaks will be baseline separated,¹⁵ a reliable *ee* determination especially for highly enantioenriched samples appears questionable. Accuracy of the method was concluded by standard addition yielding good recoveries of the (*S*)-enantiomer of 100.5 ± 0.8% (mean ± relative standard deviation [RSD]).⁹

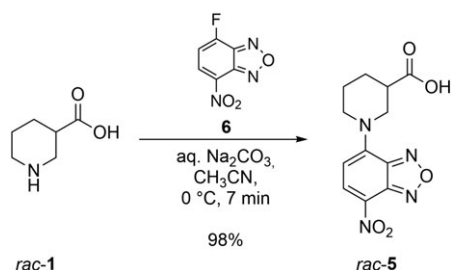
For the chiral separation of underivatized nipecotic acid, methods based on chiral ligand-exchange¹⁶ or zwitterionic chiral stationary phases^{17–19} have been reported. One disadvantage of the latter approach is that most of these stationary phases are not commercially available, but have to be prepared, which is time-consuming and therefore not appropriate for most of the potential users.^{17,18} Recently, a zwitterionic stationary phase based on quinine derivative fused with a

chiral sulfonic acid, which can be purchased under the trade name Chiralpak ZWIX(+) (Daicel), was reported to allow the separation of the nipecotic acid enantiomers with a resolution of 14.87.¹⁹ But this approach has the disadvantage that for the analysis, because nipecotic acid (**1**) is devoid of a chromophore, detectors such as an ELSD (evaporating light scattering detector) or a CAD (corona charged aerosol detector) are required. Due to the limited accessibility of ELSDs and CADs, we focused on UV/Vis-detection in order to enable application with standard HPLC equipment.

Overall, employing derivatives of **1** appears in particular a promising approach for the development of an efficient method for the chiral analysis of this compound. Providing the amino function of **1**, for example, with a chromophore would increase the sensitivity of detection of the derivative and as a consequence the upper limit of *ee* that can be determined. In addition, the elimination of the ampholytic properties of **1** in the derivative could ease the optimization of the chromatographic conditions required for the chiral separation. By being more common, also the use of UV as compared to fluorescence detection appears to be more favorable.

In 1993, derivatization of nipecotic acid with the fluorescence reagent 6-aminoquinolyl-*N*-hydroxy-succinimidyl carbamate (AQC) to give an *N*-carbamoyl nipecotic acid derivative was described. On a γ -cyclodextrin stationary phase, the enantiomers could be separated with an $R_s = 2.26$.¹⁰ However, the same derivative seems less suitable for UV/Vis-detection at the wavelength used for the excitation in fluorescence detection (226 nm). For short wavelengths, the interference resulting from contaminants are more likely, which would hamper *ee* determination.

Therefore, we deemed derivative of **1** 1-(7-nitrobenzo[*c*][1,2,5]oxadiazol-4-yl)nipecotic acid (*rac*-**5**) more suitable for chiral analysis (Scheme 1).²⁰ The low-cost reagent 4-fluoro-7-nitrobenzo[*c*][1,2,5]oxadiazole (**6**, NBD-F)²¹ required for the preparation of **5** is widely used for the analysis of amino acids like proline by HPLC, as it is known to allow the formation of stable derivatives under mild reaction conditions and to give rise to products with absorption wavelengths around 470 nm, allowing a reasonably selective UV/Vis-detection.^{22,23} In this report, we disclose an HPLC method for the chiral analysis of **1** via nipecotic acid derivative **5**, which allows the determination of *ees* up to at least



SCHEME 1 Preparation of *rac*-5 from *rac*-1 and 4-fluoro-7-nitrobenzo[*c*][1,2,5]oxadiazole (**6**, NBD-F)

99% (*ee*) for both enantiomers by means of calibration functions and the validation of said procedure.

2 | MATERIALS AND METHODS

2.1 | Derivatization: General experimental procedures

2.1.1 | Chemicals

HPLC-grade acetonitrile and formic acid were purchased from VWR International (Darmstadt, Germany). *N,N*-Diisopropylethylamine was purchased from TCI Europe (Zwijndrecht, Belgium) and was freshly distilled prior to use. *Rac*-Nipecotic acid ($\geq 98\%$) was from Sigma Aldrich (Steinheim, Germany), (+)-(*S*)-nipecotic acid (98.4%, 99.6% *ee*), (–)-(*R*)-nipecotic acid (99.6%, 99.9% *ee*), and 2,6-difluoroaniline ($> 97\%$) from TCI Europe were used as purchased. The deuterated solvents chloroform-*d* (99.8% D) and methanol-*d*₄ (99.8% D) were purchased from Euriso-top (Saint-Aubin, France).

2.1.2 | Analytical data

NMR spectra were recorded with an Avance III HD 400 MHz Bruker BioSpin (Billerica, MA) and Avance III HD 500 MHz Bruker BioSpin spectrometer. The digital resolution is stated with an accuracy of ± 0.15 Hz. MestreNova (v. 10.0.1) was used for further analysis of the spectra. IR spectra were recorded with a FT-IR spectrometer Paragon 1000 (Perkin-Elmer, Rodgau, Germany) and Spectrum v2.00 software (Perkin-Elmer). High-resolution mass spectra were measured on a Thermo Finnigan LTQ FT instrument for electrospray ionization (ESI). Specific rotations $[\alpha]_D^{25}$ ($c = \text{g} \cdot \text{cm}^{-3}$ in solvent) given as $\text{deg} \cdot \text{cm}^3 \cdot \text{g}^{-1} \cdot \text{dm}^{-1}$ were measured (pathlength *l* of 1 dm) on a Perkin Elmer 241 polarimeter with a sodium vapor lamp. For weighing, an ALC-80.4 ACCULAB and a MC 21S from Sartorius Group (Göttingen, Germany) were used.

2.1.3 | Synthesis

4-Fluoro-7-nitrobenzo[*c*][1,2,5]oxadiazole (**6**, NBD-F) was synthesized according to the literature.²⁴ The synthesis of **5** from **1** with **6** (NBD-F) was accomplished in analogy to the procedure published by Min et al. for the reaction of

piperidine-3-carboxylic acid with 7-fluoro-*N,N*-dimethylbenzo[*c*][1,2,5]oxadiazole-4-sulfonamide (DBD-F).²⁴ The applied reaction conditions are given in the general procedure (GP, Scheme 1).

2.2 | General procedure (GP)

NBD-F (**6**, 1.1 eq.) in CH₃CN was added to a solution of nipecotic acid (1 eq.) in aqueous Na₂CO₃ solution (0.0625 M). The reaction mixture was stirred at 0°C for 7 min under protection from light. The aqueous layer was extracted once with Et₂O (1 × 50 ml), and after adjustment of the pH to 3–4 with aqueous HCl solution (2 M) four additional times (4 × 100 ml). The combined organic layers were dried (Na₂SO₄), filtered, and concentrated in vacuo. The residue was resuspended in CH₂Cl₂ and after repeated evaporation dried under high vacuum to yield the desired product as a red solid.

rac-1-(7-Nitrobenzo[*c*][1,2,5]oxadiazol-4-yl)piperidine-3-carboxylic acid (*rac*-5): According to GP with *rac*-nipecotic acid (*rac*-1) (26.0 mg, 0.201 mmol) in aqueous solution of Na₂CO₃ (9.6 ml) and NBD-F (40.5 mg, 0.221 mmol) in CH₃CN (3 ml). Yield: 57 mg (98%), red amorphous powder. TLC: $R_f = 0.12$ (CH₃CN/CH₃OH = 95:5). IR (KBr): $\nu = 3427, 2928, 1608, 1553, 1293 \text{ cm}^{-1}$. ¹H NMR (500 MHz, CD₃OD, δ): 1.85–1.75 (m, 1H, CH₂), 2.02–1.94 (m, 2H, CH₂), 2.22–2.15 (m, 1H, CH₂), 2.80 (tt, $J = 9.1/4.1$ Hz, 1H, CH), 3.78 (ddd, $J = 13.4/10.1/3.0$ Hz, 1H, CH₂), 4.01 (dd, $J = 13.7/9.1$ Hz, 1H, CH₂), 4.49 (br d, 1H, CH₂), 4.72 (dd, $J = 13.7/3.1$ Hz, 1H, CH₂), 6.60 (d, $J = 9.1$ Hz, 1H, CH), 8.48 (d, $J = 9.1$ Hz, 1H, CH). ¹³C NMR (126 MHz, CD₃OD, δ): 25.4 (CH₂), 28.1 (CH₂), 42.6 (CH), 51.7 (CH₂), 52.8 (CH₂), 104.4 (CH), 123.4 (C_q), 137.1 (CH), 146.4 (C_q), 146.5 (C_q), 147.0 (C_q), 176.1 (C_q). M_r calcd. for C₁₂H₁₂N₄O₅, 292.0808; HRMS (ESI, m/z): [$M - H$][–] calcd. for C₁₂H₁₁N₄O₅, 291.0735; found, 291.0733. (*R*)-1-(7-Nitrobenzo[*c*][1,2,5]oxadiazol-4-yl)piperidine-3-carboxylic acid [(*R*)-5]: According to GP with (–)-(*R*)-nipecotic acid [(*R*)-1] (26.0 mg, 0.201 mmol) in aqueous solution of Na₂CO₃ (9.6 ml) and NBD-F (40.5 mg, 0.221 mmol) in CH₃CN (3 ml). Yield: 56 mg (96%), red amorphous powder. $[\alpha]_D^{22} = -118.0$ ($c = 0.245$ in CH₃OH). M_r calcd. for C₁₂H₁₂N₄O₅, 292.0808; HRMS (ESI, m/z): [$M - H$][–] calcd. for C₁₂H₁₁N₄O₅, 291.0735; found, 291.0738.

(*S*)-1-(7-Nitrobenzo[*c*][1,2,5]oxadiazol-4-yl)piperidine-3-carboxylic acid [(*S*)-5]: According to GP with (+)-(*S*)-nipecotic acid [(*S*)-1] (26.0 mg, 0.201 mmol) in aqueous solution of Na₂CO₃ (9.6 ml) and NBD-F (40.5 mg, 0.221 mmol) in CH₃CN (3 ml). Yield: 54 mg (93%), red amorphous powder. $[\alpha]_D^{22} = +122.8$ ($c = 0.25$ in CH₃OH). M_r calcd. for C₁₂H₁₂N₄O₅, 292.0808; HRMS (ESI, m/z): [$M - H$][–] calcd. for C₁₂H₁₁N₄O₅, 291.0735; found, 291.0733.

Analytical data obtained by ^1H NMR, ^{13}C NMR, IR and R_f value of (*R*)-**5** and (*S*)-**5** were in accord with data obtained for *rac*-**5**.

2.2.1 | Chemical purity

The water content of *rac*-**5**, (*S*)-**5** and (*R*)-**5** obtained by derivatization was determined by coulometric Karl-Fischer titration using a KF-coulometer 684 (Metrohm, Herisau, Switzerland) (solvent CH_3OH , $n = 3$). Other impurities like solvent residues or grease were identified by ^1H NMR spectroscopy. Water content was found to be lower than 1.5% (m/m) for *rac*-**5**, 1.5% (m/m) for (*S*)-**5**, and 2% (m/m) for (*R*)-**5**. ^1H NMR spectra indicated impurities of 2.5% (m/m) for *rac*-**5**, 2% (m/m) for (*S*)-**5**, and 4% (m/m) for (*R*)-**5**. Overall, the chemical purity of *rac*-**5**, (*S*)-**5**, and (*R*)-**5** can be considered as higher than 96%, 96.5%, and 94%, respectively.

2.2.2 | UV-absorption measurement

The UV-absorption spectrum of *rac*-**5** was measured in a quartz fluorescence cuvette by a Spectra Max M2e plate reader (Molecular Devices, Ismaning, Germany). The spectrum was corrected by subtraction of the spectrum of the pure solvent.

2.3 | Chromatography

2.3.1 | Instrumentation

An Agilent 1100 HPLC system consisting of a vacuum degasser, binary pump, column oven, variable wavelength UV-Vis detector, autosampler (Agilent, Waldbronn, Germany), and the stationary phase Chiralpak ID-3 column, 250×4.6 mm, $3 \mu\text{m}$ (Daicel, Illkirch, France) was used. Data analysis was performed by means of OpenLab CDS EZChrom from Agilent Technologies.

2.3.2 | Preparation of samples

Samples were dissolved in the mobile phase consisting of 3.40 ml *N,N*-diisopropylethylamine and 0.76 ml formic acid filled up with CH_3CN to 1000 ml. All concentrations of the samples used for the validation procedure represent the nominal concentration of isolated derivatized nipecotic acid **5**. The samples for method development and validation were prepared by diluting a 6 mM stock solution of **5** in the sample solvent.

2.3.3 | Investigation of chromatograms

The obtained chromatograms were examined using the following parameters calculated by OpenLab CDS EZChrom from Agilent Technologies. Resolution, R_s , retention factor, k , and symmetry factor, A_s , were calculated according to the United States Pharmacopia (USP 39 – NF 34). Due to the recommendation of the USP the following equation was used for resolution calculations: $R_s = 1.18 \cdot (t_{R1} - t_{R2}) / (w_{1,h/2} + w_{2,h/2})$ where t_{R1} and t_{R2} are the retention times

of the two compounds and $w_{1,h/2}$ and $w_{2,h/2}$ are the corresponding widths of the peaks at 50% height. For the retention factor k , void time of the stationary phase ($t_{0,SP}$) was estimated using following equation: $t_{0,SP} = 5 \cdot 10^{-4} (Ld_c^2/F)$ where L is the column length in mm, d_c is the column inner diameter in mm, and F is the flow rate in $\text{ml} \cdot \text{min}^{-1}$ and the void time of the HPLC instrument without column ($t_{0,I}$) was measured to be $t_{0,I} = 0.097 \text{ min}$.¹⁵

2.4 | HPLC method and validation

Each sample was measured in triplicate unless stated otherwise. Final chromatographic conditions were as follows: The mobile phase consisted of 20 mM formic acid and 20 mM *N,N*-diisopropylethylamine in CH_3CN , the flow rate amounted to $1 \text{ ml} \cdot \text{min}^{-1}$, injection volume to $10 \mu\text{l}$, and column temperature to 40°C . The samples were dissolved in the mobile phase and chromatograms were recorded at a detection wavelength of 490 nm. The linearity was investigated by measurement of 18 calibration levels (2, 2.5, 4, 5, 7.5, 10, 25, 50, 75, 100, 250, 500, 750, 1000, 1500, 2000, 2500, 3000 μM *rac*-**5**). Accuracy was ascertained by determination of the recovery of quality control samples (QCs) of *rac*-**5** in five different concentrations in five replicates. Precision was validated regarding repeatability by different dilutions leading to five QCs and different batches of the analyte *rac*-**5**, (*S*)-**5** and (*R*)-**5**, respectively and was calculated as RSD. Additionally, validation of accuracy and precision was extended to experiments with (*S*)-**5** and (*R*)-**5** samples of high enantiopurity spiked with defined amounts of *rac*-**5**. Furthermore, the reliable detection of small changes in the *ee* value was verified with the spiking experiments (sp-ex).

3 | RESULTS AND DISCUSSION

3.1 | HPLC method development

First, the detection wavelength was set to 490 nm, which represented the absolute maximum of the UV absorption spectrum of *rac*-**5** (100 μM in mobile phase, Figure 2a). As chiral stationary phases for enantioseparation of *rac*-**5** Astec Cyclobond I 2000 DM (Sigma Aldrich, 250×4.6 mm, $5 \mu\text{m}$) and Chiradex Gamma (Merck, Darmstadt, Germany, 250×4.6 mm, $5 \mu\text{m}$) were tested, both of which were run with a mobile phase consisting of triethylammonium acetate buffer in CH_3CN , but only Chiralpak ID-3 column (Daicel, 250×4.6 mm, $3 \mu\text{m}$) showed promising results. Consequently, all further experiments for method optimization were undertaken using this stationary phase. When CH_3CN with 20 mM of formic acid and 20 mM of *N,N*-diisopropylethylamine was used as eluent with a flow rate of $1 \text{ ml} \cdot \text{min}^{-1}$, the resulting resolution observed for *rac*-**5** appeared to be sufficient to ensure a sensitive determination of the *ee* for both enantiomers. By varying column temperature (room temperature, 30°C , 35°C , and 40°C) it could be

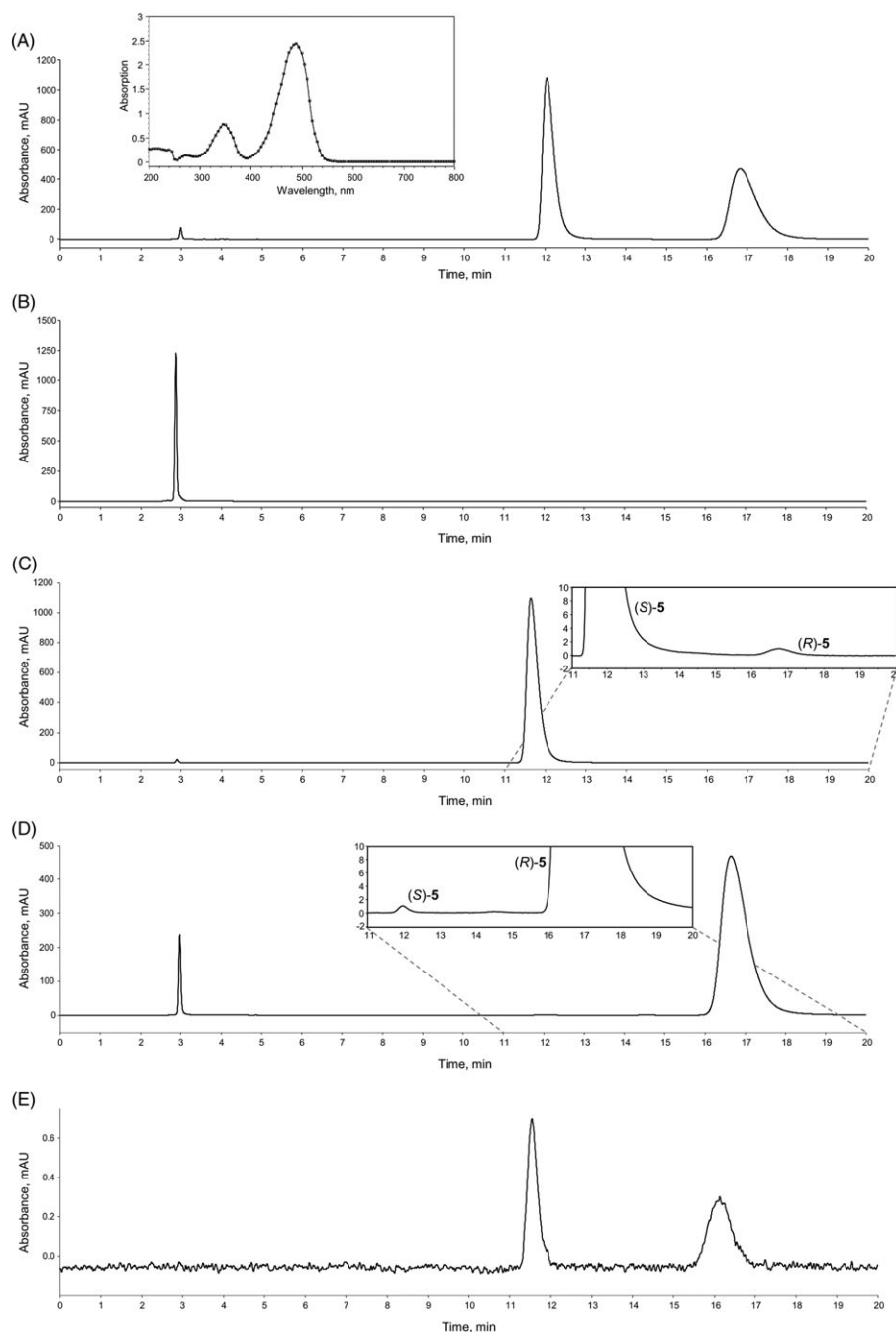


FIGURE 2 Chromatogram of (A) 3000 μM *rac*-5 (1500 μM of each enantiomer); insert shows the absorption spectrum of *rac*-5 (100 μM in the mobile phase) with the absolute maximum at 490 nm; (B) remaining residue of derivatization reaction without nipecotic acid dissolved in the mobile phase; (C) 1455 μM of (*S*)-5; (D) 1500 μM of (*R*)-5 (from TCI Europe). (E) LLOQ at 1 μM for each enantiomer (*S*)-5 and (*R*)-5 (2 μM *rac*-5). All chromatograms were recorded on a Daicel Chiralpak ID-3 (250 \times 4.6 mm, 3 μm), with a mobile phase of 20 mM formic acid and 20 mM *N,N*-diisopropylethylamine in CH_3CN at a flow rate of 1 $\text{mL}\cdot\text{min}^{-1}$ at 40°C

shown that with higher column temperature the retention time decreased, which reduced the analysis time, but at the same time the peak widths narrowed, which led to an increased resolution. When studying the effects of injection volume, it was found that the chromatographic parameters worsened, i.e., the symmetry factor A_S increased and the resolution decreased, when the volume was varied from 10 to 20 μL . Nonetheless, a reduction of the injection volume to 5 μL , although it should result in an improved resolution, was considered not appropriate, as this would most likely also

limit the quantitation range and thus also the maximal height of the *ee* values that can be determined. Accordingly, the injection volume was set to 10 μL , representing a good compromise between chromatographic resolution and quantification range. Thus, the final optimized chromatographic conditions consisted of 20 mM formic acid and 20 mM *N,N*-diisopropylethylamine in CH_3CN as mobile phase, a flow rate of 1 $\text{mL}\cdot\text{min}^{-1}$ at a column temperature of 40°C, and an injection volume of 10 μL with the samples being dissolved in the mobile phase. For the chromatograms received under

these conditions, the following analytical parameters were obtained. The resolution was found to be $R_s = 5.44$, when determined at 3000 μM of *rac*-**5**. As the sample at this concentration had led to a chromatogram with the broadest peaks and the highest symmetry factors ($A_s((S)\text{-}\mathbf{5}) = 1.73$; $A_s((R)\text{-}\mathbf{5}) = 1.67$), this value can be considered the lowest resolution for the whole concentration range studied (Figure 2a). From the same chromatogram the retention factors k for (*S*)-**5** and (*R*)-**5** were calculated to be 3.39 and 5.13, respectively. Additionally, blank samples containing only the mobile phase were injected during method development and validation. According to the lack of peaks at the retention time of *rac*-**5**, the method is free of sample carryover effects (data not shown).

3.2 | Validation

To validate the described HPLC method the following parameters were examined: specificity, lower limit of quantification (LLOQ), linearity, quantitation range, accuracy (i.e., recovery), and precision (i.e., repeatability, calculated as RSD) for both enantiomers of nipecotic acid. To this end, the particular chromatograms of *rac*-**5** were analyzed. Additionally, for determination of accuracy and precision experiments with enantiopure samples of (*S*)-**5** and (*R*)-**5** were performed.

3.2.1 | Specificity

To exclude any interference of unreacted reagents resulting from the formation of *rac*-**5** from *rac*-**1** or other components in the analytical samples, the procedure used for the synthesis of *rac*-**5** was repeated under identical conditions, except that *rac*-**1** was left out. When the thus obtained residue was subjected to the same analytical procedure as *rac*-**5** (see Figure 2b), the resulting chromatogram showed only a peak eluting near the void time. But neither any other peak nor a peak at the retention times of the enantiomers of *rac*-**5** could be detected, which were determined by injection of pure (*S*)- or (*R*)-enantiomers of **5**. (Figure 2c,d). Accordingly, the method can be considered as being specific.

3.2.2 | Linearity, range, LLOQ

Calibration functions for both enantiomers were generated based on the data obtained from the analysis of 18 concentration levels of *rac*-**5** in the concentration range from 2 to 3000 μM (for details, see Materials and Methods), by applying linear regression with $1/x^2$ weighing. For the (*S*)-enantiomer, the calibration function found was $y = 264479x + 9186$ ($r^2 = 0.9994$, y-intercept corresponding to 3.37% of the area obtained at the LLOQ) and for the (*R*)-enantiomer $y = 262519x + 16276$ ($r^2 = 0.9995$, y-intercept corresponding to 5.88% of the area obtained at LLOQ). For both enantiomers, the quantitation range reached from 1 to 1500 μM . Thus, determination of enantiopurities of nipecotic acid **1** up to 99.87% *ee* should be feasible, considering that

one enantiomer may be reliably quantified at a concentration of 1500 μM when the other enantiomer, in this case the minor isomer, is present at a concentration of 1 μM . The signal to noise (*S/N*) ratio was recorded for three 1 μM concentrations of (*S*)-**5** and (*R*)-**5**. It was found to be ≥ 22 for (*S*)-**5** and ≥ 11 for (*R*)-**5** (Figure 2e), which could be regarded as suitable for the purpose of determining *ee* values up to 99%.

3.2.3 | Accuracy, precision

To determine accuracy and precision, quality control samples were analyzed in replicates ($n = 5$) at five different concentration levels (2, 10, 750, 1500, 3000 μM of *rac*-**5**). Concentrations were calculated from the experimentally obtained areas employing the particular calibration function. Mean concentrations, accuracy, and precision are given in Table 1. Recovery was calculated as the ratio of the experimentally determined concentration \pm confidence interval ($\alpha = 0.05$) to the nominal concentration and precision as the RSD of the measured concentrations. For the (*S*)-enantiomer of **5**, recoveries between $98.8 \pm 0.6\%$ and $99.7 \pm 0.9\%$ and RSDs between 0.26% and 0.73% and for (*R*)-**5** recoveries between $99.3 \pm 0.6\%$ and $100.2 \pm 0.3\%$ and RSDs between 0.26% and 1.0% were found.

When accuracy and precision were examined for highly enantioenriched material, samples of (*S*)-**5** and (*R*)-**5**, with the concentration of the major enantiomer not exceeding 1500 μM were prepared, the concentrations thus stayed still in the previously defined linearity range. The found concentration of the (*S*)-**5** sample (from TCI Europe) with a nominal concentration of 1455 μM amounted to 1477 μM and resulted in a recovery of $101.5 \pm 1.7\%$ and the RSD was 1.3% related to the sum of both enantiomers (Table 2). According to the *ee* value of 99.60% *ee* given by the supplier, TCI Europe, the analyzed sample should contain the enantiomers (*S*)-**5** and (*R*)-**5** in concentrations of 1452 μM and 2.910 μM , respectively. With respect to the determined concentrations of 1474 μM for (*S*)-**5** and 3.014 μM for (*R*)-**5**, for the latter recovery it was found to be $103.6 \pm 2.5\%$ and RSD 1.9% and for (*S*)-**5** recovery it was $101.5 \pm 1.7\%$ and RSD 1.3%. The *ee* value calculated from these results amounts to 99.59%, which is in excellent agreement with the *ee* of 99.60% stated by the supplier.

In the case of the (*R*)-**5** sample (from TCI Europe) analyzed at a nominal concentration of 1500 μM , the concentrations calculated by means of five replicates were 1468 μM with a recovery of $97.8 \pm 2.6\%$ and RSD of 2.2% related to the sum of both enantiomers (Table 2). For the enantioenriched (*R*)-**5** (with 99.90% *ee* according to the supplier) the nominal concentrations for each enantiomer were expected to be 0.750 μM for (*S*)-**5** and 1499 μM for (*R*)-**5**. However, with the LLOQ being 1 μM for (*S*)-**5**, this value was too low for a reliable determination by our method. But for (*S*)-**5**, a concentration of 1.296 μM was found, which was thus within the quantitation range. For this, recovery

TABLE 1 Results (mean values, $n = 5$) for QC samples at five different concentration levels of *rac*-5 regarding accuracy (recovery \pm confidence interval, $\alpha = 0.05$) and precision (relative standard deviation, RSD)

Concentration (μM)	Found (mean values)		Recovery \pm CI (%)		RSD (%)	
	(S)-5	(R)-5	(S)-5	(R)-5	(S)-5	(R)-5
1500	1494	1503	99.6 \pm 0.3	100.2 \pm 0.3	0.26	0.26
750	746.0	749.3	99.5 \pm 0.5	99.9 \pm 0.5	0.43	0.44
375	370.6	372.4	98.8 \pm 0.6	99.3 \pm 0.6	0.51	0.52
5	4.974	4.980	99.5 \pm 0.8	99.6 \pm 0.9	0.62	0.75
1	0.9966	0.9954	99.7 \pm 0.9	99.5 \pm 1.3	0.73	1.0

TABLE 2 Results (mean values, $n = 5$) for samples of (S)-5 and (R)-5 regarding accuracy (recovery \pm confidence interval, $\alpha = 0.05$), precision (relative standard deviation, RSD) and the error range of the determined *ee* values (calculated with concentration \pm confidence interval, $\alpha = 0.05$)

Concentration									ee [%]	
Nominal [μM]		Found ± CI [μM]		Recovery ± CI [%]		RSD [%]		Expected ^e	Found	ee range ^f
(S)-5		1455		1477 ± 24.4		101.5 ± 1.7 ^c		1.3 ^d		
(S)-5	(R)-5	(S)-5	(R)-5	(S)-5	(R)-5	(S)-5	(R)-5			
1452 ^a	2.910 ^a	1474 ± 24.5	3.014 ± 0.1	101.5 ± 1.7	103.6 ± 2.5	1.3	1.9	99.60	99.59	99.58–99.61
(R)-5		1500		1468 ± 39.5		97.8 ± 2.6 ^c		2.2 ^d		
(S)-5	(R)-5	(S)-5	(R)-5	(S)-5	(R)-5	(S)-5	(R)-5			
0.750 ^b	1499 ^b	1.296 ± 0.1	1466 ± 39.4	172.8 ± 10.8	97.8 ± 2.6	5.1	2.2	99.90	99.82	99.81–99.84

^aExpected concentration of a 1455 μM (S)-5 sample with a given *ee* value of 99.60% *ee* stated by TCI Europe (Zwijndrecht, Belgium).

^bExpected concentration of a 1500 μM (R)-5 sample with a given *ee* value of 99.90% *ee* stated by TCI Europe (Zwijndrecht, Belgium).

^cRecovery [%] \pm CI was calculated regarding the combined concentration of (S)-5 and (R)-5 in the sample.

^dRSD [%] was calculated regarding the combined concentration of (S)-5 and (R)-5 in the sample.

^e*ee* values [%] given by TCI Europe (Zwijndrecht, Belgium).

^f*ee* range represents the range of error of the found *ee* values calculated using the confidence intervals of the found concentrations. Upper limit of error range was calculated with mean concentration + CI of the major enantiomer and the mean concentration – CI of the minor enantiomer and the lower limit of error range was calculated with mean concentration – CI of the major enantiomer and the mean concentration + CI of the minor enantiomer.

was calculated to be $172.8 \pm 10.8\%$ and RSD 5.1%. For the (R)-enantiomer (R)-5, a concentration of 1466 μM was found together with a recovery of $97.8 \pm 2.6\%$ and RSD of 2.2%. The *ee* of 99.82% calculated from the experimentally determined concentrations is in very good agreement with the *ee* of 99.90% indicated by TCI Europe. Figure 2c,d show the chromatograms observed after injections of 1455 μM of (S)-5 and 1500 μM of (R)-5. To visualize the small peaks of the minor enantiomer of the enantioenriched samples, the respective parts of both chromatograms have been enlarged.

To prove that the developed method is able to determine small changes in the *ee* values in a reliable manner, the above-mentioned enantiopure samples of (S)-5 with a concentration of 1477 μM (1474 μM of (S)-5 and 3.014 μM of (R)-5) and (R)-5 with a concentration of 1468 μM (1466 μM of (R)-5 and 1.296 μM of (S)-5) were each spiked with 5 μl (995 μl of (S)-5 or (R)-5 plus 5 μl of *rac*-5, Table 3, sp-ex 1 and sp-ex 3) and 8 μl (992 μl of (S)-5 or (R)-5 plus 8 μl of *rac*-5, Table 3, sp-ex 2 and sp-ex 4) of a 1500 μM solution of *rac*-5. The concentrations of the spiked samples measured in five replicates were calculated by means of the aforementioned calibration curves. The results were verified with the expected *ee* values for the spiked samples calculated with the expected concentrations for both enantiomers based

on the experimentally determined concentrations of the unspiked (S)-5 and (R)-5 solutions, which can be seen in Table 3.

In the case of spiking (S)-5 samples with 5 μM and 8 μM of 1500 μM of *rac*-5, concentrations of 1471 μM (S)-5 and 6.749 μM (R)-5 (Table 3, sp-ex 1) and of 1469 μM (S)-5 and 8.990 μM (R)-5 (Table 3, sp-ex 2) with *ee* value of 99.09% and 98.78% could be expected, respectively. For sp-ex 1 (Table 3), the found concentrations of 1420 μM for (S)-5 and 6.413 for (R)-5 resulted in a recovery of $96.6 \pm 0.2\%$ and an RSD of 0.18% for the major enantiomer (S)-5 and a recovery of $95.0 \pm 2.1\%$ and an RSD of 1.8% for the minor enantiomer (R)-5. The concentrations regarding sp-ex 2 (Table 3) were found to be 1413 μM for (S)-5 and 8.511 μM for (R)-5. Thus, recovery is $96.2 \pm 0.4\%$ for (S)-5 and $94.7 \pm 1.1\%$ for (R)-5 and RSD is calculated to be 0.30% for (S)-5 and 0.92% for (R)-5. For both spiking experiments, the experimentally found *ee* values of 99.10% for sp-ex 1 and of 98.80% for sp-ex 2 matched the expected *ee* values almost perfectly (Table 3). For enantioenriched samples of (R)-5, spiking with 5 μM and 8 μM of *rac*-5 would lead to concentrations of 5.040 μM of (S)-5 and 1463 μM of (R)-5 (Table 3, sp-ex 3) and 7.286 μM of (S)-5 and 1461 μM of (R)-5 (Table 3, sp-ex 4), respectively. The

TABLE 3 Validation results (mean values, $n = 5$) regarding accuracy (recovery \pm confidence interval, $\alpha = 0.05$) and precision (relative standard deviation, RSD) after spiking a 1477 μM solution of (*S*)-**5** (99.59% *ee*) with small amounts of a 1500 μM *rac*-**5** solution and a 1468 μM solution of (*R*)-**5** (99.82% *ee*) with small amounts of a 1500 μM *rac*-**5** solution, respectively. The error ranges of the determined *ee* values of (*R*)-**5** and (*S*)-**5** were calculated using the concentration \pm confidence interval ($\alpha = 0.05$).

	Concentration				<i>ee</i> (%)						
	Expected (μM) ^b		Found \pm CI (μM)		Recovery \pm CI (%)		RSD (%)		expected ^g	found	<i>ee</i> range ^h
sp-ex ^a	(<i>S</i>)- 5	(<i>R</i>)- 5	(<i>S</i>)- 5	(<i>R</i>)- 5	(<i>S</i>)- 5	(<i>R</i>)- 5	(<i>S</i>)- 5	(<i>R</i>)- 5			
1 ^c	1471	6.749	1420 \pm 3.2	6.413 \pm 0.2	96.6 \pm 0.2	95.0 \pm 2.1	0.18	1.8	99.09	99.10	99.08–99.12
2 ^d	1469	8.990	1413 \pm 5.2	8.511 \pm 0.2	96.2 \pm 0.4	94.7 \pm 1.1	0.30	0.92	98.78	98.80	98.78–98.82
3 ^e	5.040	1463	5.105 \pm 0.2	1397 \pm 12.9	101.3 \pm 3.6	95.5 \pm 0.9	2.9	0.74	99.30	99.27	99.24–99.30
4 ^f	7.286	1461	7.302 \pm 0.2	1383 \pm 11.6	100.2 \pm 2.6	94.6 \pm 0.8	2.1	0.68	99.01	98.95	98.91–98.99

^asp-ex = abbreviation for Spiking Experiment

^bExpected concentration calculated from the experimentally determined concentration for the enantioenriched (*S*)-**5** and (*R*)-**5**, respectively and the added amount of *rac*-**5**.

^csp-ex 1: spiking 995 μL of a 1477 μM (*S*)-**5** solution (99.59% *ee*) with 5 μL 1500 μM *rac*-**5** solution.

^dsp-ex 2: spiking 992 μL of a 1477 μM (*S*)-**5** solution (99.59% *ee*) with 8 μL 1500 μM *rac*-**5** solution.

^esp-ex 3: spiking 995 μL of a 1468 μM (*R*)-**5** solution (99.82% *ee*) with 5 μL 1500 μM *rac*-**5** solution.

^fsp-ex 4: spiking 992 μL of a 1468 μM (*R*)-**5** solution (99.82% *ee*) with 8 μL 1500 μM *rac*-**5** solution.

^gExpected enantiomeric excess calculated with the expected concentrations of the spiking experiments sp-ex 1–4.

^h*ee* range represents the range of error of the found *ee* values calculated using the confidence intervals of the found concentrations. Upper limit of error range was calculated with mean concentration + CI of the major enantiomer and the mean concentration – CI of the minor enantiomer and the lower limit of error range was calculated with mean concentration – CI of the major enantiomer and the mean concentration + CI of the minor enantiomer.

expected *ee* values for sp-ex 3 and sp-ex 4 were calculated to be 99.30% and 99.01% (Table 3). With found concentrations of 5.105 μM of (*S*)-**5** and 1397 μM of (*R*)-**5** in sp-ex 3, recovery amounted to 101.3 \pm 3.6% for (*S*)-**5** with RSD of 2.9% and 95.5 \pm 0.9% for (*R*)-**5** with RSD of 0.74%. For sp-ex 4, following concentrations were found: 7.302 μM for (*S*)-**5** and 1383 μM for (*R*)-**5** which led to recovery of 100.2 \pm 2.6% for (*S*)-**5** and 94.6 \pm 0.8% for (*R*)-**5** with RSDs of 2.1% for (*S*)-**5** and 0.68% for (*R*)-**5**. Due to these results, *ee* values of 99.27% for sp-ex 3 and 98.95% for sp-ex 4 could be calculated, which are in excellent accord with the expected values.

Additionally, the error ranges for the found *ee* values listed in Tables 2 and 3 were calculated using the concentration and CI values obtained for both enantiomers in quintuplicate measurements (Tables 2 and 3). The best possible *ee* value was calculated from the upper confidence limit of concentration of the major enantiomer (mean concentration + CI) and the lower confidence limit of the concentration of the minor enantiomer (mean concentration – CI). The resulting *ee* value represents the upper limit of the error range of the determined *ee* values. The lower limit of the error range was calculated from the lower confidence limit of the concentration of the major enantiomer (mean concentration – CI) and the upper confidence limit of the concentration of the minor enantiomer (mean concentration + CI) (Tables 2 and 3). For the unspiked samples an *ee* range from 99.58 to 99.61% for (*S*)-**5** and 99.81 to 99.84% for (*R*)-**5** was obtained. Spiking experiments performed with enantiopure (*S*)-**5**, yielded an *ee* error range of 99.08 to 99.12% for sp-ex 1 and an *ee* range of 98.78 to 98.82% for sp-ex 2 (for (*S*)-**5**) both including the respective *ee* values (sp-ex 1: 99.09% *ee*; sp-ex 2: 98.78% *ee*). The *ee* error ranges for sp-ex 3

and sp-ex 4 performed for (*R*)-**5** were determined with 99.24 to 99.30% and 98.91 to 98.99% for (*R*)-**5**, respectively. For sp-ex 3, the expected *ee* value was again within the confidence limits and for sp-ex 4 was very close to it (sp-ex 3: 99.30% *ee*; sp-ex 4: 99.01% *ee*).

Overall, an excellent accordance between all experimentally determined and expected *ee* values was found. Thus, the method described in this article can be considered reliable for the determination of the *ee* of nipecotic acid and for the identification of small changes of *ee* values.

4 | CONCLUSION

In this study, a reliable and sensitive HPLC method for the analysis of highly enantioenriched samples of nipecotic acid (**1**) on a chiral stationary phase has been presented. Using UV detection at 490 nm ensures a very selective and versatile method for the determination of the analyte, which should be helpful for many others users. The method was demonstrated to allow a reliable quantification of *ee* values up to 99.87% for (*R*)-**5** and 99.86% for (*S*)-**5** over a concentration range from 1 to 1500 μM for (*R*)-**5** and from 1 to 1455 μM for (*S*)-**5**. The determination of accuracy (i.e., recovery) and precision (i.e., repeatability) examined by QCs of *rac*-**5** led to recoveries between 98.8 \pm 0.6% and 99.7 \pm 0.9% with RSDs between 0.26 and 0.73% for the (*S*)-enantiomer, as well as recoveries between 99.3 \pm 0.6% and 100.2 \pm 0.3% with RSDs between 0.26 and 1.0%, demonstrating the high validity of the method. The *ee* values found for the enantioenriched substances (*S*)-**5** and (*R*)-**5** were in very good accord with the *ee* values referred by the supplier (99.59% *ee* for (*S*)-**5** and 99.82% *ee* for (*R*)-**5**) and even slight changes in

the *ee* values effected by spiking experiments could be reliably quantified.

REFERENCES

1. Four different subtypes of membrane-bound GABA transport proteins are known, whereas their nomenclature is species-dependent. Murine subtypes were indicated as mGAT1–mGAT4 corresponding to hGAT-1, hBGT-1, hGAT-2, and hGAT-3 in humans, respectively. In the following, the nomenclature for the murine systems is employed.
2. Krosgaard-Larsen P, Falch E, Larsson OM, Schousboe A. GABA uptake inhibitors: relevance to antiepileptic drug research. *Epilepsy Res.* 1987;1:77–93.
3. Wein T, Petrer M, Allmendinger L, Höfner G, Pabel J, Wanner KT. Different binding modes of small and large binders of GAT1. *ChemMedChem.* 2016;11:509–518.
4. Kragler A, Höfner G, Wanner KT. Synthesis and biological evaluation of aminomethylphenol derivatives as inhibitors of the murine GABA transporters mGAT1–mGAT4. *Eur J Med Chem* 2008;43:2404–2411.
5. Pabel J, Faust M, Prehn C, et al. Development of an (S)-1-[2-[Tris(4-methoxyphenyl)-methoxy]ethyl]piperidine-3-carboxylic acid [(S)-SNAP-5114] carba analogue inhibitor for murine γ -aminobutyric acid transporter type 4. *ChemMedChem.* 2012;7:1245–1255.
6. Miyazawa T, Iwanaga H, Yamada T, Kuwata S. Resolution of cyclic imino acid and β -amino acid enantiomers by derivatization with 2,3,4,6-tetra-O-acetyl- β -D-glucopyranosyl isothiocyanate followed by reverse-phase HPLC analysis. *Anal Lett.* 1993;26:367–378.
7. Rustum AM, Menon G, Patel S. Separation of the S(+) and R(–)-enantiomers of tiagabine•HCl and its two chiral precursors by chiral chromatography: application to chiral inversion studies. *J Pharm Biomed Anal* 1998;17:1439–1447.
8. Valsborg JS, Foged C. Synthesis of (R) and (S) 14 C-labelled Ethyl Nipecotate, for preparation of GABA uptake ligands. *J Label Compd Radiopharm* 1997;39:401–407.
9. Rustum AM. Determination of chiral purity of ethyl nipecotate using Chiralcel-OG column. *J Chromatogr A.* 1995;696:75–81.
10. Pawlowska M, Chen S, Armstrong DW. Enantiomeric separation of fluorescent, 6-aminoquinolyl-N-hydroxysuccinimidyl carbamate, tagged amino acids. *J Chromatogr A.* 1993;641:257–265.
11. Chen S. The enantioseparation of amino acids on a teicoplanin chiral stationary phase using non-aqueous mobile phases after pre-column derivatization with sulfur-containing reagents: the considerations of mobile phase composition and analyte structure variation on resolution enhancement. *Biomed Chromatogr* 2006;20:718–728.
12. Hsiao YL, Chen S. LC Separation of enantiomers on silica-bonded thioester derivatives. *Chromatographia.* 2009;70:1031–1038.
13. McGachy NT, Grinberg N, Variankaval N. Thermodynamic study of N-trifluoroacetyl-O-alkyl nipecotic acid ester enantiomers on diluted permethylated β -cyclodextrin stationary phase. *J Chromatogr A.* 2005;1064:193–204.
14. Feng Z, Gollamudi R, Han G, Tang Y, Armstrong DW. Chiral separation of nipecotic acid amides. *J Chromatogr A.* 1992;609:187–193.
15. Snyder LR, Kirkland JJ, Dolan JW. Basic concepts and the control of separation. In: *Introduction to Modern Liquid Chromatography*. Hoboken, NJ: John Wiley & Sons; 2010:19–86.
16. Miyazawa T, Minowa H, Imagawa K, Yamada T. Separation of enantiomers of non-protein amino acids by high-performance liquid chromatography on a chiral ligand-exchange column. *Chromatographia.* 2004;60:45–50.
17. Pell R, Sić S, Lindner W. Mechanistic investigations of cinchona alkaloid-based zwitterionic chiral stationary phases. *J Chromatogr A.* 2012;1269:287–296.
18. Hoffmann CV, Pell R, Lämmerhofer M, Lindner W. Synergistic effects on enantioselectivity of zwitterionic chiral stationary phases for separation of chiral acids, bases, and amino acids by HPLC. *Anal Chem* 2008;80:8780–8789.
19. Zhang T, Holder E, Franco P, Lindner W. Zwitterionic chiral stationary phases based on cinchona and chiral sulfonic acids for the direct stereoselective separation of amino acids and other amphoteric compounds. *J Sep Sci* 2014;37:1237–1247.
20. Uchiyama S, Santa T, Okiyama N, Fukushima T, Imai K. Fluorogenic and fluorescent labeling reagents with a benzofurazan skeleton. *Biomed Chromatogr* 2001;15:295–318.
21. Jung ME, Dong TA, Cai X. Improved synthesis of 4-amino-7-nitrobenz-2,1,3-oxadiazoles using NBD fluoride (NBD-F). *Tetrahedron Lett* 2011;52:2533–2535.
22. Watanabe Y, Imai K. High-performance liquid chromatography and sensitive detection of amino acids derivatized with 7-fluoro-4-nitrobenzo-2-oxa-1,3-diazole. *Anal Biochem* 1981;116:471–472.
23. Imai K, Watanabe Y. Fluorimetric determination of secondary amino acids by 7-fluoro-4-nitrobenzo-2-oxa-1,3-diazole. *Anal Chim Acta* 1981;130:377–383.
24. Min JZ, Toyooka T, Kato M, Fukushima T. Synthesis of fluorescent label, DBD- β -proline, and the resolution efficiency for chiral amines by reversed-phase chromatography. *Biomed Chromatogr* 2005;19:43–50.

How to cite this article: Schmidt SK, Höfner G, Wanner KT. Determination of enantiomeric excess of nipecotic acid as 1-(7-nitrobenzo[c][1,2,5]oxadiazol-4-yl) derivatives. *Chirality* 2017;29:48–56. doi: 10.1002/chir.22670

3.2 Second Publication

Identification of Pyrrolidine-3-acetic Acid derived Oximes as Potent Inhibitors of γ -Aminobutyric Acid Transporter 1 through Library Screening with MS Binding Assays

3.2.1 Summary of the Results

In this study, the focus was set on the identification of prospective highly affine inhibitors for mGAT1 with a 2-(pyrrolidin-3-yl)acetic acid subunit by using LC-MS/MS binding assays. To obtain the desired oxime libraries an excess of a 2-(pyrrolidin-3-yl)acetic acid derivative with an aminoxy ethyl substituent attached to the amino nitrogen (40 mM) was incubated with 28 libraries each consisting of eight different aldehydes (1 mM each) in phosphate buffer pH 6.0 (12.5 mM Na₂HPO₄, 12.5 mM NaH₂PO₄, 1 M NaCl, pH value was adjusted with 1 M HCl) with 40 % DMSO at 37 °C for 20 h. The above mentioned hydroxylamine was applied as dihydrochloride to which two equivalents of sodium hydroxide was added to compensate the acid equivalents. In contrast to the previously published method, the number of aldehydes for generation of the libraries was doubled from four to eight while maintaining the concentration of the applied hydroxylamine derivative. The completion of the oxime formation under these modified conditions and within the set time frame was exemplarily proven by ¹H NMR studies. Except for aldehyde library 26, which contains three sterically highly encumbered tritylaldehydes instead of the common reaction (20 h at 37 °C) more forcing reaction conditions (45 h at 80 °C) had to be applied to accomplish oxime library formation.

After their formation, oxime libraries were diluted with phosphate buffer pH 7.1 (12.5 mM Na₂HPO₄, 12.5 mM NaH₂PO₄, 1 M NaCl, pH value was adjusted with 1 M NaOH) and were applied in the MS Binding Assay at three different concentration levels (1 μ M, 100 nM and 10 nM).

At the highest test concentration of 1 μ M all oxime libraries were able to reduce the specific binding of the marker NO711 below 50 % and still 15 libraries below 20 % revealing a high affinity of all libraries to the target at this concentration. When using 100 nM test concentration ten libraries reduced marker binding under 50 % and still four libraries under 20 % whereas at a concentration of 10 nM only one library could reduce the marker binding below 50 %. It was decided to choose the four libraries reducing specific marker binding below 20 % at a test concentration of 100 nM for the deconvolution experiments.

For deconvolution, single oximes of the mentioned libraries were generated individually under the same conditions as used for the library generation and after subsequent dilution to 100 nM studied for their binding affinities in MS Binding Assays. Eight oximes out of 32 analyzed ones were found to reduce marker binding below 50 % and were selected to be resynthesized in

order to determine their binding affinity (pK_i values) in full-scale competitive MS Binding Assays at mGAT1 and their inhibitory activity (pIC_{50} values) using [3H]GABA uptake assays at all four GABA transporter subtypes (mGAT1-4).

All oximes identified as most affine, were found to contain a 1,1'-biphenyl residue. Their pK_i values ranged from 6.97 up to 7.87 for mGAT1 and were in good accordance with the data obtained from library screening and deconvolution experiments. The compound with the highest affinity is characterized by a 2',4'-dichlorobiphenyl moiety and with a K_i values in the low nanomolare range ($pK_i = 7.87 \pm 0.01$). Furthermore, the pIC_{50} values determined in [3H]GABA uptake assays for mGAT1 were in accord with the high affinity and revealed high subtype selectivity of the tested oximes for mGAT1 as compared to mGAT2 – mGAT4 in the range of approximately one to almost three log units regarding pIC_{50} values. Hence, a set of new potent inhibitors of mGAT1 with a 2-(pyrrolidin-3-yl)acetic acid motif was identified again proving the concept of library screening by MS Binding Assays as a powerful tool in the drug discovery process.

3.2.2. Declaration of Contribution

Synthesis of the hydroxylamine derivative as a starting material for the oxime generation, all precursor molecules and the compounds for the biological testing as well as the evaluation of all corresponding analytical data were accomplished by myself. Some aldehydes were synthesized by Hans Brabec during his bachelor thesis "*Synthese neuer Aldehyde mit Biaryl-Struktur mittels Suzuki-Miyaura-Kupplung*" which was supervised by me and Tobias Hauke. NMR studies on the kinetics of the oxime formation and oxime exchange reaction were performed together with Dr. Lars Allmendinger and Claudia Glas. All binding experiments regarding library screening and deconvolution experiments were achieved and evaluated by me. pK_i values and pIC_{50} values were determined by the technical assistants Silke Duesing-Kropp and Miriam Sandner under the supervision of Dr. Georg Höfner. I wrote the manuscript and prepared all graphics and tables, supported by Dr. Lars Allmendinger. Prof. Dr. Klaus T. Wanner corrected the manuscript. The cover image resulted in collaboration with Dr. Jörg Pabel.



Identification of Pyrrolidine-3-acetic Acid Derived Oximes as Potent Inhibitors of γ -Aminobutyric Acid Transporter 1 through Library Screening with MS Binding Assays

Simone K. Huber, Georg Höfner, and Klaus T. Wanner^{*[a]}

In this study, pyrrolidine-3-acetic acid derived oxime libraries were applied to the concept of library screening by MS Binding Assays, as a powerful technique to reveal new potent murine γ -aminobutyric acid transporter subtype (mGAT1) inhibitors. Library generation was accomplished by condensation of an excess of pyrrolidine-3-acetic acid bearing a hydroxylamine unit with various libraries, each composed of eight different aldehydes. The oxime libraries have been screened by means of competitive MS Binding Assays and, as a conse-

quence, the most active libraries were further investigated through deconvolution experiments to identify single oximes responsible for the observed activity on the target mGAT1. All identified hits were finally resynthesized to characterize them with respect to their binding affinities, and a set of new potent inhibitors with the pyrrolidine-3-acetic acid motif were found, of which the most potent oxime, possessing a 2',4'-dichlorobiphenyl residue, displayed a binding affinity in the low nanomolar range ($pK_i = 7.87 \pm 0.01$).

Introduction

The number of people throughout the world affected by neurological disorders, such as epilepsy, Alzheimer's disease, dementia, Parkinson's disease, and depression, is increasing significantly.^[1] In 2006, the World Health Organization (WHO) drew attention to the importance of the burden of neurological disorders on public health.^[2] Hence, an understanding of the abovementioned disorders and the development of more potent medications with lower side effects are huge fields of interest for research. Low concentrations of γ -aminobutyric acid (GABA)—one of the major neurotransmitters in the mammalian central nervous system (CNS)^[3]—in the synaptic cleft have been identified as being associated with diseases such as epilepsy^[4] or Alzheimer's disease.^[5] One approach to enhance the level of GABA in the synaptic cleft is to block reuptake of the neurotransmitter in presynaptic neurons and glia cells through membrane-bound GABA transporters (GATs).^[6]

Four different subtypes of human GATs are known, which are named GAT1, BGT1, GAT2, and GAT3 according to the nomenclature suggested by the Human Genome Organization (HUGO).^[7] Because GAT1 and GAT3 are the only transporters present in the CNS in notable densities, of which GAT1 is mainly expressed in neurons and GAT3 predominantly located in glia cells,^[8] both subtypes are the key targets to address for the successful enhancement of the GABA level in the synaptic cleft. There-

by, GAT1, in particular, plays a key role that has been intensively investigated over the last few years. Differently, BGT1 and GAT2 are mainly expressed in the liver and kidney and are therefore not regarded as having a significant role in the termination of GABA signaling in the CNS.^[8,9] Because the GABA transporters used herein to characterize the biological activity of the target compounds, that is, their potency to inhibit GABA uptake at different GATs, are cloned from mice, the nomenclature for the GABA transporter subtypes of this species are applied hereafter, according to which murine GABA transporters are termed as mGAT1–mGAT4.^[10]

In the late 1960s, potent inhibitors for mGAT1 were discovered, such as (*R,S*)-nipecotic acid ((*R,S*)-**2**),^[11] guvacine (**3**),^[6] and (*R,S*)-pyrrolidine-3-acetic acid ((*R,S*)-**4**); Figure 1).^[12] Relative to the substrate GABA, with an pIC_{50} value at mGAT1 of 5.14 ± 0.09 ,^[13] compounds (*R,S*)-**2** and **3** are slightly less potent ((*R,S*)-

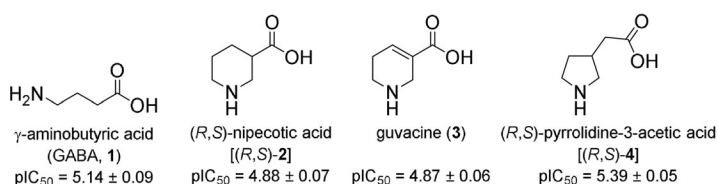


Figure 1. Structures of GABA and three different amino acids with high inhibitory potencies toward the GABA transporter mGAT1.

[a] S. K. Huber, Dr. G. Höfner, Prof. Dr. K. T. Wanner

Department of Pharmacy, Center of Drug Research, Ludwig Maximilians University of Munich, Butenandtstr. 7, 81377 Munich (Germany)
E-mail: klaus.wanner@cup.uni-muenchen.de

The ORCID identification number(s) for the author(s) of this article can be found under:
<https://doi.org/10.1002/cmdc.201800556>.

2: $pIC_{50} = 4.88 \pm 0.07$,^[14] **3**: $pIC_{50} = 4.87 \pm 0.06$ ^[15]), whereas (*R,S*)-**4** is at least equally potent toward mGAT1 ($pIC_{50} = 5.39 \pm 0.05$).^[16] For the sake of better comparability, these inhibitory potencies and the pIC_{50} values of all compounds shown in Figure 2, except for compound (*R,S*)-**8**, were determined by

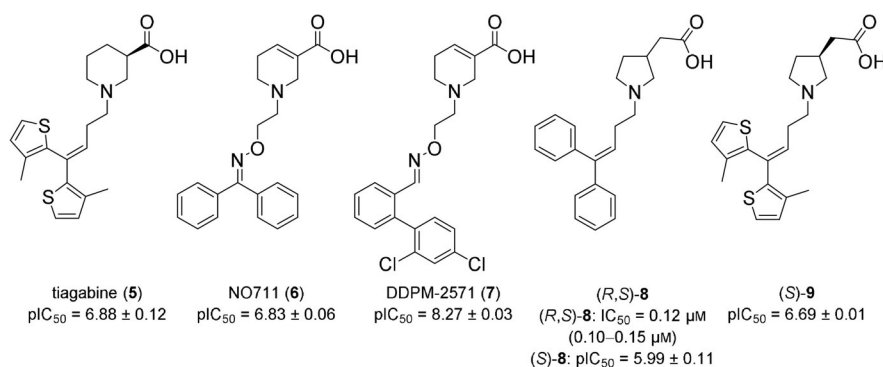


Figure 2. Inhibitors of mGAT1 based on different amino acid skeletons with lipophilic residues.

[³H]GABA uptake assays in our group by employing the same test system for all compounds.

However, the application of these potent inhibitors for mGAT1 as potential medications is limited because they are not able to cross the blood–brain barrier. Hence, inhibitors with more lipophilic character were developed over time; these are characterized by the presence of a biaryl moiety connected through an alkyl chain to the corresponding amino acid. Thus, not only the lipophilicity and brain penetration were raised, but also the inhibitory potency at mGAT1 rose by several orders of magnitude.

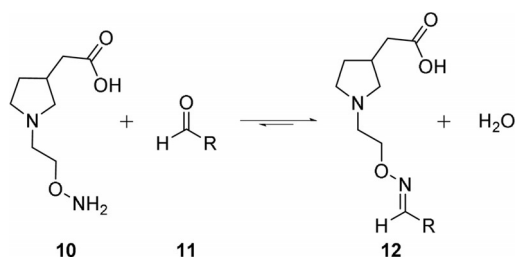
A prominent selective inhibitor of mGAT1 is the nipecotic acid derivative tiagabine (**5**), which is in clinical use ($pIC_{50} = 6.88 \pm 0.12$; Figure 2).^[15,17] Further examples with enhanced affinity toward mGAT1 are NO711^[18] and DDPM-2571,^[19] which are derived from **3** with an oxime functionality in the alkyl side chain (NO711: $pIC_{50} = 6.83 \pm 0.06$; DDPM-2571: $pIC_{50} = 8.27 \pm 0.03$; Figure 2). DDPM-2571 was found to be even more potent than **5** by almost 1.5 log units, and was applied recently in a set of in vivo studies that showed promising anxiolytic, antidepressant, and antinociceptive properties.^[20] Whereas various studies describe inhibitors of mGAT1 with nipecotic acid and guvacine substructures, only a few are known concerning mGAT1 inhibitors derived from pyrrolidine-3-acetic acid (**4**). Nevertheless, the preparations of miscellaneous pyrrolidine-3-acetic acid derivatives containing different lipophilic residues linked by alkyl, alkenyl, or alkynyl chains to the pyrrolidine nitrogen have been reported since the late 1980s; most examples are provided by a patent,^[21] but the pharmacological characterizations at GABA transporters are rather limited.^[15,22] One example is the racemic *N*-(4,4-diphenylbut-3-en-1-yl) derivative of pyrrolidine-3-acetic acid, (*R,S*)-**8**, and its enantiomer, (*S*)-**8**, which were found to be potent and selective GABA uptake inhibitors of a GABA transporter corresponding to mGAT1 in the case of (*R,S*)-**8** and mGAT1 for (*S*)-**8** ((*R,S*)-**8**: $IC_{50} = 0.12$ (0.10–0.15) μM determined on rat brain tissue, which is known to preferentially contain the rGAT subtype 1;^[22] (*S*)-**8**: $pIC_{50} = 5.99 \pm 0.11$;^[15] Figure 2). Additionally, (*S*)-pyrrolidine-3-acetic acid containing a 4,4-bis(3-methylthiophen-2-yl)but-3-en-1-yl residue, ((*S*)-**9**), was recently examined for its activity at mGAT1, and showed also a high inhibitory potency ((*S*)-**9**: $pIC_{50} = 6.69 \pm 0.01$, Figure 2), whereby the pIC_{50} value of tiaga-

bine-like derivative (*S*)-**9** is only slightly lower than that of **5** itself.^[15] Thus, substances with a pyrrolidine-3-acetic acid motif are interesting and promising scaffolds for new inhibitors of mGAT1.

Within this study, the main focus was set on the examination of lipophilic *N*-substituents carrying pyrrolidine-3-acetic acids as possible high-affinity inhibitors of mGAT1. To gain access to a broad range of structures with many different lipophilic moieties for structure–activity relationships regarding the inhibitory activity of pyrrolidine-3-acetic acid derivatives toward the target mGAT1, we decided to use the combinatorial screening concept previously published by our group.^[23] This concept is based on a simple condensation reaction of the respective amino acid scaffold through a hydroxylamine function with different aldehydes to generate oxime libraries,^[19] which are subsequently investigated with a competitive LC–MS/MS Binding Assay.^[24] With NO711 as a native marker,^[24] the LC–MS/MS Binding Assay allows the indirect determination of binding affinities of the applied competitors.^[23] This concept is exemplified in the screening of pseudostatic hydrazone libraries^[23] and stable oxime libraries;^[19] both address the target mGAT1. It was shown that the generation of libraries could be performed in the presence of the target simultaneously generating the library upon incubation with the protein, as in the case of hydrazone libraries,^[23] or in two separate steps in which the conditions of library formation are not tolerated by the target, as first implemented with oxime libraries.^[19]

For the study of pyrrolidine-3-acetic acid containing inhibitors, we focused on the identification of stable libraries with the oxime functionality due to their higher hydrolytic stability^[25] over that of the hydrazone moiety. One additional reason to focus on stable oximes is that some highly potent inhibitors containing this function are already known (e.g., NO711 and DDPM-2571; Figure 2); this indicates that the oxime functionality can undergo positive interactions with the mGAT1 protein, which might increase the chances of identifying new active mGAT1 inhibitors. Consequently, we focused on stable oxime libraries with general structure **12** (Scheme 1).

Because oxime formation is known to be very slow under physiological conditions, it was clear that this would require the generation of libraries separately from the screening experiments. Hence, the formation of oxime libraries should be



Scheme 1. Condensation reaction of hydroxylamine derivative **10** with various aldehydes **11** to yield the corresponding oximes **12**.

accomplished by reacting the pyrrolidine-3-acetic acid as a hydroxylamine derivative, **10**, with different aldehydes, **11**, as outlined in Scheme 1.

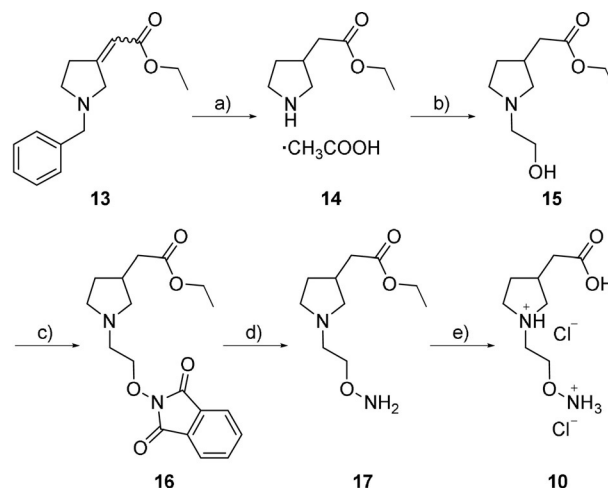
Differently to the previously reported concept,^[19] the number of aldehydes **11** in one library was intended to be doubled from four to eight to increase the throughput of the screening concept. Additionally, the number of aldehyde libraries should be increased to improve the chances of finding potent inhibitors with new substitution patterns. To realize the designated modifications, the suitability of the experimental conditions used in a recently described study for library generation had to be adapted for the use of the new hydroxylamine **10**.^[19] Also, the stability of the generated oximes had to be ensured over the incubation time. The most potent libraries identified in the screening experiments should be tested in deconvolution experiments to examine which single oximes were responsible for the affinity of the library. Subsequently, the identified single oximes should be resynthesized to determine their binding affinities (pK_i values) in full-scale competitive MS Binding Assays,^[24] and their inhibitory activities (pIC_{50} values) through [³H]GABA uptake assays,^[18] to find the most active inhibitors for mGAT1 originating from the respective set of aldehydes. Finally, all identified hits should be characterized with regard to their inhibitory potencies at all four murine GABA transporters to determine their subtype selectivity.

Results and Discussion

Chemistry

Synthesis of hydroxylamine **10**

The desired hydroxylamine **10** was synthesized by using the synthetic pathway outlined in Scheme 2. First, an *E/Z* mixture of **13**^[26] (*E/Z* ratio = 1:1) was treated with hydrogen in the presence of Pd/C for the hydrogenation of the C–C double bond and simultaneous deprotection of the benzyl group to yield pyrrolidine-3-acetic acid as acetate salt **14** (97% yield). Conversion of **14** into hydroxyethyl derivative **15** (83% yield) upon reaction with 2-bromoethanol, followed by a Mitsunobu reaction with *N*-hydroxyphthalimide as a nucleophile in the presence of DMEAD at room temperature for 20 h, yielded the corresponding *N*-hydroxyphthalimide derivative **16**. Purification of **16** was accomplished by flash

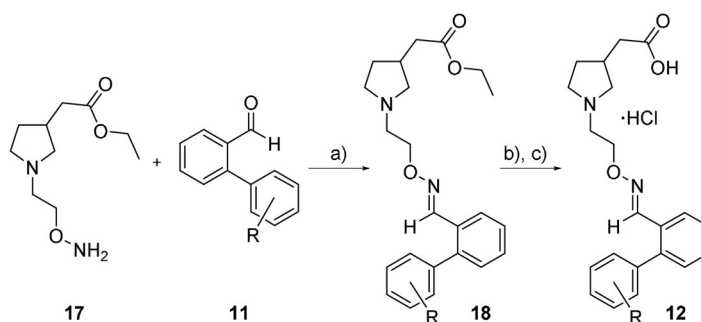


Scheme 2. Synthesis of 2-[(2-aminooxy)ethyl]pyrrolidine-3-yl]acetic acid dihydrochloride **10**: a) H₂, Pd/C, AcOH, EtOH, 50 bar, 24 h, RT, 97%; b) 2-bromoethanol, K₂CO₃, KI, THF, 24 h, reflux, 83%; c) *N*-hydroxyphthalimide, PPh₃, di-2-methoxyethyl azodicarboxylate (DMEAD), THF, 20 h, RT, 90%; d) hydrazine (50–60% solution), EtOH, 2 h, RT, 96%; e) aqueous solution of HCl (1 M), 3 h, 90 °C, 87%.

column chromatography on silica gel pre-dried at 145 °C in vacuo for 5 h. Thus, the hydrolytic instability of **16** observed during flash column chromatography with regular silica gel could be overcome. Subsequent hydrazinolysis with an aqueous hydrazine solution of **16** afforded hydroxylamine **17** in very good yield (96%). Finally, the ethyl ester was hydrolyzed by using hydrochloric acid (1 M) to afford **10**. The salt form of **10** was deduced from the results of elemental analysis performed for **10**.

Synthesis of oximes **12**

For the determination of pK_i and pIC_{50} values of the hit compounds found through the screening process described below, the individual oximes were synthesized as outlined in Scheme 3. Following a previously reported method, a hydroxylamine functionality containing a pyrrolidine-3-acetic acid derivative was reacted, such as ethyl ester **17**, with aldehydes **11** in equimolar concentrations to yield the oxime esters **18** as *E/Z* mixtures, of which the *Z* isomer is the minor isomer (1–7%, rel-



Scheme 3. Synthesis of oximes **12**: a) absolute EtOH, RT, 18 h, 48–90%; b) aqueous solution of NaOH (2 M), EtOH, RT, 24 h; c) aqueous solution of HCl (2 M) then CH₂Cl₂, 41–94% (over two steps).^[19,27]

ative to the *E* isomer).^[19] Flash column chromatography of the *E/Z* mixture yielded the pure *E* form of esters (*E*)-**18**. After subsequent cleavage of the ester function with an aqueous solution of NaOH (2 M) in EtOH, acidification with an aqueous solution of HCl (2 M), and extraction with dichloromethane, the hydrochloric acid salts, **12**, of the desired oximes were obtained.^[27]

Aldehydes 11

The required aldehydes were purchased from Sigma Aldrich (Steinheim, Germany), TCI (Zwijndrecht, Belgium), Acros (Geel, Belgium), or ABCR (Karlsruhe, Germany) and used without further purification, or synthesized through Suzuki–Miyaura cou-

pling according to a method published previously.^[28,29] The set of aldehydes used for oxime generation and screening is given in Figure 3.

Library generation

Twenty-eight different aldehyde libraries were applied in the screening, each consisting of eight aldehydes (Figure 3). For broad structural variation, libraries contained aldehydes differing with respect to their gross structure, substituents, and substitution patterns; major classes represent aromatic (e.g., in libraries 6, 7, 8, 9, 16), heteroaromatic (e.g., in libraries 1, 3, 10, 13, 24, 25, 28), and arylaliphatic aldehydes (e.g., in libraries 15, 18, 26).

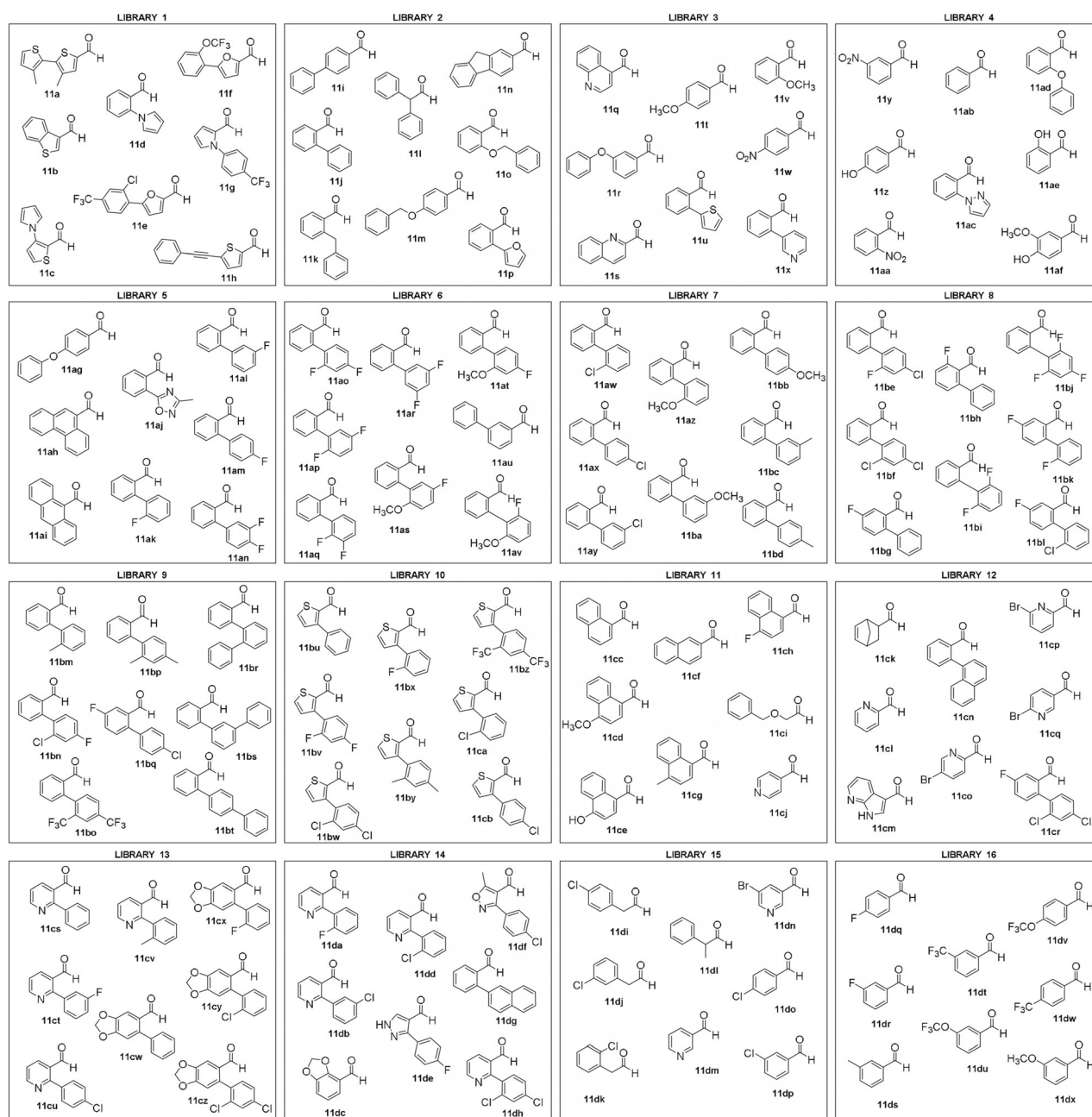


Figure 3. Aldehyde libraries 1–28 applied within the screening experiments.

Analogously to the previously published method for the MS Binding Assay based on screening of oxime libraries derived from **3**,^[19] we pre-generated the oximes in the absence of the target mGAT1 by treating each library of aldehydes (1 mM each) with an excess of the pyrrolidine-3-acetic acid containing a hydroxylamine function (40 mM) at 37 °C in phosphate buffer (pH 6.0, 12.5 mM Na₂HPO₄, 12.5 mM NaH₂PO₄, 1 M NaCl, pH value was adjusted with 1 M HCl) with a high DMSO concentration, 40%, to guarantee the solubility of all reactants.

Different from the previously described protocol, hydroxylamine **10** was applied as the dihydrochloride. To compensate for the two additional equivalents of acid introduced with **10**, two equivalents of sodium hydroxide were added to the phosphate buffer (pH 6.0) used for the incubation system. With this modification, decomposition of the free form of **10**, the preparation of which required ion-exchange chromatography with an aqueous solution of ammonia for elution, could be avoided.

Moreover, the number of aldehydes contained in one library was doubled from four to eight to increase the throughput, and hence, efficiency of the assay (Scheme 4). However, upon increasing the number of aldehydes, and thereby, maintaining a concentration of 1 mM for each aldehyde, the 10-fold excess of hydroxylamine used in the original screening protocol is re-

duced to 5-fold. ¹H NMR spectroscopy studies with reaction mixtures, by applying a reactant ratio of 1:5, confirmed that oxime formation under the newly chosen conditions was achieved within 20 h, except for library 26. For this library, containing the three sterically highly demanding tritylaldehydes **11gw**, **11gy** and **11gz**, ¹H NMR spectroscopy studies showed that these compounds could not be converted into the corresponding oximes within the original reaction time, 20 h, at 37 °C. Hence, for library 26, the abovementioned procedure for oxime generation had to be adjusted. If the components were allowed to react at an elevated temperature of 80 °C, leaving the buffer system (phosphate buffer with pH 6.0, 40% DMSO) and concentration levels of the aldehydes (1 mM each aldehyde) and hydroxylamine (40 mM) unchanged, the formation of oximes in library 26 was complete within 45 h, as revealed by monitoring the reaction through ¹H NMR spectroscopy.

Before use in the screening process, all formed oxime libraries had to be diluted with phosphate buffer (pH 7.1, 12.5 mM Na₂HPO₄, 12.5 mM NaH₂PO₄, 1 M NaCl, pH value was adjusted with 1 M NaOH) to the required test concentrations (1 μM, 100 nM, and 10 nM in the assay for each oxime), thereby warranting that the concentration of DMSO in the incubation mixture with the target mGAT1 at 37 °C did not exceed 1%. The

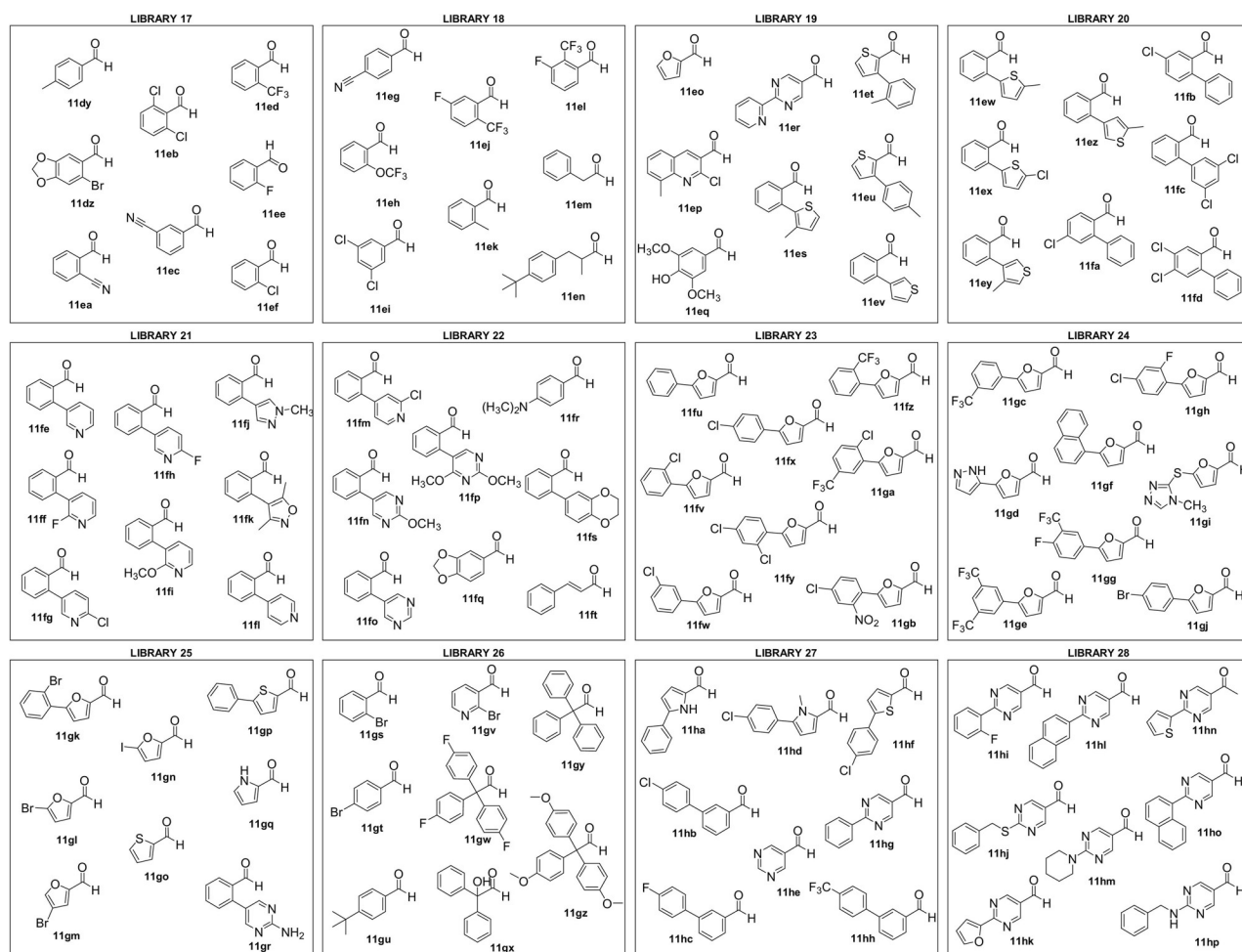
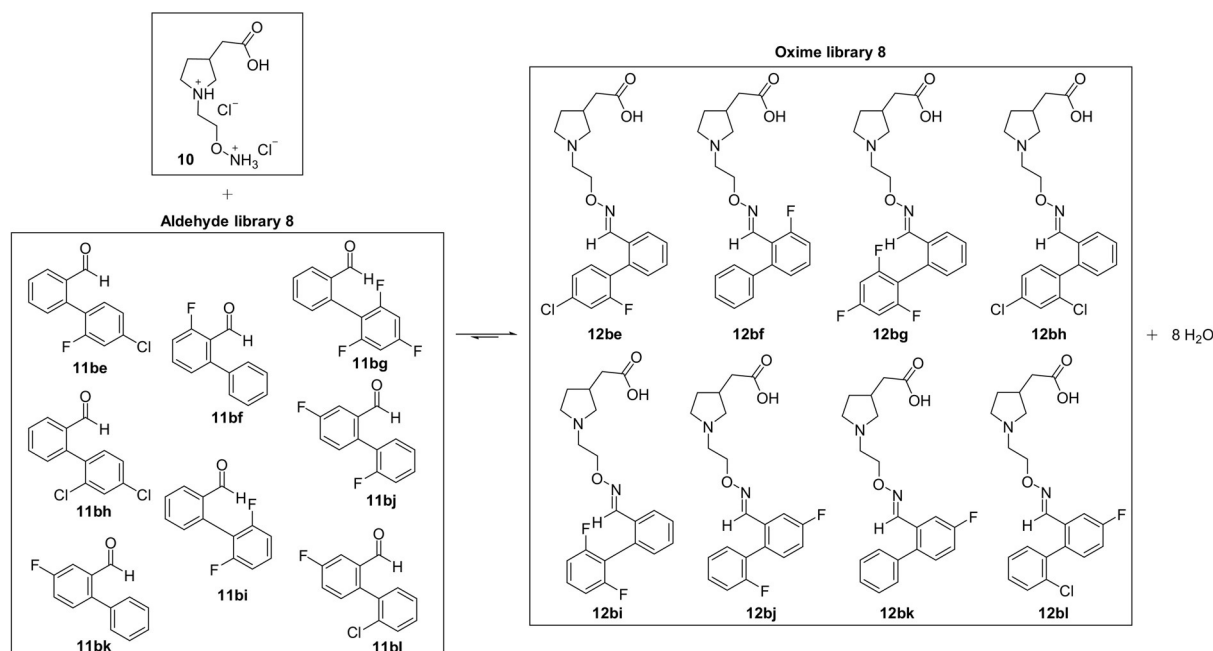


Figure 3a continued.



Scheme 4. Reaction of hydroxylamine derivative **10** with eight different aldehydes to yield corresponding oxime library **8**.

stability of the oximes in the diluted mixture was verified through fluorescence spectroscopy measurements performed immediately after the dilution step. Fluorescence measurements had the advantage that they could be rendered selective for the oxime derivatives by choosing the appropriate excitation and emission wavelengths. All applied oximes were stable for the incubation time of 4 h because the fluorescence signal remained unchanged. Additionally, an oxime exchange experiment monitored by means of ^1H NMR spectroscopy was performed. For this experiment, two equivalents of aldehyde **11t** (2 equiv, 2 mM) were added to separately prepared oxime **12ao** (1 mM), the mixture was diluted with phosphate buffer (pH 7.1; 12.5 mM Na_2HPO_4 , 12.5 mM NaH_2PO_4 , 1 M NaCl, 10% D_2O , 1% [D₆]DMSO), kept at 37 °C in an NMR tube, and subjected to ^1H NMR spectroscopy measurements every 4 h for a total of 64 h (see the Experimental Section for details). Within this period of time, the ^1H NMR spectra remained unchanged, which indicated that oxime **12ao** was stable in the presence of free aldehyde **11t** because no exchange reaction occurred.

Library screening

The affinity of the libraries was determined in competitive MS binding experiments for mGAT1 with NO711 as a reporter ligand. Experiments were performed at single points, that is, the concentrations of the test compounds were set as limits for minimal affinities. These screening experiments were performed as follows: after dilution of the generated oxime libraries to three different test concentration levels, namely, 1 μM (1st experiment), 100 nM (2nd experiment), and 10 nM (3rd experiment) with phosphate buffer (pH 7.1), the libraries were incubated with the target protein, mGAT1 (10–20 μg protein per sample in 250 μL), and the MS marker, NO711 (20 nM in the

assay), for 4 h at 37 °C in a shaking water bath. Then the protein–ligand complexes were separated by filtration, denatured by drying at 50 °C for 1 h, and finally eluted with MeOH. The amount of formerly bound, and now liberated, marker NO711 was quantified by means of LC–MS/MS (ESI). This amount of marker was indicative of the affinity of the oxime libraries. Low amounts of marker binding indicated high affinity of the oxime library, which could possibly arise from a single compound. All libraries were examined at three different concentration levels (1 μM , 100 nM, and 10 nM) to ensure a reliable differentiation of the affinity of the libraries, of which many appeared potent at the highest test concentration (1 μM).

Control experiments in which only the aldehyde libraries, without prior incubation with hydroxylamine **10** for the formation of the oximes, were applied to examine the potential inhibitory activity of the aldehydes themselves showed that they did not have a significantly impact on marker binding; NO711 binding ranged from 82 to 100% (aldehyde concentration 1 μM ; Table 1). In addition, different concentration levels of hydroxylamine **10** were screened to determine its affinity to the target because, even after full conversion toward the oximes, a high concentration of hydroxylamine, 32 mM, remained in the sample solution. After dilution of the oximes to the desired concentration for the screening experiments, the remaining hydroxylamine concentrations were still 32 μM (oxime concentration 1 μM), 3.2 μM (oxime concentration 100 nM), and 320 nM (oxime concentration 10 nM), respectively.

Fortunately, hydroxylamine **10** effected marker binding only at concentrations above 40 μM to a significant extent (400 μM : $79 \pm 3\%$; 4 mM: $37 \pm 1\%$; Figure 4). At the concentration levels prevalent in the assay, almost no reduction of marker binding could be found (40 μM : $93 \pm 2\%$; 4 μM : $93 \pm 1\%$, 400 nM: $95 \pm 2\%$; Figure 4). Accordingly, free hydroxylamine **10** will not in-

Table 1. Results of the screening of aldehyde and oxime libraries.

Library	Specific NO711 binding [%] ^[a]			
	Aldehyde library 1 μ M	1 μ M	Oxime library 100 nM	10 nM
1	95 \pm 1	22 \pm 1	74 \pm 7	91 \pm 6
2	93 \pm 1	8 \pm 1	30 \pm 2	81 \pm 2
3	93 \pm 3	17 \pm 1	66 \pm 4	89 \pm 4
4	96 \pm 2	34 \pm 3	69 \pm 8	95 \pm 7
5	82 \pm 1	7 \pm 1	31 \pm 2	85 \pm 6
6	96 \pm 3	2 \pm 1	21 \pm 2	84 \pm 6
7	94 \pm 2	2 \pm 1	18 \pm 2	80 \pm 6
8	91 \pm 1	< LLOQ ^[b]	6 \pm 1	44 \pm 4
9	97 \pm 4	< LLOQ ^[b]	11 \pm 1	57 \pm 3
10	97 \pm 4	6 \pm 1	41 \pm 6	99 \pm 1
11	99 \pm 2	33 \pm 1	80 \pm 4	87 \pm 6
12	99 \pm 1	2 \pm 1	33 \pm 4	89 \pm 3
13	93 \pm 4	11 \pm 1	55 \pm 2	91 \pm 3
14	100 \pm 2	2 \pm 1	29 \pm 1	90 \pm 3
15	96 \pm 5	17 \pm 2	65 \pm 5	94 \pm 6
16	95 \pm 1	48 \pm 6	73 \pm 1	85 \pm 2
17	93 \pm 7	28 \pm 3	65 \pm 3	87 \pm 4
18	88 \pm 7	44 \pm 5	72 \pm 5	100 \pm 5
19	96 \pm 7	7 \pm 1	54 \pm 2	92 \pm 5
20	94 \pm 2	2 \pm 1	32 \pm 1	70 \pm 3
21	89 \pm 4	27 \pm 3	97 \pm 3	98 \pm 3
22	95 \pm 3	45 \pm 4	82 \pm 6	90 \pm 6
23	87 \pm 3	20 \pm 1	76 \pm 3	93 \pm 4
24	99 \pm 3	27 \pm 1	88 \pm 2	94 \pm 3
25	92 \pm 6	43 \pm 5	77 \pm 4	92 \pm 2
26	88 \pm 1	28 \pm 3	59 \pm 2	89 \pm 6
27	91 \pm 7	32 \pm 3	71 \pm 1	90 \pm 6
28	83 \pm 5	41 \pm 2	80 \pm 4	94 \pm 7

[a] Percentage of remaining bound NO711; data represent the mean \pm standard deviation (SD) of $n=4$ experiments. [b] Level of quantified MS marker NO711 is below the lower limit of quantification (LLOQ) of 50 pM.

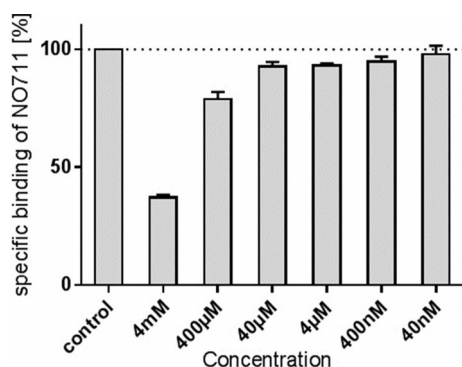


Figure 4. Control experiment applying single hydroxylamine **10** in six different concentration levels. Percentage of remaining specific bound NO711; data represent the mean \pm standard deviation (SD) of $n=4$ experiments. Control represents the specific binding of NO711 in the absence of hydroxylamine.

terfere with marker binding in the screening experiments to any reasonable extent.

The first series of screening experiments, applying the generated oxime libraries containing each oxime at a concentration of 1 μ M in the assay, revealed that all libraries reduced the specific binding of NO711 below 50%, and for 15 libraries it

was below 20% (libraries 2, 3, 5–10, 12–15, 19, 20, and 23; Table 1). Because at a test concentration of 1 μ M the affinity of all tested libraries was quite high, we decided to study the libraries at a concentration of 100 nM and furthermore at 10 nM. Whereas at a test concentration of 10 nM, only one library was left reducing the marker binding below 50% (library 8; Table 1), a distinctly broader, and hence, more useful differentiation of library affinity occurred at a test concentration of 100 nM. In this case, 10 libraries reduced the marker binding to below 50% and was even below 20% for 4 libraries (libraries 6–9; Table 1), which corresponded to an IC_{50} value of 25 nM if the affinity was due to a single library component. With four libraries reaching this limit (20% marker binding at 100 nM test concentration), the decision was made to take only these four libraries forward to the next step: the deconvolution experiments.

Deconvolution experiments

To identify the oximes responsible for reduced marker binding in each of the four most potent libraries identified, single oximes were generated by reacting the respective aldehyde (1 mM) with a large excess of hydroxylamine (40 mM) under conditions identical to those of the library screening experiments (phosphate buffer at pH 6.0 with 40% DMSO, 37 °C, 20 h). Subsequent dilution of the deconvolution samples to 100 nM and analysis of these samples by means of LC-MS/MS Binding Assays, with NO711 as a marker, provided the following results, which are summarized in Table 2. Also, the corresponding aldehydes alone without hydroxylamine were tested, and once more no significant effect on marker binding could be found for any of these compounds (83–101%; Table 2).

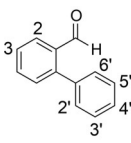
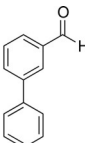
Of the 32 oximes studied, 8 oximes were found to reduce marker binding below 50% (**12ao**, **12av**, **12aw**, **12ax**, **12be**, **12bf**, **12bj**, and **12bn**; Table 2, entries 1, 8, 9, 10, 17, 18, 22, and 26), according to which results they could be expected to possess a high affinity, with an IC_{50} value at or below 100 nM.

One of these oximes was even capable of reducing MS marker binding below 20% (**12bf** of library 8, 10 \pm 1%; Table 2, entry 18); in which case, the affinity should even reach an IC_{50} value below 25 nM. The aforementioned compounds were chosen for resynthesis to determine their pK_i values in full-scale competitive MS Binding Assays.^[24]

Structure–activity relationships

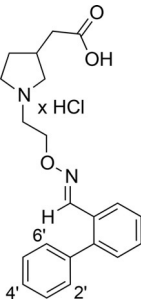
Next, all eight oximes (**12ao**, **12av**, **12aw**, **12ax**, **12be**, **12bf**, **12bj**, **12bn**) that were able to reduce the specific binding of NO711 to below 50% at a test concentration of 100 nM, and hence, classified as hits, were subsequently resynthesized to determine their binding affinities (pK_i values) in full-scale MS Binding Assays and their inhibitory potencies (pIC_{50} values) in [3 H]GABA uptake assays. The resynthesized oximes yielded pK_i values from 6.97 to 7.87 (Table 3). All determined pK_i values were in good accordance with the data obtained by library and deconvolution experiments because, for example, oxime **12bf**, with the lowest value for the remaining bound NO711 of

Table 2. Results of the deconvolution experiments for libraries 6, 7, 8, and 9 at a concentration of 100 nM.

<div><div></div><div></div></div> <div>11ao–at, 11av–az 11ba–bt11au</div>							
Entry	Compound (substitution pattern)	Specific NO711 binding [%] Aldehyde 11 ^[a] Oxime 12 ^[b]		Entry	Compound (substitution pattern)	Specific NO711 binding [%] Aldehyde 11 ^[a] Oxime 12 ^[b]	
library 6				library 7			
1	ao (2'-F,4'-F)	95 ± 6	46 ± 1	9	aw (2'-Cl)	98 ± 1	48 ± 6
2	ap (2'-F,5'-F)	97 ± 4	95 ± 1	10	ax (4'-Cl)	96 ± 2	45 ± 3
3	aq (2'-F,3'-F)	89 ± 6	72 ± 5	11	ay (3'-Cl)	95 ± 5	81 ± 8
4	ar (3'-F,5'-F)	92 ± 5	94 ± 2	12	az (2'-OMe)	86 ± 4	75 ± 2
5	as (2'-OMe,5'-F)	95 ± 5	93 ± 4	13	ba (3'-OMe)	95 ± 4	74 ± 7
6	at (2'-OMe,4'-F)	85 ± 5	61 ± 6	14	bb (4'-OMe)	91 ± 7	76 ± 1
7	au	93 ± 5	94 ± 4	15	bc (3'-Me)	89 ± 3	82 ± 4
8	av (2'-OMe,6'-F)	95 ± 5	44 ± 2	16	bd (4'-Me)	97 ± 7	61 ± 3
library 8				library 9			
17	be (2'-F,4'-Cl)	100 ± 1	33 ± 4	25	bm (2'-Me)	94 ± 4	65 ± 5
18	bf (2'-Cl,4'-Cl)	101 ± 2	10 ± 1	26	bn (2'-Cl,4'-F)	92 ± 2	30 ± 2
19	bg (3-F)	90 ± 6	67 ± 3	27	bo (2'-CF ₃ ,4'-CF ₃)	90 ± 2	86 ± 6
20	bh (2-F)	98 ± 3	70 ± 2	28	bp (2'-Me,4'-Me)	93 ± 4	66 ± 5
21	bi (2'-F,6'-F)	83 ± 1	60 ± 4	29	bq (3-F,4'-Cl)	94 ± 6	57 ± 4
22	bj (2'-F,4'-F,6'-F)	98 ± 5	43 ± 1	30	br (2'-Ph)	90 ± 6	78 ± 5
23	bk (3-F,2'-F)	98 ± 2	57 ± 3	31	bs (3'-Ph)	93 ± 5	76 ± 3
24	bl (3-F,2'-Cl)	100 ± 2	59 ± 2	32	bt (4'-Ph)	92 ± 5	89 ± 3

[a] Percentage of remaining bound NO711 in the presence of pure aldehyde at 100 nM; data represent the mean ± SD of *n* = 4 experiments. [b] Percentage of remaining bound NO711 in the presence of generated oxime in the deconvolution experiment with the respective aldehyde at 100 nM; data represent the mean ± SD of *n* = 4 experiments.

Table 3. Binding affinities (*pK_i*) from the competitive MS Binding Assay and inhibitory potencies (*pIC₅₀*) from [³H]GABA uptake experiments determined for synthesized oximes with different substitution patterns.

<div></div>							
Entry	Compound (substitution pattern) ^[a]	<i>pK_i</i> ^[b]	mGAT1	mGAT2	<i>pIC</i> ₅₀ ^[c]	mGAT3	mGAT4
1	12 ao (2'-F,4'-F)	7.31 ± 0.03	6.60 ± 0.08	73 %		82 %	85 %
2	12 av (2'-OMe,6'-F)	7.12 ± 0.03	6.57 ± 0.05	100 %		88 %	89 %
3	12 aw (2'-Cl)	7.07 ± 0.04	6.41 ± 0.08	77 %		76 %	72 %
4	12 ax (4'-Cl)	6.97 ± 0.04	6.29 ± 0.07	4.87		73 %	4.63
5	12 be (2'-F,4'-Cl)	7.13 ± 0.11	6.63 ± 0.12	4.07		64 %	4.49
6	12 bf (2'-Cl,4'-Cl)	7.87 ± 0.01	7.33 ± 0.05	4.44		4.08	4.27
7	12 bj (2'-F,4'-F,6'-F)	7.23 ± 0.03	6.55 ± 0.06	89 %		82 %	58 %
8	12 bn (2'-Cl,4'-F)	7.57 ± 0.08	7.06 ± 0.12	71 %		77 %	61 %

[a] Individually synthesized oximes (see the Experimental Section). [b] Data points for specific binding of NO711 on mGAT1 (mean ± SD, *n* = 3) in the presence of different concentrations of test compound resulted in binding curves for *K_i* determination by means of nonlinear regression. *pK_i* values represent the mean ± standard error of the mean (SEM) of three independent experiments, each performed in triplicate. [c] *pIC₅₀* values from [³H]GABA uptake assay performed with murine GABA transporter expressing HEK cells. The values represent the mean ± SEM of three (mGAT1) or one (mGAT2-4) independent experiments, each performed in triplicate. Percentage values represent remaining [³H]GABA uptake in the presence of 100 μM test compound.

$10 \pm 1\%$ (Table 2, entry 18), showed the highest pK_i value of 7.87 ± 0.01 (Table 3, entry 6) that could be determined under these conditions.

Notably, all hits contain a 1,1'-biphenyl moiety, which was derived from 1,1'-biphenyl-2-carbaldehyde with substituents at the terminal phenyl ring. The unsubstituted 1,1'-biphenyl derivative, **12j**, from library 2 was additionally applied as a single substance in the deconvolution experiments ($70 \pm 2\%$ remaining bound NO711). According to a comparison of the value observed for the regioisomeric unsubstituted biphenyl-3-carbaldehyde-derived oxime, **12au** ($94 \pm 4\%$; Table 2, entry 7), the substitution pattern of the latter compound leads to a reduced affinity toward mGAT1.

The substitution pattern of the hits can be divided into four main groups of which all members show rather high affinity toward mGAT1: oximes derived from biphenyl-2-carbaldehydes containing only chlorine (**12aw**, **12ax**, **12bf**; Table 2, entries 9, 10, and 18), oximes containing only fluorine (**12ao**, **12bj**; Table 2, entries 1 and 22), oximes containing both fluorine and chlorine substituents (**12be**, **12bn**; Table 2, entries 17 and 26), and one oxime containing a methoxy and a fluorine residue (**12av**; Table 2, entry 8). Oximes with different substituents, such as methyl groups (e.g., monosubstituted: **12bc**, **12bd**, **12bm**; disubstituted: **12bp**; Table 2, entries 15, 16, 25, and 28), trifluoromethyl groups (e.g., **12bo**; Table 2, entry 27), or additional phenyl groups (e.g., **12br**, **12bs**, **12bt**; Table 2, entries 30–32) showed a diminished binding affinity.

Among the oximes with a single chlorine substituent, the 3'-chloro-substituted oxime, **12ay** ($81 \pm 8\%$; Table 2, entry 11), represents the compound with the lowest affinity and does not reach the limit of 50% in the deconvolution experiments. For the *ortho*- and *para*-substituted derivatives, the affinity is distinctly higher and roughly the same for both compounds; pK_i value for the 2'-substituted oxime, **12aw**, is 7.07 ± 0.04 and for the 4'-substituted oxime, **12ax**, is 6.97 ± 0.04 (Table 3, entries 3 and 4). In comparison, for oxime **12bl**, which also has a 2'-chloro substituent in the second phenyl moiety, for example, **12aw**, but an additional fluoro substituent in the 3-position of the first ring, the affinity to target mGAT1 is distinctly diminished ($59 \pm 2\%$; Table 2, entry 24). The same trend, a reduced binding affinity, is also found for oxime **12bq** with 3-fluoro- and 4'-chloro substituents ($57 \pm 4\%$; Table 2, entry 29), relative to that of **12ax** with only a 4'-chloro substituent. Accordingly, *ortho* or *para* substitution in the second phenyl ring is favorable and additional 3-substitution in the first phenyl ring leads to a decrease in affinity.

If two chloro substituents are present in the terminal ring in the 2'- and 4'-positions, a significant increase in the binding affinity, by almost one log unit, results ($pK_i = 7.87 \pm 0.01$; Table 3, entry 6). The 2',4'-dichloro-substituted oxime, **12bf**, represents the oxime with the best binding affinity of all compounds studied. If, however, the first phenyl ring of the 2',4'-dichloro-substituted oxime, **12bf**, is replaced, for example, by a thiophene (**12bw**, library 10; Table 1), pyridine (**12dh**, library 14; Table 1), or a furan ring (**12fy**, library 23; Table 1), the mGAT1 affinity must have lowered because none of the libraries containing those oximes were able to reduce the specific NO711

binding under the limit of 20% to be selected for further experiments (see Table 1).

By replacing monochloro- by monofluoro-substituted compounds at the terminal ring, the negative effect on affinity is apparent because library 5, containing monofluoro-substituted oximes in the 2'-, 3'-, and 4'-positions (**12ak**, **12al**, and **12am**, respectively), is not able to decrease the remaining specific binding of NO711 to below 20% at the test concentration of 100 nM ($31 \pm 2\%$; Table 1, entry 5), and thus, it was not examined in the deconvolution experiments. A similar negative effect could be observed for oximes monosubstituted at the terminal ring with a methoxy residue. All three oximes **12az**, **12ba**, and **12bb**, with methoxy functions in the 2'-, 3'-, and 4'-positions, respectively, lead to a similar weak reduction of specific NO711 binding (at 100 nM marker concentration) to approximately 75% (Table 2, entries 12–14).

All oximes containing fluorine that reached the limit of below 50% in the deconvolution experiments carry one or two additional substituents in the terminal biphenyl subunit. Among the difluoro-substituted compounds, the 2',4'-substituted oxime, **12ao** ($pK_i = 7.31 \pm 0.03$; Table 3, entry 1), was the most active oxime, and the 2',6'-disubstituted oxime, **12bi**, could almost reach the 50% limit ($60 \pm 4\%$; Table 2, entry 21). For the 2',4',6'-trifluoro-substituted oxime, **12bj**, with an additional 6'-fluoro substituent compared with **12ao**, the pK_i value of 7.23 ± 0.03 (Table 3, entry 7) is only slightly lower than the value of **12ao**. Oximes with a second fluoro substituent in the *meta* position, in addition to the first fluorine atom in the 2'-position, show a distinctly diminished binding affinity compared with, for example, the 2',4'-difluoro-substituted compound, **12ao** (Table 2, entry 1). This is especially true for the 2',5'-disubstituted system (oxime **12ap**; $95 \pm 1\%$; Table 2, entry 2), whereas it is less pronounced for the 2',3'-disubstituted compound (oxime **12aq**; $72 \pm 5\%$; Table 2, entry 3). The 3',5'-difluoro-substituted oxime **12ar** ($94 \pm 2\%$; Table 2, entry 4) shows a similar low affinity to that of the 2',5'-difluoro-substituted compound, **12ap** (Table 2, entry 2). Hence, for all tested compounds, *meta*-fluoro substitution has a negative effect on the affinity of the oximes and *ortho* and *para* substitution is generally favorable; this is most pronounced for the chloro-substituted compounds.

A 2',4'-disubstitution appears also favorable for mixed substituted oximes containing a fluorine and a chlorine residue. Thereby, oxime **12bn**, with a chlorine in the 2'-position and a fluorine in the 4'-position, leads to a higher affinity ($pK_i = 7.57 \pm 0.08$; Table 3, entry 8) than that of regioisomeric oxime **12be** with an inverted substitution pattern ($pK_i = 7.13 \pm 0.11$; Table 3, entry 5). Considering that the affinity of oxime **12ao**, containing two fluorine substituents in the 2',4'-position, slightly diminished if the 4'-fluoro substituent was replaced by chlorine (**12be**; Table 3, entry 5), but increased upon replacement of the 2'-fluoro substituent, a 2'-chloro substituent is clearly beneficial for the binding affinity.

As already mentioned, among the difluoro-substituted compounds, the 2',4'-difluoro-substituted derivative, **12ao** (Table 2, entry 1), has an increased affinity to mGAT1 than that of the oxime with a 2',6'-disubstitution pattern, **12bi** (Table 2,

entry 21). However, the opposite is true for the mixed disubstituted oximes, **12av** and **12at**, exhibiting methoxy and fluorine residues. Here, the 2'-methoxy-6'-fluoro-substituted oxime, **12av** ($pK_i = 7.12 \pm 0.03$; Table 3, entry 2), is more active than oxime **12at** with 2'-methoxy-4'-fluoro substitution ($61 \pm 6\%$; Table 2, entry 6). Notably, if the 4'-fluoro substituent in **12at** is shifted to the 5'-position, and hence, in the *meta* position and resulting in oxime **12as**, the affinity decreases ($93 \pm 4\%$; Table 2, entry 5) according to the results already found.

In comparison with the recently published mGAT1 inhibitors obtained with oxime libraries using guvacine (**3**) as the amino acid motif,^[19] the lipophilic moieties with the same substitution pattern also turned out to yield the most potent inhibitors in this study. These guvacine-derived hits displayed slightly higher pK_i values, for example, the oxime with guvacine motif DDPM-2571, with 2',4-dichloro substitution, showed a pK_i value of 8.29 ± 0.02 , compared with 7.87 ± 0.01 for the analogous pyrrolidine-3-acetic acid derivative **12bf**. Interestingly, the methoxy group was identified as an alternative substituent that, as in oxime **12av**, gave rise to high mGAT1 affinity ($pK_i = 7.12 \pm 0.03$). Hence, known substitution patterns, such as dichloro or mixed chloro/fluoro substitution, were also confirmed to be favorable for mGAT1 binding affinity for the pyrrolidine-3-acetic acid derivatives.

Subtype selectivity—GABA uptake assays

The newly identified hits were characterized for their subtype selectivity by determining their inhibitory potencies (pIC_{50}) at all four murine GABA transporters, mGAT1–mGAT4, by means of [3H]GABA uptake assays based on HEK cells (Table 3). If the test compounds at a concentration of $100 \mu M$ were not able to reduce [3H]GABA uptake below a limit of 50% ($pIC_{50} \leq 4.00$), the percentage value of the remaining [3H]GABA uptake was given. In cases of reduction of [3H]GABA uptake below 50% , the pIC_{50} values were determined in triplicate.

Upon comparing pK_i values determined in the MS Binding Assay with the pIC_{50} values determined in [3H]GABA uptake assays on mGAT1, it appears that pK_i values are approximately up to one log unit higher, which is common in these assays and thought to be due to differences in the applied NaCl concentrations in the assays. To ensure high affinity of the marker NO711 for improved assay performance, $1 M$ NaCl is employed in MS Binding Assays and, in contrast, a NaCl concentration of $120 mM$ is used in uptake assays to comply with physiological conditions. In the present case, all pK_i values are between 0.50 (**12be**; Table 3, entry 5) and 0.71 (**12ao**; Table 3, entry 1) log units higher than the corresponding pIC_{50} values, and hence, fully in the expected range.

All studied test compounds listed in Table 3 show the highest potencies as GABA uptake inhibitors at mGAT1, with pIC_{50} values between 6.29 (**12ax**; Table 3, entry 4) and 7.33 (**12bf**; Table 3, entry 6). The potencies at GABA transporters mGAT2–mGAT4 are much lower. In most cases, the compounds are not even capable of reducing [3H]GABA uptake to 50% or lower at a test compound concentration of $100 \mu M$. In other words, the pIC_{50} values of these compounds at mGAT2–mGAT4 are below

4.0 , which is also why these pIC_{50} values are not considered to be worth determining.

In the case of oxime **12bf**—the compound identified with the highest pIC_{50} value, 7.33 ± 0.05 , for mGAT1—the potencies at the transporters mGAT2–mGAT4 are almost three log units lower (mGAT2–mGAT4, $pIC_{50} = 4.08$ – 4.44 ; Table 3, entry 6). A remarkable subtype selectivity is also found for compound **12av**, although it displays a lower pIC_{50} at mGAT1 ($pIC_{50} = 6.57 \pm 0.05$; Table 3, entry 2) than that of **12bf**. With 88 – 100% of remaining [3H]GABA uptake (at $100 \mu M$ test compound concentration), the pIC_{50} values of **12ao** at mGAT2–mGAT4 are far below 4.0 (Table 2, entry 2). Compound **12ax** also deserves attention. It shows the lowest inhibitory potency toward mGAT1 ($pIC_{50} = 6.29 \pm 0.07$; Table 3, entry 4) and, at the same time, the highest pIC_{50} values of all tested compounds toward the other transporters, mGAT2 and mGAT4 ($pIC_{50} = 4.87$ for mGAT2 and $pIC_{50} = 4.63$ for mGAT4). The subtype selectivity in favor of mGAT1 is thus markedly reduced. Overall, all test compounds in Table 3 show a clear subtype selectivity in favor of mGAT1, which is in the range of approximately one to almost three log units.

Conclusions

The concept of stable oxime library screening by using a competitive LC–MS/MS Binding Assay was successfully transferred to lipophilic N-substituted pyrrolidine-3-acetic acid derivatives. The synthesis of **10** as a hydrophilic amino acid precursor was accomplished within five steps, with an overall yield of 61% . The number of different aldehydes applied per library to receive stable oximes was this time increased from four to eight compounds to improve the throughput of this type of assay. Upon subsequent screening at different concentrations, 4 libraries out of a total of 28, containing 228 different members, were identified as being highly active toward the target mGAT1. These libraries were subjected to deconvolution experiments and led to eight hit compounds. After resynthesis of these oximes, all of which displayed a 1,1'-biphenyl moiety as part of the lipophilic domain, full competitive MS Binding Assays confirmed the identification of new potent inhibitors of mGAT1. With pK_i values ranging from 6.97 to 7.87 , these compounds represent mGAT1 inhibitors with a pyrrolidine-3-acetic acid motif with the highest binding affinity toward mGAT1 reported so far. The concept of library screening by using an oxime functionality for library generation has again been successfully applied, and the reliable application of an LC–MS/MS Binding Assay in library screening for hit identification on a specific target has been proven.

Experimental Section

Chemistry

Organic solvents used were of analytical grade and were freshly distilled prior to use, except for DMSO and absolute EtOH. Purchased reagents and reactants were used without further purification. TLC was performed on precoated silica gel F_{254} aluminum sheets (Merck). Flash column chromatography was performed on

Merck silica gel 60 (mesh 0.040–0.063 mm). NMR spectra were recorded with an Avance III HD 400 MHz Bruker BioSpin (400 MHz) spectrometer and Avance III HD 500 MHz Bruker BioSpin (500 MHz) spectrometer equipped with a CryoProbe Prodigy attachment. ^1H chemical shifts were internally referenced to tetramethylsilane (TMS) or 3-(trimethylsilyl)propionic-2,2,3,3-[D₄] acid sodium salt (TSP) for samples dissolved in D₂O. The digital resolution was stated with an accuracy of ± 0.15 Hz. MestreNova (Version 12.0.0) was used for further analysis of the spectra. IR spectra were recorded with a FTIR Paragon 1000 (PerkinElmer, Rodgau, Germany) spectrometer and Spectrum v2.00 software (PerkinElmer, Rodgau, Germany) as either KBr pellets or as films on NaCl plates. HRMS was measured on a Thermo Finnigan LTQ FT instrument for ESI or on a Thermo Finnigan MAT 95 instrument for electron impact (EI). Melting points (in $^{\circ}\text{C}$, uncorrected) were determined with a Büchi melting point B-350 apparatus. Elemental analysis for **10** was performed with an 888 Titrand (Metrohm) instrument to determine the protonation state. Purity was determined by means of qNMR spectroscopy on an Avance III HD 400 MHz Bruker BioSpin (400 MHz) spectrometer with maleic acid as an internal standard (Sigma Aldrich, Steinheim, Germany, LOT-No. BCBM8127V).^[30] Oximes **12** and **10** were $\geq 95\%$ pure. For weighing, an ALC-80.4 ACCULAB and a MC 215 scale from Sartorius Group (Göttingen, Germany) were used.

General procedure for the preparation of oximes (GP1)

Aldehyde **11** (1.0 equiv) in absolute EtOH ($c=0.1$ M) was added to a stirred solution of **10** (1.0 equiv) in absolute EtOH ($c=0.1$ M), and the resulting mixture was stirred at 60°C for 18 h. After removal of the solvent under reduced pressure, the residue was purified by flash column chromatography (silica gel, *n*-pentane/ether = 9:1 to 0:1) to yield **18** as a colorless oil.

General procedure for the hydrolysis of oximes (GP2)

A solution of ester **18** (1.0 equiv) in absolute EtOH ($c=0.1$ M) was treated with an aqueous solution of NaOH (2 M, 3.0 equiv), and the mixture was stirred at room temperature for 18 h. After cooling to 0°C , an aqueous solution of HCl (1 M) was added until pH 1 was reached. The aqueous phase was extracted with CH_2Cl_2 (3×20 mL), the combined organic layers were dried with Na_2SO_4 , and the solvent was removed under reduced pressure. The resulting oil was dissolved in double-distilled water and lyophilized to yield desired product **12** as a hydrochloride salt.

Syntheses

Synthesis of 13: Only the ^1H NMR spectroscopy analytical data for the *E/Z* mixture were reported in the literature.^[26] Thus, additional analytical data are given for the isolated isomers. (*Z*)-**13**: $R_f=0.30$ (*n*-hexanes/EtOAc 8:2); IR (film): $\tilde{\nu}=3028, 2979, 2935, 2792, 1712, 1668, 1370, 1370, 1215, 1037, 700\text{ cm}^{-1}$; ^1H NMR (400 MHz, CDCl_3 , TMS): $\delta=1.25$ (t, $J=7.1$ Hz, 3H), 2.64 (s, 4H), 3.65–3.71 (m, 4H), 4.13 (q, $J=7.1$ Hz, 2H), 5.67–5.82 (m, 1H), 7.22–7.27 (m, 1H), 7.29–7.35 ppm (m, 4H); ^{13}C NMR (100 MHz, CDCl_3 , TMS): $\delta=14.3, 33.9, 52.56, 59.1, 59.7, 60.4, 111.8, 127.1, 128.3, 128.8, 138.5, 163.5, 166.3$ ppm; IR (film): $\tilde{\nu}=3028, 2978, 2789, 1712, 1665, 1370, 1214, 1146, 1037\text{ cm}^{-1}$; HRMS (ESI⁺): m/z calcd for $\text{C}_{15}\text{H}_{19}\text{NO}_2$ [M]⁺: 245.1416; found: 245.1423. (*E*)-**13**: $R_f=0.40$ (*n*-hexanes/EtOAc 8:2); ^1H NMR (500 MHz, CDCl_3 , TMS): $\delta=1.26$ (t, $J=7.1$ Hz, 3H), 2.73 (t, $J=6.8$ Hz, 2H), 2.96 (tdd, $J=6.6, 2.5, 1.2$ Hz, 2H), 3.26 (q, $J=1.5$ Hz,

2H), 3.65 (s, 2H), 4.15 (q, $J=7.1$ Hz, 2H), 5.74 (p, $J=2.3$ Hz, 1H), 7.26–7.29 (m, 1H), 7.30–7.35 ppm (m, 4H); ^{13}C NMR (126 MHz, CDCl_3 , TMS): $\delta=14.4, 32.0, 54.1, 59.7, 60.4, 60.5, 111.4, 127.2, 128.4, 128.8, 138.5, 163.1, 166.5$ ppm; HRMS (ESI⁺): m/z calcd for $\text{C}_{15}\text{H}_{19}\text{NO}_2$ [M]⁺: 245.1416; found: 245.1411.

Synthesis of 14: Compound **13** (3.85 g, 15.7 mmol), Pd/C (10%, 929 mg, 7.85 mmol), and glacial acetic acid (2.70 mL, 47.1 mmol) in EtOH (abs., 15 mL) was introduced into an autoclave, and hydrogenation was performed at room temperature and 50 bar for 23 h. The reaction mixture was filtered through Celite and the solid was washed with EtOH (abs., 15 mL). After removal of the solvent under reduced pressure, the residue was dissolved in water (20 mL) and the aqueous phase was washed with diethyl ether (3×20 mL) and lyophilized to afford **14** as a yellow oil (3.3 g, 97%). IR (film): $\tilde{\nu}=3405, 2982, 2755, 2472, 1731, 1563, 1402, 1199, 1029\text{ cm}^{-1}$; ^1H NMR (400 MHz, CDCl_3 , TMS): $\delta=1.26$ (t, $J=7.1$ Hz, 3H), 1.64 (dq, $J=13.0, 8.7$ Hz, 1H), 1.96 (s, 3H), 2.15–2.25 (m, 1H), 2.47 (d, $J=7.5$ Hz, 2H), 2.67 (hept, $J=7.5$ Hz, 1H), 2.82 (dd, $J=11.4, 8.4$ Hz, 1H), 3.14 (ddd, $J=11.4, 8.9, 7.7$ Hz, 1H), 3.24–3.35 (m, 1H), 3.41 (dd, $J=11.4, 7.6$ Hz, 1H), 4.14 (q, $J=7.1$ Hz, 2H); ^{13}C NMR (100 MHz, CDCl_3 , TMS): $\delta=14.2, 23.6, 30.6, 34.7, 37.2, 44.1, 49.2, 60.8, 171.6, 178.4$ ppm; HRMS (ESI⁺): m/z calcd for $\text{C}_8\text{H}_{15}\text{NO}_2$ [M]⁺: 157.1103; found: 157.1109.

Synthesis of 15: K_2CO_3 (382 mg, 2.76 mmol), KI (3 mg, 0.02 mmol) and 2-bromoethanol (83 μL , 1.1 mmol) were added to a solution of **14** (200 mg, 0.921 mmol) in THF (4 mL). The resulting mixture was heated at reflux for 20 h. After cooling to room temperature, the solids were removed by filtration and the solvent was removed under reduced pressure. The residue was purified by column chromatography on silica gel (MeCN/ $\text{NEt}_3=97:3$) to yield **15** as a yellow oil (153 mg, 83%); $R_f=0.10$ (MeCN/ NEt_3 97:3); IR (film): $\tilde{\nu}=3389, 2954, 1729, 1376, 1191, 1051, 880\text{ cm}^{-1}$; ^1H NMR (400 MHz, CDCl_3 , TMS): $\delta=1.26$ (t, $J=7.1$ Hz, 3H), 1.40–1.54 (m, 1H), 2.08 (dddd, $J=13.1, 9.1, 7.4, 5.9$ Hz, 1H), 2.30 (dd, $J=9.3, 6.2$ Hz, 1H), 2.39 (d, $J=7.4$ Hz, 2H), 2.50–2.80 (m, 6H), 2.82 (dd, $J=9.3, 7.4$ Hz, 1H), 3.61 (t, $J=5.4$ Hz, 2H), 4.13 ppm (q, $J=7.1$ Hz, 2H); ^{13}C NMR (100 MHz, CDCl_3 , TMS): $\delta=14.3, 30.5, 33.8, 40.0, 53.4, 57.2, 59.5, 59.7, 60.3, 172.8$ ppm; HRMS (ESI⁺): m/z calcd for $\text{C}_{10}\text{H}_{20}\text{NO}_3$ [$M+H$]⁺: 202.1438; found: 202.1439.

Synthesis of 16: Compound **15** (235 mg, 1.17 mmol), *N*-hydroxyphthalimide (324 mg, 1.98 mmol), and triphenylphosphine (531 mg, 1.98 mmol) were dissolved in THF (5 mL) before DMEAD (479 mg, 2.04 mmol) was added slowly and the solution was stirred for 17 h at room temperature. After removal of the solvent under reduced pressure, the residue was dissolved in CH_2Cl_2 (20 mL) and the organic layer was washed with water (3×15 mL), dried over sodium sulfate, and the solvent was again removed in vacuo. The resulting oil was purified by column chromatography on silica gel, which was pre-dried at 145°C in vacuo for 5 h (diethyl ether/ $\text{NEt}_3=95:5$), to afford **16** as a light yellow oil (364 mg, 90%). $R_f=0.81$ (diethyl ether/ NEt_3 95:5); IR (film): $\tilde{\nu}=3059, 2981, 1731, 1693, 1434, 1267, 1178, 1029\text{ cm}^{-1}$; ^1H NMR (400 MHz, CDCl_3 , TMS): $\delta=1.25$ (t, $J=7.1$ Hz, 3H), 1.37 (ddt, $J=12.7, 8.1, 6.4$ Hz, 1H), 2.01 (dddd, $J=13.0, 9.1, 7.7, 5.6$ Hz, 1H), 2.25–2.37 (m, 3H), 2.45–2.56 (m, 1H), 2.60 (td, $J=8.6, 5.7$ Hz, 1H), 2.64–2.73 (m, 1H), 2.83–2.98 (m, 3H), 4.12 (q, $J=7.1$ Hz, 2H), 4.32 (t, $J=5.5$ Hz, 2H), 7.72–7.81 (m, 2H), 7.81–7.90 ppm (m, 2H); ^{13}C NMR (100 MHz, CDCl_3 , TMS): $\delta=14.3, 30.6, 33.7, 40.0, 53.9, 54.1, 60.1, 60.2, 76.1, 123.5, 129.0, 134.4, 163.5, 172.7$ ppm; HRMS (ESI⁺): m/z calcd for $\text{C}_{18}\text{H}_{23}\text{N}_2\text{O}_5$ [$M+H$]⁺: 347.1601; found: 347.1607.

Synthesis of 17: A solution of hydrazine (50–60%, 21 μ L, 0.33 mmol) was added to a stirred solution of **16** (57 mg, 0.17 mmol) in EtOH (abs., 2 mL), and the solution was stirred for 2 h at room temperature. The resulting slurry was filtered, the filtrate was washed with ice-cold CH_2Cl_2 (10 mL), and the solvent was removed in vacuo. Again ice-cold CH_2Cl_2 (10 mL) was added to the residue and the resulting mixture was filtered. Evaporation under reduced pressure afforded **17** as a colorless oil (34 mg, 96%). IR (film): $\tilde{\nu}$ = 2958, 2933, 2792, 1732, 1591, 1374, 1277, 1191, 1156, 1031 cm^{-1} ; ^1H NMR (400 MHz, CDCl_3 , TMS): δ = 1.25 (t, J = 7.1 Hz, 3H), 1.46 (ddt, J = 12.6, 8.2, 6.2 Hz, 1H), 2.09 (dddd, J = 13.0, 9.4, 7.8, 6.0 Hz, 1H), 2.20 (dd, J = 9.3, 6.9 Hz, 1H), 2.39 (d, J = 7.5 Hz, 2H), 2.52 (td, J = 8.6, 6.0 Hz, 1H), 2.56–2.63 (m, 1H), 2.63–2.76 (m, 3H), 2.91 (dd, J = 9.3, 7.8 Hz, 1H), 3.78 (t, J = 5.6 Hz, 2H), 4.12 ppm (q, J = 7.1 Hz, 2H); ^{13}C NMR (100 MHz, CDCl_3 , TMS): δ = 14.3, 30.5, 33.7, 40.0, 54.2, 54.9, 60.3, 60.4, 74.2, 172.8 ppm; HRMS (ESI $^+$): m/z calcd for $\text{C}_{10}\text{H}_{21}\text{N}_2\text{O}_3$ [$M+H$] $^+$: 217.1547; found: 217.1548.

Synthesis of 10: Compound **17** (57 mg, 0.26 mmol) was dissolved in an aqueous solution of HCl (1 M, 2.6 mL, 2.6 mmol) and the reaction mixture was stirred at 95 $^\circ\text{C}$ for 4 h. After cooling to room temperature, the mixture was washed with CH_2Cl_2 (3 \times 5 mL) and the aqueous layer was lyophilized to yield the product as colorless amorphous solid (60 mg, 87%); in the NMR spectra two different conformers in a ratio of 1:1.18 could be identified; mp: 58–64 $^\circ\text{C}$; IR (KBr): $\tilde{\nu}$ = 3383, 2957, 2671, 1722, 1454, 1408, 1199, 1044, 1019 cm^{-1} ; HRMS (ESI $^+$): m/z calcd for $\text{C}_8\text{H}_{17}\text{N}_2\text{O}_3$ [$M+H$] $^+$: 189.1234; found: 189.1233. Conformer 1 (major): ^1H NMR (500 MHz, 0.1 DCI in D_2O , TPS): δ = 1.90 (dddd, J = 13.7, 9.5, 7.9, 5.9 Hz, 1H), 2.32 (dq, J = 13.7, 8.1 Hz, 1H), 2.56–2.70 (m, 2H), 2.70–2.80 (m, 1H), 2.86–2.98 (m, 1H), 3.31 (ddd, J = 11.8, 9.6, 7.2 Hz, 1H), 3.64 (tt, J = 4.0, 1.5 Hz, 2H), 3.77 (ddd, J = 14.1, 7.6, 5.3 Hz, 1H), 3.96 (dd, J = 11.3, 7.0 Hz, 1H), 4.45 ppm (ddd, J = 5.6, 4.3, 1.5 Hz, 2H); ^{13}C NMR (126 MHz, 0.1 DCI in D_2O , TPS): δ = 31.1, 35.9, 39.4, 40.0, 55.4, 55.5, 56.8, 61.6, 72.6, 72.6, 178.8, 179.0 ppm; Conformer 2 (minor): ^1H NMR (500 MHz, 0.1 DCI in D_2O , TPS): δ = 1.74 (dddd, J = 13.6, 11.6, 9.3, 7.5 Hz, 1H), 2.42 (dtd, J = 13.7, 7.2, 2.1 Hz, 1H), 2.56–2.70 (m, 2H), 2.86–2.98 (m, 1H), 3.21 (td, J = 11.5, 6.9 Hz, 1H), 3.51 (d, J = 8.2 Hz, 2H), 3.64 (tt, J = 4.0, 1.5 Hz, 2H), 3.81 (ddd, J = 11.2, 7.3, 1.9 Hz, 1H), 4.45 ppm (ddd, J = 5.6, 4.3, 1.5 Hz, 2H); ^{13}C NMR (126 MHz, 0.1 DCI in D_2O , TPS): δ = 32.4, 35.3, 39.4, 40.0, 55.4, 55.5, 58.0, 61.1, 72.6, 72.6, 178.8, 179.0 ppm.

Synthesis of 18ao: According to GP1, compound **18ao** was obtained as a colorless oil (84 mg, 87%) from hydroxylamine **17** (50 mg, 0.23 mmol) and **11ao** (50.4 mg, 0.231 mmol). R_f = 0.17 (diethyl ether 100%); IR (film): $\tilde{\nu}$ = 3066, 2960, 2790, 1732, 1620, 1509, 1270, 1141, 954 cm^{-1} ; ^1H NMR (400 MHz, CDCl_3 , TMS): δ = 1.24 (t, J = 7.1 Hz, 3H), 1.45 (ddt, J = 12.6, 8.1, 6.1 Hz, 1H), 2.07 (dddd, J = 13.6, 9.3, 7.8, 6.0 Hz, 1H), 2.20 (dd, J = 9.0, 7.2 Hz, 1H), 2.38 (d, J = 7.5 Hz, 2H), 2.47–2.65 (m, 2H), 2.65–2.83 (m, 3H), 2.91 (dd, J = 9.0, 7.9 Hz, 1H), 4.11 (q, J = 7.1 Hz, 2H), 4.24 (t, J = 5.9 Hz, 2H), 6.84–6.93 (m, 1H), 6.93–6.99 (m, 1H), 7.21 (td, J = 8.5, 6.5 Hz, 1H), 7.24–7.26 (m, 1H), 7.37–7.45 (m, 2H), 7.93 (d, J = 2.0 Hz, 1H), 7.95–8.01 ppm (m, 1H); ^{13}C NMR (100 MHz, CDCl_3 , TMS): δ = 14.2, 30.5, 33.7, 40.0, 54.3, 55.0, 60.3, 60.4, 73.1, 104.2 (t, $J_{\text{C(F)}} = 25.9$ Hz), 111.5 (dd, $J_{\text{C(F)}} = 21.0$, 4.0 Hz), 123.3 (dd, $J_{\text{C(F)}} = 16.4$, 4.0 Hz), 125.9, 128.4, 129.5, 130.8, 132.6 (dd, $J_{\text{C(F)}} = 9.5$, 4.7 Hz), 134.6, 147.0, 159.6 (dd, $J_{\text{C(F)}} = 249.8$, 12.4 Hz), 162.7 (dd, $J_{\text{C(F)}} = 249.9$, 11.8 Hz), 172.8 ppm; ^{19}F NMR (376 MHz, CDCl_3): δ = –110.2 (p, J = 8.0 Hz), –110.3 ppm (q, J = 8.6 Hz); HRMS (EI $^+$): m/z calcd for $\text{C}_{23}\text{H}_{26}\text{F}_2\text{N}_2\text{O}_3$ [M] $^+$: 416.1911; found: 416.1909.

Synthesis of 18av: According to GP1, compound **18av** was obtained as a colorless oil (17 mg, 48%) from hydroxylamine **17**

(17.8 mg, 0.0825 mmol) and **11av** (19.0 mg, 0.0825 mmol). R_f = 0.08 (diethyl ether 100%); IR (film): $\tilde{\nu}$ = 3065, 2960, 2794, 1732, 1615, 1470, 1239, 1155, 1083 cm^{-1} ; ^1H NMR (400 MHz, CD_2Cl_2 , TMS): δ = 1.22 (t, J = 7.1 Hz, 3H), 1.39 (ddt, J = 12.5, 8.0, 6.2 Hz, 1H), 2.01 (dddd, J = 13.4, 9.3, 7.8, 5.7 Hz, 1H), 2.18 (dd, J = 9.2, 6.5 Hz, 1H), 2.29–2.39 (m, 2H), 2.44–2.56 (m, 2H), 2.60 (td, J = 8.4, 6.2 Hz, 1H), 2.63–2.77 (m, 2H), 2.79 (dd, J = 9.2, 7.5 Hz, 1H), 3.74 (s, 3H), 4.08 (q, J = 7.2 Hz, 2H), 4.17 (t, J = 5.9 Hz, 2H), 6.74–6.87 (m, 2H), 7.17–7.28 (m, 1H), 7.30–7.48 (m, 3H), 7.78 (s, 1H), 7.96 ppm (dd, J = 7.7, 1.6 Hz, 1H); ^{13}C NMR (100 MHz, CD_2Cl_2 , TMS): δ = 14.6, 31.1, 34.4, 40.5, 54.6, 55.3, 56.6, 60.7, 60.8, 73.6, 107.3 (d, $J_{\text{C(F)}} = 2.9$ Hz), 108.6 (d, $J_{\text{C(F)}} = 23.0$ Hz), 116.6 (d, $J_{\text{C(F)}} = 19.4$ Hz), 125.9, 128.6, 129.8, 130.4 (d, $J_{\text{C(F)}} = 10.6$ Hz), 132.0, 132.0, 132.2, 147.5, 158.6 (d, $J_{\text{C(F)}} = 6.8$ Hz), 160.9 (d, $J_{\text{C(F)}} = 243.5$ Hz), 173.2 ppm; ^{19}F NMR (376 MHz, CD_2Cl_2): δ = –114.3 ppm; HRMS (ESI $^+$): m/z calcd for $\text{C}_{24}\text{H}_{30}\text{FN}_2\text{O}_4$ [$M+H$] $^+$: 429.2184; found: 429.2181.

Synthesis of 18aw: According to GP1, compound **18aw** was obtained as a colorless oil (39 mg, 68%) from hydroxylamine **17** (30 mg, 0.14 mmol) and **11aw** (30 mg, 0.14 mmol). R_f = 0.15 (diethyl ether, 100%); IR (film): $\tilde{\nu}$ = 3061, 2958, 2791, 1732, 1467, 1188, 1155, 1034, 756 cm^{-1} ; ^1H NMR (400 MHz, CD_2Cl_2 , TMS): δ = 1.21 (t, J = 7.1 Hz, 3H), 1.39 (ddt, J = 12.6, 8.2, 6.2 Hz, 1H), 2.01 (dddd, J = 13.3, 9.3, 7.9, 5.7 Hz, 1H), 2.17 (dd, J = 9.2, 6.5 Hz, 1H), 2.29–2.38 (m, 2H), 2.43–2.56 (m, 2H), 2.59 (td, J = 8.3, 6.1 Hz, 1H), 2.61–2.76 (m, 2H), 2.79 (dd, J = 9.1, 7.6 Hz, 1H), 4.08 (q, J = 7.1 Hz, 2H), 4.17 (t, J = 5.9 Hz, 2H), 7.18–7.30 (m, 2H), 7.31–7.39 (m, 2H), 7.39–7.47 (m, 2H), 7.46–7.54 (m, 1H), 7.76 (s, 1H), 7.90–8.03 ppm (m, 1H); ^{13}C NMR (100 MHz, CD_2Cl_2 , TMS): δ = 14.5, 30.9, 34.2, 40.4, 54.5, 55.2, 60.5, 60.7, 73.6, 125.8, 127.2, 128.6, 129.7, 129.9, 130.7, 131.0, 132.1, 133.7, 138.8, 139.6, 147.1, 173.0 ppm; HRMS (ESI $^+$): m/z calcd for $\text{C}_{23}\text{H}_{28}\text{ClN}_2\text{O}_3$ [$M+H$] $^+$: 415.1783; found: 415.1781.

Synthesis of 18ax: According to GP1, compound **18ax** was obtained as a colorless oil (48 mg, 72%) from hydroxylamine **17** (35 mg, 0.16 mmol) and **11ax** (35 mg, 0.16 mmol). R_f = 0.17 (diethyl ether, 100%); IR (film): $\tilde{\nu}$ = 3062, 2958, 2792, 1733, 1473, 1200, 1156, 1035, 761 cm^{-1} ; ^1H NMR (500 MHz, CD_2Cl_2 , TMS): δ = 1.14 (t, J = 7.2 Hz, 3H), 1.33 (ddt, J = 12.7, 8.1, 6.3 Hz, 1H), 1.94 (dddd, J = 13.4, 9.3, 7.9, 5.8 Hz, 1H), 2.12 (dd, J = 8.9, 6.7 Hz, 1H), 2.27 (d, J = 7.5 Hz, 2H), 2.37–2.48 (m, 2H), 2.49–2.57 (m, 1H), 2.59–2.70 (m, 2H), 2.73 (dd, J = 8.9, 7.7 Hz, 1H), 4.00 (q, J = 7.2 Hz, 2H), 4.13 (t, J = 5.9 Hz, 2H), 7.15–7.20 (m, 2H), 7.22 (dd, J = 7.5, 1.5 Hz, 1H), 7.30 (td, J = 7.6, 1.5 Hz, 1H), 7.32–7.39 (m, 3H), 7.85 (dd, J = 7.8, 1.3 Hz, 1H), 7.90 ppm (s, 1H); ^{13}C NMR (126 MHz, CD_2Cl_2 , TMS): δ = 13.3, 29.8, 33.1, 39.2, 53.3, 54.0, 59.3, 59.6, 72.5, 125.3, 127.1, 127.7, 128.8, 129.2, 129.4, 130.3, 132.8, 137.4, 140.0, 146.4, 171.8 ppm; HRMS (ESI $^+$): m/z calcd for $\text{C}_{23}\text{H}_{28}\text{ClN}_2\text{O}_3$ [$M+H$] $^+$: 415.1783; found: 415.1781.

Synthesis of 18be: According to GP1, compound **18be** was obtained as a colorless oil (60 mg, 75%) from hydroxylamine **17** (50 mg, 0.23 mmol) and **11be** (54 mg, 0.23 mmol). R_f = 0.15 (diethyl ether, 100%); IR (film): $\tilde{\nu}$ = 3065, 2958, 2791, 1738, 1731, 1607, 1277, 1156, 893 cm^{-1} ; ^1H NMR (500 MHz, CDCl_3 , TMS): δ = 1.24 (t, J = 7.1 Hz, 3H), 1.45 (ddt, J = 12.6, 8.2, 6.2 Hz, 1H), 2.07 (dddd, J = 13.6, 9.3, 7.8, 6.0 Hz, 1H), 2.19 (dd, J = 9.3, 6.9 Hz, 1H), 2.38 (d, J = 7.5 Hz, 2H), 2.52 (td, J = 8.7, 6.0 Hz, 1H), 2.59 (dq, J = 9.2, 7.2 Hz, 1H), 2.66–2.82 (m, 3H), 2.90 (dd, J = 9.2, 7.8 Hz, 1H), 4.11 (q, J = 7.1 Hz, 2H), 4.24 (t, J = 5.9 Hz, 2H), 7.14–7.23 (m, 3H), 7.23–7.26 (m, 1H), 7.37–7.46 (m, 2H), 7.93 (d, J = 2.0 Hz, 1H), 7.95–8.01 ppm (m, 1H); ^{13}C NMR (126 MHz, CDCl_3 , TMS): δ = 14.2, 30.5, 33.7, 40.0, 54.3, 55.0, 60.3, 60.4, 73.1, 116.6 (d, $J_{\text{C(F)}} = 25.8$ Hz), 124.6 (d, $J_{\text{C(F)}} = 3.7$ Hz), 125.8 (d, $J_{\text{C(F)}} = 16.4$ Hz), 126.0, 128.5, 129.5, 130.6, 130.7, 132.6 (d, $J_{\text{C(F)}} = 4.1$ Hz), 134.4, 134.7 (d, $J_{\text{C(F)}} = 9.9$ Hz), 146.9, 159.3

(d, $J_{\text{CF}}=250.5$ Hz), 172.8 ppm; ^{19}F NMR (376 MHz, CDCl_3): $\delta = -112.1$ ppm; HRMS (EI^+): m/z calcd for $\text{C}_{23}\text{H}_{26}\text{FCIN}_2\text{O}_3$ [M] $^+$: 432.1616; found: 432.1612.

Synthesis of 18bf: According to GP1, compound **18bf** was obtained as a colorless oil (48 mg, 77%) from hydroxylamine **17** (30 mg, 0.14 mmol) and **11bf** (35 mg, 0.14 mmol). $R_f=0.11$ (diethyl ether, 100%); IR (film): $\tilde{\nu}=3059, 2957, 2925, 1733, 1586, 1466, 1154, 1035, 762\text{ cm}^{-1}$; ^1H NMR (400 MHz, CDCl_3 , TMS): $\delta=1.24$ (t, $J=7.1$ Hz, 3H), 1.44 (ddt, $J=12.6, 8.3, 6.1$ Hz, 1H), 2.07 (dddd, $J=13.5, 9.3, 7.7, 5.9$ Hz, 1H), 2.18 (dd, $J=9.3, 6.9$ Hz, 1H), 2.38 (d, $J=7.5$ Hz, 2H), 2.47–2.55 (m, 1H), 2.55–2.64 (m, 1H), 2.64–2.81 (m, 3H), 2.90 (dd, $J=9.2, 7.6$ Hz, 1H), 4.11 (q, $J=7.2$ Hz, 2H), 4.22 (t, $J=5.9$ Hz, 2H), 7.14–7.21 (m, 2H), 7.30 (dd, $J=8.2, 2.1$ Hz, 1H), 7.36–7.44 (m, 2H), 7.48 (d, $J=2.1$ Hz, 1H), 7.80 (s, 1H), 7.90–8.06 ppm (m, 1H); ^{13}C NMR (100 MHz, CDCl_3 , TMS): $\delta=14.2, 30.5, 33.7, 40.0, 54.2, 55.0, 60.2, 60.4, 73.1, 125.8, 127.1, 128.5, 129.4, 130.2, 130.6, 132.3, 134.3, 134.4, 137.0, 138.0, 146.7, 172.8$ ppm; HRMS (ESI^+): m/z calcd for $\text{C}_{23}\text{H}_{27}\text{Cl}_2\text{N}_2\text{O}_3$ [$M+H$] $^+$: 449.1393; found: 449.1393.

Synthesis of 18bj: According to GP1, compound **18bj** was obtained as a colorless oil (48 mg, 82%) from hydroxylamine **17** (29.3 mg, 0.135 mmol) and **11bj** (32.0 mg, 0.135 mmol). $R_f=0.14$ (diethyl ether, 100%); IR (film): $\tilde{\nu}=3065, 2959, 2792, 1732, 1463, 1274, 1233, 1154, 1034, 998, 788\text{ cm}^{-1}$; ^1H NMR (400 MHz, CD_2Cl_2 , TMS): $\delta=1.22$ (t, $J=7.1$ Hz, 3H), 1.40 (ddt, $J=12.7, 8.2, 6.3$ Hz, 1H), 2.02 (dddd, $J=13.5, 9.2, 7.9, 5.7$ Hz, 1H), 2.18 (dd, $J=9.2, 6.5$ Hz, 1H), 2.29–2.38 (m, 2H), 2.51 (dtd, $J=14.2, 8.1, 7.4, 3.4$ Hz, 2H), 2.55–2.62 (m, 1H), 2.62–2.76 (m, 2H), 2.79 (dd, $J=9.0, 7.6$ Hz, 1H), 4.08 (q, $J=7.1$ Hz, 2H), 4.17 (t, $J=5.9$ Hz, 2H), 6.74–6.86 (m, 2H), 7.22–7.33 (m, 1H), 7.41–7.54 (m, 2H), 7.87 (t, $J=1.2$ Hz, 1H), 7.91–7.99 ppm (m, 1H); ^{13}C NMR (100 MHz, CD_2Cl_2 , TMS): $\delta=14.5, 30.9, 34.3, 40.4, 54.5, 55.1, 60.5, 60.7, 73.7, 100.8$ (ddd, $J_{\text{CF}}=28.5, 25.7, 2.5$ Hz), 113.3 (td, $J_{\text{CF}}=21.5, 5.2$ Hz), 126.8, 128.0, 129.5, 129.9, 131.9, 132.0, 146.6, 160.7 (ddd, $J_{\text{CF}}=248.3, 14.9, 10.2$ Hz), 163.2 (dt, $J_{\text{CF}}=234.0, 15.8$ Hz), 173.0 ppm; ^{19}F NMR (376 MHz, CD_2Cl_2): $\delta=-108.6$ (t, $J=6.2$ Hz), -109.8 ppm (d, $J=6.7$ Hz); HRMS (ESI^+): m/z calcd for $\text{C}_{23}\text{H}_{26}\text{F}_3\text{N}_2\text{O}_3$ [$M+H$] $^+$: 435.1890; found: 435.1888.

Synthesis of 18bn: According to GP1, compound **18bn** was obtained as a colorless oil (59 mg, 84%) from hydroxylamine **17** (35 mg, 0.16 mmol) and **11bn** (38 mg, 0.16 mmol). $R_f=0.15$ (diethyl ether, 100%); IR (film): $\tilde{\nu}=3064, 2958, 2792, 1733, 1601, 1257, 1156, 1060, 898\text{ cm}^{-1}$; ^1H NMR (400 MHz, CDCl_3 , TMS): $\delta=1.24$ (t, $J=7.1$ Hz, 3H), 1.44 (ddt, $J=11.7, 8.2, 6.1$ Hz, 1H), 2.07 (dddd, $J=13.3, 9.4, 7.9, 6.0$ Hz, 1H), 2.19 (dd, $J=8.8, 7.3$ Hz, 1H), 2.38 (d, $J=7.5$ Hz, 2H), 2.51 (td, $J=8.4, 6.6$ Hz, 1H), 2.58 (dq, $J=9.1, 7.3$ Hz, 1H), 2.64–2.83 (m, 3H), 2.90 (dd, $J=9.0, 7.9$ Hz, 1H), 4.11 (q, $J=7.1$ Hz, 2H), 4.23 (t, $J=5.8$ Hz, 2H), 7.04 (ddd, $J=8.4, 8.0, 2.6$ Hz, 1H), 7.14–7.24 (m, 3H), 7.37–7.47 (m, 2H), 7.80 (s, 1H), 7.92–8.05 ppm (m, 1H); ^{13}C NMR (100 MHz, CDCl_3 , TMS): $\delta=14.2, 30.5, 33.7, 40.0, 54.3, 55.0, 60.3, 60.4, 73.1, 114.1$ (d, $J_{\text{CF}}=21.1$ Hz), 116.9 (d, $J_{\text{CF}}=24.7$ Hz), 125.7, 128.4, 129.4, 130.4, 130.7, 132.5 (d, $J_{\text{CF}}=8.7$ Hz), 134.3 (d, $J_{\text{CF}}=10.3$ Hz), 134.6 (d, $J_{\text{CF}}=3.7$ Hz), 138.2, 146.9, 162.1 (d, $J_{\text{CF}}=250.4$ Hz), 172.8 ppm; ^{19}F NMR (376 MHz, CDCl_3): $\delta=-112.2$ ppm; HRMS (EI^+): m/z calcd for $\text{C}_{23}\text{H}_{26}\text{FCIN}_2\text{O}_3$ [M] $^+$: 432.1616; found: 432.1604.

Synthesis of 12ao: According to GP2, compound **12ao** was obtained as a colorless, amorphous powder (54 mg, 87%) from **18ao** (61.0 mg, 0.146 mmol) and NaOH (17.6 mg, 0.439 mmol, 220 μL); mp: 60–62 °C; IR (KBr): $\tilde{\nu}=3416, 2950, 2618, 2562, 1719, 1618, 1508, 1419, 1269, 1140, 942, 764\text{ cm}^{-1}$; ^1H NMR (500 MHz, 0.1 M NaOD/ $\text{CD}_3\text{OD}=1:2$, TPS): $\delta=1.46$ (ddt, $J=12.9, 8.2, 6.3$ Hz, 1H), 2.04 (dddd, $J=13.8, 8.9, 7.6, 6.4$ Hz, 1H), 2.18 (dd, $J=9.6, 7.7$ Hz,

1H), 2.22 (dd, $J=14.2, 8.1$ Hz, 1H), 2.25 (dd, $J=24.0, 10.7$ Hz, 1H), 2.46–2.59 (m, 2H), 2.67–2.83 (m, 3H), 2.94 (dd, $J=9.6, 7.9$ Hz, 1H), 4.23 (t, $J=5.8$ Hz, 2H), 7.06–7.16 (m, 2H), 7.27–7.37 (m, 2H), 7.49 (td, $J=7.6, 1.5$ Hz, 1H), 7.54 (td, $J=7.5, 1.6$ Hz, 1H), 7.87 (dd, $J=7.7, 1.5$ Hz, 1H), 7.91 ppm (d, $J=2.2$ Hz, 1H); ^{13}C NMR (126 MHz, 0.1 M NaOD/ $\text{CD}_3\text{OD}=1:2$, TPS): $\delta=33.1, 37.6, 46.2, 56.9, 57.4, 63.2, 75.4, 106.6$ (t, $J_{\text{CF}}=26.2$ Hz), 114.5 (dd, $J_{\text{CF}}=21.5, 3.7$ Hz), 126.3 (dd, $J_{\text{CF}}=16.4, 3.8$ Hz), 129.0, 131.5, 133.0, 133.2, 133.8, 135.6 (dd, $J_{\text{CF}}=9.7, 4.5$ Hz), 137.7, 150.9, 162.5 (dd, $J_{\text{CF}}=247.4, 12.2$ Hz), 165.9 (dd, $J_{\text{CF}}=248.2, 11.7$ Hz), 183.9 ppm; ^{19}F NMR (376 MHz, 0.1 M NaOD/ $\text{CD}_3\text{OD}=1:2$): $\delta=-111.5$ (d, $J=7.6$ Hz), -112.5 ppm (d, $J=7.6$ Hz); HRMS (ESI^+): m/z calcd for $\text{C}_{21}\text{H}_{23}\text{F}_2\text{N}_2\text{O}_3$ [$M+H$] $^+$: 389.1671; found: 389.1671.

Synthesis of 12av: According to GP2, compound **12av** was obtained as a colorless, amorphous powder (41 mg, 89%) from **18av** (45.0 mg, 0.105 mmol) and NaOH (12.6 mg, 0.315 mmol); mp: 54–59 °C; IR (KBr): $\tilde{\nu}=3441, 2942, 2622, 2562, 1719, 1616, 1469, 1238, 1074, 786\text{ cm}^{-1}$; ^1H NMR (500 MHz, 0.1 M NaOD/ $\text{CD}_3\text{OD}=1:2$, TPS): $\delta=1.45$ (ddt, $J=13.0, 8.0, 6.4$ Hz, 1H), 2.03 (dddd, $J=13.7, 9.0, 7.6, 6.4$ Hz, 1H), 2.17 (dd, $J=9.3, 8.0$ Hz, 1H), 2.21 (dd, $J=14.2, 8.0$ Hz, 1H), 2.24 (dd, $J=14.3, 7.6$ Hz, 1H), 2.45–2.60 (m, 2H), 2.67–2.81 (m, 3H), 2.93 (dd, $J=9.3, 8.1$ Hz, 1H), 3.75 (s, 3H), 4.21 (t, $J=5.8$ Hz, 2H), 6.87 (t, $J=8.7$ Hz, 1H), 6.97 (d, $J=8.5$ Hz, 1H), 7.22 (dd, $J=7.6, 1.0$ Hz, 1H), 7.41–7.54 (m, 3H), 7.78 (s, 1H), 7.88 ppm (d, $J=7.7$ Hz, 1H); ^{13}C NMR (126 MHz, 0.1 M NaOD/ $\text{CD}_3\text{OD}=1:2$, TPS): $\delta=33.1, 37.6, 46.2, 56.9, 57.3, 58.6, 63.2, 75.3, 110.0$ (d, $J_{\text{CF}}=2.8$ Hz), 110.8 (d, $J_{\text{CF}}=22.8$ Hz), 118.8 (d, $J_{\text{CF}}=19.3$ Hz), 128.5, 131.2, 132.7, 133.3 (d, $J_{\text{CF}}=10.7$ Hz), 133.7, 134.3, 134.8, 151.2, 160.9 (d, $J_{\text{CF}}=6.9$ Hz), 163.1 (d, $J_{\text{CF}}=242.6$ Hz), 183.9 ppm; ^{19}F NMR (376 MHz, 0.1 M NaOD/ $\text{CD}_3\text{OD}=1:2$): $\delta=-115.7$ ppm; HRMS (ESI^+): m/z calcd for $\text{C}_{22}\text{H}_{26}\text{FN}_2\text{O}_4$ [$M+H$] $^+$: 401.1871; found: 401.1868.

Synthesis of 12aw: According to GP2, compound **12aw** was obtained as a colorless, amorphous powder (23 mg, 81%) from **18aw** (28.0 mg, 0.0675 mmol) and NaOH (8.1 mg, 0.20 mmol); mp: 56–60 °C; IR (KBr): $\tilde{\nu}=3444, 3054, 2924, 2854, 2616, 2553, 2480, 1716, 1467, 1429, 1201, 1069, 757\text{ cm}^{-1}$; ^1H NMR (500 MHz, 0.1 M NaOD/ $\text{CD}_3\text{OD}=1:2$, TPS): $\delta=1.45$ (ddt, $J=12.9, 8.1, 6.3$ Hz, 1H), 2.02 (dddd, $J=13.7, 9.1, 7.6, 6.4$ Hz, 1H), 2.16 (dd, $J=9.6, 7.9$ Hz, 1H), 2.20 (dd, $J=14.2, 8.1$ Hz, 1H), 2.24 (dd, $J=14.3, 7.3$ Hz, 1H), 2.45–2.60 (m, 2H), 2.66–2.81 (m, 3H), 2.93 (dd, $J=9.6, 7.8$ Hz, 1H), 4.21 (t, $J=5.8$ Hz, 2H), 7.22–7.25 (m, 1H), 7.25–7.30 (m, 1H), 7.42–7.47 (m, 2H), 7.47–7.51 (m, 1H), 7.51–7.56 (m, 2H), 7.76 (s, 1H), 7.88 ppm (dd, $J=7.6, 1.5$ Hz, 1H); ^{13}C NMR (126 MHz, 0.1 M NaOD/ $\text{CD}_3\text{OD}=1:2$, TPS): $\delta=33.1, 37.6, 46.2, 56.9, 57.3, 63.2, 75.4, 128.5, 130.1, 131.3, 132.3, 132.6, 132.8, 132.9, 133.1, 134.4, 135.8, 141.2, 142.3, 150.9, 183.9$ ppm; HRMS (ESI^+): m/z calcd for $\text{C}_{21}\text{H}_{24}\text{ClN}_2\text{O}_3$ [$M+H$] $^+$: 387.1475; found: 387.1473.

Synthesis of 12ax: According to GP2, compound **12ax** was obtained as a colorless, amorphous powder (22 mg, 77%) from **18ax** (28 mg, 0.068 mmol) and NaOH (8.1 mg, 0.20 mmol, 101 μL); mp: 59–65 °C; IR (KBr): $\tilde{\nu}=3443, 2945, 2622, 2562, 1720, 1473, 1201, 1089, 762\text{ cm}^{-1}$; ^1H NMR (500 MHz, 0.1 M NaOD/ $\text{CD}_3\text{OD}=1:2$, TPS): $\delta=1.47$ (ddt, $J=13.0, 8.1, 6.5$ Hz, 1H), 2.05 (dddd, $J=13.7, 9.1, 7.6, 6.5$ Hz, 1H), 2.19 (dd, $J=9.6, 7.8$ Hz, 1H), 2.22 (dd, $J=14.5, 8.0$ Hz, 1H), 2.25 (dd, $J=14.2, 7.4$ Hz, 1H), 2.47–2.61 (m, 2H), 2.71–2.86 (m, 3H), 2.96 (dd, $J=9.5, 7.9$ Hz, 1H), 4.26 (t, $J=5.8$ Hz, 2H), 7.22–7.31 (m, 2H), 7.36 (dd, $J=7.6, 1.3$ Hz, 1H), 7.43–7.50 (m, 3H), 7.52 (td, $J=7.5, 1.4$ Hz, 1H), 7.86 (dd, $J=7.8, 1.0$ Hz, 1H), 8.00 ppm (s, 1H); ^{13}C NMR (126 MHz, 0.1 M NaOD/ $\text{CD}_3\text{OD}=1:2$, TPS): $\delta=33.1, 37.6, 46.2, 56.9, 57.4, 63.2, 75.4, 129.2, 131.0, 131.4, 132.2, 133.0, 133.1, 133.9, 136.5, 141.1, 143.8, 151.4, 183.9$ ppm; HRMS (ESI^+): m/z calcd for $\text{C}_{21}\text{H}_{24}\text{ClN}_2\text{O}_3$ [$M+H$] $^+$: 387.1475; found: 387.1471.

Synthesis of 12be: According to GP2, compound **12be** was obtained as a colorless, amorphous powder (38 mg, 71%) from **18be** (57.0 mg, 0.132 mmol) and NaOH (15.8 mg, 0.395 mmol, 198 μ L); mp: 69–72 °C; IR (KBr): $\tilde{\nu}$ = 3422, 2945, 2477, 1718, 1606, 1474, 1402, 1211, 1078, 892, 765 cm^{-1} ; ^1H NMR (500 MHz, 0.1 M NaOD/ CD_3OD = 1:2, TPS): δ = 1.46 (ddt, J = 12.9, 8.1, 6.3 Hz, 1 H), 2.04 (dddd, J = 13.8, 9.0, 7.7, 6.6 Hz, 1 H), 2.17 (dd, J = 9.6, 7.8 Hz, 1 H), 2.22 (dd, J = 14.2, 8.0 Hz, 1 H), 2.25 (dd, J = 14.3, 7.3 Hz, 1 H), 2.47–2.62 (m, 2 H), 2.66–2.80 (m, 3 H), 2.94 (dd, J = 9.5, 7.9 Hz, 1 H), 4.21 (t, J = 5.9 Hz, 2 H), 7.26–7.38 (m, 4 H), 7.47–7.59 (m, 2 H), 7.85 (dd, J = 7.6, 1.6 Hz, 1 H), 7.92 ppm (d, J = 2.1 Hz, 1 H); ^{13}C NMR (126 MHz, 0.1 M NaOD/ CD_3OD = 1:2, TPS): δ = 33.1, 37.6, 46.2, 56.9, 57.4, 63.2, 75.3, 119.0 (d, $J_{\text{C,F}}$ = 26.3 Hz), 127.8 (d, $J_{\text{C,F}}$ = 3.6 Hz), 129.0 (d, $J_{\text{C,F}}$ = 16.2 Hz), 129.2, 131.7, 133.0, 133.2, 133.6, 135.5 (d, $J_{\text{C,F}}$ = 4.0 Hz), 137.3, 137.6 (d, $J_{\text{C,F}}$ = 10.3 Hz), 150.9, 162.2 (d, $J_{\text{C,F}}$ = 248.5 Hz), 183.9 ppm; ^{19}F NMR (376 MHz, 0.1 M NaOD/ CD_3OD = 1:2): δ = –112.6 ppm; HRMS (ESI $^+$): m/z calcd for $\text{C}_{21}\text{H}_{23}\text{FCIN}_2\text{O}_3$ [$M+H$] $^+$: 405.1376; found: 405.1374.

Synthesis of 12bf: According to GP2, compound **12bf** was obtained as a colorless, amorphous powder (19 mg, 58%) from **18bf** (32 mg, 0.071 mmol) and NaOH (8.6 mg, 0.21 mmol; 107 μ L); mp: 50–55 °C; IR (KBr): $\tilde{\nu}$ = 3422, 2942, 2794, 2462, 1702, 1586, 1466, 1203, 1101, 1069, 807, 763 cm^{-1} ; ^1H NMR (500 MHz, 0.1 M NaOD/ CD_3OD = 1:2, TPS): δ = 1.46 (ddt, J = 12.9, 8.2, 6.4 Hz, 1 H), 2.03 (dddd, J = 13.5, 8.7, 7.6, 6.5 Hz, 1 H), 2.16 (dd, J = 9.3, 8.4 Hz, 1 H), 2.21 (dd, J = 14.2, 8.0 Hz, 1 H), 2.25 (dd, J = 14.2, 7.4 Hz, 1 H), 2.44–2.58 (m, 2 H), 2.61–2.81 (m, 3 H), 2.92 (dd, J = 9.5, 7.9 Hz, 1 H), 4.18 (t, J = 5.8 Hz, 2 H), 7.20–7.25 (m, 1 H), 7.27 (d, J = 8.2 Hz, 1 H), 7.46 (dd, J = 8.2, 2.1 Hz, 1 H), 7.51 (pd, J = 7.4, 1.6 Hz, 2 H), 7.60 (d, J = 2.1 Hz, 1 H), 7.80 (s, 1 H), 7.84 ppm (dd, J = 7.6, 1.6 Hz, 1 H); ^{13}C NMR (126 MHz, 0.1 M NaOD/ CD_3OD = 1:2, TPS): δ = 37.6, 46.2, 50.3, 50.5, 50.7, 50.8, 51.0, 51.2, 51.4, 57.3, 63.2, 75.3, 129.1, 130.3, 131.6, 131.9, 132.8, 133.1, 135.4, 150.6, 183.9 ppm; HRMS (ESI $^+$): m/z calcd for $\text{C}_{21}\text{H}_{23}\text{Cl}_2\text{N}_2\text{O}_3$ [$M+H$] $^+$: 421.1080; found: 421.1079.

Synthesis of 12bj: According to GP2, compound **12bj** was obtained as a colorless, amorphous powder (20 mg, 41%) from **18bj** (48 mg, 0.11 mmol) and NaOH (13 mg, 0.33 mmol, 166 μ L); mp: 49–51 °C; IR (KBr): $\tilde{\nu}$ = 3422, 2954, 2612, 2557, 1719, 1638, 1599, 1435, 1119, 1028, 997, 840 cm^{-1} ; ^1H NMR (500 MHz, 0.1 M NaOD/ CD_3OD = 1:2, TPS): δ = 1.46 (ddt, J = 12.9, 8.0, 6.4 Hz, 1 H), 2.04 (dddd, J = 13.6, 9.2, 7.7, 6.1 Hz, 1 H), 2.16 (dd, J = 9.7, 7.7 Hz, 1 H), 2.21 (dd, J = 14.1, 8.0 Hz, 1 H), 2.25 (dd, J = 14.2, 7.5 Hz, 1 H), 2.46–2.62 (m, 2 H), 2.62–2.80 (m, 3 H), 2.93 (dd, J = 9.7, 7.8 Hz, 1 H), 4.18 (t, J = 5.8 Hz, 2 H), 6.96–7.06 (m, 2 H), 7.27–7.36 (m, 1 H), 7.49–7.61 (m, 2 H), 7.81–7.91 (m, 1 H), 7.93 ppm (s, 1 H); ^{13}C NMR (126 MHz, 0.1 M NaOD/ CD_3OD = 1:2, TPS): δ = 33.1, 37.6, 46.2, 56.9, 57.3, 63.2, 75.4, 103.9–102.3 (m), 115.9 (td, $J_{\text{C,F}}$ = 21.3, 4.8 Hz), 129.9, 130.6, 132.2, 132.8, 134.0, 134.5, 150.5, 163.1 (ddd, $J_{\text{C,F}}$ = 247.3, 15.2, 9.9 Hz), 165.7 (dt, $J_{\text{C,F}}$ = 248.8, 15.5 Hz), 171.1, 183.9 ppm; ^{19}F NMR (376 MHz, 0.1 M NaOD/ CD_3OD = 1:2): δ = –108.9 (t, J = 6.4 Hz), –111.1 ppm (d, J = 6.3 Hz); HRMS (ESI $^+$): m/z calcd for $\text{C}_{21}\text{H}_{22}\text{F}_3\text{N}_2\text{O}_3$ [$M+H$] $^+$: 407.1577; found: 407.1577.

Synthesis of 12bn: According to GP2, compound **12bn** was obtained as a colorless, amorphous powder (44 mg, 92%) from **18bn** (47 mg, 0.11 mmol) and NaOH (13 mg, 0.33 mmol); mp: 64–67 °C; IR (KBr): $\tilde{\nu}$ = 3429, 2951, 2625, 2562, 1720, 1601, 1474, 1257, 1198, 1060, 897, 765 cm^{-1} ; ^1H NMR (500 MHz, 0.1 M NaOD/ CD_3OD = 1:2, TPS): δ = 1.45 (ddt, J = 12.9, 8.1, 6.4 Hz, 1 H), 2.03 (ddt, J = 13.7, 9.4, 7.5 Hz, 1 H), 2.16 (dd, J = 9.6, 7.9 Hz, 1 H), 2.21 (dd, J = 14.3, 8.0 Hz, 1 H), 2.24 (dd, J = 14.2, 7.5 Hz, 1 H), 2.45–2.60 (m, 2 H), 2.64–2.84 (m, 3 H), 2.93 (dd, J = 9.4, 8.0 Hz, 1 H), 4.20 (t, J = 5.8 Hz, 2 H), 7.18–7.27 (m, 2 H), 7.31 (dd, J = 8.5, 6.1 Hz, 1 H), 7.38 (dd, J = 8.7, 2.6 Hz, 1 H),

7.46–7.56 (m, 2 H), 7.78 (s, 1 H), 7.86 ppm (dd, J = 7.6, 1.6 Hz, 1 H); ^{13}C NMR (126 MHz, 0.1 M NaOD/ CD_3OD = 1:2, TPS): δ = 33.1, 37.6, 46.2, 56.9, 57.3, 63.2, 75.4, 117.2 (d, $J_{\text{C,F}}$ = 21.4 Hz), 119.4 (d, $J_{\text{C,F}}$ = 25.1 Hz), 128.8, 131.5, 132.9, 133.2, 133.3, 135.6 (d, $J_{\text{C,F}}$ = 8.9 Hz), 136.8 (d, $J_{\text{C,F}}$ = 10.5 Hz), 137.8 (d, $J_{\text{C,F}}$ = 3.7 Hz), 141.2, 150.7, 165.2 (d, $J_{\text{C,F}}$ = 249.0 Hz), 183.9 ppm; ^{19}F NMR (376 MHz, 0.1 M NaOD/ CD_3OD = 1:2): δ = –113.4 ppm; HRMS (ESI $^+$): m/z calcd for $\text{C}_{21}\text{H}_{23}\text{FCIN}_2\text{O}_3$ [$M+H$] $^+$: 405.1376; found: 405.1373.

Oxime exchange experiments

Phosphate buffer (990 μ L, pH 7.1, 12.5 mM Na_2HPO_4 , 12.5 mM NaH_2PO_4 , 1 M NaCl, pH value adjusted with 1 M NaOH, 10% D_2O) was added to a solution of oxime **12ao** (0.477 mg, 1 μ mol) and **11t** (0.272 mg, 2 μ mol) in $[\text{D}_6]\text{DMSO}$ (10 μ L) in an NMR tube. ^1H NMR spectra (64 scans) were measured at 37 °C with water suppression directly after the preparation of the sample and every 4 h over a 64 h period. No changes to the spectra could be observed over the duration of the experiment.

MS binding experiments

Generation of pre-equilibrated libraries: To obtain **10** as a free base, an aqueous solution of NaOH (1 M, 2.0 equiv) in phosphate buffer (pH 6.0, 12.5 mM Na_2HPO_4 , 12.5 mM NaH_2PO_4 , 1 M NaCl, pH value adjusted with 1 M HCl) was added to **10** as a dihydrochloride salt dissolved in phosphate buffer (pH 6.0) to a nominal concentration of 400 mM of **10**. This solution (10 μ L) was added to a mixture containing eight solutions of individual aldehydes in DMSO (20 mM, 5 μ L each) and phosphate buffer (pH 6.0, 50 μ L). These library mixtures were incubated for 20 h at 37 °C in a shaking water bath to guarantee full conversion into the corresponding oximes. Before binding experiments, all pre-equilibrated libraries were freshly diluted with phosphate buffer at pH 7.1 (12.5 mM Na_2HPO_4 , 12.5 mM NaH_2PO_4 , 1 M NaCl, pH value adjusted with 1 M NaOH) and DMSO to obtain the generated oximes in final concentrations of 10 μ M (1st experiment), 1 μ M (2nd experiment), and 100 nM (3rd experiment) in phosphate buffer (pH 7.1) containing 10% DMSO (v/v).

Generation of pre-equilibrated single oximes for deconvolution experiments: The pre-equilibrated single oximes for deconvolution were obtained in the same way as that described for pre-equilibrated libraries, except that one solution of a single aldehyde in DMSO (20 mM, 5 μ L) and additional DMSO (35 μ L) were used. Before binding experiments, all pre-equilibrated deconvolution batches were freshly diluted with phosphate buffer at pH 7.1 (12.5 mM Na_2HPO_4 , 12.5 mM NaH_2PO_4 , 1 M NaCl, pH value adjusted with 1 M NaOH) and DMSO to obtain the generated oximes in final concentrations of 1 μ M in phosphate buffer (pH 7.1) containing 10% DMSO.

Aldehyde libraries: Aldehyde libraries were obtained by dissolving eight individual aldehydes in phosphate buffer (pH 7.1) containing 10% DMSO to obtain final concentrations of 10 μ M (1st experiment), 1 μ M (2nd experiment), or 100 nM (3rd experiment).

mGAT1 membrane preparation: Membrane preparations of HEK293 cells stably expressing mGAT1 $^{[18]}$ were prepared as described previously and stored at –80 °C. $^{[24,31]}$ On the day of the assay, an aliquot was rapidly thawed and diluted in a 20-fold volume of a cold 0.9% (m/v) aqueous solution of NaCl. After centrifugation at 20500 rpm and 4 °C for 20 min (CP56GII, P70AT, Hitachi Ltd., Tokyo, Japan), the resulting pellet was resuspended in ice-

cold phosphate buffer at pH 7.1 to a protein concentration of approximately 0.1 mg mL^{-1} , as previously described.^[31]

Library screening: Library screening was performed in 1.2 mL polypropylene deep-well plates (Sarstedt, Nümbrecht, Germany) analogously to a procedure previously described.^[19,23] Samples ($n = 4$) were prepared in phosphate buffer (pH 7.1) with 1% DMSO in total volume of 250 μL per sample containing the mGAT1 membrane preparation (50 μL , approximately 20 μg protein per sample, see above), NO711 (25 μL , final concentration in the assay 20 nM), and the pre-equilibrated libraries (25 μL ; final concentration one-tenth of the corresponding stock solution containing the pre-equilibrated libraries, as described above) and incubated for 4 h at 37 °C in a shaking water bath. Incubation was stopped by transferring aliquots (200 μL) of each sample to a 96-well filter plate (Acroprep Advance, glass fiber, 1.0 μm , 350 μL , Pall, Dreieich, Germany) with a 12-channel pipette followed by subsequent vacuum filtration. After washing with an ice-cold aqueous solution of NaCl (1 M, $5 \times 150 \mu\text{L}$ per well) by using a 12-channel pipette, the filter plate was dried (60 min, 50 °C) and cooled to room temperature. Subsequently, the marker was liberated by elution of the filter plate with MeOH ($3 \times 100 \mu\text{L}$ per well) into a 1.2 mL polypropylene 96-well plate (Sarstedt, Nümbrecht, Germany). Each sample was supplemented with 1 nM [$^2\text{H}_{10}$]NO711 (200 μL , in MeOH) as an internal standard. All samples were completely dried (17 h, 50 °C). For quantification by means of LC–MS/MS (ESI), samples were reconstituted in 10 mM ammonium formate buffer (200 μL ; pH 7.0/MeOH (95:5 v/v)). In the same way, aldehyde libraries (see above) and **10** (final concentrations in the assay 40 μM , 4 μM , or 400 nM) were investigated. Total binding and nonspecific binding of NO711 were determined in analogously constituted samples lacking any inhibitor or in the presence of 100 mM GABA, respectively.

Deconvolution: The experiments were performed in the same manner as the experiments described for the library screening, expect that an aliquot (25 μL) of a pre-equilibrated batch of a single oxime was employed.

LC–MS/MS (ESI) analysis: Quantification of NO711 by means of LC–MS/MS (ESI) was performed as described by using an API 3200 triple-quadrupole mass spectrometer.^[24,31] To assure reliable quantification, each day a binding experiment was performed, also matrix blanks (generated analogously to that described for binding samples, but in the absence of NO711 and [$^2\text{H}_{10}$]NO711), a zero sample (matrix blank with 1 nM [$^2\text{H}_{10}$]NO711) and matrix standards (generated by supplementing matrix blanks with different concentrations of NO711 (50 μM , 100 μM , 200 μM , 500 μM , 1 nM, 2.5 nM, and 5 nM) and [$^2\text{H}_{10}$]NO711 (1 nM) were investigated and individual calibration curves for marker quantification were generated therefrom. Derived from the external calibration curve, the LLOQ could be determined to 50 μM and results below this limit were described as < LLOQ in Table 1.^[19,23]

Competition experiments with isolated oximes: The experiments were performed as described recently, but substituting the original incubation buffer for phosphate buffer (pH 7.1, 12.5 mM Na_2HPO_4 , 12.5 mM NaH_2PO_4 , 1 M NaCl, pH value adjusted with 2 M NaOH).^[24,31]

Analysis of competitive binding experiments: Marker depletion was negligible (< 10%) in all binding experiments. Specific binding was defined as the difference between the total and nonspecific binding. Nonspecific binding less than 50 μM (LLOQ) was not determined experimentally, but was extrapolated by linear regression from nonspecifically bound NO711 concentrations of $\geq 50 \mu\text{M}$. The concentration of a competitor that inhibited 50% of specific bind-

ing (IC_{50}) was calculated from competition curves by plotting NO711 specific binding concentrations versus the log of competitor concentration (eight different concentrations per competitor) with Prism 5.04 (GraphPad Software, San Diego, CA, USA) by using the equation for one-site competition and nonlinear curve fitting. Specific binding determined for control samples in the absence of any competitor was set to 100%, whereas the bottom level was set to 0% (corresponding to the nonspecific binding of NO711). K_i values were calculated according to a report by Cheng and Prusoff and expressed as $\text{p}K_i$ values.^[32] All results were expressed as the mean \pm SEM (unless stated otherwise). $\text{p}K_i$ values were determined in at least three separate experiments.

GABA uptake assays: [^3H]GABA uptake assays were performed as previously described.^[18]

Acknowledgements

We gratefully thank Dr. Marc Marull and Dr. Markus Betz for the synthesis of 3-(2-ethoxy-2-oxoethyl)pyrrolidin-1-ium acetate (**14**). Special thanks go to Silke Duesing-Kropp and Miriam Sandner for excellent technical support.

Conflict of interest

The authors declare no conflict of interest.

Keywords: binding assays • high-throughput screening • inhibitors • mass spectrometry • oximes

- [1] GBD 2015 Neurological Disorder Collaborator Group, *Lancet Neurol.* **2017**, *16*, 877–897.
- [2] J. Aarli, D. Tarun, A. Janca, A. Muscetta, *Neurological Disorders: Public Health Challenges*, World Health Organization, Geneva, **2006**.
- [3] A. V. Kalueff, D. J. Nutt, *Depression Anxiety* **2007**, *24*, 495–517.
- [4] D. M. Treiman, *Epilepsia* **2001**, *42*, 8–12.
- [5] a) K. L. Lancôt, N. Herrmann, P. Mazzotta, L. R. Khan, N. Ingber, *Can. J. Psychiatry* **2004**, *49*, 439–453; b) R. A. Rissmann, A. L. De Blas, D. M. Armstrong, *J. Neurochem.* **2007**, *103*, 1285–1292.
- [6] P. Krogsgaard-Larsen, E. Falch, O. M. Larsson, A. Schousboe, *Epilepsy Res.* **1987**, *1*, 77–93.
- [7] K. K. Madsen, P. C. Rasmus, O. M. Larsson, P. Krogsgaard-Larsen, A. Schousboe, H. S. White, *J. Neurochem.* **2009**, *109*, 139–144.
- [8] Y. Zhou, S. Holmseth, C. Guo, B. Hassel, G. Höfner, H. S. Huitfeldt, K. T. Wanner, N. C. Danbolt, *J. Biol. Chem.* **2012**, *287*, 35733–35746.
- [9] Y. Zhou, S. Holmseth, R. Hua, A. C. Lehre, A. M. Olofsson, I. Poblete-Naredo, S. A. Kempson, N. C. Danbolt, *Am. J. Physiol. Renal. Physiol.* **2012**, *302*, F316–F328.
- [10] K. K. Madsen, H. S. White, A. Schousboe, *Pharmacol. Ther.* **2010**, *125*, 394–401.
- [11] P. Krogsgaard-Larsen, G. A. R. Johnston, *J. Neurochem.* **1975**, *25*, 797–802.
- [12] O. M. Larsson, P. Thorbek, P. Krogsgaard-Larsen, A. Schousboe, *J. Neurochem.* **1981**, *37*, 1509–1516.
- [13] T. Wein, K. T. Wanner, *J. Mol. Model.* **2010**, *16*, 155–161.
- [14] T. Hellenbrand, G. Höfner, T. Wein, K. T. Wanner, *Bioorg. Med. Chem.* **2016**, *24*, 2072–2096.
- [15] T. Wein, M. Petrera, L. Allmendinger, G. Höfner, J. Pabel, K. T. Wanner, *ChemMedChem* **2016**, *11*, 509–518.
- [16] The pIC_{50} values were determined by using the [^3H]GABA uptake assay in three independent experiments, as described in ref. [18].
- [17] a) E. B. Nielsen, P. D. Suzdak, K. E. Andersen, L. J. Knutsen, U. Sonnewald, C. Braestrup, *Eur. J. Pharmacol.* **1991**, *196*, 257–266; b) B. S. Meldrum, A. G. Chapman, *Epilepsia* **1999**, *40*, S2–S6.

- [18] A. Kragler, G. Höfner, K. T. Wanner, *Eur. J. Med. Chem.* **2008**, *43*, 2404–2411.
- [19] F. T. Kern, K. T. Wanner, *ChemMedChem* **2015**, *10*, 396–410.
- [20] K. Sałat, A. Podkowa, N. Malikowska, F. Kern, J. Pabel, E. Wojcieszak, K. Kulig, K. T. Wanner, B. Strach, E. Wyska, *Neuropharmacology* **2017**, *113*, 331–342.
- [21] W. E. Bondinell, J. J. Lafferty, C. L. Zirkle (Smithkline Beckman Corporation, Philadelphia, USA), US Pat. No. US4514414, **1985**.
- [22] F. E. Ali, W. E. Bondinell, P. A. Dandridge, J. S. Frazee, E. Garvey, G. R. Girard, C. Kaiser, T. W. Ku, J. J. Lafferty, G. I. Moonsammy, H. Oh, J. A. Rush, S. E. Setler, O. D. Stringer, J. W. Venslavsky, B. W. Volpe, L. M. Yunker, C. L. Zirkle, *J. Med. Chem.* **1985**, *28*, 653–660.
- [23] M. Sindelar, K. T. Wanner, *ChemMedChem* **2012**, *7*, 1678–1690.
- [24] C. Zepperitz, G. Höfner, K. T. Wanner, *ChemMedChem* **2006**, *1*, 208–217.
- [25] a) H. Brunner, M. Schönherr, M. Zabel, *Tetrahedron: Asymmetry* **2001**, *12*, 2671–2675; b) J. Kalia, R. T. Raines, *Angew. Chem. Int. Ed.* **2008**, *47*, 7523–7526; *Angew. Chem.* **2008**, *120*, 7633–7636.
- [26] W. J. Kim, M. H. Park, J. D. Ha, K. U. Baik (Korea Research Institute of Chemical Technology, Daejeon, Korea), Eur. Pat. No. EP0550025 A1, **1992**.
- [27] K. E. Andersen, J. Lau, B. F. Lundt, H. Petersen, P. O. Huusfeldt, P. D. Suzdak, M. D. B. Swedberg, *Bioorg. Med. Chem.* **2001**, *9*, 2773–2785.
- [28] M. Sindelar, T. A. Lutz, M. Petrera, K. T. Wanner, *J. Med. Chem.* **2013**, *56*, 1323–1340.
- [29] H. Irngartinger, T. Escher, *Tetrahedron* **1999**, *55*, 10753–10760.
- [30] G. F. Pauli, S.-N. Chen, C. Simmler, D. C. Lankin, T. Gödecke, B. U. Jaki, J. B. Friesen, J. B. McAlpine, J. G. Napolitano, *J. Med. Chem.* **2014**, *57*, 9220–9231.
- [31] C. Zepperitz, G. Höfner, K. T. Wanner, *Anal. Bioanal. Chem.* **2008**, *391*, 309–316.
- [32] Y.-C. Cheng, W. H. Prusoff, *Biochem. Pharmacol.* **1973**, *22*, 3099–3108.

Manuscript received: August 16, 2018

Version of record online: November 28, 2018

3.3 Third Publication

Application of the Concept of Oxime Library Screening by Mass Spectrometry (MS) Binding Assays to Pyrrolidine-3-carboxylic Acid Derivatives as Potential Inhibitors of γ -Aminobutyric Acid Transporter 1 (GAT1)

3.3.1 Summary of the Results

Various publications about differently affine inhibitors for mGAT1 with nipecotic acid or guvacine motif are known, but with regard to compounds delineated from other amino acid moieties only few information is published so far. To reduce this gap of information, the concept of oxime library screening by means of LC-MS/MS binding assays was transferred to substances with a pyrrolidine-3-carboxylic acid substructure.

The desired oximes libraries were prepared by reaction of 28 sub-libraries with eight different aldehydes (1 mM each) with an excess of an pyrrolidine-3-carboxylic acid derivative possessing a hydroxylamine functionality (40 mM) which had been synthesized in six steps with an overall yield of 43 %. The oxime library generation was accomplished in the absence of the target mGAT1 at 37 °C for 20 h using a non-physiological buffer system with a pH value of 6.0 (12.5 mM Na₂HPO₄, 12.5 mM NaH₂PO₄, 1 M NaCl, pH value was adjusted with 1 M HCl) containing 40 % DMSO. The completion of oxime formation was verified exemplarily by ¹H NMR measurements. Only three sterically highly demanding tritylaldehydes of one library were not fully converted to the corresponding oximes within the reaction time of 20 h, but after raising the reaction temperature to 80 °C the oximes were successfully formed within 45 h.

After formation, all 28 freshly prepared oxime libraries were diluted with phosphate buffer pH 7.1 (12.5 mM Na₂HPO₄, 12.5 mM NaH₂PO₄, 1 M NaCl, pH value was adjusted with 1 M NaOH) to the desired screening concentration level of 1 μ M. In the MS Binding Assay, eight libraries were able to reduce the specific marker binding under 50 % and three libraries still reduced the marker binding below 20 % which corresponds to an IC₅₀ value of 250 nM at the concentration of 1 μ M if only one oxime is responsible for the affinity. In order to identify the most potent oximes these three oxime libraries were forwarded to the next step – the deconvolution experiments.

Therefore, each single oxime of the three active libraries was generated by reacting the respective aldehydes (1 mM) with an excess of hydroxylamine (40 mM) under conditions identical to these applied for oxime library formation. After dilution of the thus generated samples to the concentration of 1 μ M applied in the screening assay with phosphate buffer pH 7.1 the performed MS Binding Assays revealed that none of the single oximes was able to reduce marker binding to 20 % and only one compound was able to reach the limit of 50 %

Results and Discussion

marker binding. Hence, the three most potent oximes effecting the lowest remaining marker binding in the three sub-libraries were selected for resynthesis and determination of their binding affinities in full-scale competitive MS binding assays. Furthermore, their inhibitory activities in [^3H]GABA uptake assays at all four GABA transporter subtypes (mGAT1-4) and thus their subtype selectivities were determined. All three compounds were found to contain a 1,1'-biphenyl moiety with different substituents at the terminal phenyl ring. The oximes derivatives with a 2',4'-dichloro ($pK_i = 6.41 \pm 0.02$) and a 2'-methoxy-4'-fluoro substitution ($pK_i = 6.39 \pm 0.03$) yielded the highest pK_i values. When exchanging the chlorine in the 4'-position of the 2',4'-dichloro derivative with a fluorine the affinity is reduced to a pK_i values of 6.16 ± 0.03 . Interestingly, when compared to the corresponding oximes with 2-(pyrrolidin-3-yl)acetic acid motif for the three substances all determined pK_i values were lower. For the 2',4'-dichloro substituted oxime the difference amounts to approximately 1.5 log unit, but for the 2'-methoxy-4'-fluorine derivative with pyrrolidine-3-carboxylic acid moiety the pK_i value is roughly 0.7 log units lower indicating that substitution with a methoxy group has a favorable effect on the affinity for pyrrolidine-3-carboxylic acid derivatives. The pIC_{50} values for mGAT1 of the [^3H]GABA uptake assays confirmed the affinity towards the target and pIC_{50} values for mGAT2 – mGAT4 showed high subtype selectivity regarding mGAT1.

Overall, three oximes with pK_i values between 6.16 and 6.41 with a pyrrolidine-3-carboxylic acid motif were identified and structure-activity-relationships for mGAT1 inhibition were expanded in particular with regard to the amino acid moiety.

3.3.2 Declaration of Contribution

Synthesis of the hydroxylamine derivative as a starting material for the oxime generation, all precursor molecules and the compounds for the biological testing as well as the evaluation of all corresponding analytical data were accomplished by myself. Some aldehydes were synthesized by Hans Brabec during his bachelor thesis "*Synthese neuer Aldehyde mit Biaryl-Struktur mittels Suzuki-Miyaura-Kupplung*" which was supervised by me and Tobias Hauke. NMR studies on the subject of kinetics and oxime exchange experiment were performed together with Dr. Lars Allmendinger and Claudia Glas. All binding experiments regarding library screening and deconvolution experiments were achieved and evaluated by me. pK_i values and pIC_{50} values were determined by the technical assistants Silke Duesing-Kropp and Miriam Sandner under the supervision of Dr. Georg Höfner. I wrote the manuscript and prepared all graphics and tables, supported by Dr. Lars Allmendinger. Prof. Dr. Klaus T. Wanner corrected the manuscript.

Application of the Concept of Oxime Library Screening by Mass Spectrometry (MS) Binding Assays to Pyrrolidine-3-carboxylic Acid Derivatives as Potential Inhibitors of γ -Aminobutyric Acid Transporter 1 (GAT1)

Simone K. Huber, Georg Höfner, and Klaus T. Wanner*

Department of Pharmacy – Center of Drug Research, Ludwig Maximilians-Universität München, Butenandtstr. 7, 81377 Munich, Germany

*corresponding author. E-mail address: klaus.wanner@cup.uni-muenchen.de

Abstract

In the present study, the concept of oxime library screening by MS Binding Assays was successfully extended to N-substituted lipophilic pyrrolidine-3-carboxylic acid derivatives in the pursuit of varying the amino acid motif in order to identify new inhibitors for GAT1 and to broaden structure-activity-relationships for this target, the most abundant GABA transporter in the central nervous system. For the screening, 28 different oxime sub-libraries were employed that were generated by simple condensation reaction of an excess of pyrrolidine-3-carboxylic acid derivatives carrying a hydroxylamine functionality with various sub-libraries each assembled of eight aldehydes with broadly varying chemical structures and functionalities. The compounds responsible for the activity of an oxime sub-library were identified by deconvolution experiments performed by employing single oximes. Binding affinities of the oxime hits were confirmed in full-scale competitive MS Binding Assays. Thereby, oxime derivatives with a 1,1'-biphenyl moiety were found as the first inhibitors of mGAT1 comprising a pyrrolidine-3-carboxylic acid motif with affinities in the submicromolar range.

1. Introduction

γ -Aminobutyric acid (GABA) is the major inhibitory neurotransmitter in the mammalian central nervous system (CNS).¹ A decreased GABAergic signaling and the resulting imbalance between excitatory neurotransmission effected by glutamate and inhibitory neurotransmission mediated by GABA² is assumed to be the cause for severe neurological diseases such as epilepsy³, Alzheimer's disease⁴, or depression⁵. Hence, as a rational approach for the treatment of the above mentioned diseases, the membrane bound GABA transporters (GATs) responsible for the reuptake of GABA in the presynaptic neurons and glia cells to enhance the level of GABA in the synaptic cleft may be blocked.⁶

The GABA transporter proteins exist in four different subtypes which are termed mGAT1, mGAT2, mGAT3, and mGAT4 when cloned from mice,⁷ whereas according to the Human Genome Organization (HUGO)⁸, they are indicated as GAT1 (=mGAT1), BGT1 (=mGAT2), GAT2 (=mGAT3), and GAT3 (=mGAT4). Of these, only mGAT1 and mGAT4 are found in the CNS in densities high enough to play a significant role in the determination of GABAergic

neurotransmission. Thereby, mGAT1 is the predominant GABA transporter located in neurons and mGAT4 is mainly responsible for the reuptake of GABA in glia cells.⁹ Being predominantly expressed in the kidney and liver and only in very low densities and in specific areas of the brain, mGAT2 and mGAT3 are not likely to be notably involved in termination of GABAergic neurotransmission in the CNS.¹⁰

Some cyclic analogues of GABA including 6-membered amino acids like nipecotic acid (**1**)¹¹ or 5-membered amino acids such as 2-(pyrrolidin-3-yl)acetic acid (**2**)¹² and pyrrolidine-3-carboxylic acid (**3**)¹³ have been found to be potent inhibitors of mGAT1. Although these small amino acids reveal good functional activities at the target mGAT1 with 2-(pyrrolidin-3-yl)acetic acid as the most potent inhibitor among these amino acids ($pIC_{50} = 5.39 \pm 0.05$ in [³H]GABA uptake assays, Figure 1)¹⁴ followed by nipecotic acid ($pIC_{50} = 4.88 \pm 0.07$, Figure 1)¹⁵ and pyrrolidine-3-carboxylic acid ($pIC_{50} = 4.17 \pm 0.06$, Figure 1)¹⁶, their benefit for pharmacological treatment is limited due to their inability to cross the blood brain barrier. Derivatives of nipecotic acid and of the related unsaturated amino acid guvacine bearing aromatic residues linked with an all carbon or heteroatom carbon chain to the amino nitrogen appeared to possess in addition to an increased lipophilicity also an improved membrane permeability. For example, tiagabine (**4**) ($pIC_{50} = 6.88 \pm 0.12$, Figure 1)¹⁷, which is in clinical use for the treatment of epilepsy and NO711 (**5**) ($pIC_{50} = 6.83 \pm 0.06$, Figure 1),¹⁸ a widely used experimental drug with an oxime functionality in the alkyl chain are selective inhibitors for mGAT1 with substantially enhanced inhibitory activity and known to be capable of passing the blood brain barrier.

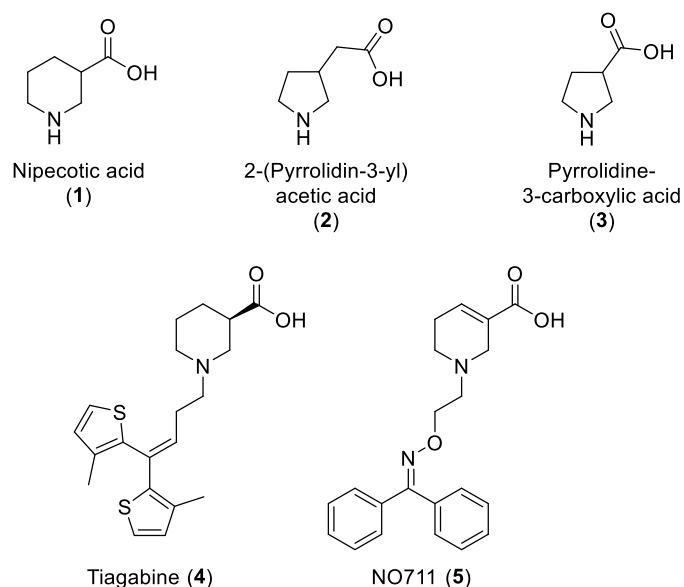
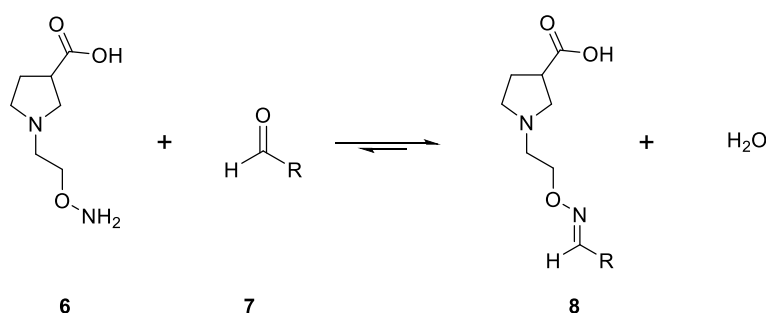


Figure 1: Selected potent inhibitors of mGAT1.

A whole plethora of additional substances with mainly nipecotic acid and guvacine as polar subunit have been developed. These are varying with respect to the structure of aromatic residues, substituents, and the length and the functionalities embedded in the linkers,¹⁹ providing a tremendous amount of information regarding structure-activity-relationships

(SARs) of mGAT1 ligands.²⁰ However, when it comes to SARs for mGAT1 inhibitors derived from amino acid moieties different from nipecotic acid (**1**) and guvacine, some, but only a limited amount of literature has yet been published which is for example true for 2-(pyrrolidin-3-yl)acetic acid (**2**) derived inhibitors¹⁴, but in the case of compounds with a pyrrolidine-3-carboxylic acid (**3**) subunit no publication is known so far.

Hence, in the present study, we aimed at the generation of SARs for pyrrolidine-3-carboxylic acid (**3**) derived mGAT1 inhibitors by an extensive variation of the lipophilic domain linked to the amino acid subunit. To this end, a concept for combinatorial screening developed by us and used for the identification of potent inhibitors with a guvacine²¹ and 2-(pyrrolidin-3-yl)acetic acid¹⁴ subunit should be followed. This method comprises the generation of oxime sub-libraries and their screening by means of competitive mGAT1 MS Binding Assays.²² In the present case, the hydroxylamine containing pyrrolidine-3-carboxylic acid **6** should be reacted with a set of sub-libraries containing various aldehydes to give the corresponding oxime sub-libraries as outlined in Scheme 1 and thus giving easy access to a broad variety of potential mGAT1 inhibitors.



Scheme 1: Reaction of hydroxylamine derivative **6** with sub-libraries containing various aldehydes **7** possessing different lipophilic residues to afford corresponding oximes **8**.

As in related studies, also here competitive MS Binding Assays for mGAT1 with NO711 (**5**) as MS marker²³ should be used to determine the binding affinities²⁴ of the individual compound sub-libraries.

In analogy to the screening of oxime sub-libraries derived from 2-(pyrrolidin-3-yl)acetic acid (**2**),¹⁴ in this study oximes sub-libraries should be generated by employing sub-libraries with eight different aldehydes in the absence of the target, mGAT1, to allow the use of a non-physiological buffer system with a pH of 6.0 required for oxime formation in a reasonable period of time. Of course appropriate studies had to be performed to warrant completion of sub-library generation within the set time frame and also to ascertain the stability of the generated oximes over the incubation period. The oxime sub-libraries found most potent during the library screening would have to be subjected to deconvolution experiments, i.e. tests of single oximes in the same manner as the sub-library to identify hit compounds. For hit validation, the respective oximes should be resynthesized and characterized in full-scale competitive MS

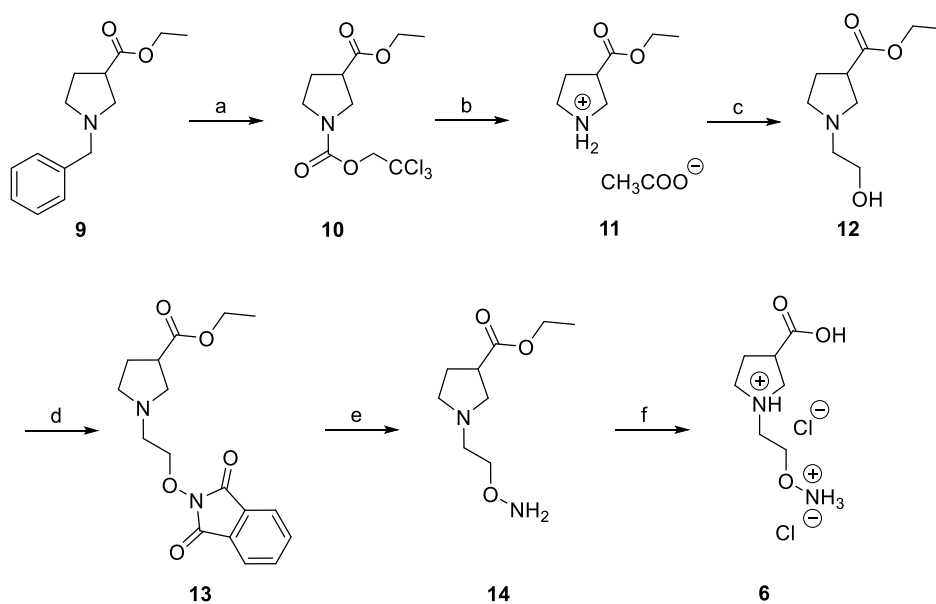
Binding Assays²⁴ providing their pK_i values as well as in [^3H]GABA uptake assays¹⁸ for all four murine GABA transporters to gain insights in their functional activity (pIC_{50} values) at mGAT1–4. All in all, by this MS Binding Assays based screening of easily to generate oxime sub-libraries an extension of structure-activity-relationships of pyrrolidine-3-carboxylic acid (**3**) derived mGAT1 inhibitors should be achieved.

2. Results and Discussion

2.1. Chemistry

2.1.1. Synthesis of hydroxylamine building block **6**

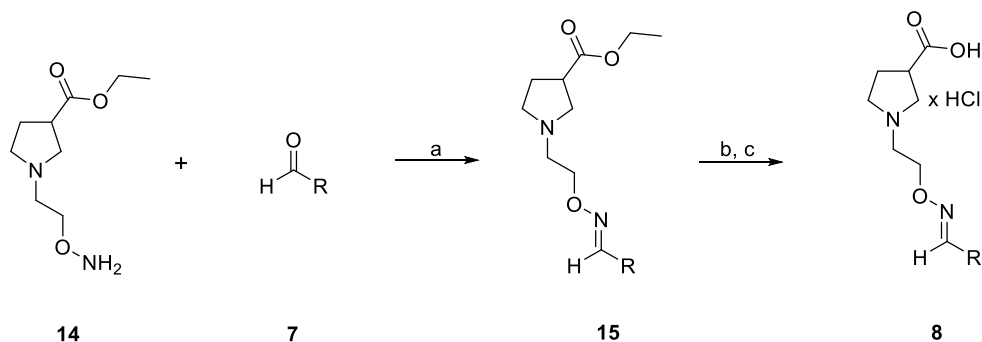
Synthesis of hydroxylamine **6** was accomplished according to the synthetic sequence outlined in Scheme 2. At first, the benzyl protecting group of the pyrrolidine-3-carboxylic acid ester **9**²⁵ was substituted by a Troc protecting group using 2,2,2-trichloroethyl chloroformate to generate **10** (yield 90%), which upon subsequent deprotection of **10** with zinc powder in acetic acid afforded pyrrolidine-3-carboxylic acid ethylester **11** as acetate salt in high yield (87%). According to literature²⁶, this two-step procedure is required for the deprotection of the amino nitrogen in **9** as a hydrogenolytic procedure employing Pd/C as catalyst for the direct removal of the benzyl moiety gives rise to extensive decomposition. Employing **11** in a nucleophilic substitution reaction at 2-bromoethanol furnished alcohol **12** (yield 76%) which when subjected to a Mitsunobu reaction with *N*-hydroxyphthalimide as nucleophile in the presence of di(2-methoxyethyl)azodicarboxylate (DMEAD) and triphenylphosphine provided the corresponding *N*-hydroxyphthalimide derivative **13** in very good yield (83%). Upon purification by flash column chromatography, **13** appeared to be hydrolytically labile. This problem could, however, be overcome when pre-dried silica gel was used (145 °C for 5 hours *in vacuo*). Treatment of **13** with aqueous hydrazine solution to remove the phthalic acid protecting group afforded hydroxylamine **14**, which was finally subjected to carboxylic acid ester hydrolysis by treatment with 1 M HCl to give 1-[2-(aminooxy)ethyl]pyrrolidine-3-carboxylic acid (**6**) as dihydrochloride salt with an overall yield of 43% over six steps.



Scheme 2: Synthesis of 1-[2-(aminooxy)ethyl]pyrrolidine-3-carboxylic acid (**6**) as dihydrochloride. Reagents and conditions: (a) 2,2,2-trichloroethyl chloroformate, K_2CO_3 , CH_3CN , 60 °C, 3 h, 90%; (b) Zn, AcOH, rt, 4 h, 87%; (c) 2-bromoethanol, K_2CO_3 , KI, THF, 24 h, reflux, 76%; (d) *N*-hydroxyphthalimide, PPh_3 , DMEAD, THF, 20 h, rt, 81%; (e) hydrazine (50–60% solution), EtOH, 2 h, rt, 92%; (f) aq. HCl (1 M), 3 h, 90 °C, 97%.

2.1.2. Synthesis of oximes **8**

The individual oximes required for further hit characterization in MS Binding Assays (pK_i) and [3H]GABA uptake studies (pIC_{50}) were synthesized as described in Scheme 3 in analogy to the recently published approaches.^{14,21} Hence, hydroxylamine **14** was reacted with a single aldehyde, which gave the respective oxime **15** as an *E/Z*-mixture. The *E*-isomer as the major isomer (amount of *Z*-isomer was approximately 2–7% compared to *E*-isomer) was isolated via column chromatography followed by alkaline hydrolysis of the ester function using aqueous NaOH solution (2 M) in EtOH. Finally, acidification with aqueous HCl solution and extraction with dichloromethane yielded the desired oximes **8** as hydrochloric acid salts.²⁷



Scheme 3: Synthesis of oximes **8**. (a) abs. EtOH, rt, 18 h, 69–81%; (b) aq. NaOH (2 M), EtOH, rt, 24 h; (c) aq. HCl (2 M) then CH_2Cl_2 , 70–89% (over two steps).^{14,22,27}

2.1.3. Aldehydes **7**

Aldehydes required for the formation of the oxime sub-libraries 1–28 (see e.g. sub-library 8, Scheme 4) were either purchased from Sigma Aldrich (Steinheim, Germany), TCI (Zwijndrecht, Belgium), Acros (Geel, Belgium), or ABCR (Karlsruhe, Germany) and used without further purification or synthesized via Suzuki-Miyaura coupling according to the method published previously.^{28,29,30} Aldehydes applied for the oxime generation and screening have been grouped in aldehyde sub-libraries 1–28, which are given in Figure 2 and each of which contains eight constituents.

Third publication

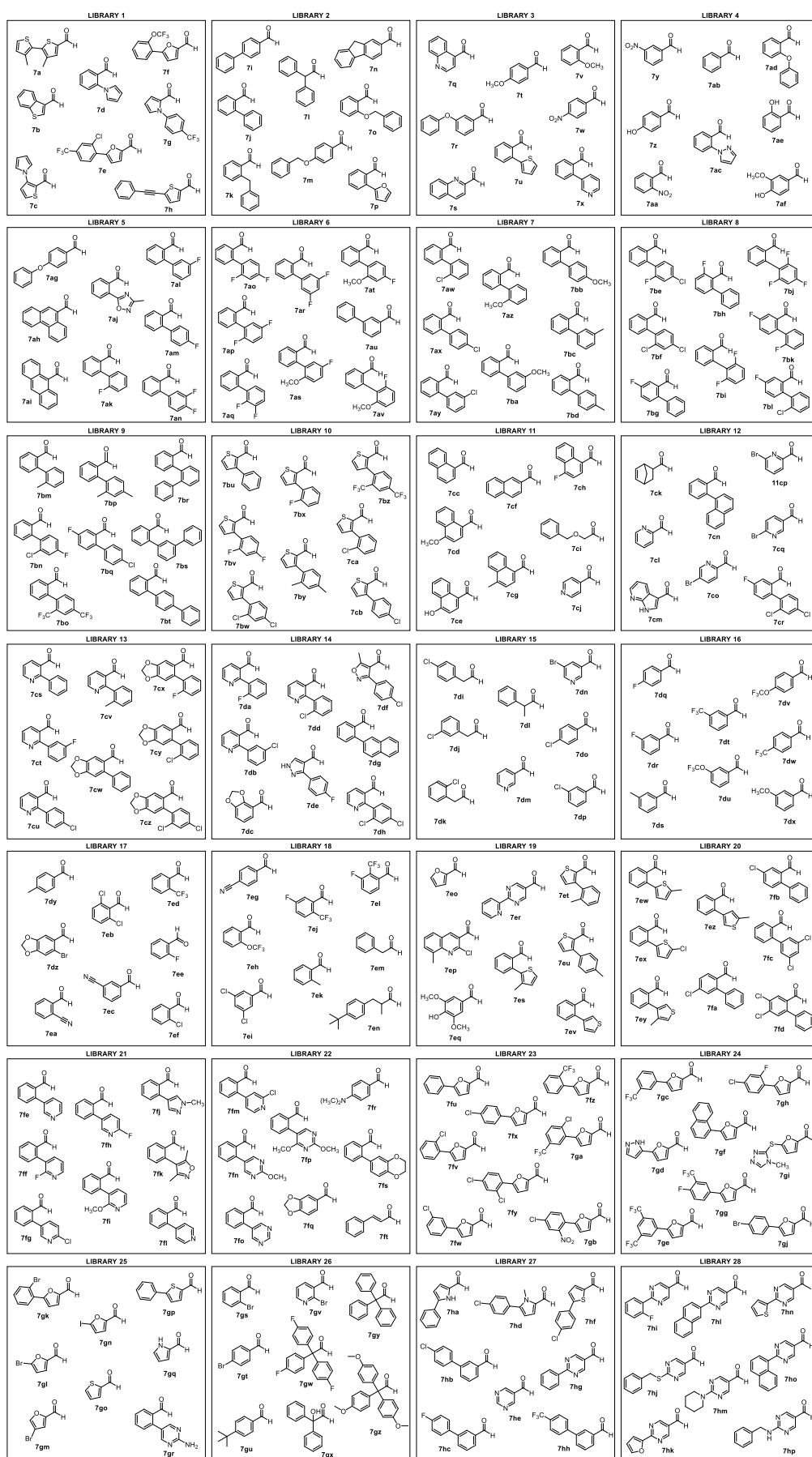
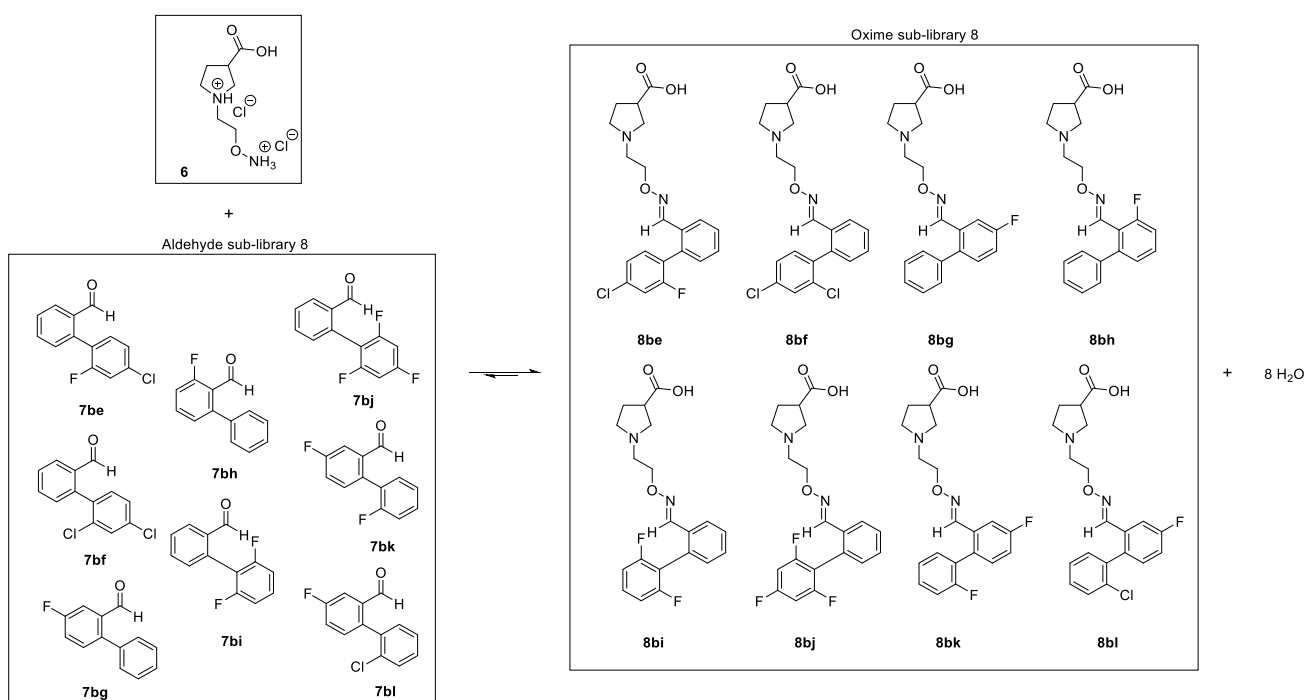


Figure 2: Aldehyde sub-libraries 1–28 which were employed for oxime sub-library generation and subsequent screening experiments.

2.2. Library screening employing LC-MS/MS Binding Assays

2.2.1. Sub-library generation

For the generation of the oxime sub-libraries, which was performed in the absence of the target mGAT1, an excess of pyrrolidine-3-carboxylic acid derived hydroxylamine **6** (40 mM) was reacted with the individual aldehyde sub-libraries (1 mM each) at 37 °C in a 6:4 mixture of phosphate buffer (pH 6.0, 12.5 mM Na₂HPO₄, 12.5 mM NaH₂PO₄, 1 M NaCl, pH value was adjusted with 1 M HCl) and DMSO as exemplarily displayed in Scheme 4. The aldehyde sub-libraries 1–28 employed in the present study were identical with those used in a former related study¹⁴, each containing the same eight constituents overall representing a broad variety of different chemical structures (Scheme 4). As attempts to purify and liberate the free hydroxylamine from its dihydrochloride salt by ion-exchange chromatography using aqueous ammonia solution as eluent led to decomposition of the compound, the dihydrochloride derivative **6** was directly employed for oxime generation, however, two equivalents of sodium hydroxide were added to reaction mixture (phosphate buffer, pH 6.0, DMSO = 6:4) to compensate for the two acid equivalents from the disalt **6**.



Scheme 4: Exemplary chosen reaction of hydroxylamine derivative **6** with aldehyde sub-library 8 containing of eight different aldehydes to yield corresponding oxime sub-library 8.

As verified by ¹H NMR spectroscopy studies, oxime formation was complete within 20 h at 37 °C applying the mentioned buffer system and a reactant ratio of 5:1

(hydroxylamine/aldehydes). This, however, did not apply for sub-library 26 containing the three sterically highly encumbered tritylaldehydes **7gw**, **7gy**, and **7gz**. As these did not show any significant sign of oxime formation within the defined time, the reaction temperature was risen to 80 °C, while leaving all other parameters unchanged. Oxime formation was then completed within 45 h.

The thus generated oxime sub-libraries were finally diluted to a concentration of 1 µM for individual oximes present in the sub-library with phosphate buffer (pH 7.1, 12.5 mM Na₂HPO₄, 12.5 mM NaH₂PO₄, 1 M NaCl, pH value was adjusted with 1 M NaOH). That way also the DMSO content was reduced to ≤ 1%, thus matching conditions found earlier to be suitable for the incubation with the target mGAT1 (performed at 37 °C for 4 h).^{14,21} According to fluorescence spectroscopy measurements performed with single oximes generated with an excess of hydroxylamine as described before and diluted to the test concentration of 1 µM, the test compounds are stable over the incubation time of 4 h as no change of the intensity of the fluorescence signal occurs. Furthermore, exemplarily an oxime exchange experiment using ¹H NMR spectroscopy was performed to determine the stability of oximes in the presence of a competing free aldehyde. For this purpose, 4-methoxybenzaldehyde **7t** (2 mM) was added to a solution of oxime **8av** (1 mM) in phosphate buffer pH 7.1 (12.5 mM Na₂HPO₄, 12.5 mM NaH₂PO₄, 1 M NaCl, 10% D₂O) in an NMR tube kept at 37 °C. No change over a period of 64 h of repeatedly taken NMR spectra occurred indicating that no exchange reaction took place.

2.2.2. Sub-library screening

For the determination of the activity of the oxime sub-libraries in competitive MS Binding Assays, the freshly diluted oxime sub-libraries were incubated with the target mGAT1 (10–20 µg protein per sample in 250 µL) and the MS marker NO711 (final concentration in the assay 20 nM) for 4 h at 37 °C. Thereafter, the protein-ligand-complexes were separated from the non-bound components by filtration and were dried for 1 h at 50 °C to improve the efficiency of the subsequent step, i.e. the treatment of the filter plates to denature protein-ligand complexes and elute the formerly bound MS marker. Quantification of the liberated MS marker NO711 by LC-MS/MS (ESI), finally revealed the affinity of a particular sub-library towards the target – the amount of formerly bound MS marker being inversely proportional to the sub-library affinity. In an already previously published screening study¹⁴, control experiments had revealed that the individual aldehyde sub-libraries (with 1 µM of each aldehyde) themselves do not have a significant effect on MS marker binding (reduction of bound NO711 from 82% to 100%; in oxime sub-libraries only neglectable amounts should be present).

Third publication

When only hydroxylamine **6** which is present in excess in the screening experiments was studied for its potential to reduce MS marker binding towards the target, only marginal effects were detected (at 40 μM **6** leads to remaining marker binding of $98 \pm 1\%$).

Table 1: Results of the screening of oximes sub-libraries at a concentration level of 1 μM .

Oxime sub-library	Specific NO711 binding [%] ^a	Oxime sub-library	Specific NO711 binding [%] ^a
1	66 ± 2	15	57 ± 3
2	59 ± 1	16	87 ± 6
3	65 ± 6	17	85 ± 3
4	79 ± 2	18	91 ± 5
5	49 ± 2	19	55 ± 4
6	20 ± 2	20	36 ± 3
7	34 ± 3	21	76 ± 3
8	13 ± 2	22	81 ± 4
9	19 ± 2	23	68 ± 2
10	54 ± 3	24	84 ± 4
11	85 ± 4	25	85 ± 1
12	48 ± 2	26	69 ± 4
13	69 ± 2	27	91 ± 5
14	49 ± 4	28	89 ± 2

^a Percentage of remaining specific bound NO711; data represent the mean \pm standard deviation (SD) of n = 4 experiments.

As summarized in Table 1, with the test concentration for the oximes set to 1 μM , eight sub-libraries were found to reduce marker binding below 50% (sub-library 5–9, 12, 14 and 20). Aiming at identification of only the most potent inhibitors out of the 28 sub-libraries studied, we decided to define the limit to 20% under which sub-libraries had to decrease the marker binding to be selected for further investigations, which correspond to an IC_{50} value of 250 nM provided the observed affinity results from a single constituent. The thus defined requirement, the reduction of the specific NO711 binding below 20% was fulfilled by three sub-libraries (sub-library 6, 8 and 9, Table 1). These sub-libraries were subjected to deconvolution experiments, whereas all other sub-libraries, the MS marker binding values of which ranged from $34 \pm 3\%$ (sub-library 7, Table 1) to $91 \pm 5\%$ (sub-library 18, Table 1) were excluded from further studies.

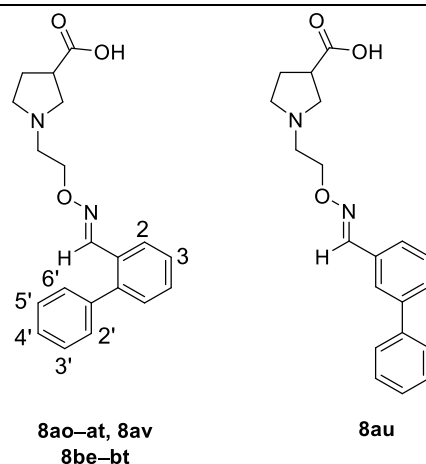
2.2.3. Deconvolution experiments

For the deconvolution experiments, single oximes of the three sub-libraries designated as active, sub-libraries 6,8, and 9, were generated by incubation of the respective aldehydes (1 mM) with an excess of hydroxylamine **6** (40 mM) under conditions identical to those used for oxime sub-library generation (phosphate buffer pH 6.0 with 40% DMSO, 37 °C, 20 h) and then diluted to the test concentration of 1 μ M (as in the assay with phosphate buffer pH 7.1). To examine that the single fragments of the oxime formation were not able to reduce the specific marker binding themselves, the individual aldehydes applied in the deconvolution experiments were tested in the absence of hydroxylamine whereby they showed no significant impact on the marker binding (87–98%, data not shown).

The results of the deconvolution experiments are presented in Table 2. None of the screened oximes was able to reduce marker binding to the set limit of 20% or below, that had been used before as limit for the library screening. Even when adapting the limit for the reduction of MS marker binding to 50% corresponding to an IC_{50} value of 1 μ M, only one oxime, **8bf**, could almost reach this criterion ($52 \pm 2\%$, Table 2, entry 10). Hence, it was decided to resynthesize this compound to determine its pK_i value in full-scale competitive MS Binding Assays²³. In order to verify the validity of the results obtained from the deconvolution experiments and to gain insight into structure-activity-relationships for this class of compounds and to expand the SARs for mGAT1 in general, also the two most active oximes of sub-library 6 and 9 were selected for resynthesis and further evaluation of the binding affinity towards the target (sub-library 6, oxime **8av**: $63 \pm 1\%$, entry 8 and sub-library 9, oxime **8bn**: $62 \pm 2\%$, entry 18; Table 2).

Third publication

Table 2: Results of the deconvolution experiments of oximes **8** of sub-library 6, 8 and 9 at a concentration level of 1 μM .



Entry	Oxime (substitution pattern)	Specific NO711 binding [%] ^a	Entry	Oxime (substitution pattern)	Specific NO711 binding [%] ^a	Entry	Oxime (substitution pattern)	Specific NO711 binding [%] ^a
Sub-library 6			Sub-library 8			Sub-library 9		
1	8ao (2'-F,4'-F)	87 \pm 2	9	8be (2'-F,4'-Cl)	78 \pm 5	17	8bm (2'-Me)	83 \pm 1
2	8ap (2'-F,5'-F)	96 \pm 4	10	8bf (2'-Cl,4'-Cl)	52 \pm 2	18	8bn (2'-Cl,4'-F)	62 \pm 2
3	8aq (2'-F,3'-F)	95 \pm 6	11	8bg (3-F)	77 \pm 6	19	8bo (2'-CF ₃ ,4'-CF ₃)	88 \pm 2
4	8ar (3'-F,5'-F)	83 \pm 5	12	8bh (2-F)	76 \pm 2	20	8bp (2'-Me,4'-Me)	77 \pm 1
5	8as (2'-OMe,5'-F)	83 \pm 2	13	8bi (2'-F,6'-F)	81 \pm 3	21	8bq (3-F,4'-Cl)	79 \pm 2
6	8at (2'-OMe,4'-F)	76 \pm 3	14	8bj (2'-F,4'-F,6'-F)	76 \pm 2	22	8br (2'-Ph)	70 \pm 5
7	8au	94 \pm 2	15	8bk (3-F,2'-F)	79 \pm 3	23	8bs (3'-Ph)	69 \pm 2
8	8av (2'-F,6'-OMe)	63 \pm 1	16	8bl (3-F,2'-Cl)	77 \pm 3	24	8bt (4'-Ph)	86 \pm 6

^aPercentage of remaining specific bound NO711 in the presence of generated oxime in the deconvolution experiment with the respective aldehyde at 1 μM ; data represent the mean \pm standard deviation (SD) of n = 4 experiments.

2.2.4. Structure-activity-relationships

After resynthesis, the three selected oximes **8av**, **8bf**, and **8bn** were characterized for their binding affinities for mGAT1 (pK_i values) in full-scale MS Binding Assays and their inhibitory potencies at mGAT1–4 (pIC_{50} values) in [3H]GABA uptake assays. The results are summarized in Table 3. All three compounds have a 1,1'-biphenyl moiety with different substituents at the terminal phenyl ring in common. Oxime **8av** with 2'-fluoro-6'-methoxy substitution and the 2',4'-dichloro derivative **8bf** yielded very high and similar pK_i values, which amounted to 6.39 ± 0.03 (for **8av**, Table 3, entry 1) and to 6.41 ± 0.02 (for **8bf**, Table 3, entry 2).

Upon exchange of the 4'-chloro substituent in the 2',4'-dichloro substituted oxime **8bf** by a 4'-fluoro atom, a slightly reduction of the binding affinity from 6.41 ± 0.02 (**8bf**, Table 3; entry 2) to 6.16 ± 0.03 (**8bn**, Table 3, entry 3) occurs. As can be seen from the remaining MS marker binding in the deconvolution experiment, a switch of the positions of the 2'-chloro-4'-fluoro substituents in **8bn** resulting in **8be** (2'-F,4'-Cl, Table 2; entry 9) leads to a reduced affinity (compare **8bn**, Table 2, entry 18, $62 \pm 2\%$ with **8be**, Table 2, entry 9, $78 \pm 5\%$). The affinity of the latter compound, **8be**, is further lowered, the remaining MS marker binding amounting then to $87 \pm 2\%$ when the 4'-chloro substituent still present in **8be** is replaced by a fluorine atom as well (2'-F,4'-F, **8ao**, Table 2, entry 1). Hence, a chlorine substituent in 2'-position of the studied oximes increases the affinity to mGAT1 to a larger extent than a fluorine residue.

The oxime **8av** bearing a methoxy group in 6'-position and a fluorine in 2'-position showed a high affinity ($pK_i = 6.39 \pm 0.03$, Table 3, entry 1) which, in contrast, is significantly lower when the fluorine residue is shifted to the meta (**8as**, $83 \pm 2\%$, Table 2, entry 5) or para position (**8at**, $76 \pm 3\%$, Table 2, entry 6).

As compared to the homologous compounds in which the pyrrolidine ring is provided with an acetic acid residue instead of a carboxylic acid function in 3-position¹⁴, oximes **8av**, **8bf** and **8bn** though possessing identical lipophilic residues showed in each case (for the individual pairs of compounds) lower affinities towards mGAT1. For example, the pK_i value of the 2',4'-dichloro-substituted oxime **8bf** ($pK_i = 6.41 \pm 0.02$) is approximately 1.5 log unit lower than the pK_i value of the respective homologous oxime bearing an acetic acid moiety at the pyrrolidine ring ($pK_i = 7.87 \pm 0.01$)¹⁴. In other words, reduction of the acetic acid chain in 3-position of the pyrrolidine ring to a carboxylic acid function leads to a loss of affinity of almost 1.5 log units. Interestingly, in case of 2'-fluoro-6'-methoxy-substituted oxime **8av** ($pK_i = 6.39 \pm 0.03$), the difference between its pK_i value and the pK_i value of the homologous 2-(pyrrolidin-3-yl)acetic acid derivative ($pK_i = 7.12 \pm 0.03$)¹⁴ was less pronounced implying that the presence of a methoxy group had a more favorable effect in **8av** than in the homologous compound.

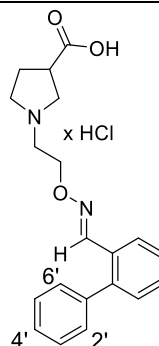
2.2.5. Subtype selectivity

In order to characterize the potencies at mGAT1 and their subtype selectivity regarding mGAT1 over the other murine GABA transporter subtypes mGAT2–mGAT4, the novel oximes **8av**, **8bf**, and **8bn** were furthermore characterized in [³H]GABA uptake assays.

The results are given in Table 3. In those cases where [³H]GABA uptake was reduced to 50% or below ($\sim \text{pIC}_{50} \geq 4.0$) at a test compound concentration of 100 μM , pIC_{50} values were determined in three independent experiments for mGAT1 whereas in a single experiment for mGAT2–4. For less potent compounds only the percentage value of the remaining [³H]GABA uptake is given. As can be seen from the data in Table 3, the inhibitory potencies (pIC_{50} values) of the studied compounds at mGAT1 are approximately one log unit lower than the corresponding binding affinities (pK_i values). This phenomenon repeatedly observed and reported in previous publications may be attributed to the different assay conditions used for MS Binding Assays as compared to the [³H]GABA uptake assays. Still the determined pIC_{50} and pK_i values for mGAT1 are in good accordance to each other. With the highest pIC_{50} value found for mGAT2–4 amounting to 4.30 (for **8bf** at mGAT2, Table 3, entry 2) and all other potencies being so low that only the percentage value or remaining [³H]GABA uptake ($\sim \text{pIC}_{50} \leq 4.0$) has been determined, the hit compounds **8av**, **8bf**, and **8bn** show a distinct subtype selectivity in favor of mGAT1 of more than 1.3 log units (compare e.g. data for mGAT1 with those for mGAT2–4 found for **8bf**, Table 3, entry 2).

Third publication

Table 3: Binding affinities (pK_i) from competitive MS Binding Assays and inhibitory potencies (pIC_{50}) from [3H]GABA uptake experiments determined for synthesized oximes with following substitution pattern.



Entry	compound (substitution pattern) ^a	pK_i^b	pIC_{50}^c			
			mGAT1	mGAT2	mGAT3	mGAT4
1	8av (2'-F,6'-OMe)	6.39 ± 0.03	5.72 ± 0.04	86%	93%	89%
2	8bf (2'-Cl,4'-Cl)	6.41 ± 0.02	5.64 ± 0.11	4.30	62%	56%
3	8bn (2'-Cl,4'-F)	6.16 ± 0.03	5.32 ± 0.07	52%	75%	66%

^aIndividually synthesized oximes (see experimental section). ^bData points for specific binding of NO711 on mGAT1 (mean ± SD, n = 3) in the present of different concentrations of test compound resulted in binding curves for K_i determination by nonlinear regression. pK_i values represent the mean ± SEM of three independent experiments, each performed in triplicate. ^c pIC_{50} values from [3H]GABA uptake assays performed with murine GABA transporters expressing HEK cells. The values represent the mean ± SEM of three (mGAT1) or one (mGAT2–4) independent experiments, each performed in triplicates. Percentage values represent remaining [3H]GABA uptake in present of 100 μ M test compound.

3. Conclusion

In this study, the library screening concept based on competitive LC-MS/MS Binding Assays established in our group has been applied to oximes possessing a pyrrolidine-3-carboxylic acid as polar domain to identify novel inhibitors for the GABA transporter mGAT1. The studied oxime sub-libraries could be easily generated by reacting an excess of 1-[2-(aminooxy)ethyl]pyrrolidine-3-carboxylic acid (**6**) with the respective aldehyde sub-libraries, of which 28 were employed, each containing eight different aldehydes representing a broad range of different structures. Screening of these oxime sub-libraries in competitive MS Binding Assays for mGAT1 revealed three sub-libraries that were able to reduce the specific binding of the marker under the defined limit of 20% when applied in 1 μ M concentration for the individual oximes. These sub-libraries were subsequently selected for deconvolution experiments performed in analogy to library screening except that only single oximes were applied, to identify the oxime with the highest affinities.

The three oximes found to be the most active in the deconvolution experiments were resynthesized and subjected to full-scale MS Binding Assays and [3 H]GABA uptake assays to determine their binding affinities and inhibitory potencies. Oximes with a 2',4'-dichlorobiphenyl residue (**8bf**: $pK_i = 6.41 \pm 0.02$) and a 2'-fluoro-6'-methoxy residue (**8av**: $pK_i = 6.39 \pm 0.03$) were found to be the most affine inhibitors, representing the first submicromolar mGAT1 inhibitors delineated from pyrrolidine-3-carboxylic acid. Interestingly, two of the three pyrrolidine-3-carboxylic acid derivatives with the highest affinities for mGAT1 out of 224 different oximes studied displayed a 2',4'-dichloro and 2'-chloro-4'-fluoro substitution pattern at the terminal phenylring identical to that of the most potent oximes out of a homologous series of compounds with a 2-(pyrrolidin-3-yl)acetic acid instead of pyrrolidine-3-carboxylic acid as polar subunit. But the best binding oximes from this series showed a significant lower affinity for mGAT than the corresponding 2-(pyrrolidin-3-yl)acetic acid derived compounds reported earlier¹⁴.

Overall, variation of the amino acid motif in order to extend structure-activity-relationships were accomplished and three oximes with pK_i values between 6.16 and 6.41 were identified representing mGAT1 inhibitors derived from pyrrolidine-3-carboxylic acid with the highest binding affinities published so far. Therefore, the concept of oxime library screening using competitive MS Binding Assays has again proven to be a reliable readout tool to identify the most potent substances out of a given set of different structures.

4. Experimental Section

4.1. Chemistry

General: Organic solvents used were of analytical grade and were freshly distilled prior to use except for DMSO and absolute EtOH. Purchased reagents and reactants were used without further purification. TLC was performed on pre-coated silica gel F₂₅₄ aluminum sheets (Merck). Flash column chromatography was performed on Merck silica gel 60 (mesh 0.040–0.063 mm). NMR spectra were recorded with an Avance III HD 400 MHz Bruker BioSpin (400 MHz) spectrometer and Avance III HD 500 MHz Bruker BioSpin (500 MHz) spectrometer equipped with a CryoProbe Prodigy. ¹H chemical shifts were internally referenced to tetramethylsilane (TMS) or 3-(trimethylsilyl)propionic-2,2,3,3-*d*₄ acid sodium salt (TSP) for samples dissolved in D₂O. MestreNova (Version 12.0.0) was used for further analysis of the spectra. IR spectra were recorded with a FT-IR spectrometer Paragon 1000 (Perkin-Elmer, Rodgau, Germany) and Spectrum v2.00 software (Perkin-Elmer, Rodgau, Germany) as either KBr pellets or as films on NaCl plates. High resolution mass spectra (HRMS) were measured on a Thermo Finnigan LTQ FT instrument for electrospray ionization (ESI) or on a Thermo Finnigan MAT 95 instrument for electron impact (EI). Melting points (in °C, uncorrected) were determined with a Büchi melting point B-350 apparatus. Determination of the protonation state of hydroxylamine **6** was performed with an 888 Titrand (Metrohm). Purity was determined using qNMR on the Avance III HD 400 MHz Bruker BioSpin (400 MHz) spectrometer with maleic acid as internal standard (Sigma Aldrich, Steinheim, Germany, LOT-No.: BCBM8127V).³¹ Oximes **8** and hydroxylamine **6** were ≥95% pure. For weighing, an ALC-80.4 ACCULAB and a MC 21S from Sartorius Group (Göttingen, Germany) were used.

4.2. General procedures

4.2.1. General procedure for the preparation of oximes (GP1): Aldehyde **7** (1.0 eq.) in absolute EtOH (c = 0.1 M) was added to a stirred solution of hydroxylamine ethylester **14** (1.0 eq.) in absolute EtOH (c = 0.1 M) and the resulting mixture was stirred at 60 °C for 18 h. After removing of the solvent under reduced pressure, the residue was purified by flash column chromatography (silica gel, *n*-pentane/ether + 1% NEt₃ = 9:1 to 7:3) to yield **15** as a colorless oil.

4.2.2. General procedure for the hydrolysis of oximes (GP2): A solution of ester **15** (1.0 eq.) in absolute EtOH (c = 0.1 M) was treated with aqueous NaOH solution (2 M, 3.0 eq.) and the mixture was stirred at room temperature for 18 h. After cooling to 0 °C, aqueous HCl

solution (1 M) was added until pH 1 was reached. The aqueous phase was extracted with CH₂Cl₂ (3 x 20 mL), the combined organic layers were dried with Na₂SO₄ and the solvent was removed under reduced pressure. The resulting oil was dissolved in double-distilled water and lyophilized to yield the desired product **8** as hydrochloride.

4.3. Synthesized substances

4.3.1. 1-[2-(Aminooxy)ethyl]pyrrolidine-3-carboxylic acid –hydrogen chloride (1/2) (6): **14** (27 mg, 0.13 mmol) was dissolved in aqueous HCl solution (1 M, 1.33 mL, 1.33 mmol) and the reaction mixture was stirred at 95 °C for 4 h. After cooling to room temperature, the mixture was washed with CH₂Cl₂ (3 x 10 mL) and the aqueous layer was lyophilized to yield the product **6**. Colorless amorphous solid (32 mg, 97%): mp: 66–69°C. IR (KBr): $\tilde{\nu}$ = 3423, 2959, 2692, 1726, 1624, 1451, 1400, 1199 cm⁻¹. ¹H NMR (400 MHz, D₂O, TPS) δ = 1.92 (ddd, *J* = 12.8, 10.1, 6.4 Hz, 1H), 2.05 (ddd, *J* = 13.1, 7.9, 5.2 Hz, 1H), 2.41–2.57 (m, 2H), 2.73 (h, *J* = 7.9 Hz, 2H), 2.81–2.98 (m, 2H), 3.06 (t, *J* = 8.9 Hz, 1H), 3.84 (t, *J* = 5.6 Hz, 2H) ppm. ¹³C NMR (101 MHz, D₂O, TPS) δ = 30.9, 47.7, 55.8, 56.5, 60.1, 76.7, 186.5 ppm. HRMS (ESI⁺): [M+H]⁺ calcd. for C₇H₁₅N₂O₃, 175.1077; found: 175.1077.

4.3.2. 1-[2-((*E*)-[(2'-Fluoro-6'-methoxy[1,1'-biphenyl]-2-yl)methylidene]amino)oxyethyl]pyrrolidine-3-carboxylic acid (8av): According to **GP2: 15av** (38 mg, 0.092 mmol) and NaOH (11 mg, 0.28 mmol). Colorless, amorphous powder (27 mg, 70%). mp: 61–64°C. IR (KBr): $\tilde{\nu}$ = 3426, 3054, 2940, 2570, 1727, 1615, 1469, 1238, 1074, 786 cm⁻¹. ¹H NMR (500 MHz, 0.1 M NaOD/CD₃OD = 1:2, TPS) δ = 1.94–2.08 (m, 2H), 2.46 (q, *J* = 8.4 Hz, 1H), 2.55 (td, *J* = 9.6, 1.8 Hz, 1H), 2.76 (qt, *J* = 13.1, 6.5 Hz, 2H), 2.81–2.93 (m, 2H), 3.05 (t, *J* = 9.0 Hz, 1H), 3.75 (s, 3H), 4.22 (t, *J* = 5.8 Hz, 2H), 6.88 (t, *J* = 8.7 Hz, 1H), 6.98 (d, *J* = 8.5 Hz, 1H), 7.23 (dd, *J* = 7.5, 1.3 Hz, 1H), 7.43–7.49 (m, 2H), 7.51 (td, *J* = 7.5, 1.6 Hz, 1H), 7.80 (s, 1H), 7.88 (dd, *J* = 7.7, 1.4 Hz, 1H). ppm. ¹³C NMR (126 MHz, 0.1 M NaOD/CD₃OD = 1:2, TPS) δ = 31.2, 48.0, 57.0, 58.7, 60.9, 75.3, 110.1 (d, *J*_{CF} = 2.8 Hz), 110.8 (d, *J*_{CF} = 22.9 Hz), 118.7 (d, *J*_{CF} = 19.3 Hz), 128.5, 131.2, 132.7, 133.4 (d, *J*_{CF} = 10.5 Hz), 133.7, 134.3, 134.7, 151.4, 160.8 (d, *J*_{CF} = 6.7 Hz), 163.1 (d, *J*_{CF} = 242.5 Hz), 185.2 ppm. ¹⁹F NMR (376 MHz, D₂O): δ = –115.8 ppm. HRMS (ESI⁺): [M+H]⁺ calcd. for C₂₁H₂₄FN₂O₄, 387.1715; found: 387.1715.

4.3.3. 1-[2-((*E*)-[(2',4'-Dichloro[1,1'-biphenyl]-2-yl)methylidene]amino)oxyethyl]pyrrolidine-3-carboxylic acid (8bf): According to **GP2: 15bf** (40 mg, 0.092 mmol) and NaOH (11 mg, 0.28 mmol). Colorless, amorphous powder (35 mg, 86%). mp: 63–67°C. IR (KBr): $\tilde{\nu}$ = 3431, 3060, 2949, 2560, 1728, 1585, 1466, 1443, 1203, 1101, 1069, 764 cm⁻¹. ¹H NMR (500 MHz, 0.1 M NaOD/CD₃OD = 1:2, TPS) δ = 1.91–2.09 (m, 2H), 2.46 (q, *J* = 8.3 Hz, 1H), 2.55

(t, J = 9.1 Hz, 1H), 2.73 (dddd, J = 12.9, 11.4, 9.0, 4.8 Hz, 2H), 2.83 (ddd, J = 13.3, 8.9, 4.9 Hz, 1H), 2.89 (dtd, J = 9.7, 8.5, 7.1 Hz, 1H), 3.04 (t, J = 8.9 Hz, 1H), 4.19 (t, J = 5.8 Hz, 2H), 7.21–7.25 (m, 1H), 7.27 (d, J = 8.2 Hz, 1H), 7.46 (dd, J = 8.2, 2.1 Hz, 1H), 7.47–7.57 (m, 2H), 7.61 (d, J = 2.1 Hz, 1H), 7.81 (s, 1H), 7.85 (dd, J = 6.9, 1.6 Hz, 1H) ppm. ^{13}C NMR (126 MHz, 0.1 M NaOD/CD₃OD = 1:2, TPS) δ = 31.2, 48.0, 57.0, 60.9, 75.4, 129.1, 129.1, 130.3, 131.6, 131.9, 132.9, 133.0, 133.2, 135.4, 136.8, 137.3, 140.3, 140.9, 150.8, 185.2 ppm. HRMS (ESI⁺): [M+H]⁺ calcd. for C₂₀H₂₁Cl₂N₂O₃, 407.0924; found: 407.0926.

4.3.4. 1-[2-((*E*)-[(2'-Chloro-4'-fluoro[1,1'-biphenyl]-2-yl)methylidene]amino)oxy)ethyl]pyrrolidine-3-carboxylic acid (8bn): According to **GP2**: **15bn** (20 mg, 0.048 mmol) and NaOH (5.7 mg, 0.14 mmol). Colorless, amorphous powder (18 mg, 89%): mp: 51–53°C. IR (KBr): $\tilde{\nu}$ = 3424, 3054, 2947, 2561, 1726, 1601, 1500, 1474, 1445, 1389, 1257, 1198, 1059, 897, 764 cm⁻¹. ^1H NMR (500 MHz, 0.1 M NaOD/CD₃OD = 1:2, TPS) δ = 1.96–2.17 (m, 2H), 2.64 (q, J = 8.5 Hz, 1H), 2.74 (t, J = 9.1 Hz, 1H), 2.84–2.92 (m, 2H), 2.92–2.98 (m, 2H), 3.14 (t, J = 9.2 Hz, 1H), 4.25 (t, J = 5.6 Hz, 2H), 7.19–7.27 (m, 2H), 7.31 (dd, J = 8.5, 6.1 Hz, 1H), 7.39 (dd, J = 8.7, 2.6 Hz, 1H), 7.47–7.58 (m, 2H), 7.82 (s, 1H), 7.87 (dd, J = 7.3, 1.4 Hz, 1H) ppm. ^{13}C NMR (126 MHz, 0.1 M NaOD/CD₃OD = 1:2, TPS) δ = 31.1, 47.8, 56.9, 57.0, 60.7, 74.7, 117.2 (d, J_{CF} = 21.3 Hz), 119.4 (d, J_{CF} = 25.2 Hz), 128.9, 131.5, 133.0, 133.0, 133.4, 135.6 (d, J_{CF} = 8.9 Hz), 136.7 (d, J_{CF} = 10.6 Hz), 137.6 (d, J_{CF} = 3.1 Hz), 141.3, 151.3, 165.2 (d, J_{CF} = 249.1 Hz), 184.6 ppm. ^{19}F NMR (376 MHz, MeOD): δ = –113.3 ppm. HRMS (ESI⁺): [M+H]⁺ calcd. for C₂₀H₂₁FCIN₂O₃, 391.1219; found: 391.1219.

4.3.5. 3-Ethyl 1-(2,2,2-trichloroethyl)pyrrolidine-1,3-dicarboxylate (10): Potassium carbonate (451 mg, 3.26 mmol) and 2,2,2-trichloroethyl chloroformate (390 μL , 2.86 mmol) were added to a solution of **9** (475 mg, 2.04 mmol) in acetonitrile (8 mL) and the resulting reaction mixture was stirred at 60 °C for 3 h. After cooling to room temperature the suspension was diluted with EtOAc (15 mL) and was filtrated. The solvent was removed *in vacuo* and the crude product was purified by flash column chromatography (silica gel, *n*-pentane/ether = 8:2). Colorless oil (583 mg, 90%): R_f = 0.27 (*n*-pentane:ether = 8:2). IR (Film): $\tilde{\nu}$ = 2984, 2892, 1727, 1417, 1181, 1125, 716 cm⁻¹. ^1H NMR (400 MHz, tetrachlorethane-*d*₂, 100 °C, TMS) δ = 1.25 (t, J = 7.1 Hz, 3H), 2.08–2.21 (m, 2H), 3.05 (p, J = 7.2 Hz, 1H), 3.47 (dt, J = 10.8, 7.3 Hz, 1H), 3.58 (dt, J = 11.0, 6.8 Hz, 1H), 3.62–3.74 (m, 2H), 4.15 (q, J = 7.2 Hz, 2H), 4.71 (s, 2H) ppm. ^{13}C NMR (101 MHz, tetrachlorethane-*d*₂, 100 °C, TMS) δ = 14.2, 28.6, 43.0, 45.7, 48.5, 61.0, 75.2, 96.0, 152.7, 172.5 ppm. HRMS (EI⁺): [M]⁺ calcd. for C₁₀H₁₄Cl₃NO₄, 316.9988; found: 316.9972.

4.3.6. Ethyl pyrrolidine-3-dicarboxylate–acetic acid (11): Zinc powder (614 mg, 9.39 mmol) was added to a solution of **10** (997 mg, 3.13 mmol) in acetic acid (7 mL) and the reaction mixture was stirred at room temperature for 4 h. The suspension was filtrated over Celite® and the solid washed with CH₂Cl₂ (15 mL). The solvent and excess acetic acid were removed *in vacuo* by co-evaporation with toluene (3 x 10 mL). Slightly yellow oil (552 mg, 87%): IR (Film): $\tilde{\nu}$ = 3054, 2986, 1731, 1567, 1557, 1453, 1213, 1025, 736 cm⁻¹. ¹H NMR (500 MHz, CD₃OD, TMS) δ = 1.18 (t, *J* = 7.1 Hz, 3H), 1.99 (s, 3H), 2.15 (dq, *J* = 13.4, 7.1 Hz, 1H), 2.22–2.35 (m, 1H), 3.18–3.29 (m, 3H), 3.35–3.44 (m, 2H), 3.61 (q, *J* = 7.0 Hz, 2H) ppm. ¹³C NMR (126 MHz, CD₃OD, TMS) δ = 18.4, 22.5, 29.6, 43.5, 47.4, 49.5, 58.4, 175.0, 180.9 ppm. HRMS (EI⁺): [M]⁺ calcd. for C₇H₁₃NO₂, 143.0946; found: 143.0945.

4.3.7. Ethyl 1-(2-hydroxyethyl)pyrrolidine-3-carboxylate (12): K₂CO₃ (510 mg, 3.69 mmol), KI (4 mg, 0.03 mmol) and 2-bromoethanol (101 μ L, 1.35 mmol) were added to a solution of **11** (250 mg, 1.23 mmol) in THF (4 mL). The resulting mixture was heated to reflux for 20 h. After cooling to room temperature the solids were removed by filtration and the solvent was removed under reduced pressure. The residue was purified by column chromatography on silica gel (MeCN/NEt₃ = 95:5). Yellow oil (175 mg, 76%): *R*_f = 0.11 (MeCN/NEt₃ = 95:5). IR (Film): $\tilde{\nu}$ = 3406, 2954, 2805, 1733, 1448, 1372, 1198, 1177, 1056, 881 cm⁻¹. ¹H NMR (500 MHz, CDCl₃, TMS) δ = 1.27 (t, *J* = 7.1 Hz, 3H), 2.08–2.16 (m, 2H), 2.65 (dt, *J* = 9.1, 7.0 Hz, 1H), 2.66–2.75 (m, 2H), 2.74–2.79 (m, 1H), 2.80 (dd, *J* = 8.5, 5.7 Hz, 1H), 2.97 (dd, *J* = 9.2, 8.4 Hz, 1H), 3.04 (qd, *J* = 8.0, 6.5 Hz, 1H), 3.66 (t, *J* = 5.4 Hz, 2H), 4.15 (q, *J* = 7.1 Hz, 2H) ppm. ¹³C NMR (126 MHz, CDCl₃, TMS) δ = 14.2, 27.7, 42.1, 53.5, 56.4, 57.0, 59.6, 60.8, 174.8 ppm. HRMS (ESI⁺): [M+H]⁺ calcd. for C₉H₁₈NO₃, 188.1281; found: 188.1281.

4.3.8. Ethyl 1-{2-[(1,3-dioxo-2,3-dihydro-1*H*-isoindol-2-yl)oxy]ethyl}pyrrolidine-3-carboxylate (13): **12** (152 mg, 0.812 mmol), *N*-hydroxyphthalimide (225 mg, 1.38 mmol), triphenylphosphine (369 mg, 1.38 mmol) were dissolved in THF (4 mL), DMEAD (333 mg, 1.42 mmol) was added slowly and the solution was stirred for 17 h at room temperature. After removing the solvent under reduced pressure, the residue was dissolved in CH₂Cl₂ (20 mL), the organic layer was washed with water (3 x 15 mL), dried over sodium sulfate and the solvent was again removed *in vacuo*. The resulting oil was purified by column chromatography on silica gel, which was pre-dried at 145 °C *in vacuo* for 5 h (Ether/NEt₃ = 95:5). Colorless oil (219 mg, 81%): *R*_f = 0.67 (ether/NEt₃ = 95:5). IR (Film): $\tilde{\nu}$ = 2978, 2800, 1789, 1731, 1467, 1374, 1188, 1023, 878, 702 cm⁻¹. ¹H NMR (500 MHz, CDCl₃, TMS) δ = 1.26 (t, *J* = 7.1 Hz, 3H), 2.00–2.09 (m, 2H), 2.54 (dt, *J* = 8.9, 7.7 Hz, 1H), 2.68 (dd, *J* = 9.1, 7.1 Hz, 1H), 2.82–3.03 (m, 4H), 3.09 (t, *J* = 8.8 Hz, 1H), 4.13 (q, *J* = 7.2 Hz, 2H), 4.28–4.39 (m, 2H), 7.75 (dd, *J* = 5.5, 3.1 Hz, 2H), 7.84 (dd, *J* = 5.4, 3.1 Hz, 2H) ppm. ¹³C NMR (126 MHz, CDCl₃, TMS) δ = 14.2, 27.7, 42.1,

53.6, 54.0, 57.0, 60.6, 76.3, 123.5, 129.0, 134.4, 163.5, 174.9 ppm. HRMS (EI⁺): [M]⁺ calcd. for C₁₇H₂₀N₂O₅, 332.1372; found: 332.1366.

4.3.9. Ethyl 1-[2-(aminooxy)ethyl]pyrrolidine-3-carboxylate (14): Hydrazine solution (50–60%, 15 µL, 0.24 mmol) was added to a stirred solution of **13** (40 mg, 0.12 mmol) in EtOH (abs., 2 mL) and the solution was stirred for 2 h at room temperature. The resulting slurry was filtered, the filtrate was washed with ice-cold CH₂Cl₂ (5 mL) and the solvent was removed *in vacuo*. Again ice-cold CH₂Cl₂ (5 mL) was added to the residue and the resulting mixture was filtered. Evaporation under reduced pressure afforded the product **14**. Colorless oil (22 mg, 92%): IR (Film): $\tilde{\nu}$ = 2959, 2950, 2802, 1731, 1592, 1372, 1194, 1032 cm⁻¹. ¹H NMR (500 MHz, CDCl₃, TMS) δ = 1.26 (t, *J* = 7.1 Hz, 3H), 2.00–2.22 (m, 2H), 2.50 (dt, *J* = 8.6, 7.7 Hz, 1H), 2.59–2.77 (m, 3H), 2.81 (ddd, *J* = 9.0, 7.0, 5.7 Hz, 1H), 2.96–3.11 (m, 2H), 3.80 (t, *J* = 5.5 Hz, 2H), 4.14 (q, *J* = 7.1 Hz, 2H) ppm. ¹³C NMR (126 MHz, CDCl₃, TMS) δ = 14.2, 27.7, 42.1, 54.3, 54.4, 57.1, 60.7, 74.1, 175.0 ppm. HRMS (ESI⁺): [M+H]⁺ calcd. for C₉H₁₉N₂O₃, 203.1390; found: 203.1389.

4.3.10. Ethyl 1-[2-(((*E*)-[(2'-fluoro-6'-methoxy[1,1'-biphenyl]-2-yl)methylidene]amino)oxy)ethyl]pyrrolidine-3-carboxylate (15av): According to **GP1**: Hydroxylamine **14** (30 mg, 0.15 mmol) and **7av** (34 mg, 0.15 mmol). Colorless oil (50 mg, 81%). *R*_f = 0.18 (*n*-pentane:ether = 8:2, 1% NEt₃). IR (Film): $\tilde{\nu}$ = 3062, 2958, 2937, 2804, 1731, 1614, 1580, 1469, 1438, 1275, 1239, 1196, 1175, 1083, 943 cm⁻¹. ¹H NMR (500 MHz, CD₂Cl₂, TMS) δ = 1.22 (t, *J* = 7.1 Hz, 3H), 1.97–2.08 (m, 2H), 2.53 (dt, *J* = 8.7, 7.3 Hz, 1H), 2.60–2.70 (m, 2H), 2.72 (tdd, *J* = 5.7, 2.4, 1.5 Hz, 2H), 2.85 (t, *J* = 8.9 Hz, 1H), 2.96 (qd, *J* = 8.2, 6.7 Hz, 1H), 3.74 (s, 3H), 4.09 (q, *J* = 7.1 Hz, 2H), 4.19 (t, *J* = 5.8 Hz, 2H), 6.77–6.85 (m, 2H), 7.20–7.28 (m, 1H), 7.32–7.38 (m, 1H), 7.38–7.47 (m, 2H), 7.79 (d, *J* = 1.1 Hz, 1H), 7.96 (dd, *J* = 7.7, 1.5 Hz, 1H) ppm; ¹³C NMR (126 MHz, CD₂Cl₂, TMS) δ = 14.4, 28.1, 42.5, 54.6, 54.8, 56.5, 57.5, 60.9, 73.4, 107.1 (d, *J*_{CF} = 2.8 Hz), 108.4 (d, *J*_{CF} = 23.0 Hz), 116.4 (d, *J*_{CF} = 19.3 Hz), 125.8, 128.5, 129.7, 130.3 (d, *J*_{CF} = 10.6 Hz), 131.8, 132.1, 132.1, 147.5, 158.4 (d, *J*_{CF} = 6.9 Hz), 160.7 (d, *J*_{CF} = 243.7 Hz), 175.2 ppm; ¹⁹F NMR (376 MHz, CD₂Cl₂) δ = –114.3 ppm. HRMS (ESI⁺): [M+H]⁺ calcd. for C₂₃H₂₈FN₂O₄, 415.2028; found: 415.2024.

4.3.11. Ethyl 1-[2-(((*E*)-[(2',4'-dichloro[1,1'-biphenyl]-2-yl)methylidene]amino)oxy)ethyl]pyrrolidine-3-carboxylate (15bf): According to **GP1**: Hydroxylamine **14** (30 mg, 0.15 mmol) and **7bf** (37 mg, 0.15 mmol). Colorless oil (48 mg, 74%). *R*_f = 0.24 (*n*-pentane:ether = 8:2, 1% NEt₃). IR (Film): $\tilde{\nu}$ = 3061, 2970, 2936, 2804, 1732, 1466, 1444, 1192, 1176, 1036, 761 cm⁻¹. ¹H NMR (500 MHz, CD₂Cl₂, TMS) δ = 1.22 (t, *J* = 7.1 Hz, 3H), 1.98–2.07 (m, 2H), 2.54 (dt, *J* = 8.8, 7.2 Hz, 1H), 2.63 (dt, *J* = 8.8, 6.7 Hz, 1H), 2.67 (dd, *J* = 9.3, 6.6 Hz, 1H), 2.70

(td, $J = 5.7, 1.7$ Hz, 2H), 2.84 (t, $J = 8.8$ Hz, 1H), 2.96 (qd, $J = 8.2, 6.6$ Hz, 1H), 4.10 (q, $J = 7.1$ Hz, 2H), 4.18 (t, $J = 5.8$ Hz, 2H), 7.18–7.24 (m, 2H), 7.34 (dd, $J = 8.2, 2.1$ Hz, 1H), 7.40–7.47 (m, 2H), 7.51 (d, $J = 2.1$ Hz, 1H), 7.77 (s, 1H), 7.91–7.97 (m, 1H) ppm. ^{13}C NMR (126 MHz, CD_2Cl_2 , TMS) $\delta = 14.4, 28.1, 42.5, 54.6, 54.8, 57.5, 60.9, 73.6, 126.1, 127.6, 128.9, 129.7, 129.8, 130.7, 131.1, 132.9, 134.6, 134.7, 137.5, 138.4, 146.9, 175.3$ ppm. HRMS (ESI⁺): $[\text{M}+\text{H}]^+$ calcd. for $\text{C}_{22}\text{H}_{25}\text{Cl}_2\text{N}_2\text{O}_3$, 435.1237; found: 435.1236.

4.3.12. Ethyl 1-[2-(((*E*)-[(2'-chloro-4'-fluoro[1,1'-biphenyl]-2-yl)methylidene)amino)oxy)ethyl]pyrrolidine-3-carboxylate (15bn): According to **GP1**: Hydroxylamine **14** (30 mg, 0.15 mmol) and **7bn** (35 mg, 0.15 mmol). Colorless oil (43 mg, 69%). $R_f = 0.21$ (*n*-pentane:ether = 8:2, 1% NEt_3). IR (Film): $\tilde{\nu} = 3059, 2961, 2930, 2805, 1731, 1601, 143, 1257, 1198, 1059, 1035, 897, 762$ cm^{-1} . ^1H NMR (500 MHz, CDCl_3 , TMS) $\delta = 1.25$ (t, $J = 7.1$ Hz, 3H), 2.00–2.18 (m, 2H), 2.51 (q, $J = 8.2$ Hz, 1H), 2.65 (dd, $J = 12.3, 5.0$ Hz, 1H), 2.72–2.88 (m, 3H), 2.99–3.11 (m, 2H), 4.14 (q, $J = 7.2$ Hz, 2H), 4.26 (t, $J = 5.7$ Hz, 2H), 7.05 (td, $J = 8.2, 2.6$ Hz, 1H), 7.16–7.25 (m, 3H), 7.38–7.45 (m, 2H), 7.81 (s, 1H), 7.94–7.99 (m, 1H) ppm. ^{13}C NMR (126 MHz, CD_2Cl_2 , TMS) $\delta = 14.2, 27.7, 42.1, 54.3, 54.6, 57.1, 60.7, 72.8, 114.1$ (d, $J_{\text{CF}} = 21.1$ Hz), 116.9 (d, $J_{\text{CF}} = 24.6$ Hz), 125.7, 128.4, 129.5, 130.5, 130.6, 132.5 (d, $J_{\text{CF}} = 8.8$ Hz), 134.3 (d, $J_{\text{CF}} = 10.3$ Hz), 134.5 (d, $J_{\text{CF}} = 3.7$ Hz), 138.2, 147.0, 162.1 (d, $J_{\text{CF}} = 250.5$ Hz), 174.9 ppm. ^{19}F NMR (376 MHz, CDCl_3) $\delta = -112.1$ ppm. HRMS (ESI⁺): $[\text{M}+\text{H}]^+$ calcd. for $\text{C}_{22}\text{H}_{25}\text{FCIN}_2\text{O}_3$, 419.1532; found: 419.1530.

4.4. Oxime exchange experiment: Phosphate buffer (990 μL , pH 7.1, 12.5 mM Na_2HPO_4 , 12.5 mM NaH_2PO_4 , 1 M NaCl, pH value adjusted with 1 M NaOH, 10% D_2O) was added to a solution of oxime **8av** (0.423 mg, 1 μmol) and 4-methoxybenzaldehyde **7t** (0.272 mg, 2 μmol) in $\text{DMSO}-d_6$ (10 μL) in an NMR tube. ^1H NMR spectra (64 scans) were measured at 37 °C with water suppression directly after the preparation of the sample and every 4 h over a 64 h period. No change of the spectra could be observed over the experiment time.

4.5. LC-MS/MS binding experiments

4.5.1. Generation of pre-equilibrated sub-libraries: To obtain the hydroxylamine **6** as a free base, aqueous NaOH solution (1 M, 2.0 eq.) in phosphate buffer (pH 6.0, 12.5 mM Na_2HPO_4 , 12.5 mM NaH_2PO_4 , 1 M NaCl, pH value adjusted with 1 M HCl) was added to hydroxylamine **6** as dihydrochloride dissolved in phosphate buffer (pH 6.0) to a nominal concentration of 400 mM of **6**. This solution (10 μL) was added to a mixture containing eight solutions of individual aldehydes in DMSO (20 mM, 5 μL each) and phosphate buffer (pH 6.0, 50 μL). These sub-library mixtures were incubated for 20 h at 37 °C in a shaking water bath to

guarantee full conversion into the corresponding oximes. In case of sub-library 26, oxime generation was achieved at 80 °C for 45 h. Before the binding experiments, all pre-equilibrated sub-libraries were freshly diluted with phosphate buffer pH 7.1 (12.5 mM Na₂HPO₄, 12.5 mM NaH₂PO₄, 1 M NaCl, pH value adjusted with 1 M NaOH) and DMSO to obtain the generated oximes in final concentrations of 10 µM in phosphate buffer (pH 7.1) containing 10% DMSO v/v.

4.5.2. Generation of pre-equilibrated single oximes for deconvolution experiments: The pre-equilibrated single oximes for deconvolution were obtained in the same way as described for pre-equilibrated sub-libraries, except that one solution of a single aldehyde in DMSO (20 mM, 5 µL) and additional DMSO (35 µL) were used. Before the binding experiments, all pre-equilibrated deconvolution batches were freshly diluted with phosphate buffer pH 7.1 (12.5 mM Na₂HPO₄, 12.5 mM NaH₂PO₄, 1 M NaCl, pH value adjusted with 1 M NaOH) and DMSO to obtain the generated oximes in final concentrations of 10 µM in phosphate buffer (pH 7.1) containing 10% DMSO.

4.5.3. mGAT1 membrane preparation: Membrane preparations of HEK293 cells stably expressing mGAT1¹⁸ were prepared as described previously and stored at –80 °C.^{23,32} On the day of the assay, an aliquot was rapidly thawed and diluted in a 20-fold volume of cold aqueous 0.9% NaCl solution (m/v). After centrifugation at 20500 rpm and 4 °C for 20 min (CP56GII, P70AT, Hitachi Ltd., Tokyo, Japan), the resulting pellet was resuspended in ice-cold phosphate buffer pH 7.1 to a protein concentration of approximately 0.1 mg mL⁻¹ as previously described.³²

4.5.4. Library screening: Library screening was performed in 1.2 mL polypropylene deep-well plates (Sarstedt, Nümbrecht, Germany) in analogy to a procedure previously described.^{16,21,22} Samples (n = 4) were prepared in phosphate buffer (pH 7.1) with 1% DMSO in total volume of 250 µL per sample containing the mGAT1 membrane preparation (50 µL, approximately 20 µg protein per sample, see above), NO711 (25 µL, final concentration in the assay 20 nM) and the pre-equilibrated sub-libraries (25 µL, final concentration one tenth of the corresponding stock solution containing the pre-equilibrated sub-libraries as described above) and incubated for 4 h at 37 °C in a shaking water bath. Incubation was stopped by transferring aliquots of 200 µL of each sample onto a 96-well filter plate (Acroprep Advance, glass fiber, 1.0 µm, 350 µL, Pall, Dreieich, Germany) with a 12-channel pipette followed by subsequent vacuum filtration. After washing with ice-cold aqueous NaCl solution (1 M, 5 x 150 µL per well) by using a 12-channel pipette, the filter plate was dried (60 min, 50 °C) and cooled to room temperature. Subsequently, the marker was liberated by elution of the filter plate with MeOH

(3 x 100 μ L per well) into a 1.2 mL polypropylene 96-well plate (Sarstedt, Nümbrecht, Germany). Each sample was supplemented with 1 nM [$^2\text{H}_{10}$]NO711 (200 μ L, in MeOH) as an internal standard. All samples were dried to completeness (17 h, 50 $^{\circ}\text{C}$). For quantification by LC-MS/MS (ESI), samples were reconstituted in 200 μ L of 10 mM ammonium formate buffer [pH 7.0/MeOH (95:5 v/v)]. In the same way, aldehyde sub-libraries (see above) and hydroxylamine **6** (final concentrations in the assay 40 μ M, 4 μ M or 400 nM) were investigated. Total binding and nonspecific binding of NO711 were determined in analogously constituted samples lacking any inhibitor or in the presence of 100 mM GABA, respectively.

4.5.5. Deconvolution: The experiments were performed in the same manner as the experiments described for the library screening, expect that an aliquot of 25 μ L of a pre-equilibrated batch of a single oxime was employed.

4.5.6. LC-MS/MS (ESI) analysis: Quantification of NO711 by LC-MS/MS (ESI) was performed as described by using an API 3200 triple-quadrupole mass spectrometer.^{23,32} To assure reliable quantification, each day a binding experiment was performed, also matrix blanks (generated analogously as described for binding samples but in the absence of NO711 and [$^2\text{H}_{10}$]NO711), a zero sample (matrix blank with 1 nM [$^2\text{H}_{10}$]NO711) and matrix standards (generated by supplementing matrix blanks with different concentrations of NO711 (50 pM, 100 pM, 200 pM, 500 pM, 1 nM, 2.5 nM and 5 nM) and 1 nM of [$^2\text{H}_{10}$]NO711) were investigated and individual calibration curves for marker quantification were generated therefrom. Derived from the external calibration curve, the lower limit of quantification (LLOQ) could be determined to 50 pM.

4.5.7. Competition experiments applying isolated oximes: The experiments were performed as described recently^{23,32}, but substituting the original incubation buffer for phosphate buffer (pH 7.1, 12.5 mM Na_2HPO_4 , 12.5 mM NaH_2PO_4 , 1 M NaCl, pH value adjusted with 2 M NaOH).

4.5.8. Analysis of competitive binding experiments: Marker depletion was negligible (<10%) in all binding experiments. Specific binding was defined as the difference between the total and nonspecific binding. Nonspecific binding less than 50 pM (LLOQ) was not determined experimentally, but was extrapolated by linear regression from nonspecifically bound NO711 concentrations of ≥ 50 pM. The concentration of a competitor that inhibited 50% of specific binding (IC_{50}) was calculated from competition curves by plotting NO711 specific binding concentrations against the log of competitor concentration (eight different concentrations per competitor) with Prism 5.04 (GraphPad Software, San Diego, CA, USA) using the equation for

one-site competition and nonlinear curve fitting. Specific binding determined for control samples in the absence of any competitor was set to 100%, whereas the bottom level was set to 0% (corresponds to the nonspecific binding of NO711). K_i values were calculated according to Cheng and Prusoff³³ and are expressed as pK_i values. All results are expressed as the mean standard error of the mean \pm SEM (unless stated otherwise). pK_i values were determined in at least three separate experiments.

4.5.9. GABA uptake assays: [³H]GABA uptake assays were performed as previously described.¹⁸

Acknowledgement

Special thanks go to Silke Duesing-Kropp and Miriam Sandner for excellent technical support.

Conflict of interest

The authors declare no conflict of interest.

Keywords: LC-MS/MS binding assays, mGAT1, library screening, mass spectrometry, pyrrolidine-3-carboxylic acid.

1. Krogsgaard-Larsen P. *Med Res Rev.* 1988;8:27–56.
2. Foster AC, Kemp JA. *Curr. Opin Pharmacol.* 2006;6:7–17.
3. Treiman DM. *Epilepsia* 2001;42(Suppl. 3):8–12.
4. (a) Rissmann RA, De Blas AL, Armstrong DM. *J. Neurochem.* 2007;103:1285–1292. (b) Lanctôt KL, Herrmann N, Mazzotta P, Khan LR, Ingber N. *Can. J. Psychiatry* 2004;49:439–453.
5. Kalueff AV, Nutt DJ. *Depression Anxiety* 2007;24:495–517.
6. Krogsgaard-Larsen P, Falch E, Larsson OM, Schousboe A. *Epilepsy Res.* 1987;1:77–93.
7. (a) Liu QR, Lopez-Corcuera B, Mandiyan S, Nelson H, Nelson N. *J. Biol. Chem.* 1993;268:2106–2112. (b) Madsen KK, White HS, Schousboe A. *Pharmacol Ther.* 2010;125:394–401.
8. Madsen KK, Rasmus PC, Larsson OM, Krogsgaard-Larsen P, Schousboe A, White HS. *J. Neurochem.* 2009;109:139–144.
9. Zhou Y, Holmseth S, Guo C, Hassel B, Höfner G, Huitfeldt HS, Wanner KT, Danbolt NC. *J. Biol. Chem.* 2012;287:35733–35746.
10. Zhou Y, Holmseth S, Hua R, Lehre AC, Olofsson AM, Poblete-Naredo I, Kempson SA, Danbolt NC. *Am. J. Physiol. Renal. Physiol.* 2012;302:F316–F328.
11. Krogsgaard-Larsen P, Johnston GAR. *J. Neurochem.* 1975;25:797–802.

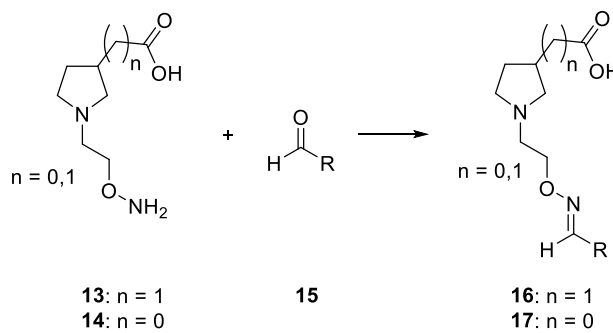
12. Larsson OM, Thorbek P, Krogsgaard-Larsen P, Schousboe A. *J. Neurochem.* 1981;37:1509–1516.
13. Krogsgaard-Larsen P. *Mol. Cell. Biochem.* 1980;31:105–121.
14. Huber SK, Wanner KT. *ChemMedChem* 2018;23:2488–2503.
15. Hellenbrand T, Höfner G, Wein T, Wanner KT. *Bioorg. Med. Chem.* 2016;24:2072–2096.
16. Wein T, Wanner KT. *J. Mol. Model* 2010;16:155–161.
17. Wein T, Petrera M, Allmendinger L, Höfner G, Pabel J, Wanner KT. *ChemMedChem* 2016;11:509–518.
18. Kragler A, Höfner G, Wanner KT. *Eur. J. Med. Chem.* 2008;43:2404–2411.
19. Hog S, Greenwood JR, Madsen KB, Larsson OM, Frolund B, Schousboe A, Krogsgaard-Larsen P, Clausen RP. *Curr. Top. Med. Chem.* 2006;6:1861–1882.
20. Soudijn W, van Wijngaarden I. *Curr. Med. Chem.* 2000;7:1063–1079.
21. Kern FT, Wanner KT. *ChemMedChem* 2015;10:396–410.
22. Sindelar M, Wanner KT. *ChemMedChem* 2012;7:1678–1690.
23. Zepperitz C, Höfner G, Wanner KT. *ChemMedChem* 2006;1:208–217.
24. Höfner G, Wanner KT. *Angew. Chem Int. Ed.* 2003;42:5235–5237.
25. Johnson G, Drummond JT, Boxer PA, Bruns RF. *J. Med. Chem.* 1992;35:233–241.
26. Schwarzer MF. *Synthese potentieller GABA-uptake-inhibitoren mit bicyclischer Struktur durch 1,3-dipolare Cycloadditionen und [2+2]-Photocycloadditionen.* München: Verl. Dr. Hut; 2008.
27. Andersen KE, Lau J, Lundt BF, Petersen H, Huusfeldt PO, Suzdak PD, Swedberg MDB: *Bioorg. Med. Chem.* 2001, 9, 2773–2785.
28. Sindelar M, Lutz TA, Petrera M, Wanner KT. *J. Med. Chem.* 2013;56:1323–1340.
29. Irgartinger H, Escher T. *Tetrahedron* 1999;55:10753–10760.
30. Hauke TJ, Wein T, Höfner G, Wanner KT. *J. Med. Chem.* 2018;61:10310–10332.
31. Pauli GF, Chen S-N, Simmler C, Lankin DC, Gödecke T, Jaki BU, Friesen JB, McAlpine JB, Napolitano JG. *J. Med. Chem.* 2014;57:9220–9231.
32. Zepperitz C, Höfner G, Wanner KT. *Anal. Bioanal. Chem.* 2008;391:309–316.
33. Cheng YC, Prusoff WH. *Biochem. Pharmacol.* 1973;22:3099–3108.

4 Further Experiments

In the following section, kinetic experiments and stability experiments are presented in detail.

4.1 Generation of Oxime Libraries – Kinetic Experiments

Oxime libraries were pre-generated in absence of the target mGAT1 by reacting each library consisting of eight different aldehydes **15** (1 mM each aldehyde) with an excess of either 2-(pyrrolidin-3-yl)acetic acid ($n = 1$) or pyrrolidine-3-carboxylic acid ($n = 0$) derived hydroxylamine (40 mM) at 37 °C in phosphate buffer (pH 6.0, 12.5 mM Na_2HPO_4 , 12.5 mM NaH_2PO_4 , 1 M NaCl, pH value was adjusted with 1 M HCl) with a DMSO concentration of 40 % as outlined in Scheme 3.



Scheme 3: Synthesis of oximes **13** ($n = 1$) and **14** ($n = 0$). Conditions: phosphate buffer (pH 6.0, 12.5 mM Na_2HPO_4 , 12.5 mM NaH_2PO_4 , 1 M NaCl, pH value was adjusted with 1 M HCl) + 40 % DMSO at 37 °C.

In order to ensure completion of oxime formation within the defined time of 20 h under these conditions the oxime generation reaction was exemplarily monitored by the means of ^1H NMR spectroscopy using the aldehydes 4-nitrobenzaldehyde **15a**, biphenyl-2-carbaldehyde **15b**, 4-methoxybenzaldehyde **15c** and 2-methoxybenzaldehyde **15d** (Figure 8). The aldehyde **15c** was only used to examine kinetics with 2-(pyrrolidin-3-yl)acetic acid derivative **13** but not with the other hydroxylamine **14**. Since it showed similar reaction times as biphenyl-2-carbaldehyde **15b** with **13** no new information regarding reaction time for oxime generation with **14** was expected.

For simplification only one single aldehyde at once was used for these kinetic experiments so the analysis of the obtained spectra could be reduced to one vanishing aldehyde proton signal and one emerging oxime proton signal, respectively. However, to maintain the concentration ratio between the reactants at 1:5 one single aldehyde was applied with in a higher concentration of 8 mM and was reacted with 40 mM of hydroxylamine. All samples were then prepared in phosphate buffer (pH 6.0, 12.5 mM Na_2HPO_4 , 12.5 mM NaH_2PO_4 , 1 M NaCl, 10 % D_2O) containing 40 % $\text{DMSO}-d_6$ at 37 °C and the spectra were recorded with a proton pulse sequence including an excitation sculpting block for water suppression. The spectra were

Further Experiments

recorded before the addition of hydroxylamine **13**, directly after the addition of **13** and was repeated for 20 hours with a time increment of 10 minutes. For the sake of clarity only the significant signals of e. g. the aldehyde proton or the oxime proton were labeled in the spectra. Additionally, signals which were found to play a role within the reaction (e.g. intermediates) were also labeled with a rectangle.

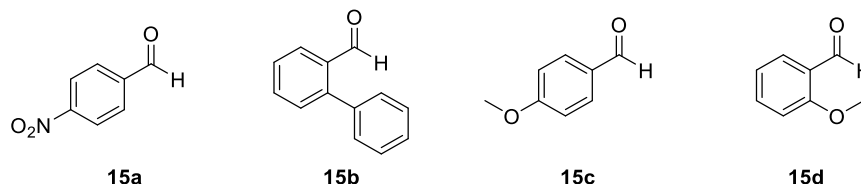


Figure 8: Applied single aldehydes for kinetic experiments.

4.1.1 Kinetic Experiments using 2-(Pyrrolidin-3-yl)acetic acid derived Hydroxylamine

4.1.1.1 Reaction with Single Aldehydes

2-{1-[(2-Aminoxy)ethyl]pyrrolidine-3-yl}acetic acid **13** was applied within the first set of kinetic experiments to begin with 4-nitrobenzaldehyde (**15a**) as reactant. In the pure aldehyde spectrum without hydroxylamine the signal for the aldehyde proton at $\delta = 9.99$ ppm and one additional signal at $\delta = 5.92$ ppm were obtained (first spectrum of Figure 9). As the reaction took place in aqueous media, the formation of the hydrate of 4-nitrobenzaldehyde (**15a**) is possible and the methine proton of its hydrate could be observed (see Scheme 4).

Five minutes after addition of hydroxylamine **13** to aldehyde **15a**, analysis of the spectrum revealed that considerable amounts of aldehyde were still present. Besides the signal for the aldehyde proton ($\delta = 9.99$ ppm) and the signal at $\delta = 5.92$ ppm two additional signals appeared: one at $\delta = 8.31$ ppm, which was considered to refer to the imine proton (*E*-configuration) of the final product **16a** identified by the fact that it is increasing over time and the other one at $\delta = 5.59$ ppm which is the dominant signal 5 min after the addition of the hydroxylamine (Figure 9).

Further Experiments

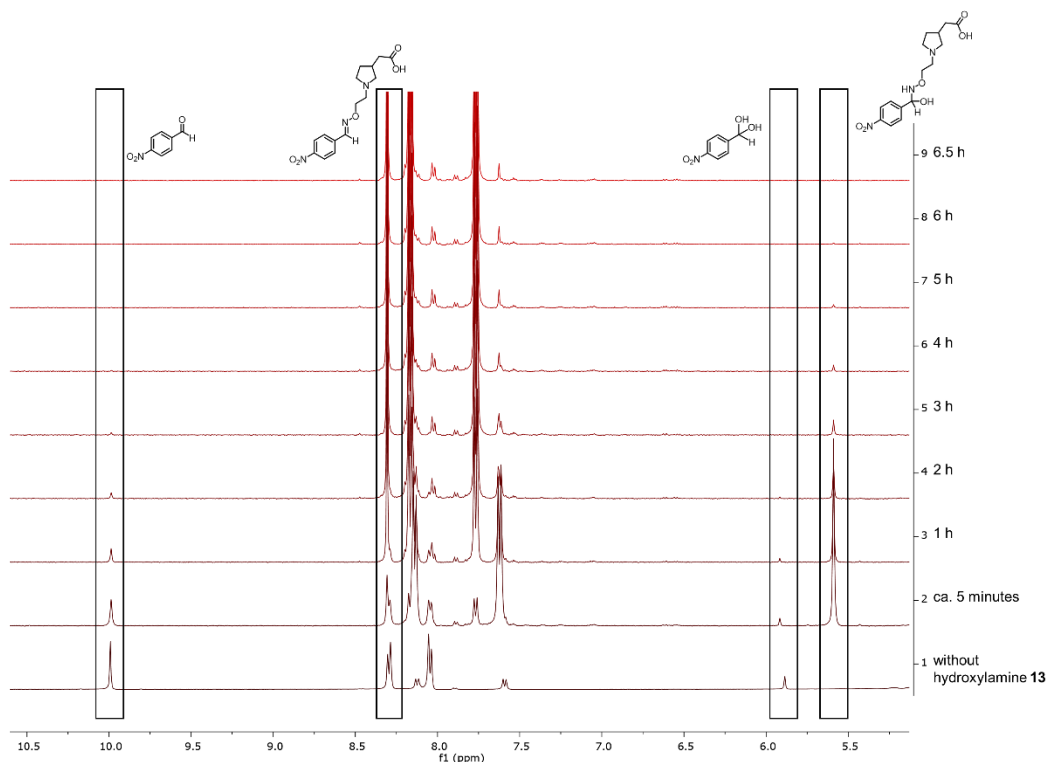
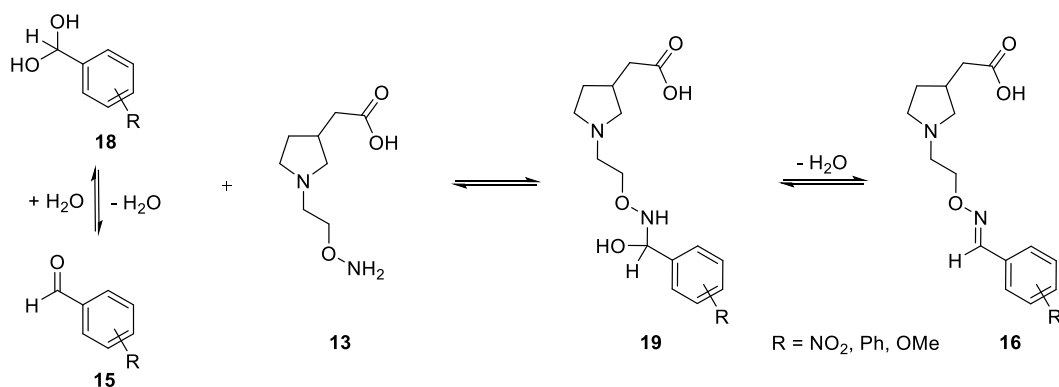


Figure 9: ^1H NMR spectra obtained from the reaction of 4-nitrobenzaldehyde (**15a**, $\delta = 9.99$ ppm, 8 mM) with hydroxylamine **13** (40 mM) to oxime **16a** ($\delta = 8.31$ ppm) after 1) ca. 5 min., 2) 1 h, 3) 2 h, 4) 3 h, 5) 4 h, 6) 5 h, 7) 6 h, 8) 6.5 h at 37°C . Hydrate **18a** of 4-nitrobenzaldehyde observed at $\delta = 5.92$ ppm; intermediate **19a** observed at $\delta = 5.59$ ppm.

This signal can be explained when looking at the proposed reaction mechanism depicted in Scheme . Aldehyde **15a** and its corresponding hydrate **18a** are attacked by hydroxylamine **1** yielding hemiaminal **19a** as intermediate which under dehydration finally leads to oxime **16a**. Since **19a** is formed very fast in large amounts – the signal of the methine proton from the hemiaminal moiety is present in the first spectrum recorded after 5 min and still detected after 6 h when no aldehyde nor hydrate signal is detectable – the dehydration can be considered as the rate determining step of the overall condensation reaction.



Scheme 4: Formation of hydrate **18** and condensation reaction of hydroxylamine **13** with respective aldehydes **15** via tetrameric intermediates **19** to the corresponding oximes **16**.

Further Experiments

The spectrum recorded after 6.5 h finally revealed that all hemiaminal intermediate was fully consumed and the signal for the oxime proton at $\delta = 8.31$ ppm reached its maximum intensity indicating the complete conversion into oxime **16a** (Figure 9). The decrease of the absolute signal integrals referring to the reactants i.e. aldehyde **15a**, hydrate **18a**, and intermediate **19a** (highlighted in rectangles) as a sum and the increase of the product signal referring to the oxime **16a** (highlighted in rectangles) are plotted versus time in one single diagram. The exponential decay of the reactants and the exponential growth of the product are clearly depicted in Figure 10.

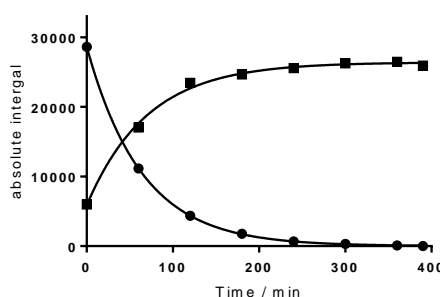


Figure 10: Kinetic plot of reactants and product during oxime formation **16a**.

To verify the assumption, that the mentioned species were components of the same equilibrium ^1H 2D EXSY NMR experiments were performed. These experiments exploit exactly the same pulse sequence as the 2D NOESY experiment. A typical sequence is depicted in Figure 11. This pulse sequence consists of a first preparation 90°_x pulse that transfers all magnetization to the x-y-plane where the spins evolve according to their Larmor frequencies. Subsequent to the evolution phase t_1 another 90°_x pulse is followed rebuilding z-magnetization. After the second pulse a very crucial delay is followed which is called the mixing time t_M . During this period magnetization transfer is accomplished due to nuclear Overhauser effect caused by spatial proximity of neighbored protons. Finally, another 90°_x pulse transfers the remaining magnetization from z- to the x-y-plane where the resulting FID is acquired.⁶⁶ In the 2D NOESY spectrum recorded in phase-sensitive mode the off diagonal peaks representing NOEs have opposite phase and sign to those of the diagonal peaks which are made apparent by the processing software using different colors. The transfer of magnetization between two neighboring spins occurs during the mixing time due to cross-relaxation, but if two spins exchange sites e.g. in molecules that are in an equilibrium this magnetization is also transferred during t_M from one spin to the other. Since these spins have been labeled before during t_1 with their Larmor frequencies i.e. chemical shifts, the cross peaks in the resulting spectrum marks physically identical proton exchanging sites in two different species. These particular cross peaks have the same phase and sign as the diagonal peaks and are therefore depicted in the same color. To distinguish between the two different phases of the cross peaks

Further Experiments

– opposite sign to the diagonal peaks caused by NOEs and the same sign due to exchange signals – 2D EXSY spectra are therefore mandatorily recorded in phase-sensitive mode.

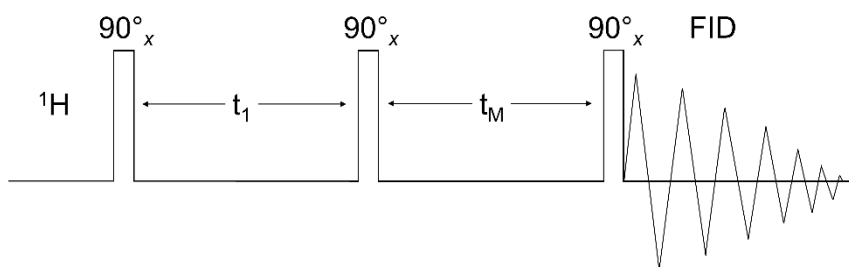


Figure 11: Pulse sequence of 2D NOESY/EXSY experiments according to literature.⁶⁶

The usefulness and reliability of 2D EXSY to verify the proposed reaction mechanism which are the basis of the considerations regarding the results of the kinetic investigations are easily demonstrated with the equilibrium between free aldehyde **15a** and corresponding hydrate **18a** which reflects the situation in solution before the addition of the respective hydroxylamine. To slow down the exchange rate the reaction temperature of this and all following experiments was set to 25 °C. Figure 12 nicely depicts the equilibrium between the aldehyde **15a** ($\delta = 9.99$ ppm) and hydrate **18a** proton ($\delta = 5.92$ ppm) and are pictured as red contours. In contrast, cross peaks resulting from NOEs e.g. between aldehyde proton and the aromatic protons in *ortho* position ($\delta = 8.06$ ppm) or hydrate proton and its aromatic *ortho* protons ($\delta = 7.60$ ppm) are shown in blue contours.

Further Experiments

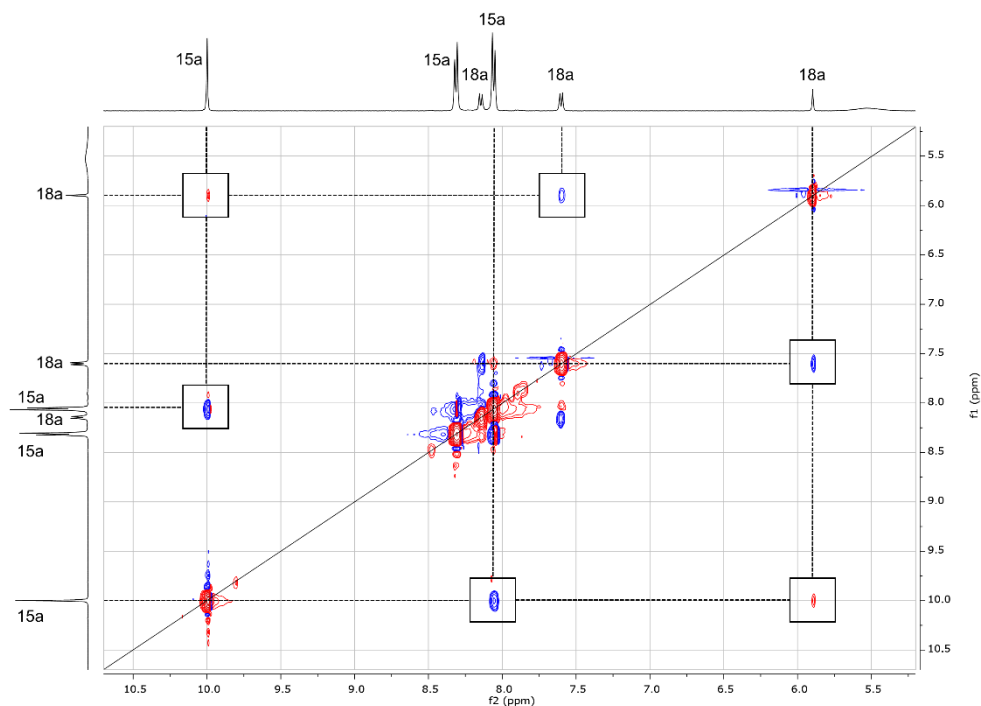


Figure 12: EXSY experiment of pure 4-nitrobenzaldehyde (**15a**) ($\delta = 9.99$ ppm, 8 mM) at 25 °C. Mixing time (t_M) was 1 s. F_1 dimension contained 256 points, F_2 dimension contained 1024 points. Number of scans was 4. NOE signals are characterized by contrary phases, exchange signals by the same phase as the diagonal line.

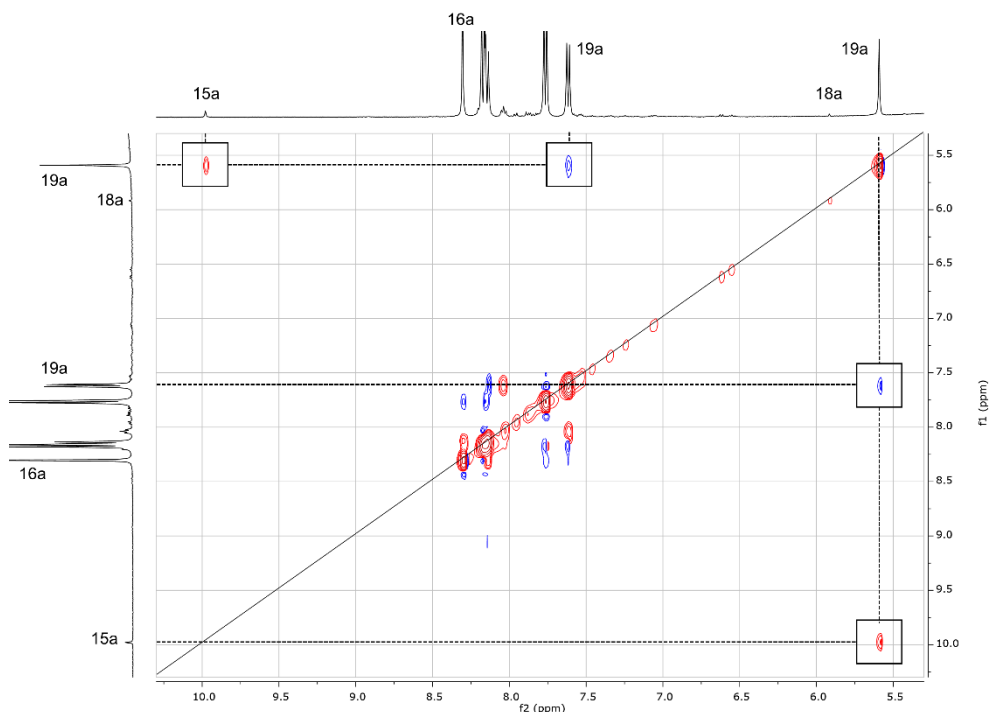
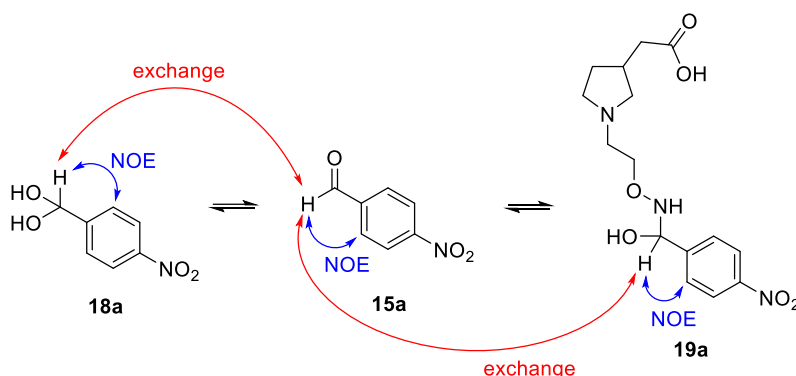


Figure 13: EXSY experiment of the reaction of 4-nitrobenzaldehyde (**15a**) ($\delta = 9.99$ ppm, 8 mM) with hydroxylamine **13** (40 mM) to oxime **16a** at 25 °C. Mixing time (t_M) was 1 s. F_1 dimension contained 256 points, F_2 dimension contained 1024 points. Number of scans was 4. NOE signals are characterized by contrary phases, exchange signals by the same phase as the diagonal line.

Further Experiments

The EXSY experiment was then applied to the whole reaction mixture using 40 mM of hydroxylamine **13**. An equilibrium between the aldehyde **15a** ($\delta = 9.99$ ppm) and another species, referred to the signal at $\delta = 5.59$ ppm was detected leading to the conclusion that this signal is a result of the methine proton of intermediate **19a** (red contour in rectangle, Figure 13). Additionally, the NOE signal between the methine proton and the aromatic protons in *ortho* position ($\delta = 7.62$ ppm) of intermediate **19a** were observed (blue contour in rectangle, Figure 13). All NOEs and exchange signals which were detected in the described ^1H 2D NMR experiments are summarized in Scheme 5.



Scheme 5: Observed NOEs and exchange signals of the shown equilibrium between aldehyde **15a**, its hydrate **18a** and the intermediate **19a** of the reaction with hydroxylamine **13**.

In contrast to **15a**, no formation of the corresponding hydrate species was observed in the spectra of the pure aldehydes **15b-d** (first spectrum of Figure 14, Figure 15 and Figure 16), but directly after the addition of the hydroxylamine **13** one new signal was detected at $\delta = 5.43$ ppm for **15b** and **15c** and $\delta = 5.70$ ppm for **15d**, respectively, which vanished over the reaction time. Because the shift of the intermediate **19a** observed in the kinetic experiments applying 4-nitrobenzaldehyde **15a** was in the same chemical shift region ($\delta = 5.59$ ppm), it was assumed that the newly observed signals are also due to the fast reaction of the aldehyde **15b-d** and the hydroxylamine **13** to the respective hemiaminal **19b-d**. Applying the other three aldehydes to the above mentioned conditions, reaction times of 4.5 h for biphenyl-2-carbaldehyde (**15b**) (Figure 14), 5 h for 4-methoxybenzaldehyde (**15c**) (Figure 15) and the fastest reaction time of 45 minutes for 2-methoxybenzaldehyde (**15d**) (Figure 16) were determined.

Further Experiments

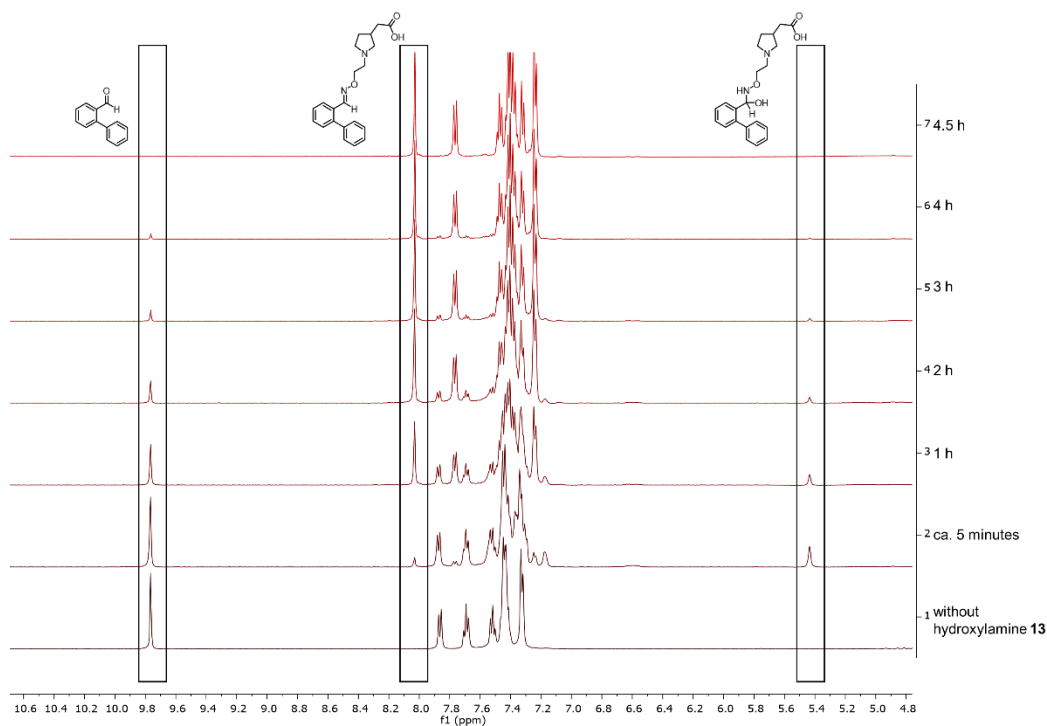


Figure 14: ^1H NMR spectra obtained from the reaction of biphenyl-2-carbaldehyde (**15b**, $\delta = 9.77$ ppm, 8 mM) with hydroxylamine **13** (40 mM) to oxime **16b** ($\delta = 8.03$ ppm) after 1) ca. 5 minutes, 2) 1 h, 3) 2 h, 4) 3 h, 5) 4 h, 6) 4.5 h at 37 °C. Intermediate **19b** could be observed at $\delta = 5.43$ ppm.

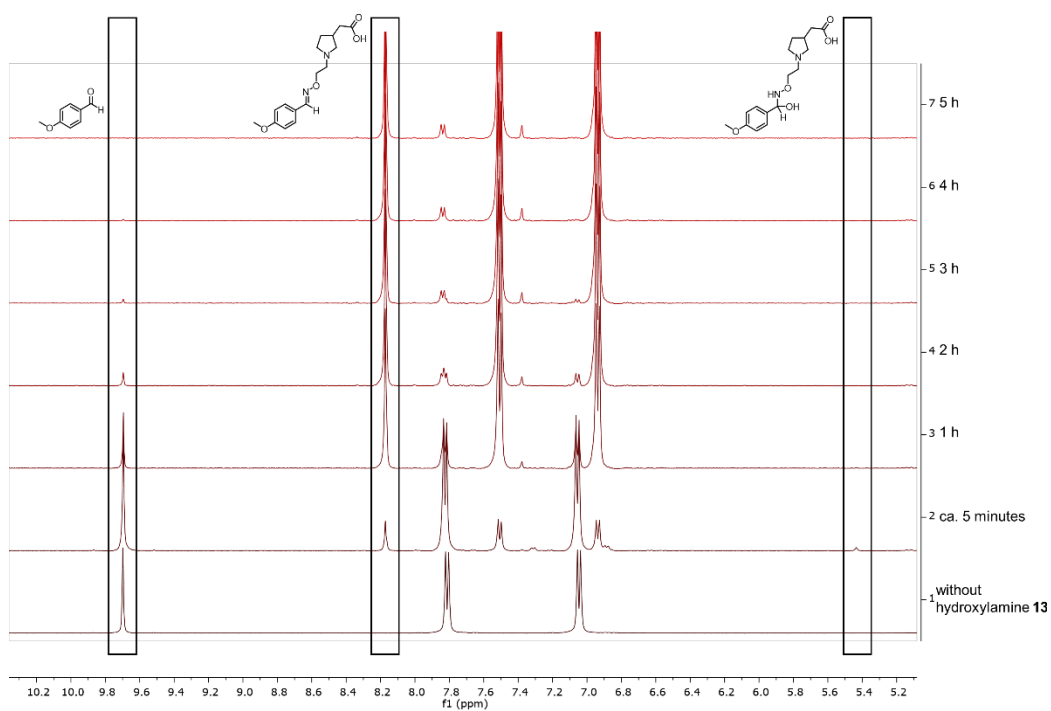


Figure 15: ^1H NMR spectra obtained from the reaction of 4-methoxybenzaldehyde (**15c**, $\delta = 9.70$ ppm, 8 mM) with hydroxylamine **13** (40 mM) to oxime **16c** ($\delta = 8.17$ ppm) after 1) ca. 5 minutes, 2) 1 h, 3) 2 h, 4) 3 h, 5) 4 h, 6) 5 h at 37 °C. Intermediate **19c** could be observed at $\delta = 5.43$ ppm.

Further Experiments

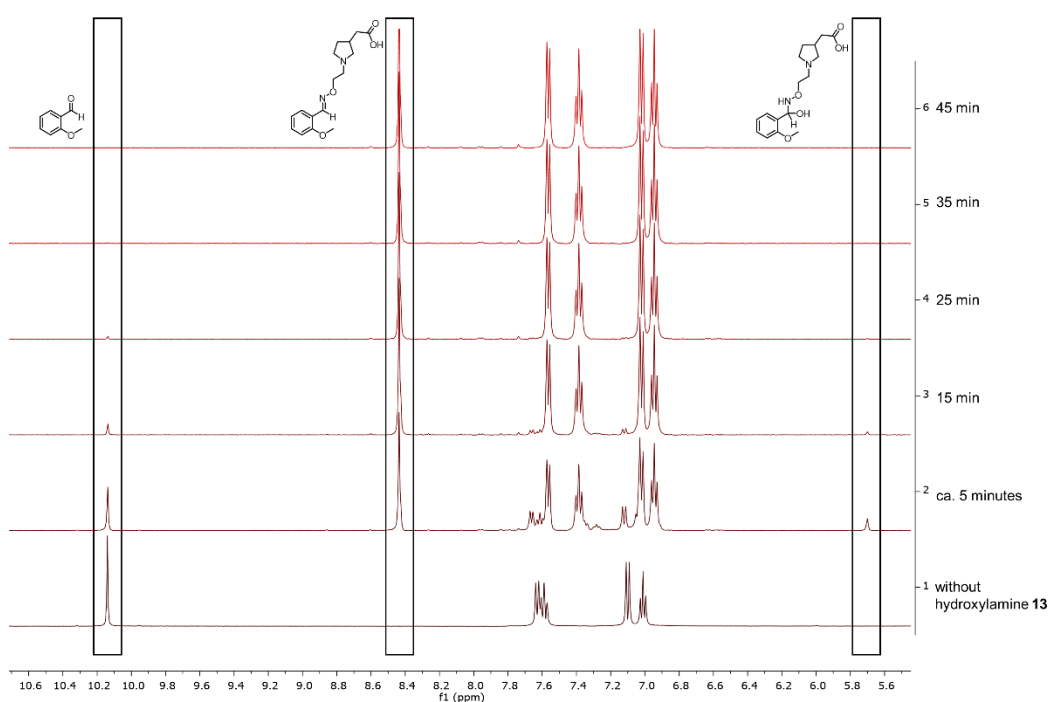


Figure 16: ^1H NMR spectra obtained from the reaction of 2-methoxybenzaldehyde (**15d**, $\delta = 10.14$ ppm, 8 mM) with hydroxylamine **13** (40 mM) to oxime **16d** ($\delta = 8.44$ ppm) after 1) ca. 5 minutes, 2) 15 min, 3) 25 min, 4) 35 min, 5) 45 min at 37 °C. Intermediate **19d** could be observed at $\delta = 5.70$ ppm.

Again, by plotting the sum of the decreasing absolute integral of the reactants – aldehyde and intermediate – and the increasing absolute integral of the oximes versus time the exponential character of all three reactions were observed (Figure 17).

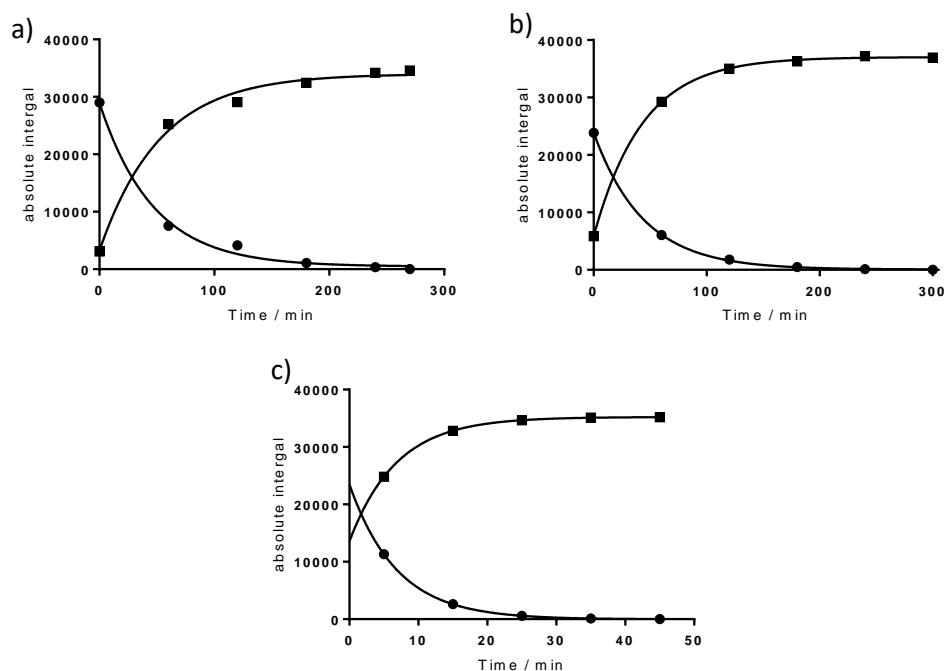


Figure 17: Kinetic plot of reactants and product during a) oxime formation **16b**, b) oxime formation **16c**, and c) oxime formation **16d**.

Further Experiments

4.1.1.2 Kinetic Experiments regarding Library 26

Since the composition of library 26 (Figure 18) was different to all other libraries due to three extraordinary sterically demanding aldehydes (**15i**, **15k** and **15l**) as well as one alkyl aldehyde (**15j**) it was individually tested again by applying standard conditions to verify if those aldehydes presumably slow reacting lead to desired oximes in an appropriate time.

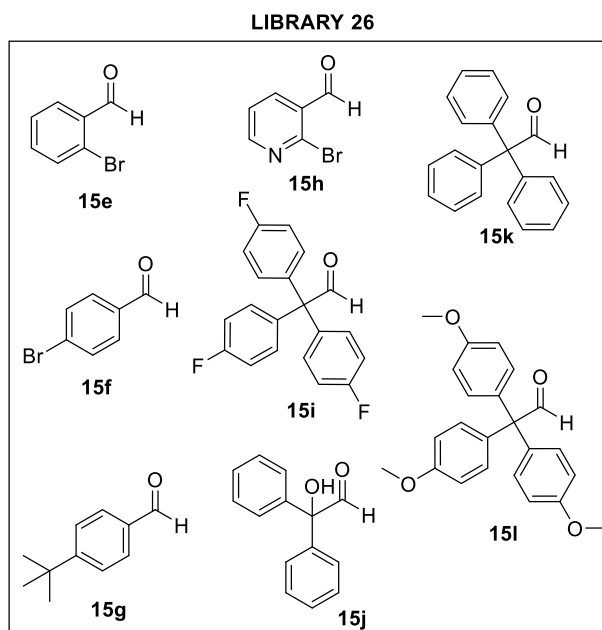


Figure 18: Aldehydes of library 26.

All aldehydes from library 26 were applied in a concentration level of 1 mM. Fortunately, all aldehyde protons could be detected as separate signals in the ^1H NMR spectrum which was recorded before the addition of hydroxylamine **13** (first spectrum, Figure 19). After adding hydroxylamine **13**, five aldehyde signals disappeared over the time period of approximately 11 h, while three signals remained even after 20 h at 37 °C (Figure 19) with no noticeable decrease. This three signals were assumed to refer to the three aldehydes **15i**, **15k** and **15l**. To verify this assumption, the solution of the kinetic experiments was subsequently spiked with one additional equivalent of each aldehyde recording an ^1H NMR spectrum after each addition. After spiking experiment 1 **15k** ($\delta = 10.22$ ppm), after spiking experiment 2 **15i** ($\delta = 10.18$ ppm) and after spiking experiment 3 **15l** ($\delta = 10.10$ ppm, Figure 20), respectively, were identified to not react sufficiently fast enough to the corresponding oximes like aldehydes **15e**, **15f**, **15g**, **15h** and **15j** from the same library. Unfortunately, no conclusion could be drawn with this experimental setup if the tritylaldehydes did not react at all or just incompletely to their corresponding oximes because the relative decrease of the integrals could not be determined. Therefore, in all further experiments 1,3,5-trimethoxybenzene (1 mM, $\delta = 6.05$ ppm) was added as an internal standard to guarantee valid quantification of the aldehyde signals.

Further Experiments

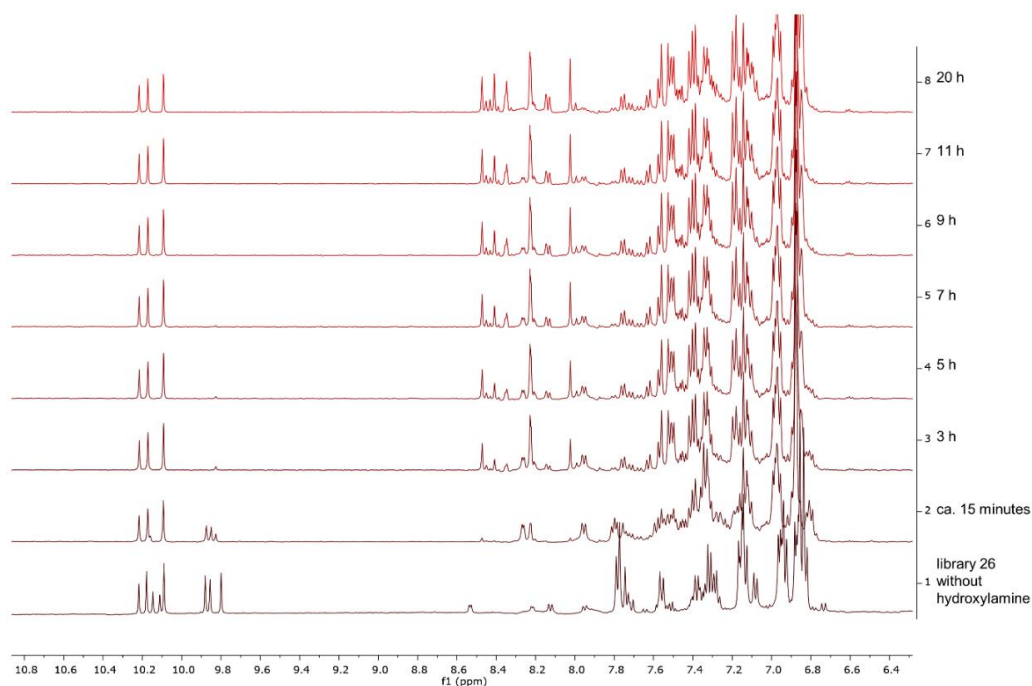


Figure 19: ^1H NMR spectra obtained from the reaction of library 26 ($\delta = 9.80\text{--}10.22$ ppm, 8×1 mM) with hydroxylamine **13** (40 mM) after 1) ca. 15 minutes, 2) 3 h, 3) 5 h, 4) 7 h, 5) 9 h, 6) 11 h, 7) 20 h at 37°C . First spectrum shows library 26 without hydroxylamine **13**.

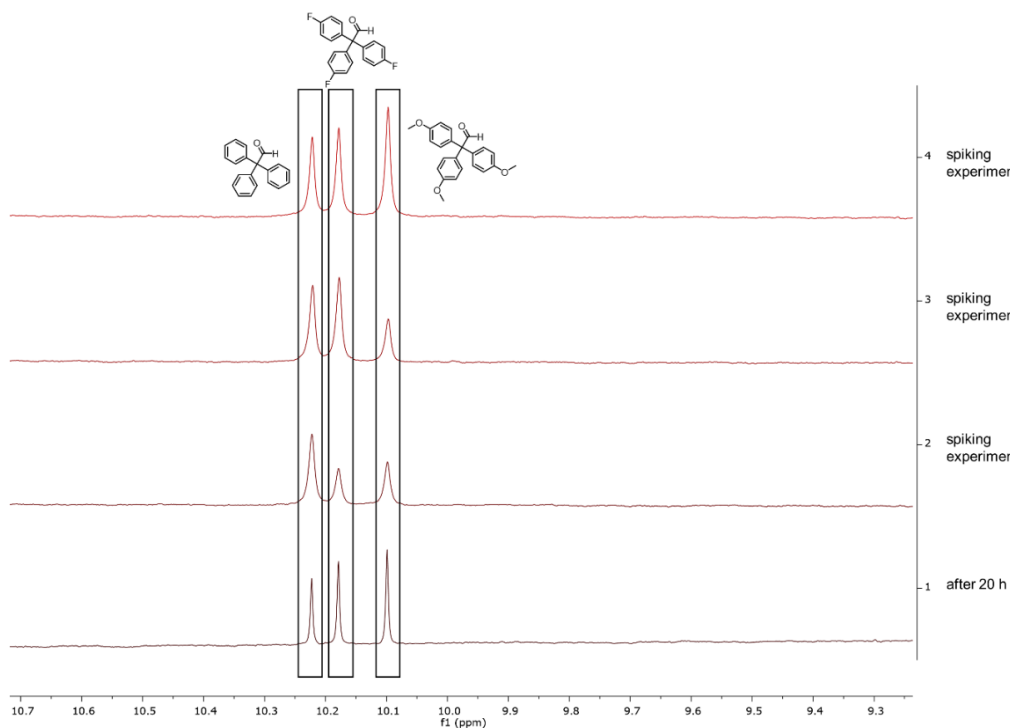


Figure 20: Spiking experiments with reaction solution of the kinetic experiment with library 26 (8×1 mM) and hydroxylamine **13** at 37°C . Addition of one equivalent of **15k** in spiking experiment 1 ($\delta = 10.22$ ppm), one equivalent of **15i** in spiking experiment 2 ($\delta = 10.18$ ppm) and one equivalent of **15l** in spiking experiment 3 ($\delta = 10.10$ ppm).

Further Experiments

Hence, conditions for oxime generation of library 26 had to be adopted and therefore should be reacted at an elevated temperature leaving the buffer system (phosphate buffer with pH 6.0, 40 % DMSO) and the concentration levels of the aldehydes (1 mM each aldehyde) and the hydroxylamine (40 mM) unchanged. Temperature of 80 °C was chosen to be tested first as this is the highest possible temperature without reaching the boiling point of the aqueous amount of the reaction media to prevent potential damage of the NMR instrument during the measurements.

First, all single tritylaldehydes were tested under the newly chosen conditions alone to determine the time till full conversion was reached. After 45 h no aldehyde signal was detected in all three experiments (Figure 21 for **15k**, Figure 22 for **15i**, Figure 23 for **15l**). Once again, library 26 was reacted under the new conditions with hydroxylamine – this time for 45 h – and full conversion to the oximes were verified by the disappearance of all aldehyde signals (Figure 24).

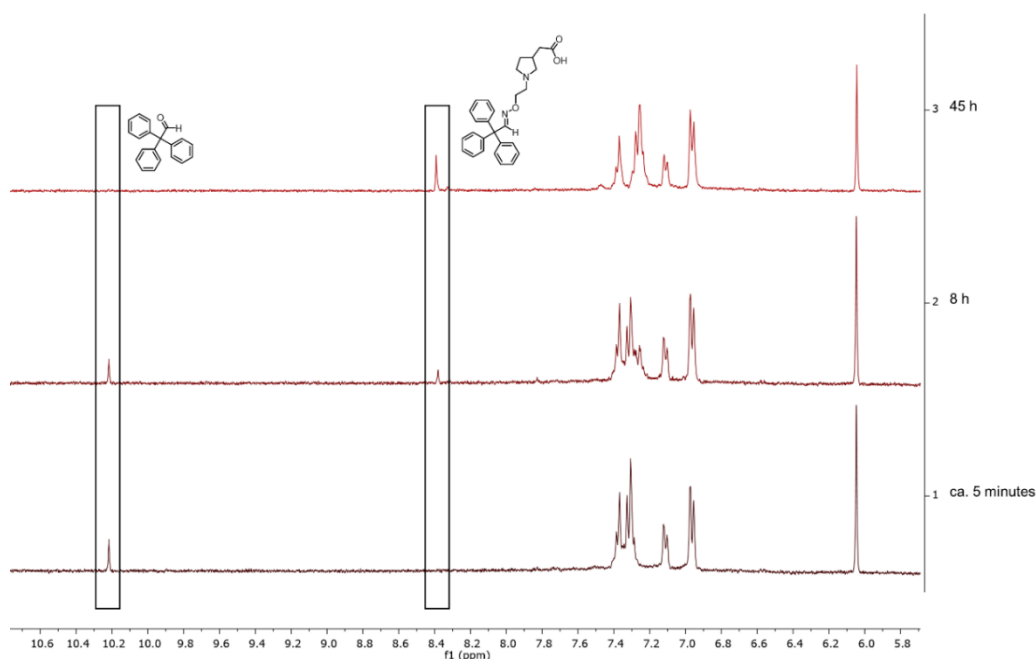


Figure 21: ^1H NMR spectra obtained from the reaction of single aldehyde **15k** ($\delta = 10.22$ ppm, 1 mM) with hydroxylamine **13** (40 mM) to corresponding oximes **16k** ($\delta = 8.38$ ppm) after 1) ca. 5 minutes, 2) 8 h, 3) 45 h at 80 °C. Internal standard is 1,3,5-trimethoxybenzene ($\delta = 6.05$ ppm, 1 mM).

Further Experiments

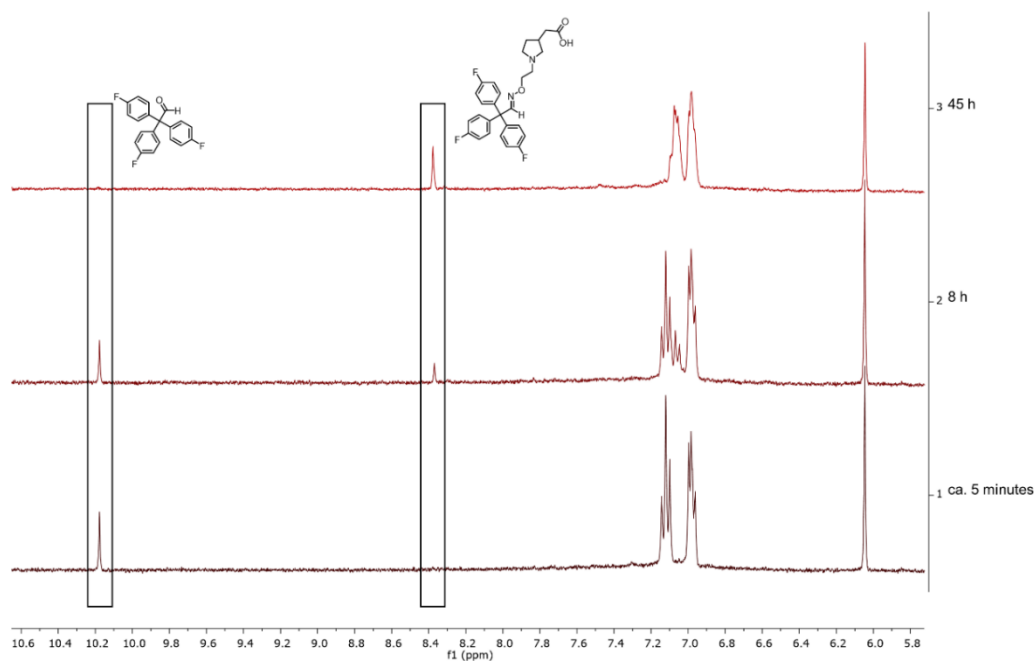


Figure 22: ^1H NMR spectra obtained from the reaction of single aldehyde **15i** ($\delta = 10.18$ ppm, 1 mM) with hydroxylamine **13** (40 mM) to corresponding oximes **16i** ($\delta = 8.37$ ppm) after 1) ca. 5 minutes, 2) 8 h, 3) 45 h at 80 °C. Internal standard is 1,3,5-trimethoxybenzene ($\delta = 6.05$ ppm, 1 mM).

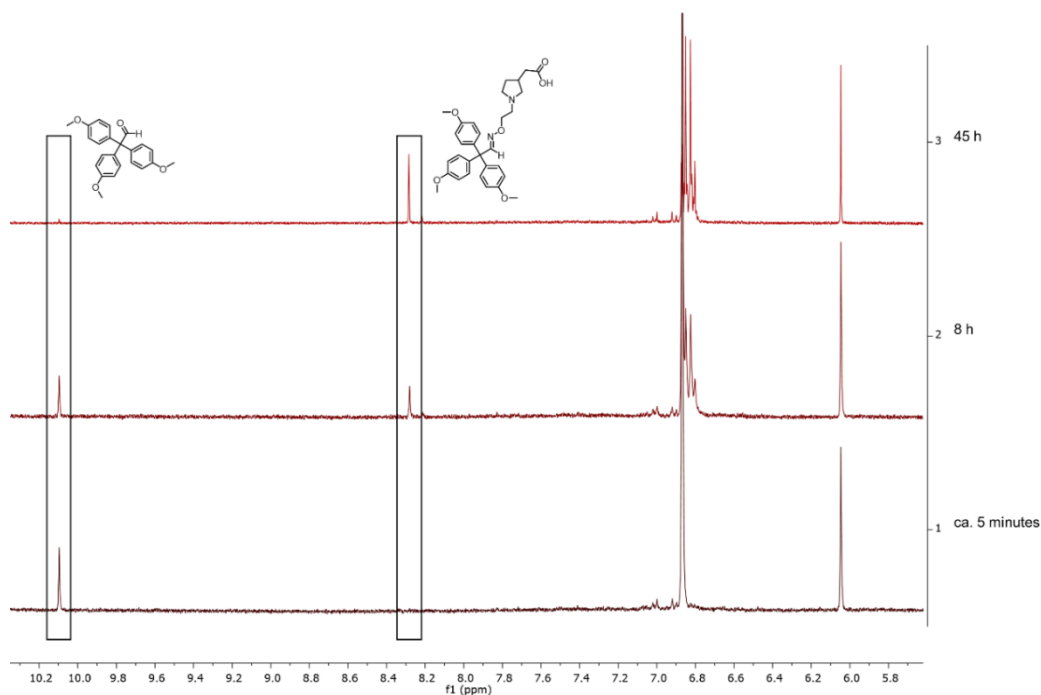


Figure 23: ^1H NMR spectra obtained from the reaction of single aldehyde **15l** ($\delta = 10.10$ ppm, 1 mM) with hydroxylamine **13** (40 mM) to corresponding oximes **16l** ($\delta = 8.28$ ppm) after 1) ca. 5 minutes, 2) 8 h, 3) 45 h at 80 °C. Internal standard is 1,3,5-trimethoxybenzene ($\delta = 6.05$ ppm, 1 mM).

Further Experiments

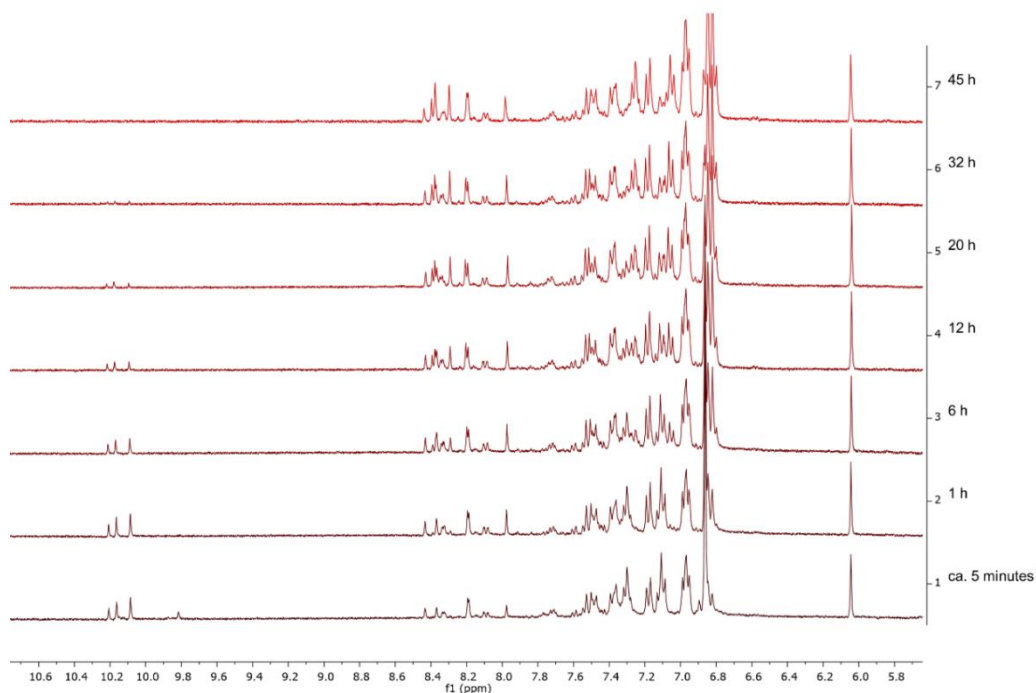


Figure 24: ¹H NMR spectra obtained from the reaction of library 26 (δ = 9.80–10.22 ppm, 8 x 1 mM) with hydroxylamine **13** (40 mM) after 1) ca. 5 minutes, 2) 1 h, 3) 6 h, 4) 12 h, 5) 20 h, 6) 32 h, 7) 45 h at 80 °C. Internal standard is 1,3,5-trimethoxybenzene (δ = 6.05 ppm, 1 mM).

Further Experiments

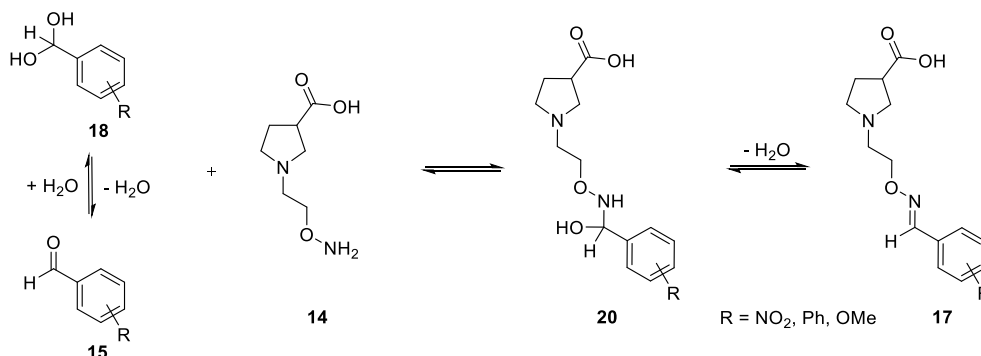
4.1.2 Kinetic Experiments using Pyrrolidine-3-carboxylic acid derived Hydroxylamine

4.1.2.1 Reaction with Single Aldehydes

The experiments utilizing 2-{1-[(2-aminooxy)ethyl]pyrrolidine-3-yl}carboxylic acid **14** was examined under the same conditions as used before for the oxime generation. By applying phosphate buffer (pH 6.0, 12.5 mM Na₂HPO₄, 12.5 mM NaH₂PO₄, 1 M NaCl, pH value adjusted with 1 M HCl, 10 % D₂O) with 40 % DMSO-*d*₆ at 37 °C, the three different single aldehydes **15a**, **15b** and **15d** were tested with an elevated concentration of 8 mM to be converted to the corresponding oximes within 20 h. Again, signal of the aldehyde proton and the signal of the oxime proton were monitored and upon the disappearance of the aldehyde signal the equilibrium was seen as fully on the site of the product.

Again, the spectra were recorded with a proton pulse sequence including an excitation sculpting block for water suppression. The spectra were recorded before the addition of the hydroxylamine **14**, directly after the addition of **14** and repeated for 20 hours with a time increment of 10 minutes. For the sake of clarity only the significant signals of e. g. the aldehyde proton or the oxime proton are labeled in the spectra. Additionally, signals which were found to play a role within the reaction (e.g. intermediates) were also labeled with a rectangle.

For the full conversion of 4-nitrobenzaldehyde **15a** with **14** to oxime **17a** (δ = 8.33 ppm, Figure 25) and of biphenyl-2-carbaldehyde **15b** with **14** to oxime **17b** (δ = 8.04 ppm, Figure 26) with reaction times of 6 h and 4 h were required, respectively and the fastest reaction time of 55 minutes was detected for the formation of oxime **17d** (δ = 8.42 ppm, Figure 27) from 2-methoxybenzaldehyde **15d** as already determined by using 2-(pyrrolidin-3-yl)acetic acid derivative **13**. Not surprisingly, hydrate formation was again detected for 4-nitrobenzaldehyde (**18a**, δ = 5.93 ppm, Figure 25) in phosphate buffer containing 40 % DMSO and for all three kinetic experiments the intermediates **20** of the condensation reaction were seen in the spectra at δ = 5.61 ppm for **20a**, δ = 5.45 ppm for **20b** and δ = 5.71 ppm for **20d**, respectively. The proposed reaction mechanism is shown in Scheme 6.



Scheme 6: Formation of hydrate **18** and condensation reaction of hydroxylamine **14** with respective aldehydes **15** via tetrameric intermediates **20** to the corresponding oximes **17**.

Further Experiments

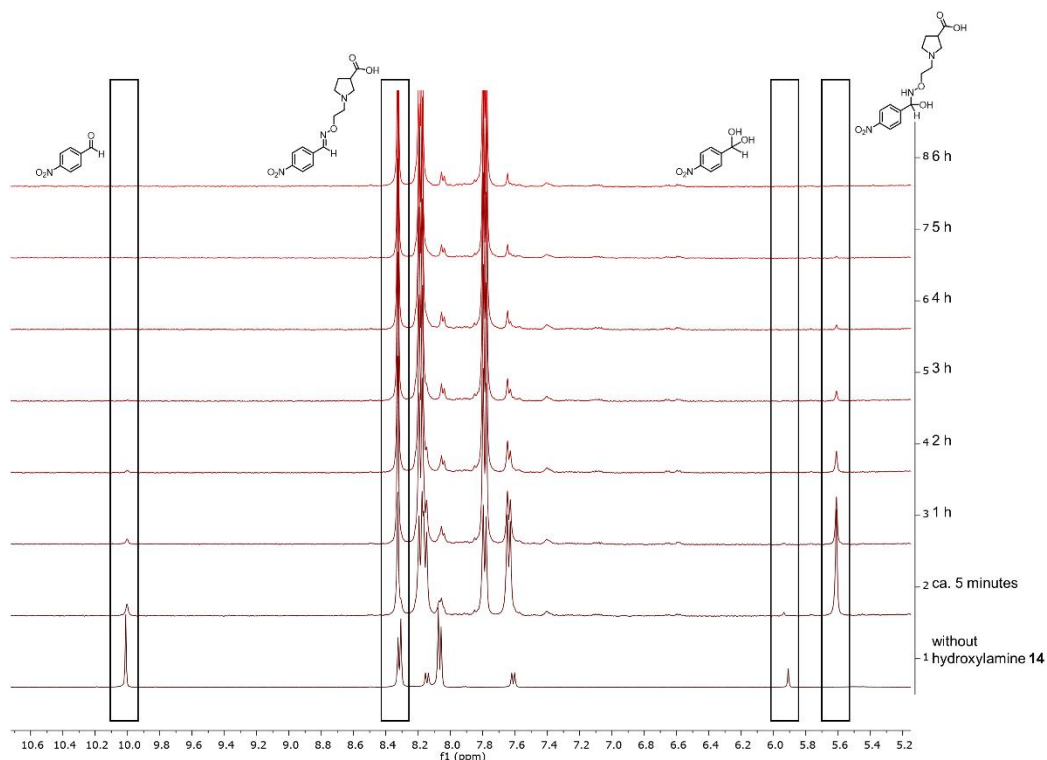


Figure 25: ^1H NMR spectra obtained from the reaction of 4-nitrobenzaldehyde (**15a**, $\delta = 9.99$ ppm, 8 mM) with hydroxylamine **14** (40 mM) to oxime **17a** ($\delta = 8.33$ ppm) after 1) ca. 5 minutes, 2) 1 h, 3) 2 h, 4) 3 h, 5) 4 h, 6) 5 h, 7) 6 h at 37 °C. Hydrate of 4-nitrobenzaldehyde **18a** observed at 5.93 ppm; intermediate **20a** observed at $\delta = 5.61$ ppm.

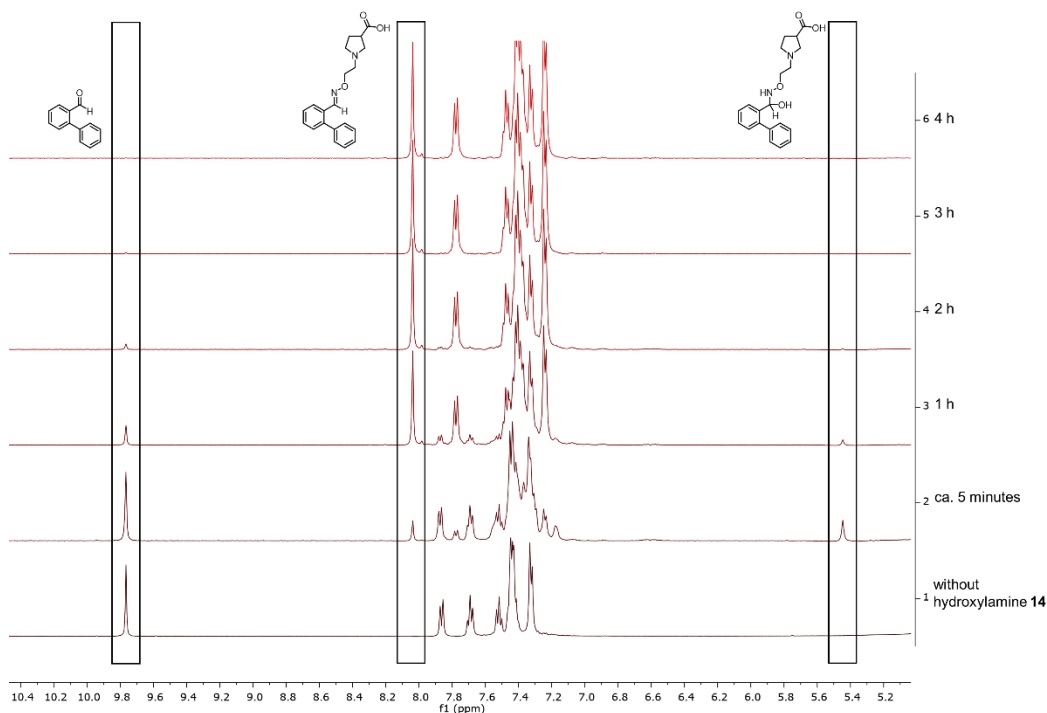


Figure 26: ^1H NMR spectra obtained from the reaction of biphenyl-2-carbaldehyde (**15b**, $\delta = 9.77$ ppm, 8 mM) with hydroxylamine **14** (40 mM) to oxime **17b** ($\delta = 8.04$ ppm) after 1) ca. 5 minutes, 2) 1 h, 3) 2 h, 4) 3 h, 5) 4 h at 37 °C. Intermediate **20b** could be observed at $\delta = 5.45$ ppm.

Further Experiments

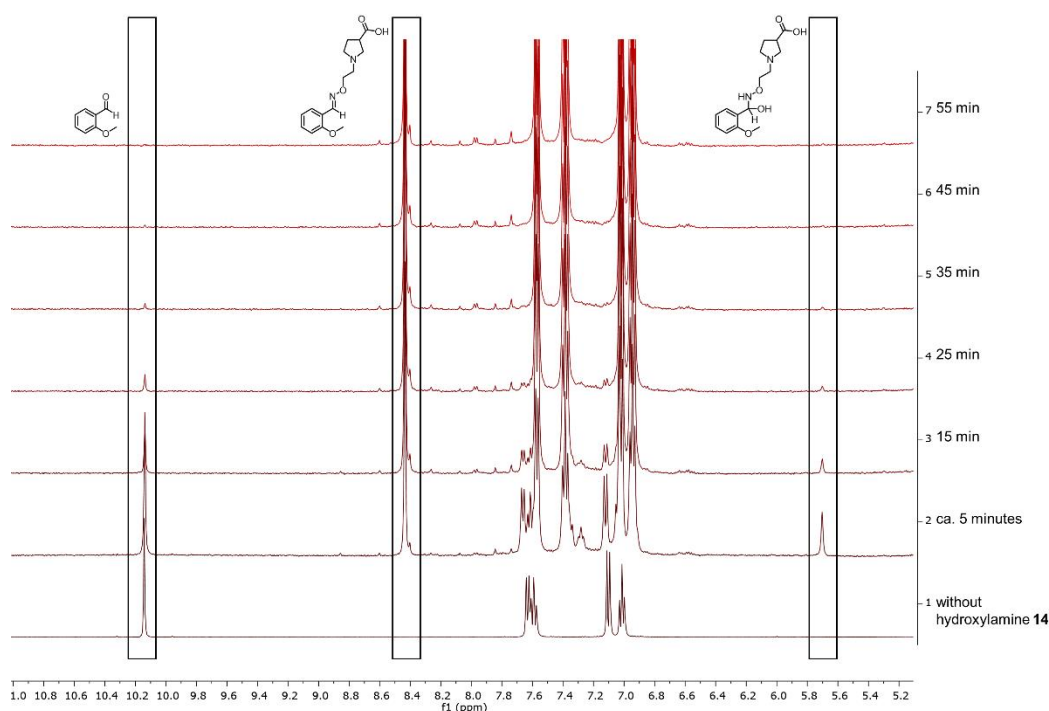


Figure 27: ^1H NMR spectra obtained from the reaction of 2-methoxybenzaldehyde (**15d**, $\delta = 10.14$ ppm, 8 mM) with hydroxylamine **14** (40 mM) to oxime **17d** ($\delta = 8.42$ ppm) after 1) ca. 5 minutes, 2) 15 min, 3) 25 min, 4) 35 min, 5) 45 min, 6) 55 min at 37 °C. Intermediate **20d** could be observed at $\delta = 5.71$ ppm.

The sum of the decreasing absolute integrals of the signals of the aldehydes, hydrate (in the case of aldehyde **15a**) and the intermediates and the increasing absolute integrals of the product signal are again plotted versus time in which the exponential decay of the reactants and the exponential increase of the oximes are clearly observed (Figure 28).

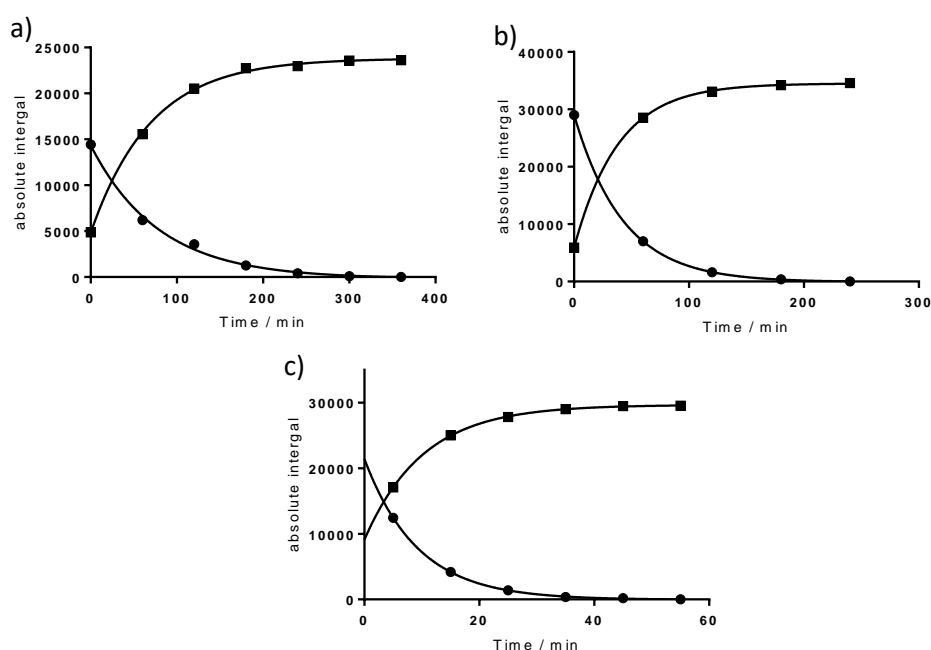


Figure 28: Kinetic plot of reactants and product during a) oxime formation **17a**, b) oxime formation **17b**, and c) oxime formation **17d**.

Further Experiments

4.1.2.2 Kinetic Experiments regarding Library 26

When library 26 (Figure 18, 1 mM of each aldehyde) was reacted with pyrrolidine-3-carboxylic acid derived hydroxylamine **14** as reactant the three sterically hindered tritylaldehydes **15k** ($\delta = 10.22$ ppm), **15i** ($\delta = 10.18$ ppm) and **15l** ($\delta = 10.10$ ppm) were again not fully converted to the corresponding oximes as all three aldehyde signals were still detected after 20 h reaction time at 37 °C (Figure 29). By raising the reaction temperature to 80 °C, the single oximes were generated within 45 h which can be seen in Figure 30 for aldehyde **15k**, in Figure 31 for **15i** and in Figure 32 for **15l**, respectively. As expected full conversion of all oximes in the whole library could be accomplished by reacting the mentioned library 26 at 80 °C for 45 h (Figure 33). Accordingly, this particular oxime library was generated separately from all other libraries.

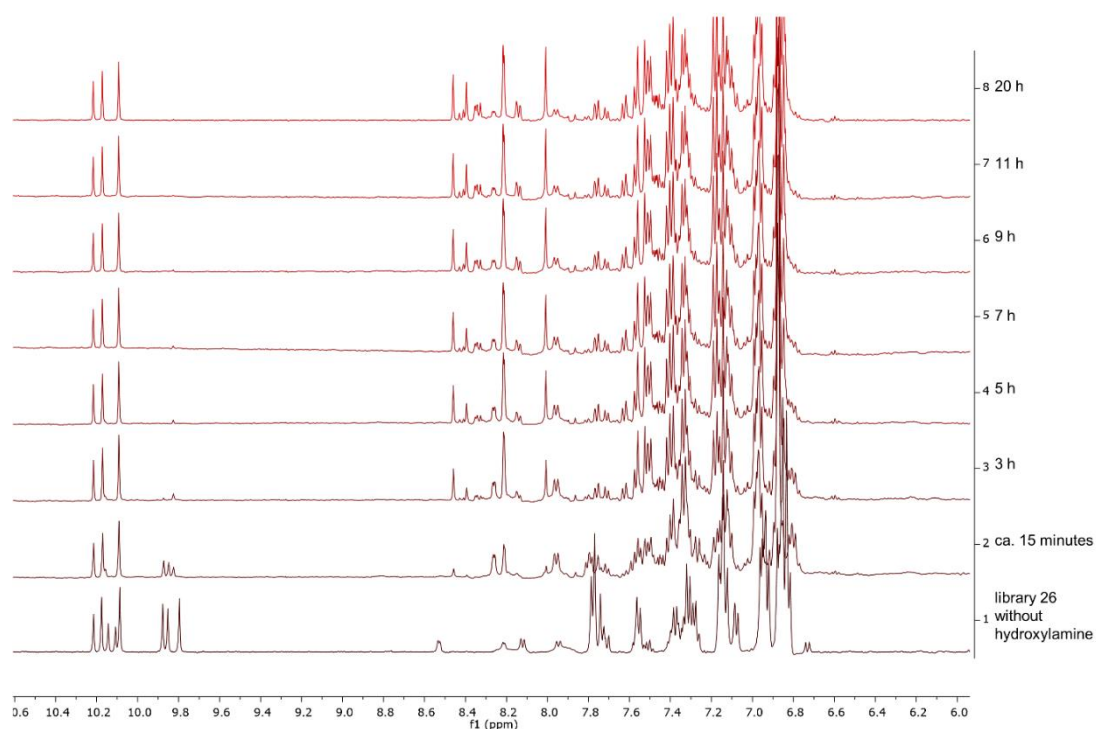


Figure 29: ^1H NMR spectra obtained from the reaction of library 26 ($\delta = 9.80\text{--}10.22$ ppm, 8×1 mM) with hydroxylamine **14** (40 mM) after 1) ca. 15 minutes, 2) 3 h, 3) 5 h, 4) 7 h, 5) 9 h, 6) 11 h, 7) 20 h at 37 °C. First spectrum shows library 26 without hydroxylamine **14**.

Further Experiments

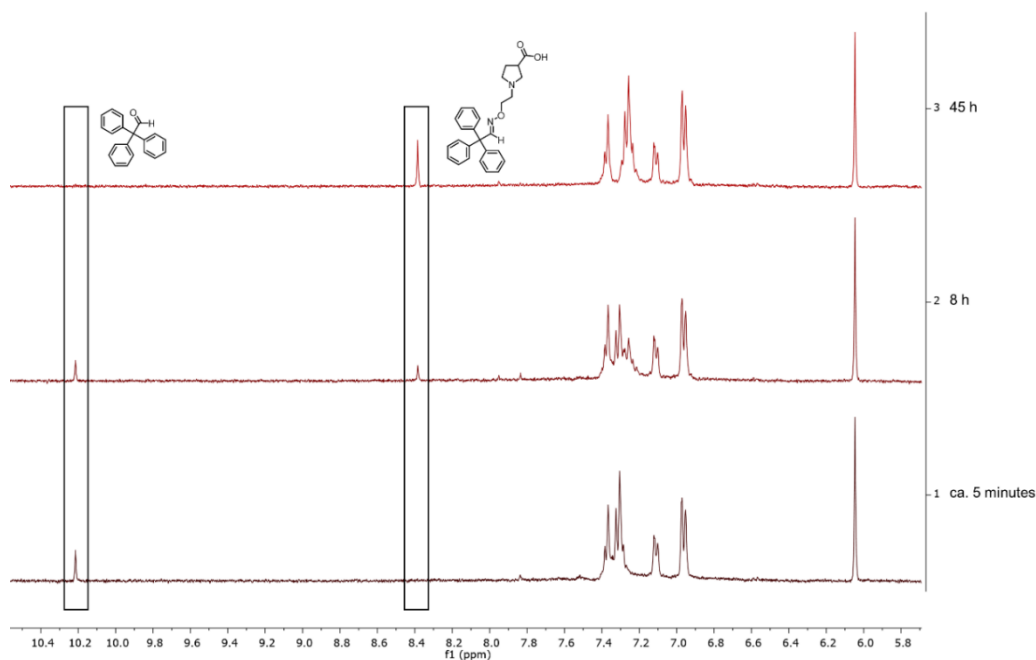


Figure 30: ^1H NMR spectra obtained from the reaction of single aldehyde **15k** ($\delta = 10.22$ ppm, 1 mM) with hydroxylamine **14** (40 mM) to corresponding oximes **17k** ($\delta = 8.38$ ppm) after 1) ca. 5 minutes, 2) 8 h, 3) 45 h at 80 °C. Internal standard is 1,3,5-trimethoxybenzene ($\delta = 6.05$ ppm, 1 mM).

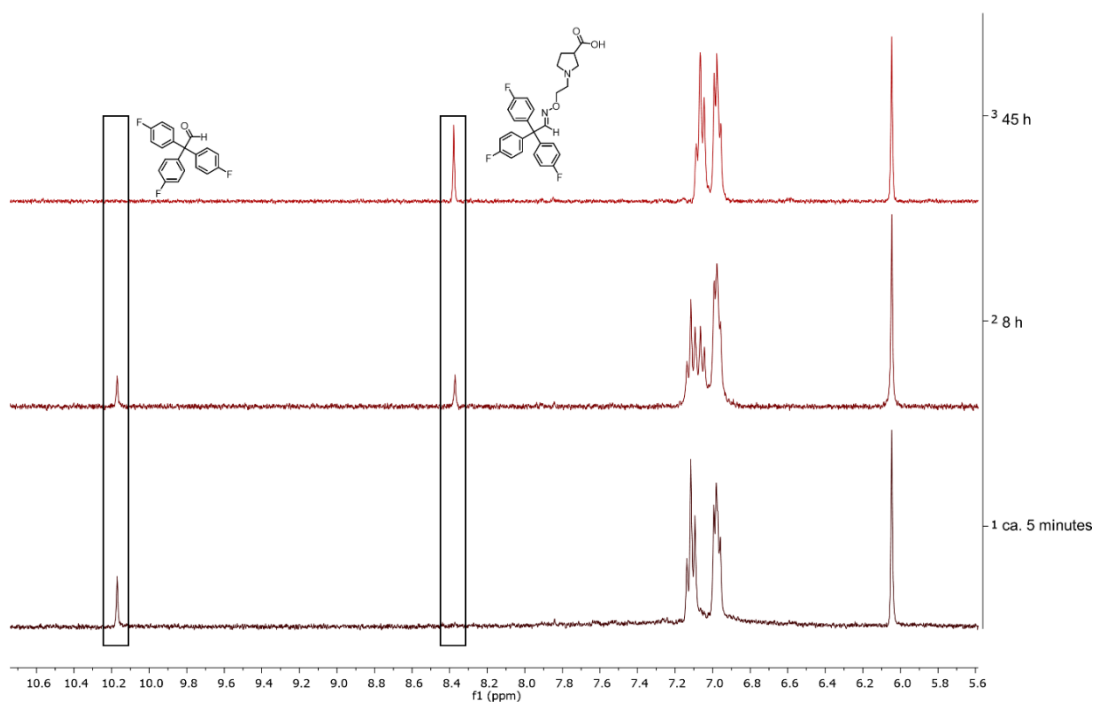


Figure 31: ^1H NMR spectra obtained from the reaction of single aldehyde **15i** ($\delta = 10.18$ ppm, 1 mM) with hydroxylamine **14** (40 mM) to corresponding oximes **17i** ($\delta = 8.37$ ppm) after 1) ca. 5 minutes, 2) 8 h, 3) 45 h at 80 °C. Internal standard is 1,3,5-trimethoxybenzene ($\delta = 6.05$ ppm, 1 mM).

Further Experiments

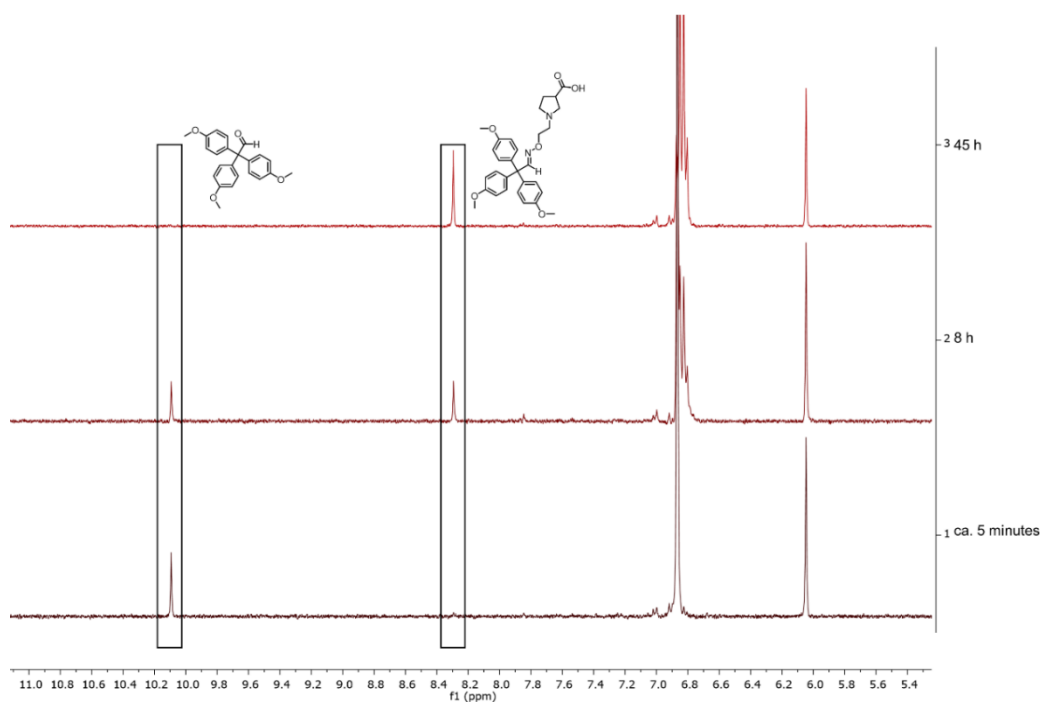


Figure 32: ^1H NMR spectra obtained from the reaction of single aldehyde **15I** ($\delta = 10.10$ ppm, 1 mM) with hydroxylamine **14** (40 mM) to corresponding oximes **17i** ($\delta = 8.29$ ppm) after 1) ca. 5 minutes, 2) 8 h, 3) 45 h at 80 °C. Internal standard is 1,3,5-trimethoxybenzene ($\delta = 6.05$ ppm, 1 mM).

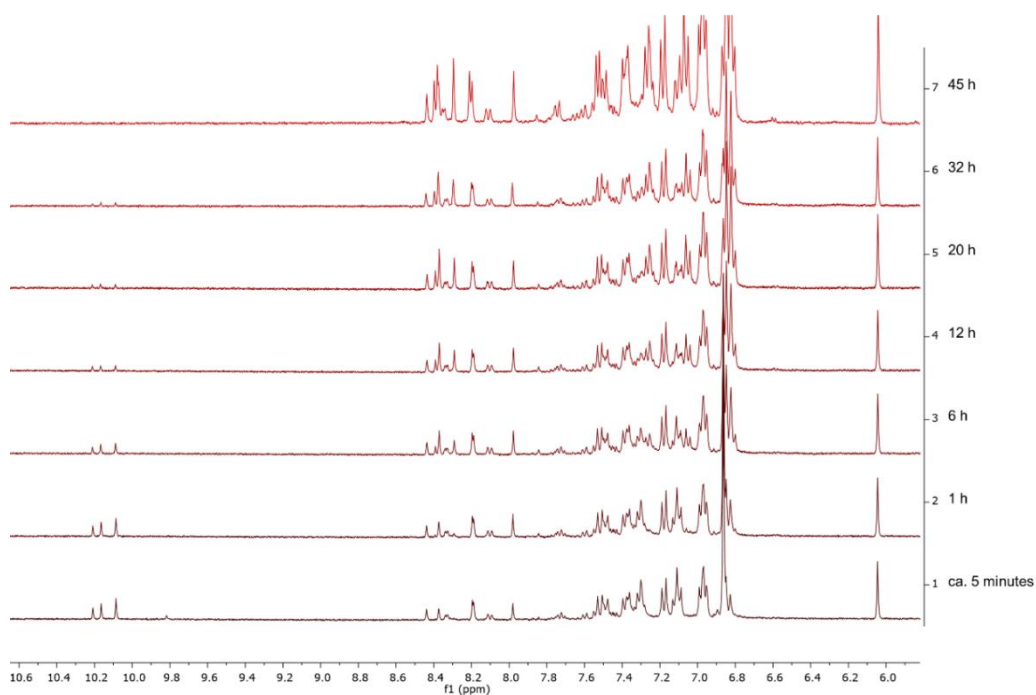


Figure 33: ^1H NMR spectra obtained from the reaction of library **26** ($\delta = 9.80\text{--}10.22$ ppm, 8 x 1 mM) with hydroxylamine **14** (40 mM) after 1) ca. 5 minutes, 2) 1 h, 3) 6 h, 4) 12 h, 5) 20 h, 6) 32 h, 7) 45 h at 80 °C. Internal standard is 1,3,5-trimethoxybenzene ($\delta = 6.05$ ppm, 1 mM).

4.2 Generated Libraries – Stability Experiments

Due to the fact that after the oxime generation samples had to be diluted for the screening experiments stability measurement had to be performed to proof that they do not undergo hydrolysis and that their concentrations do not change throughout the whole biological evaluation. Since the final concentrations applied for screening were too low for ^1H NMR spectroscopy measurements UV or fluorescence measurements were chosen to detect any decrease in concentration of formed oximes. Therefore, subsequent to the oxime generation the samples with eight different oximes were diluted with phosphate buffer (pH 7.1, 12.5 mM Na_2HPO_4 , 12.5 mM NaH_2PO_4 , 1 M NaCl, pH value was adjusted with 1 M NaOH) containing 1 % DMSO for the incubation with the target mGAT1 at 37 °C for 4 h. For oximes with 2-(pyrrolidin-3-yl)acetic acid motif three different concentration levels of 1 μM , 100 nM and 10 nM, respectively and for pyrrolidine-3-carboxylic acid derived oximes only one concentration of 1 μM were used for these experiments. The samples of the kinetic experiments which were obtained by applying the single aldehydes **15a**, **15b**, **15c**, **15d**, **15k**, **15i** and **15l** were used and the fluorescence measurements were recorded on a Spectra-Max M2e Plate Reader (Molecular Devices) and were analyzed by using Soft-Max Pro 5.4 software. In the case of 4-nitrobenzaldehyde derived oxime **16a** additional measurements were recorded by using Cary Eclipse fluorescence spectrophotometer (Varian) equipped with Cary Temperature Controller and were analyzed by Cary Eclipse software (version: 1.1.(132)).

First, absorption spectra of the oxime and the corresponding aldehydes were recorded, but in the cases of oxime derived from **15a**, **15b**, **15c** and **15d** the spectra did not differentiate in such manner that only the oxime was excited when using one particular wavelength without exciting the aldehyde to some extent. But by using fluorescence measurements, it was possible to determine an emission wavelength for each oxime at which the corresponding aldehyde had only a small contribution to the fluorescence signal ($\leq 5\%$). For the tritylaldehyde derived oximes **16k**, **16i**, **16l**, **17k**, **17i** and **17l** absorption behavior of oximes and aldehydes were indeed different, but for the sake of comparability and to receive the highest possible signal for all concentration levels to observe changes in the fluorescence signal in a reliable manner, it was decided to examine the stability of the oximes resulting from tritylaldehydes in the same way as for the other compounds, i.e. by using fluorescence measurements. Hence, suitable condition for each oxime had to be identified to determine the stability of the equilibrium indicated by a stable fluorescence signal for the incubation time of 4 h.

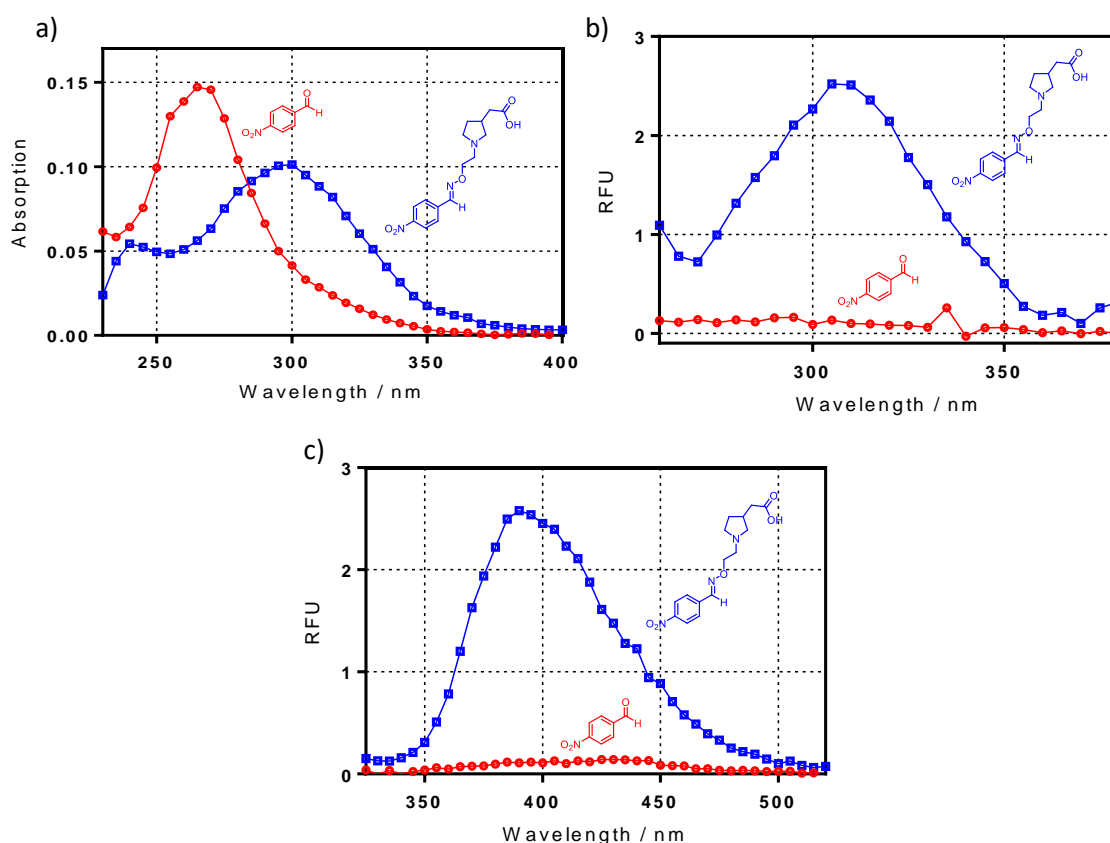
To observe changes in the equilibrium towards the reactants in a reliable way, linearity between the fluorescence signal and concentration of the oxime had to be proven. Therefore, different concentration levels including the concentrations at which stability should be verified were measured using the determined wavelength for each oxime in triplicates.

Further Experiments

After proofing linearity, the steady state of the equilibrium of the freshly diluted oximes were examined using the wavelengths as determined before for 4 h at 37 °C.

4.2.1 Stability Experiments using 2-(Pyrrolidin-3-yl)acetic acid derived Oximes

Absorption spectrum of oxime **16a** – obtained by the reaction of **13** with 4-nitrobenzaldehyde **15a** – overlapped significantly with the spectrum of the aldehyde **15a** (Figure 34a) but fluorescence measurements revealed the maximum excitation wavelength of $\lambda = 305$ nm and emission wavelength of $\lambda = 390$ nm whereas the aldehyde **15a** constituted 4.3 % of the total emission (Figure 34b and Figure 34c). Linearity was found for concentrations between 12.5 μ M and 100 nM (Figure 35a) and by employing 10 μ M and 1 μ M no change of the fluorescence signal was detected (Figure 36a and Figure 36b), respectively. But using 100 nM concentration the fluorescence signal was too low (RFU = 0.09) to detect changes in the signal. To overcome this problem, Cary Eclipse fluorescence spectrophotometer (Varian) equipped with Cary Temperature Controller was used because this device was able to reveal higher signal intensities for the same concentrations which could be seen as linearity was limited to concentration levels up to 5 μ M (Figure 35b). Hence, stability for sample with 100 nM concentration level was successfully measured with fluorescence intensity which allowed to detect changes of the signal (RFU = 0.4, Figure 36c).



Further Experiments

Figure 34: a) UV spectra (absorption versus wavelength, nm), b) excitation spectra [RFU versus wavelength, nm ($\lambda_{\text{ex}} = 260\text{--}380$ nm, $\lambda_{\text{em}} = 400$ nm)] and c) fluorescence spectra [RFU versus wavelength, nm ($\lambda_{\text{ex}} = 305$ nm, $\lambda_{\text{em}} = 335\text{--}520$ nm)]. Each spectrum obtained by measurements of 4-nitrobenzaldehyde (**15a**) (10 μM , red) and oxime **16a** (10 μM , blue). Spectra were recorded in phosphate buffer (pH 7.1) with 1 % DMSO at 37 $^{\circ}\text{C}$ and were corrected by subtraction of the spectrum of the pure solvent as blank.

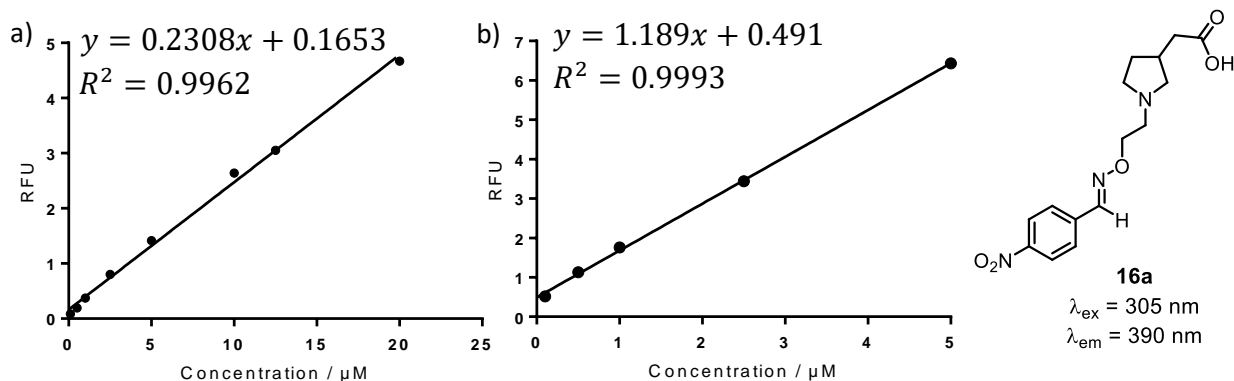


Figure 35: Determination of the linear range (RFU versus concentration, μM) in regard to oxime **16a** at different concentration levels in phosphate buffer (pH 7.1) with 1 % DMSO at 37 $^{\circ}\text{C}$ ($\lambda_{\text{ex}} = 305$ nm, $\lambda_{\text{em}} = 390$ nm). Measurements were recorded on a) Spectra-Max M2e Plate Reader or b) Cary Eclipse fluorescence spectrophotometer (Varian) equipped with Cary Temperature Controller.

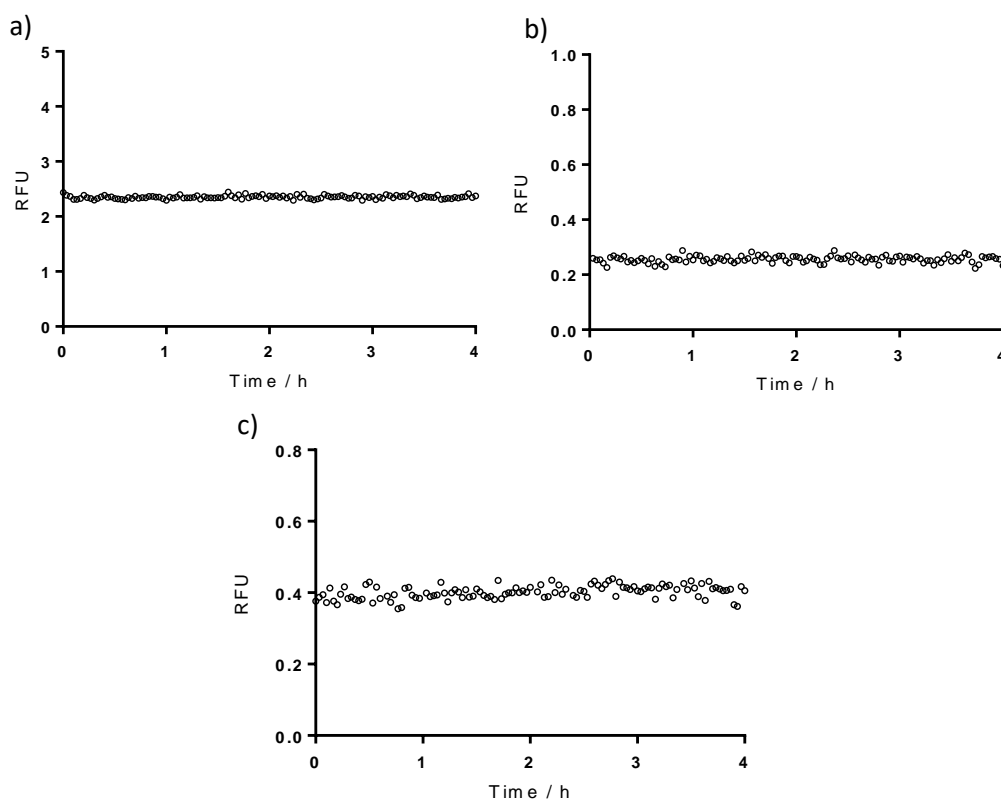


Figure 36: Monitoring of the fluorescence emission of oxime **16a** for possible change of the reaction equilibrium towards the starting materials 4-nitrobenzaldehyde (**15a**) and hydroxylamine **13** at 37 $^{\circ}\text{C}$ for 4 h after dilution with phosphate buffer (pH 7.1 + 1 % DMSO) to concentration levels of a) 10 μM , b) 1 μM and c) 0.1 μM ($\lambda_{\text{ex}} = 305$ nm, $\lambda_{\text{em}} = 390$ nm).

Further Experiments

In the case of biphenyl-2-carbaldehyde derived oxime **16b**, again no wavelength could be determined at which exclusively or mostly the oxime **16b** was detected (Figure 37a) without disturbance from the aldehyde **15b**. Excitation wavelength and emission wavelength was found to be $\lambda = 250$ nm and $\lambda = 385$ nm, respectively (Figure 37b and Figure 37c) under which the contribution of the aldehyde to the emission signal is 1.8%. Linearity was determined between 12.5 μ M and 100 nM with R^2 of 0.9977 (Figure 38) and on this basis, stability was proven at three concentration levels of 10 μ M, 1 μ M and 100 nM (Figure 39).

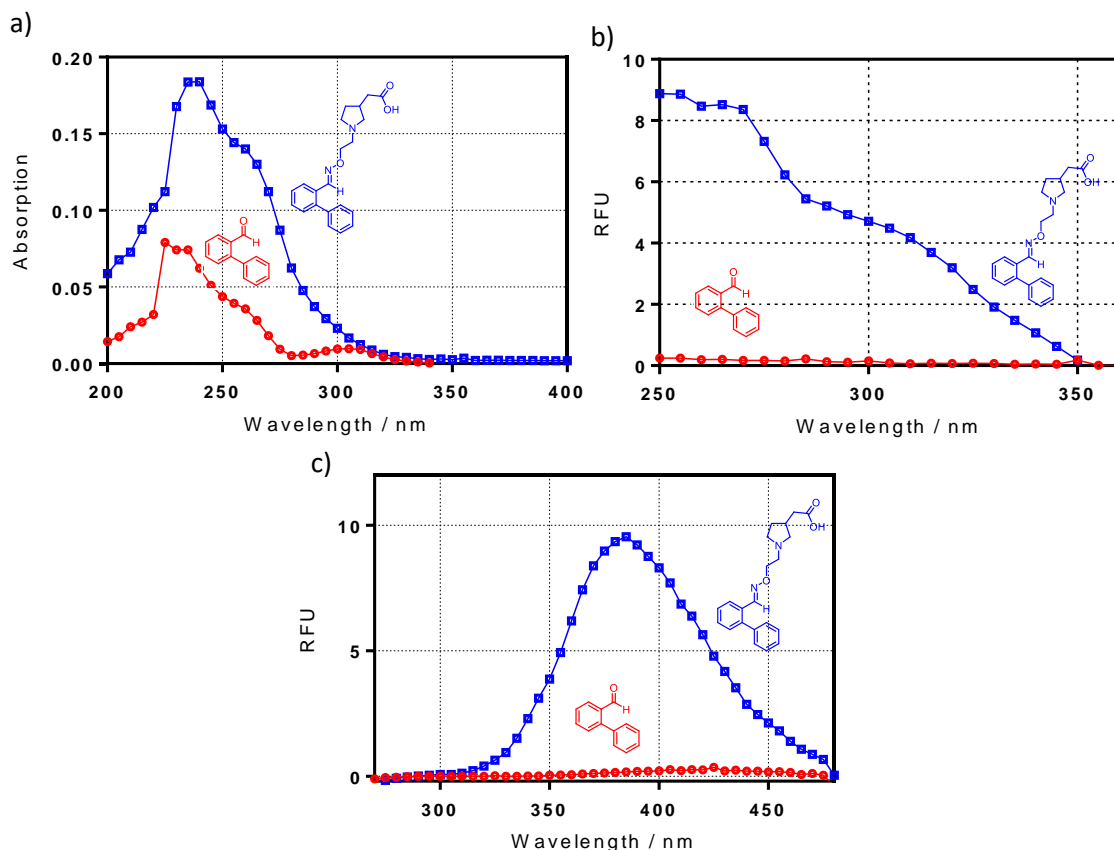
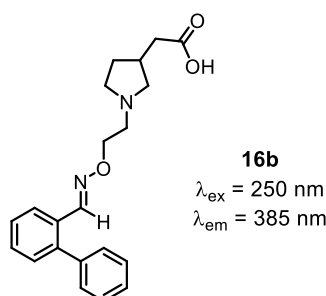
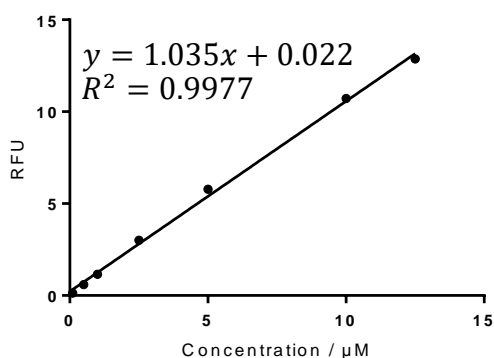


Figure 37: a) UV spectra (absorption versus wavelength, nm), b) excitation spectra [RFU versus wavelength, nm ($\lambda_{\text{ex}} = 250\text{--}360$ nm, $\lambda_{\text{em}} = 370$ nm)] and c) fluorescence spectra [RFU versus wavelength, nm ($\lambda_{\text{ex}} = 250$ nm, $\lambda_{\text{em}} = 270\text{--}470$ nm)]. Each spectrum obtained by measurements of biphenyl-2-carbaldehyde (**15b**) (10 μ M, red) and oxime **16b** (10 μ M, blue). Spectra were recorded in phosphate buffer (pH 7.1) with 1 % DMSO at 37 °C and were corrected by subtraction of the spectrum of the pure solvent as blank.



Further Experiments

Figure 38: Determination of the linear range [RFU versus concentration, μM ($R^2 = 0.9977$)] in regard to oxime **16b** in different concentration levels (12.5 μM , 10 μM , 5 μM , 2.5 μM , 1 μM , 0.5 μM , 0.1 μM) in phosphate buffer (pH 7.1) with 1 % DMSO at 37 °C ($\lambda_{\text{ex}} = 250 \text{ nm}$, $\lambda_{\text{em}} = 385 \text{ nm}$).

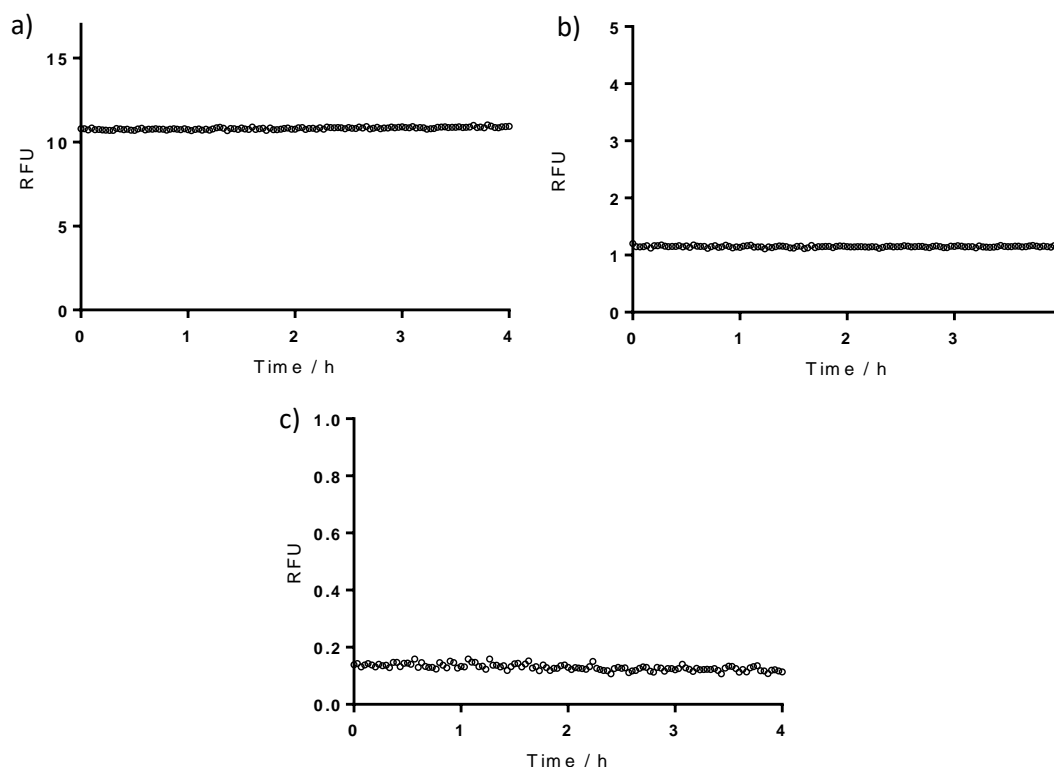


Figure 39: Monitoring of the fluorescence emission of oxime **16b** for possible change of the reaction equilibrium towards the starting materials biphenyl-2-carbaldehyde (**15b**) and hydroxylamine **13** at 37 °C for 4 h after dilution with phosphate buffer (pH 7.1 + 1 % DMSO) to concentration levels of a) 10 μM , b) 1 μM and c) 0.1 μM ($\lambda_{\text{ex}} = 250 \text{ nm}$, $\lambda_{\text{em}} = 385 \text{ nm}$).

4-Methoxybenzaldehyde **15c** itself and the corresponding oxime **16c** showed almost the same absorption maxima (Figure 40a) but excitation and emission spectra revealed maxima at $\lambda = 310 \text{ nm}$ for excitation and $\lambda = 395 \text{ nm}$ for emission with a contribution of 1.0 % of aldehyde **15c** to the emission intensity (Figure 40b and Figure 40c). Using concentration levels from 20 μM to 100 nM linearity was confirmed (Figure 41) and stability was again demonstrated for all three concentration levels (Figure 42).

Further Experiments

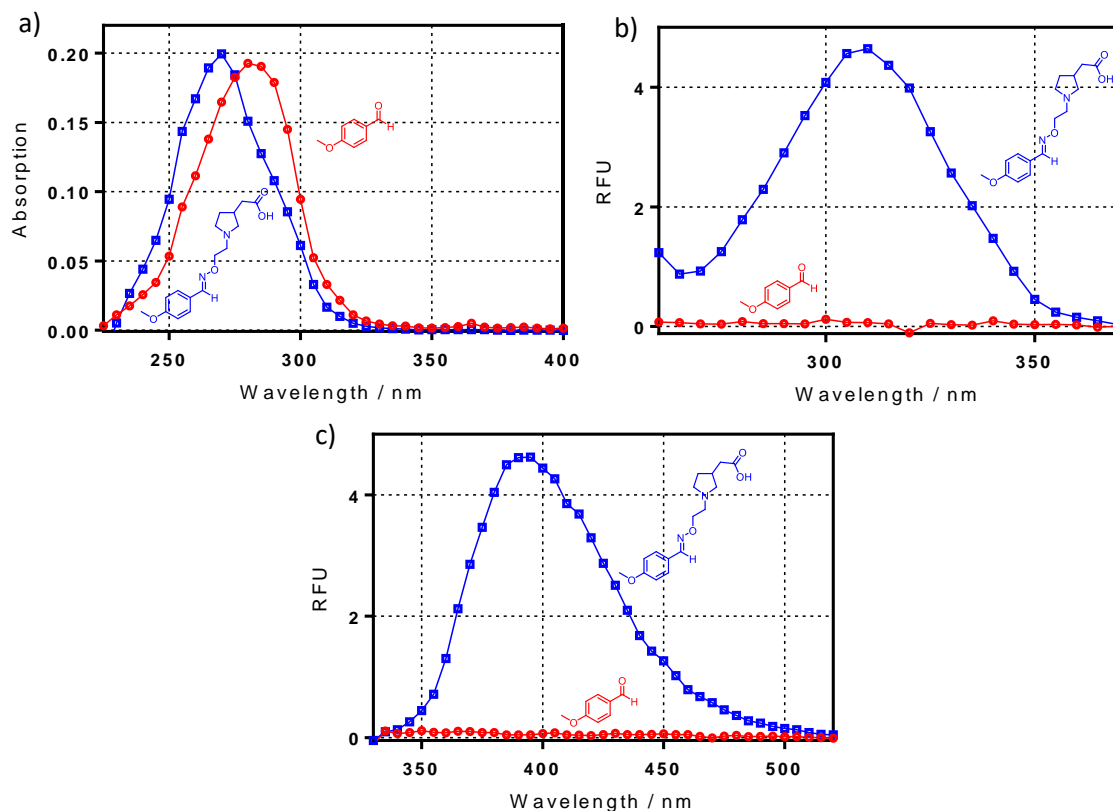


Figure 40: a) UV spectra (absorption versus wavelength, nm), b) excitation spectra [RFU versus wavelength, nm ($\lambda_{\text{ex}} = 260\text{--}370$ nm, $\lambda_{\text{em}} = 400$ nm)] and c) fluorescence spectra [RFU versus wavelength, nm ($\lambda_{\text{ex}} = 310$ nm, $\lambda_{\text{em}} = 330\text{--}520$ nm)]. Each spectrum obtained by measurements of 4-methoxybenzaldehyde (**15c**) (10 μM , red) and oxime **16c** (10 μM , blue). Spectra were recorded in phosphate buffer (pH 7.1) with 1 % DMSO at 37 °C and were corrected by subtraction of the spectrum of the pure solvent as blank.

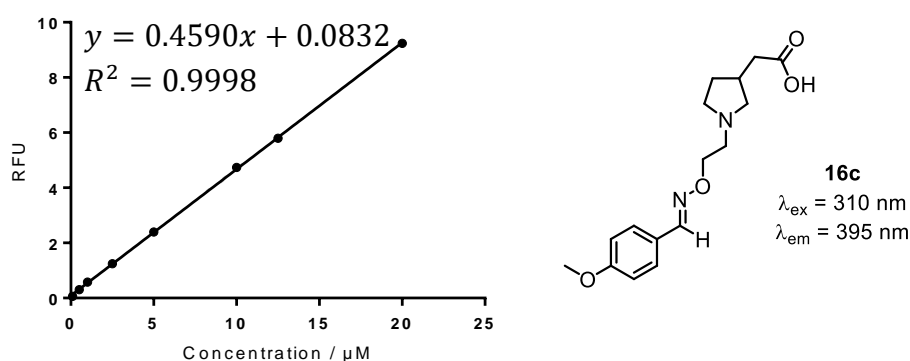


Figure 41: Determination of the linear range [RFU versus concentration, μM ($R^2 = 0.9998$)] in regard to oxime **16c** in different concentration levels (20 μM , 12.5 μM , 10 μM , 5 μM , 2.5 μM , 1 μM , 0.5 μM , 0.1 μM) in phosphate buffer (pH 7.1) with 1 % DMSO at 37 °C ($\lambda_{\text{ex}} = 310$ nm, $\lambda_{\text{em}} = 395$ nm).

Further Experiments

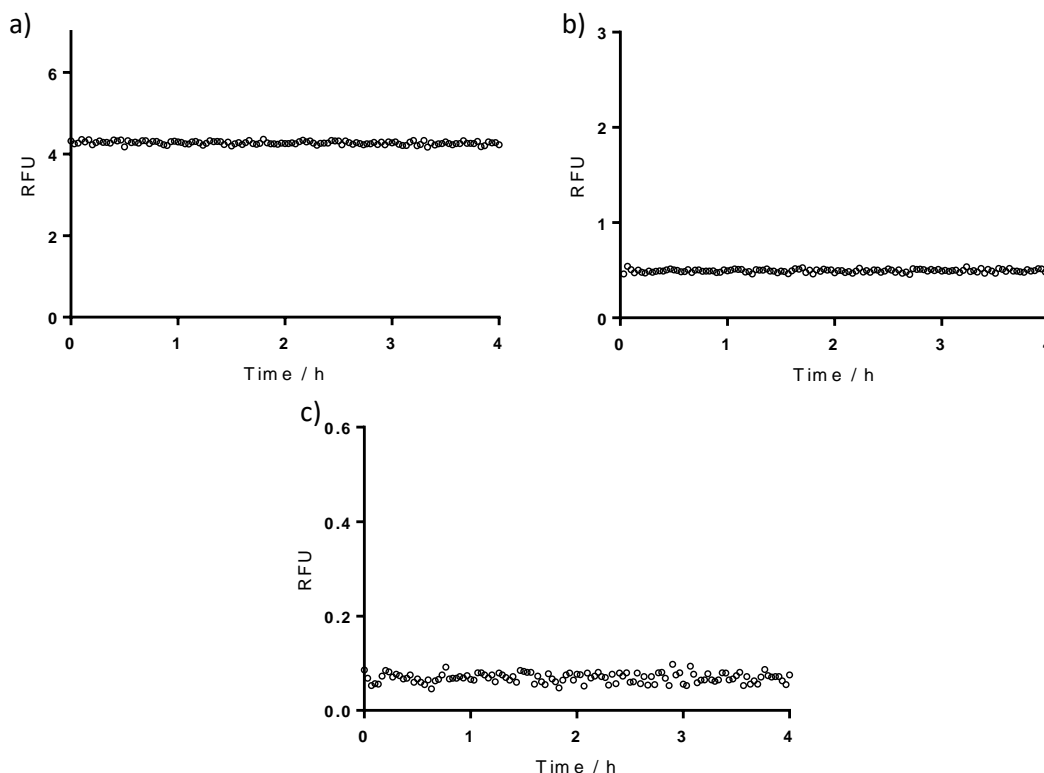


Figure 42: Monitoring of the fluorescence emission of oxime **16c** for possible change of the reaction equilibrium towards the starting materials 4-methoxybenzaldehyde (**15c**) and hydroxylamine **13** at 37 °C for 4 h after dilution with phosphate buffer (pH 7 + 1 % DMSO) to concentration levels of a) 10 μM, b) 1 μM and c) 0.1 μM ($\lambda_{\text{ex}} = 310 \text{ nm}$, $\lambda_{\text{em}} = 395 \text{ nm}$).

The overlay of both absorption spectra for oxime **16d** and the corresponding aldehyde **15d** showed again that exclusive detection of oxime **16d** was not possible (Figure 43a). By using excitation wavelength of $\lambda = 265 \text{ nm}$ (Figure 43b) maximum for the emission wavelength of $\lambda = 380 \text{ nm}$ was observed, but with these conditions the aldehyde had 7.6 % contribution to the emission signal, which was not within the defined limit of 5 % or less contribution of the pure aldehyde to the fluorescence signal. So, I decided to use $\lambda = 370 \text{ nm}$ as emission wavelength to decrease the contribution to 2.1 % (Figure 43c). Subsequently, linearity was shown for concentration levels from 12.5 μM to 100 nM (Figure 44) and oxime **16d** was proven to be stable after dilution to three different concentrations implied by stable fluorescence signals (Figure 45).

Further Experiments

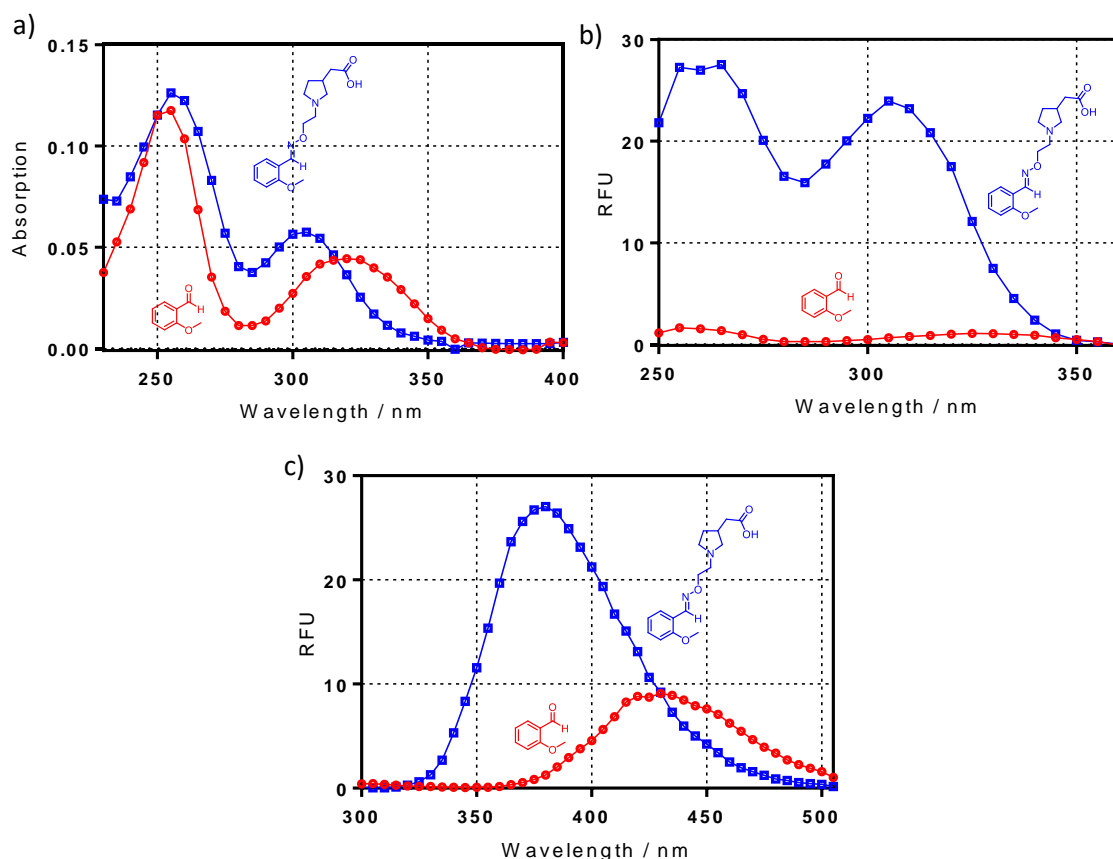


Figure 43: a) UV spectra (absorption versus wavelength, nm), b) excitation spectra [RFU versus wavelength, nm ($\lambda_{\text{ex}} = 250\text{--}360$ nm, $\lambda_{\text{em}} = 370$ nm)] and c) fluorescence spectra [RFU versus wavelength, nm ($\lambda_{\text{ex}} = 265$ nm, $\lambda_{\text{em}} = 300\text{--}500$ nm)]. Each spectrum obtained by measurements of 2-methoxybenzaldehyde (**15d**) (10 μM , red) and oxime **16d** (10 μM , blue). Spectra were in phosphate buffer (pH 7.1) with 1 % DMSO at 37 °C and were corrected by subtraction of the spectrum of the pure solvent as blank.

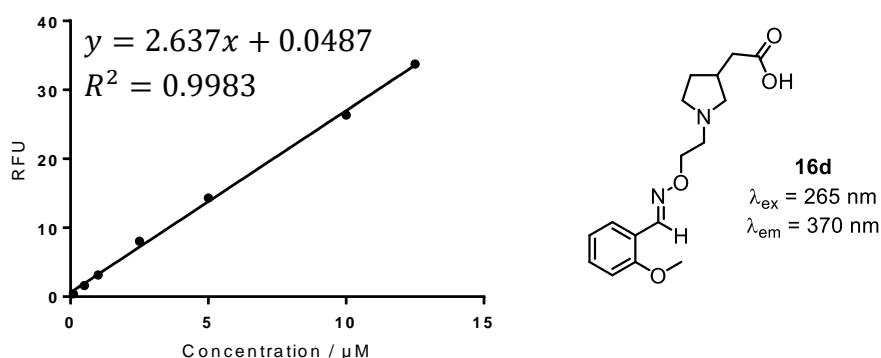


Figure 44: Determination of the linear range [RFU versus concentration, μM ($R^2 = 0.9983$)] in regard to oxime **16d** in different concentration levels (12.5 μM , 10 μM , 5 μM , 2.5 μM , 1 μM , 0.5 μM , 0.1 μM) in phosphate buffer (pH 7.1) with 1 % DMSO at 37 °C ($\lambda_{\text{ex}} = 265$ nm, $\lambda_{\text{em}} = 370$ nm).

Further Experiments

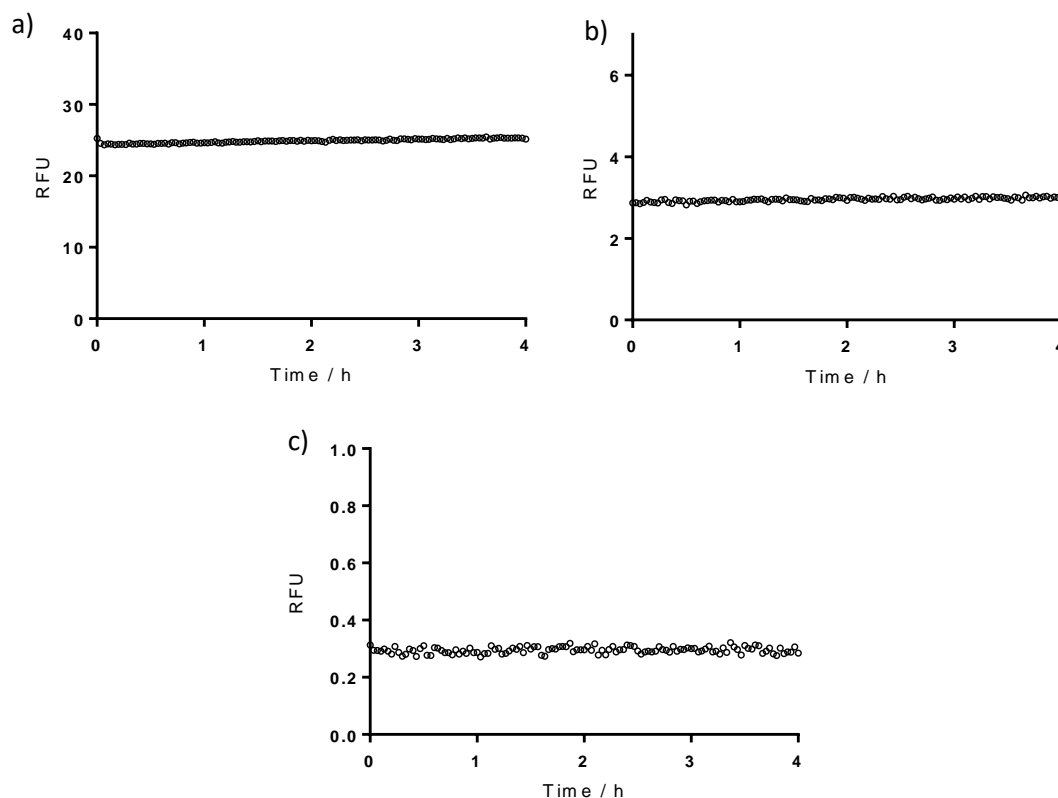
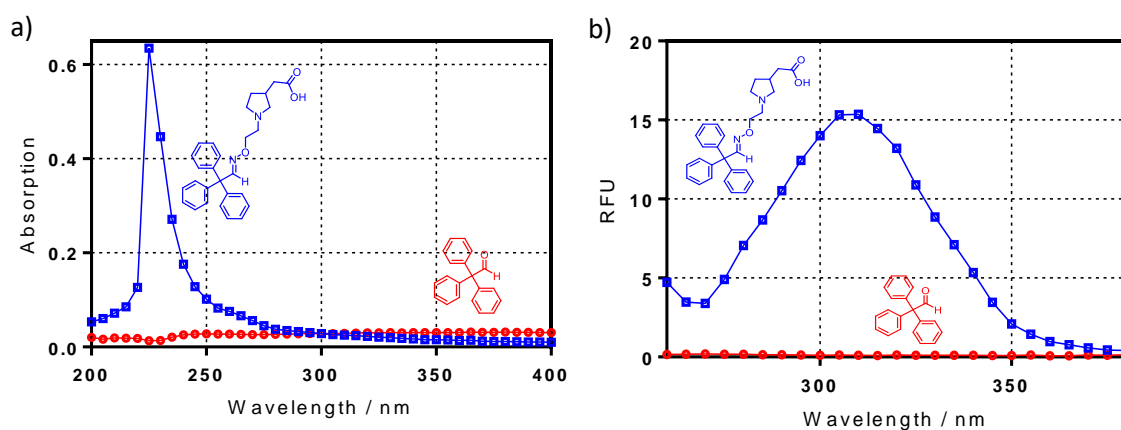


Figure 45: Monitoring of the fluorescence emission of oxime **16d** for possible change of the reaction equilibrium towards the starting materials 2-methoxybenzaldehyde (**15d**) and hydroxylamine **13** at 37 °C for 4 h after dilution with phosphate buffer (pH 7.1 + 1 % DMSO) to concentration levels of a) 10 μM, b) 1 μM and c) 0.1 μM ($\lambda_{\text{ex}} = 265 \text{ nm}$, $\lambda_{\text{em}} = 370 \text{ nm}$).

For the unsubstituted tritylaldehyde **15k** and its oxime derivative **16k** absorption (Figure 46a), excitation (Figure 46b) and emission spectra (Figure 46c) were recorded to obtain maximum wavelength of $\lambda = 310 \text{ nm}$ for excitation and $\lambda = 390 \text{ nm}$ for emission of oxime **16k**. The contribution of the aldehyde **15k** to the emission signal is 0.5%. By applying concentration levels from 20 μM to 100 nM linearity was investigated (Figure 47) and measurements with concentrations of 10 μM, 1 μM and 100 nM confirmed the stability of the oxime **16k** of 4 h, respectively (Figure 48).



Further Experiments

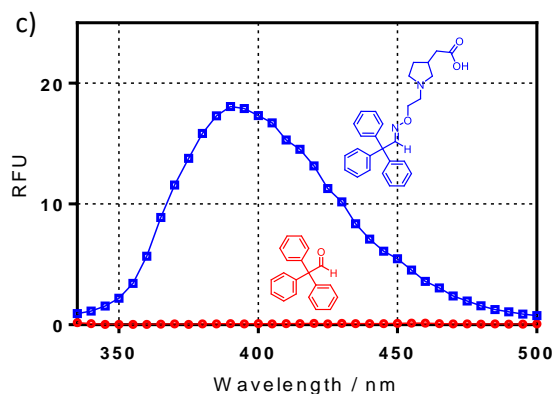


Figure 46: a) UV spectra (absorption versus wavelength, nm), b) excitation spectra [RFU versus wavelength, nm ($\lambda_{\text{ex}} = 250\text{--}380$ nm, $\lambda_{\text{em}} = 400$ nm)] and c) fluorescence spectra [RFU versus wavelength, nm ($\lambda_{\text{ex}} = 310$ nm, $\lambda_{\text{em}} = 335\text{--}500$ nm)]. Each spectrum obtained by measurements of tritylaldehyde **15k** (10 μM , red) and oxime **16k** (10 μM , blue). Spectra were recorded in phosphate buffer (pH 7.1) with 1 % DMSO at 37 °C and were corrected by subtraction of the spectrum of the pure solvent as blank.

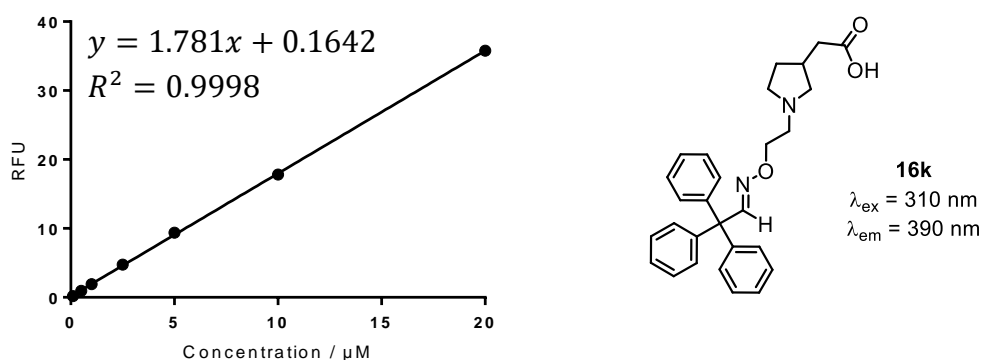
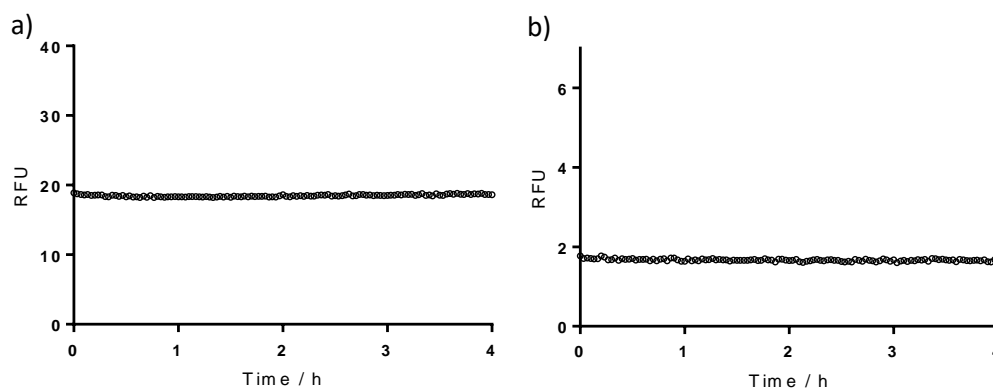


Figure 47: Determination of the linear range [RFU versus concentration, μM ($R^2 = 0.9998$)] in regard to oxime **16k** in different concentration levels (20 μM , 10 μM , 5 μM , 2.5 μM , 1 μM , 0.5 μM , 0.1 μM) in phosphate buffer (pH 7.1) with 1 % DMSO at 37 °C ($\lambda_{\text{ex}} = 310$ nm, $\lambda_{\text{em}} = 390$ nm).



Further Experiments

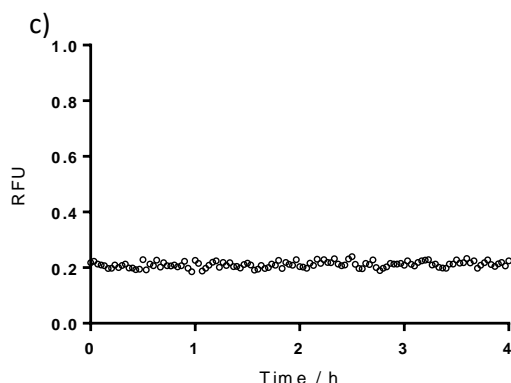
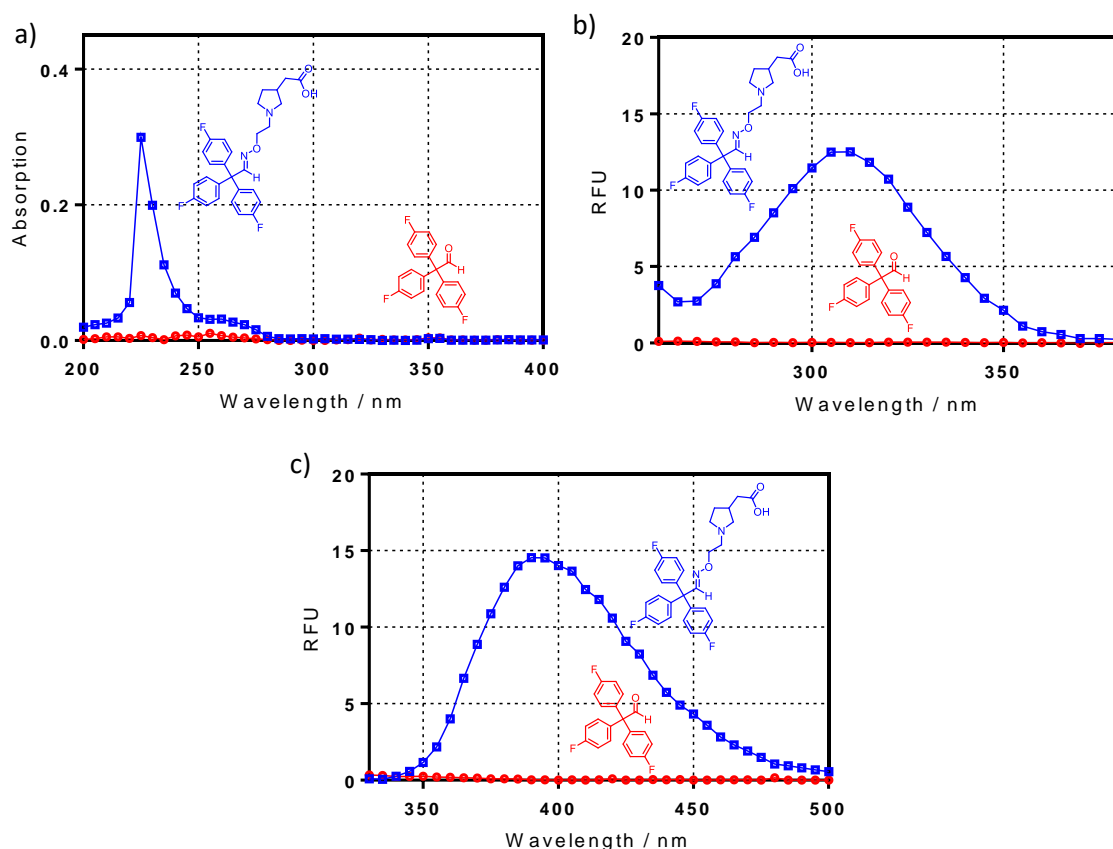


Figure 48: Monitoring of the fluorescence emission of oxime **16k** for possible change of the reaction equilibrium towards the starting materials tritylaldehyde **15k** and hydroxylamine **13** at 37 °C for 4 h after dilution with phosphate buffer (pH 7.1 + 1 % DMSO) to concentration levels of a) 10 μ M, b) 1 μ M and c) 0.1 μ M (λ_{ex} = 310 nm, λ_{em} = 390 nm).

Fluorescence measurements of oxime **16i** resulting from fluoro-substituted tritylaldehyde showed excitation maximum of λ = 310 nm and emission maximum at λ = 390 nm whereas the aldehyde **15i** constituted 0.2 % of the total emission (Figure 49b and Figure 49c). Linear range was determined from 20 μ M to 100 nM (Figure 50) and no change of the fluorescence signal was observed for the employed concentrations 10 μ M, 1 μ M and 100nM (Figure 51).



Further Experiments

Figure 49: a) UV spectra (absorption versus wavelength, nm), b) excitation spectra [RFU versus wavelength, nm ($\lambda_{\text{ex}} = 260\text{--}380$ nm, $\lambda_{\text{em}} = 400$ nm)] and c) fluorescence spectra [RFU versus wavelength, nm ($\lambda_{\text{ex}} = 310$ nm, $\lambda_{\text{em}} = 330\text{--}500$ nm)]. Each spectrum obtained by measurements of tritylaldehyde **15i** (10 μM , red) and oxime **16i** (10 μM , blue). Spectra were in phosphate buffer (pH 7.1) with 1 % DMSO at 37 $^{\circ}\text{C}$ and were corrected by subtraction of the spectrum of the pure solvent as blank.

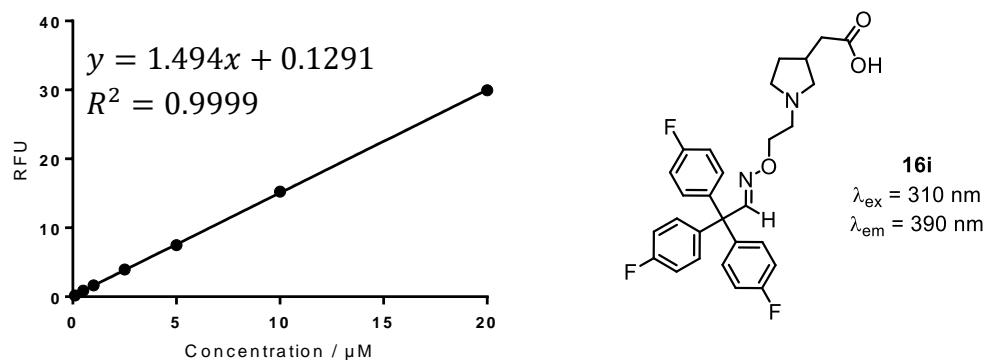


Figure 50: Determination of the linear range [RFU versus concentration, μM ($R^2 = 0.9999$)] in regard to oxime **6i** in different concentration levels (20 μM , 10 μM , 5 μM , 2.5 μM , 1 μM , 0.5 μM , 0.1 μM in phosphate buffer (pH 7.1) with 1 % DMSO at 37 $^{\circ}\text{C}$ ($\lambda_{\text{ex}} = 310$ nm, $\lambda_{\text{em}} = 390$ nm).

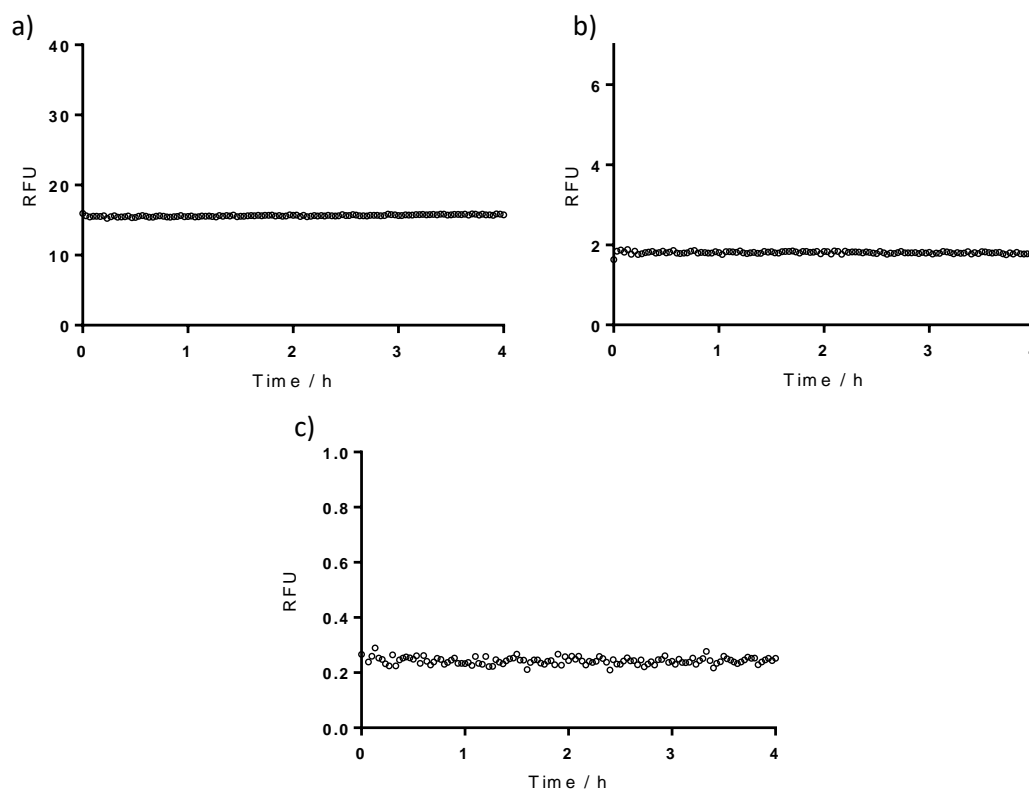


Figure 51: Monitoring of the fluorescence emission of oxime **16i** for possible change of the reaction equilibrium towards the starting materials tritylaldehyde **15i** and hydroxylamine **13** at 37 $^{\circ}\text{C}$ for 4 h after dilution with phosphate buffer (pH 7.1 + 1 % DMSO) to concentration levels of a) 10 μM , b) 1 μM and c) 0.1 μM ($\lambda_{\text{ex}} = 310$ nm, $\lambda_{\text{em}} = 390$ nm).

Further Experiments

In the case of oxime **16I**, the maximum excitation wavelength of $\lambda = 310$ nm (Figure 52b) was used to observe the maximum for the emission wavelength of $\lambda = 390$ nm (Figure 52c) with contribution of aldehyde **15I** to the fluorescence signal of 1.0 %. Thus, linearity was found for concentrations between 20 μ M and 100 nM (Figure 53) and stability was proven at all three concentrations of 10 μ M, 1 μ M and 100 nM over the incubation time of 4 h (Figure 54).

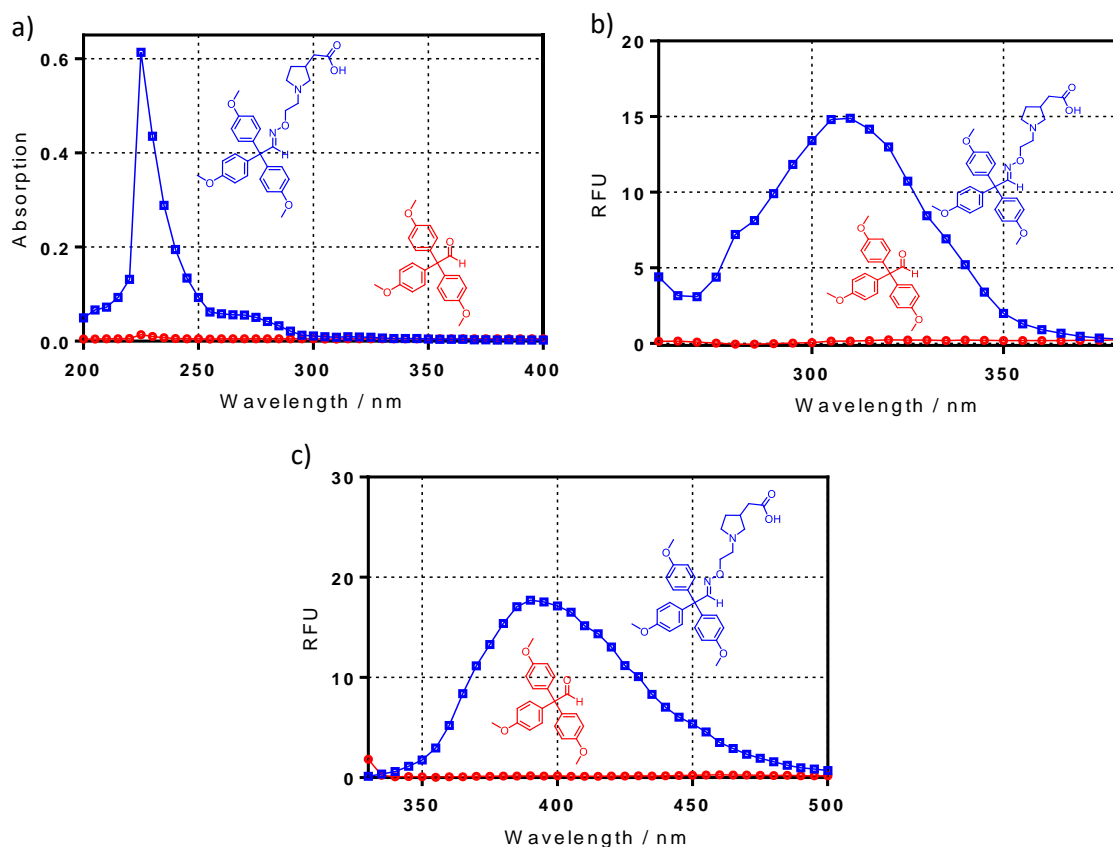
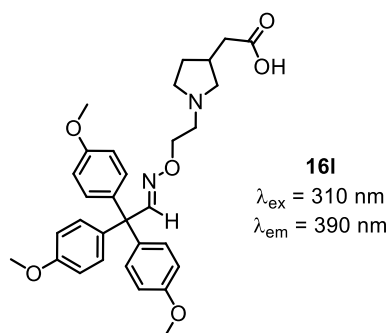
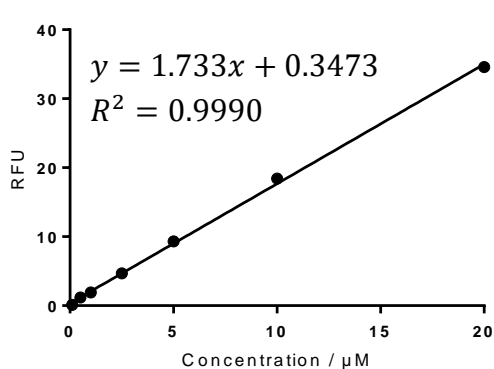


Figure 52: a) UV spectra (absorption versus wavelength, nm), b) excitation spectra [RFU versus wavelength, nm ($\lambda_{\text{ex}} = 260\text{--}380$ nm, $\lambda_{\text{em}} = 400$ nm)] and c) fluorescence spectra [RFU versus wavelength, nm ($\lambda_{\text{ex}} = 310$ nm, $\lambda_{\text{em}} = 330\text{--}500$ nm)]. Each spectrum obtained by measurements of tritylaldehyde **15I** (10 μ M, red) and oxime **16I** (10 μ M, blue). Spectra were recorded in phosphate buffer (pH 7.1) with 1 % DMSO at 37 °C and were corrected by subtraction of the spectrum of the pure solvent as blank.



Further Experiments

Figure 53: Determination of the linear range [RFU versus concentration, μM ($R^2 = 0.9990$)] in regard to oxime **16I** in different concentration levels (20 μM , 10 μM , 5 μM , 2.5 μM , 1 μM , 0.5 μM , 0.1 μM) in phosphate buffer (pH 7.1) with 1 % DMSO at 37 °C ($\lambda_{\text{ex}} = 310 \text{ nm}$, $\lambda_{\text{em}} = 390 \text{ nm}$).

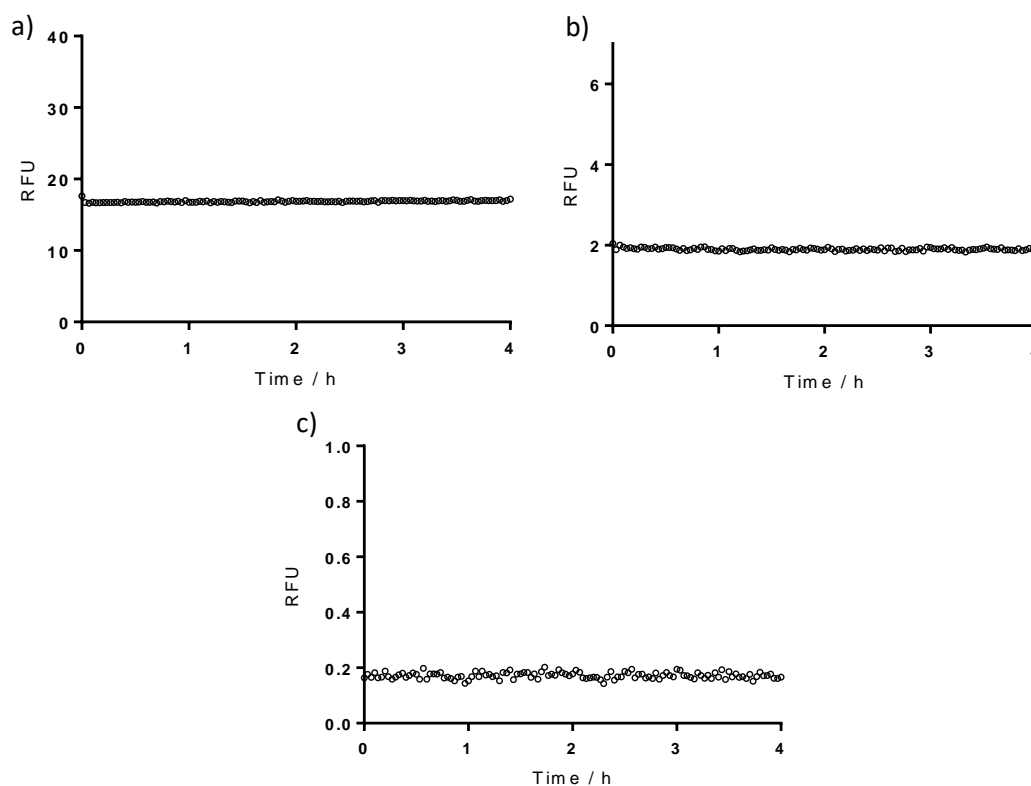


Figure 1: Monitoring of the fluorescence emission of oxime **16I** for possible change of the reaction equilibrium towards the starting materials tritylaldehyde **15I** and hydroxylamine **13** at 37 °C for 4 h after dilution with phosphate buffer (pH 7.1 + 1 % DMSO) to concentration levels of a) 10 μM , b) 1 μM and c) 0.1 μM ($\lambda_{\text{ex}} = 310 \text{ nm}$, $\lambda_{\text{em}} = 390 \text{ nm}$).

Further Experiments

4.2.2 Stability Experiments using Pyrrolidine-3-carboxylic acid derived Oximes

By employing oxime **17a** utilizing pyrrolidine-3-carboxylic acid and the corresponding aldehyde **15a**, overlapping absorption spectra were again observed (Figure 55a) and excitation and emission wavelength of $\lambda = 310$ nm (Figure 55b) and $\lambda = 390$ nm (Figure 55c) were determined, respectively. Under these conditions contribution of **15a** is 4.9 % to the fluorescence signal. Using concentration levels from 20 μ M to 100 nM linearity was confirmed (Figure 56) and stability implied by stable fluorescence signal was again demonstrated by employing 10 μ M and 1 μ M (Figure 57).

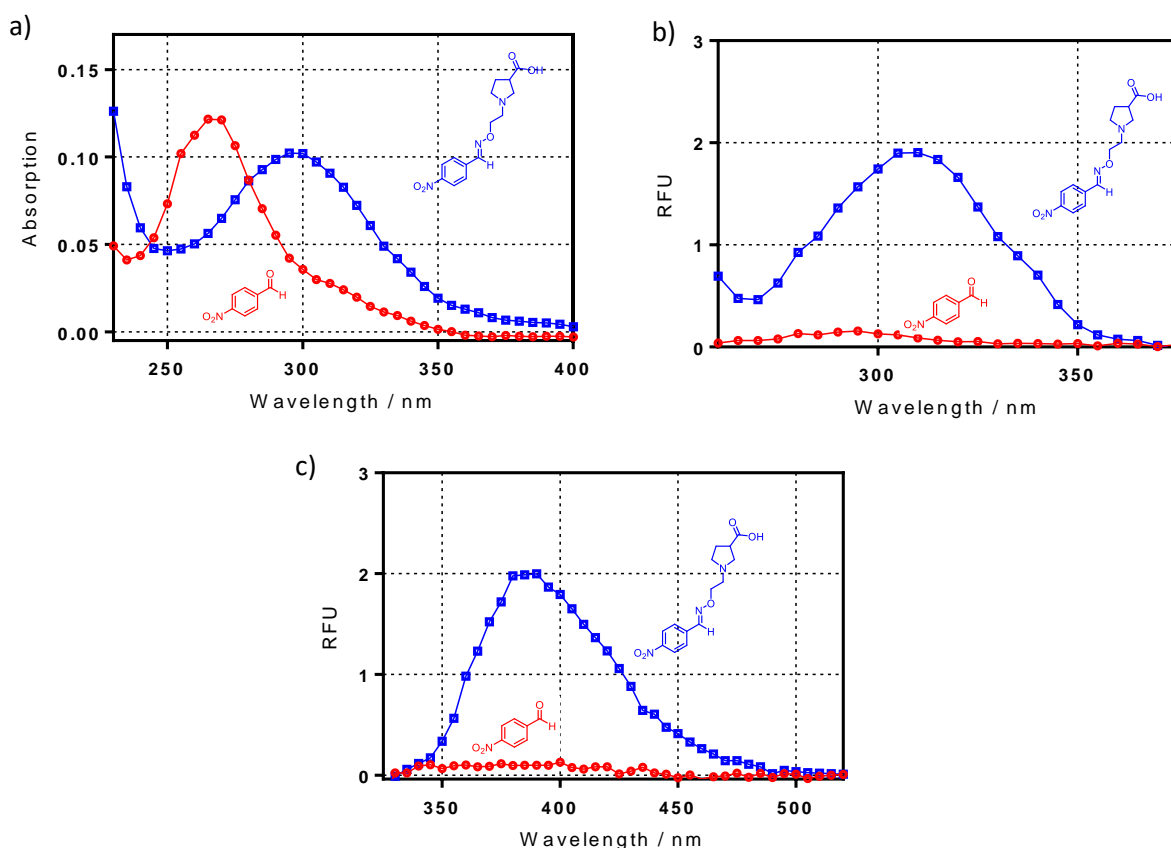


Figure 55: a) UV spectra (absorption versus wavelength, nm), b) excitation spectra [RFU versus wavelength, nm ($\lambda_{\text{ex}} = 260\text{--}375$ nm, $\lambda_{\text{em}} = 400$ nm)] and c) fluorescence spectra [RFU versus wavelength, nm ($\lambda_{\text{ex}} = 310$ nm, $\lambda_{\text{em}} = 330\text{--}520$ nm)]. Each spectrum obtained by measurements of 4-nitrobenzaldehyde (**15a**) (10 μ M, red) and oxime **17a** (10 μ M, blue). Spectra were recorded in phosphate buffer (pH 7.1) with 1 % DMSO at 37 $^{\circ}$ C and were corrected by subtraction of the spectrum of the pure solvent as blank.

Further Experiments

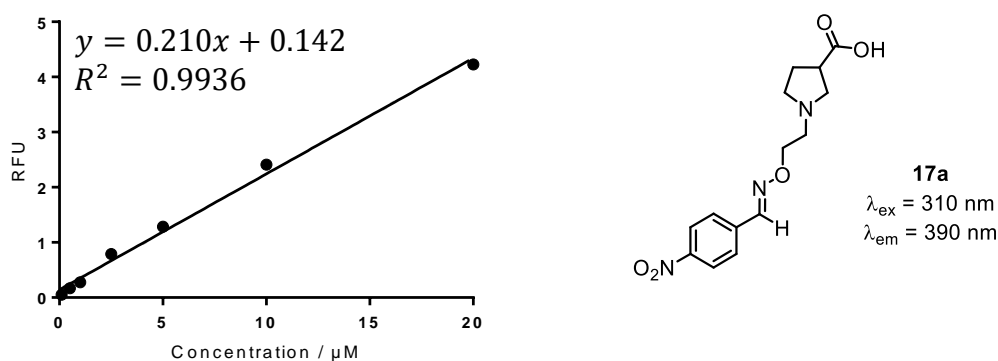


Figure 56: Determination of the linear range [RFU versus concentration, μM ($R^2 = 0.9936$)] in regard to oxime **17a** in different concentration levels (20 μM , 10 μM , 5 μM , 2.5 μM , 1 μM , 0.5 μM , 0.1 μM in phosphate buffer (pH 7.1) with 1 % DMSO at 37 °C ($\lambda_{\text{ex}} = 310 \text{ nm}$, $\lambda_{\text{em}} = 390 \text{ nm}$).

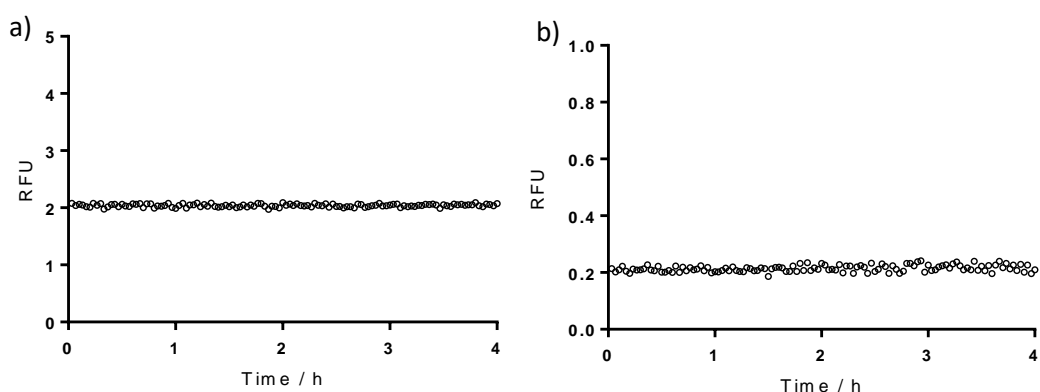


Figure 57: Monitoring of the fluorescence emission of oxime **17a** for possible change of the reaction equilibrium towards the starting materials 4-nitrobenzaldehyde (**15a**) and hydroxylamine **14** at 37 °C for 4 h after dilution with phosphate buffer (pH 7.1 + 1 % DMSO) to concentration levels of a) 10 μM and b) 1 μM ($\lambda_{\text{ex}} = 310 \text{ nm}$, $\lambda_{\text{em}} = 390 \text{ nm}$).

For biphenyl-2-carbaldehyde (**15b**) and its oxime derivative **17b** absorption, excitation and emission spectra were recorded to obtain maximum wavelength of $\lambda = 265 \text{ nm}$ for excitation (Figure 58b) and $\lambda = 380 \text{ nm}$ for emission (Figure 58c) of oxime **17b** whereas aldehyde **15b** contributed 1.7 % of the signal. Subsequently, linearity was demonstrated for concentration levels from 10 μM to 100 nM (Figure 59) and oxime **17b** was proven to be stable after dilution to 10 μM and 1 μM (Figure 60).

Further Experiments

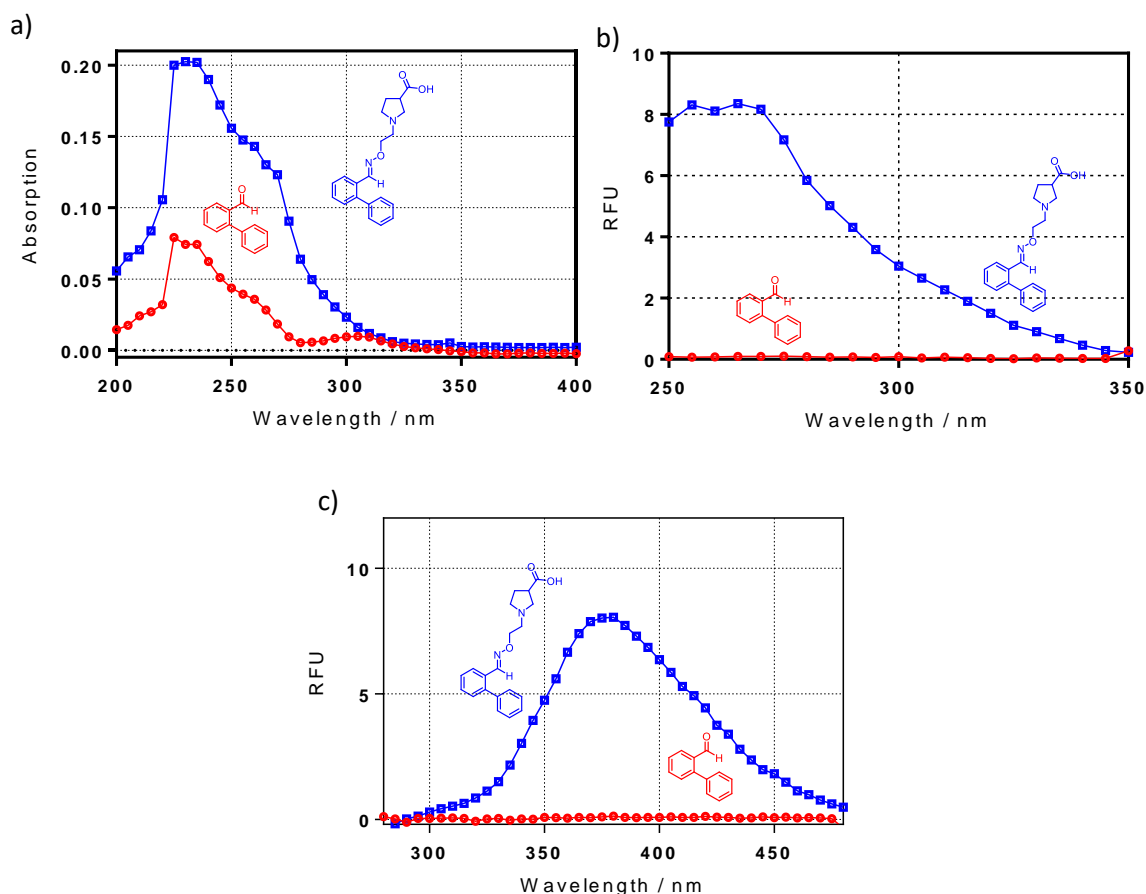


Figure 58: a) UV spectra (absorption versus wavelength, nm), b) excitation spectra [RFU versus wavelength, nm ($\lambda_{\text{ex}} = 250\text{--}350\text{ nm}$, $\lambda_{\text{em}} = 370\text{ nm}$)] and c) fluorescence spectra [RFU versus wavelength, nm ($\lambda_{\text{ex}} = 265\text{ nm}$, $\lambda_{\text{em}} = 280\text{--}480\text{ nm}$)]. Each spectrum obtained by measurements of biphenyl-2-carbaldehyde (**15b**) (10 μM , red) and oxime **17b** (10 μM , blue). Spectra were recorded in phosphate buffer (pH 7.1) with 1 % DMSO at 37 $^{\circ}\text{C}$ and were corrected by subtraction of the spectrum of the pure solvent as blank.

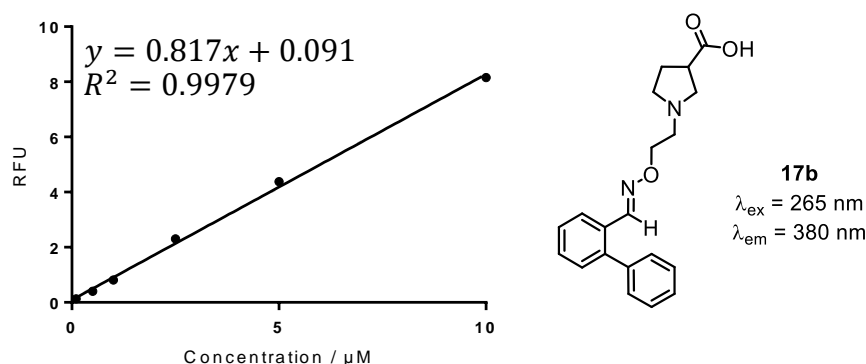


Figure 59: Determination of the linear range [RFU versus concentration, μM ($R^2 = 0.9979$)] in regard to oxime **17b** in different concentration levels (10 μM , 5 μM , 2.5 μM , 1 μM , 0.5 μM , 0.1 μM) in phosphate buffer (pH 7.1) with 1 % DMSO at 37 $^{\circ}\text{C}$ ($\lambda_{\text{ex}} = 265\text{ nm}$, $\lambda_{\text{em}} = 380\text{ nm}$).

Further Experiments

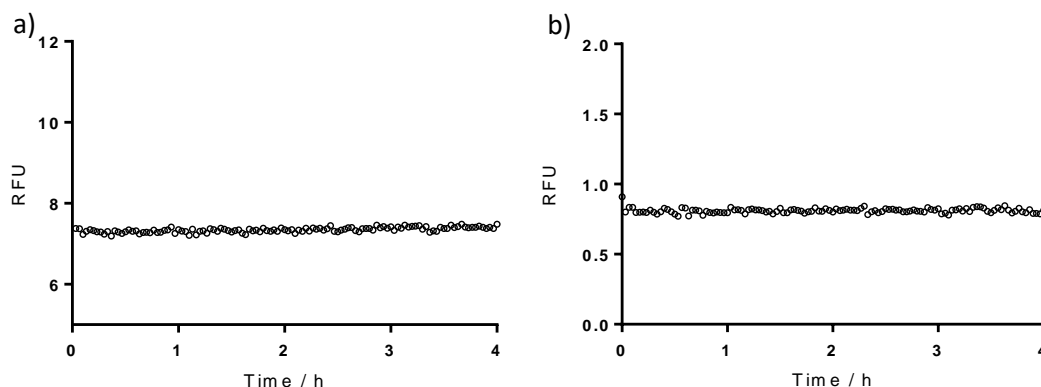
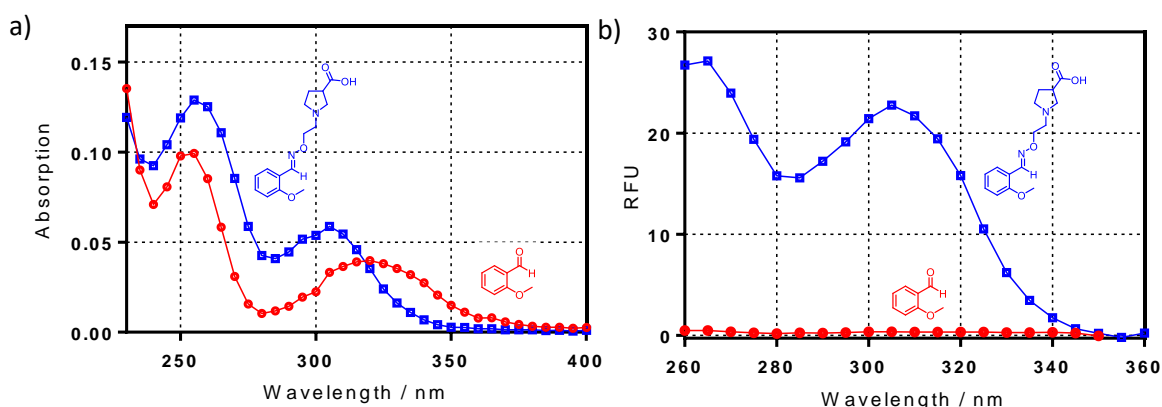


Figure 60: Monitoring of the fluorescence emission of oxime **17b** for possible change of the reaction equilibrium towards the starting materials 2-methoxybenzaldehyde (**15b**) and hydroxylamine **14** at 37 °C for 4 h after dilution with phosphate buffer (pH 7.1 + 1 % DMSO) to concentration levels of a) 10 μM and b) 1 μM ($\lambda_{\text{ex}} = 265 \text{ nm}$, $\lambda_{\text{em}} = 380 \text{ nm}$).

Absorption spectra of oxime **17d** resulting from 2-methoxybenzaldehyde and the aldehyde **15d** itself overlapped revealing that detection of only oxime **17d** was not possible without exciting aldehyde **15d** (Figure 61a). By using excitation wavelength of $\lambda = 265 \text{ nm}$ – the maximum of excitation spectra (Figure 61b) – emission wavelength of $\lambda = 380 \text{ nm}$ was determined (Figure 61c). As already observed with 2-(pyrrolidin-3-yl)acetic acid derivative **16d**, the contribution of **15d** to the fluorescence signal is over the set limit of 5 % and therefore, emission wavelength of $\lambda = 370 \text{ nm}$ was chosen to be used for the stability experiments decreasing contribution to 3.7 %. Linear range was investigated within concentrations from 10 μM to 100 nM with correlation factor of 0.9969 (Figure 62) and oxime **17d** was confirmed to be stable after dilution to the concentration levels 10 μM and 1 μM , respectively (Figure 63).



Further Experiments

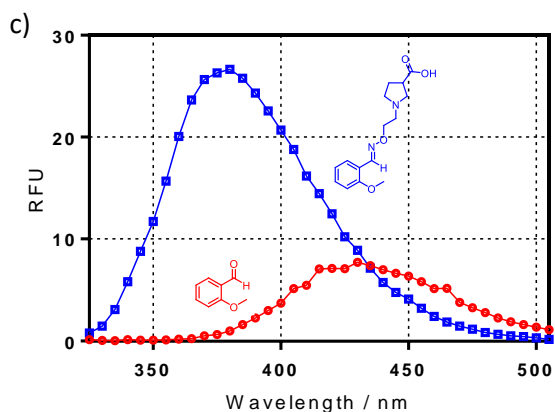


Figure 61: a) UV spectra (absorption versus wavelength, nm), b) excitation spectra [RFU versus wavelength, nm ($\lambda_{\text{ex}} = 260\text{--}360$ nm, $\lambda_{\text{em}} = 370$ nm)] and c) fluorescence spectra [RFU versus wavelength, nm ($\lambda_{\text{ex}} = 265$ nm, $\lambda_{\text{em}} = 335\text{--}505$ nm)]. Each spectrum obtained by measurements of 2-methoxybenzaldehyde (**15d**) (10 μM , red) and oxime **17d** (10 μM , blue). Spectra were recorded in phosphate buffer (pH 7.1) with 1 % DMSO at 37 $^{\circ}\text{C}$ and were corrected by subtraction of the spectrum of the pure solvent as blank.

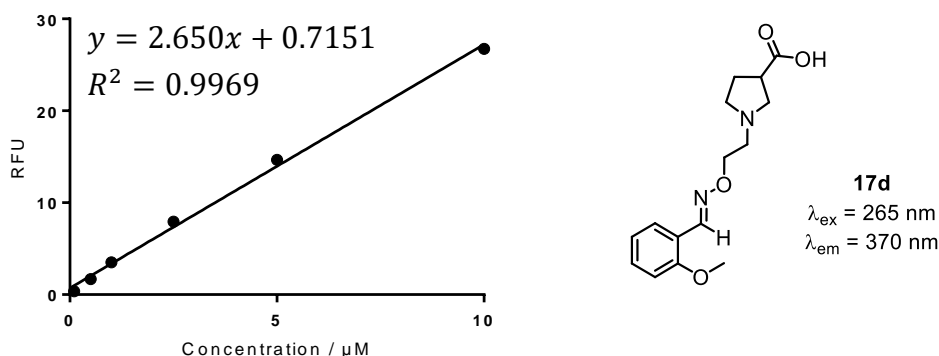


Figure 62: Determination of the linear range [RFU versus concentration, μM ($R^2 = 0.9969$)] in regard to oxime **17d** in different concentration levels (10 μM , 5 μM , 2.5 μM , 1 μM , 0.5 μM , 0.1 μM in phosphate buffer (pH 7.1) with 1 % DMSO at 37 $^{\circ}\text{C}$ ($\lambda_{\text{ex}} = 265$ nm, $\lambda_{\text{em}} = 370$ nm).

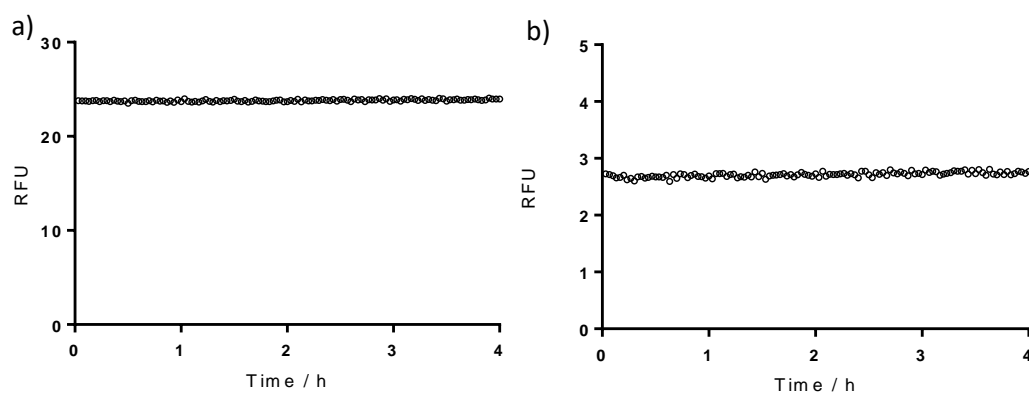


Figure 63: Monitoring of the fluorescence emission of oxime **17d** for possible change of the reaction equilibrium towards the starting materials 2-methoxybenzaldehyde (**15d**) and hydroxylamine **14** at 37 $^{\circ}\text{C}$ for 4 h after dilution with phosphate buffer (pH 7.1 + 1 % DMSO) to concentration levels of a) 10 μM and b) 1 μM ($\lambda_{\text{ex}} = 265$ nm, $\lambda_{\text{em}} = 370$ nm).

Further Experiments

Fluorescence measurements of oxime **17k** resulting from unsubstituted tritylaldehyde **15k** showed excitation maximum of $\lambda = 310$ nm (Figure 64b) and emission maximum at $\lambda = 390$ nm (Figure 64c) whereas the aldehyde **15k** constituted 0.5 % of the total emission. Using concentration levels from 20 μM to 100 nM linear range was investigated (Figure 65) and stability was again demonstrated for the concentration levels 10 μM and 1 μM (Figure 66).

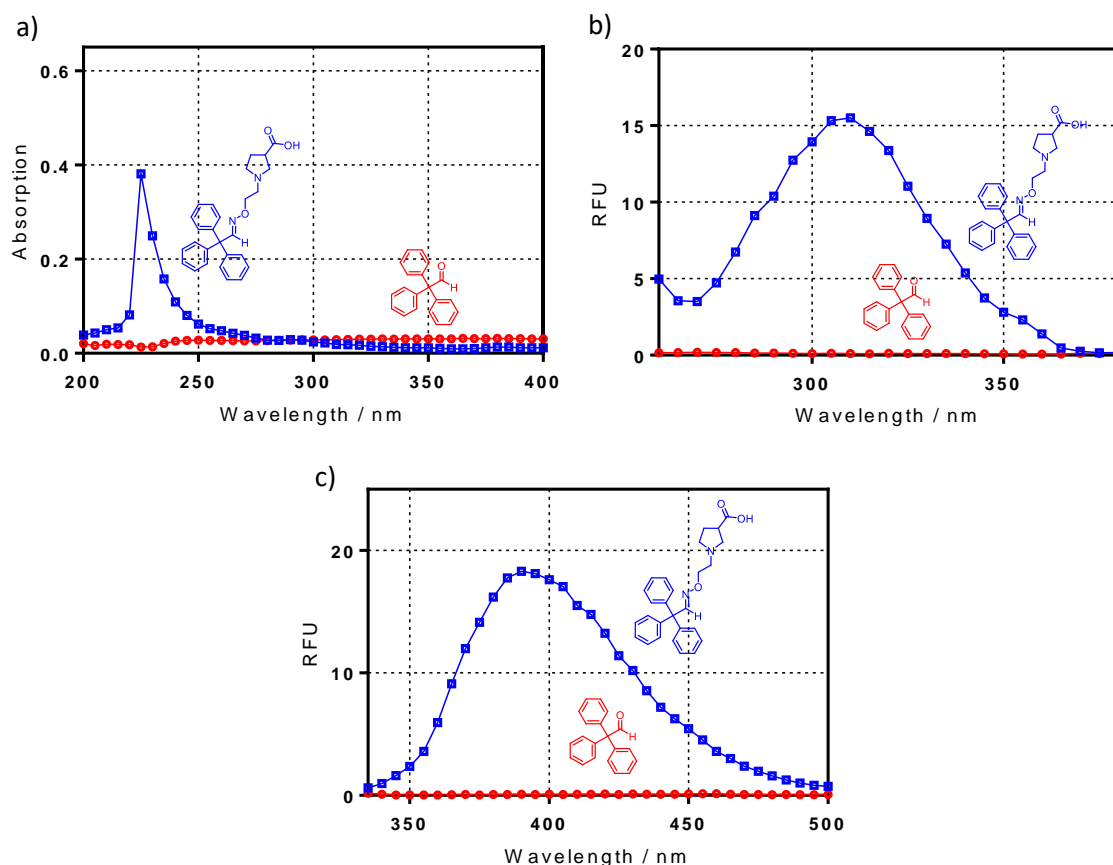
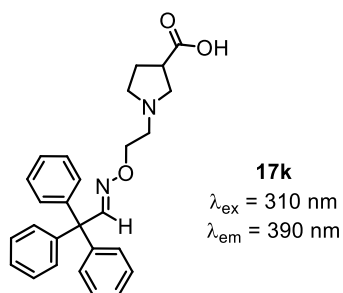
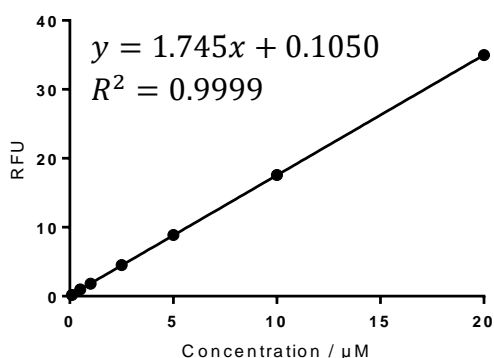


Figure 64: a) UV spectra (absorption versus wavelength, nm), b) excitation spectra [RFU versus wavelength, nm ($\lambda_{\text{ex}} = 260\text{--}380$ nm, $\lambda_{\text{em}} = 400$ nm)] and c) fluorescence spectra [RFU versus wavelength, nm ($\lambda_{\text{ex}} = 310$ nm, $\lambda_{\text{em}} = 335\text{--}500$ nm)]. Each spectrum obtained by measurements of tritylaldehyde **15k** (10 μM , red) and oxime **17k** (10 μM , blue). Spectra were in phosphate buffer (pH 7.1) with 1 % DMSO at 37 °C and were corrected by subtraction of the spectrum of the pure solvent as blank.



Further Experiments

Figure 65: Determination of the linear range [RFU versus concentration, μM ($R^2 = 0.9999$)] in regard to oxime **17k** in different concentration levels (20 μM , 10 μM , 5 μM , 2.5 μM , 1 μM , 0.5 μM , 0.1 μM) in phosphate buffer (pH 7.1) with 1 % DMSO at 37 °C ($\lambda_{\text{ex}} = 310 \text{ nm}$, $\lambda_{\text{em}} = 390 \text{ nm}$).

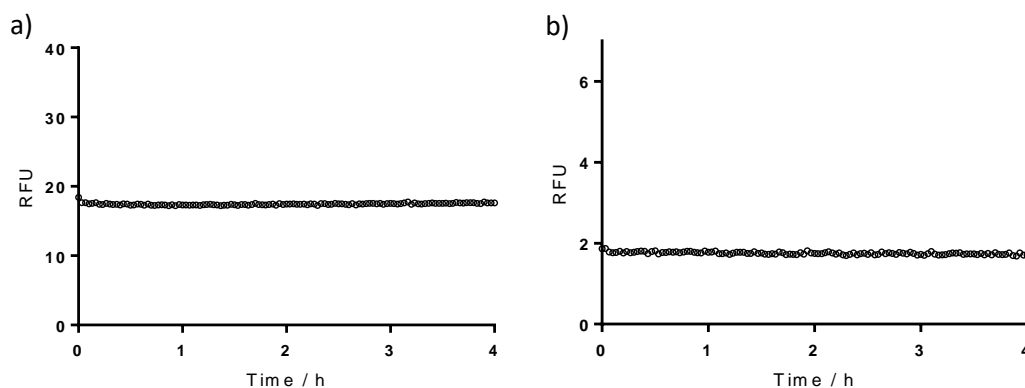
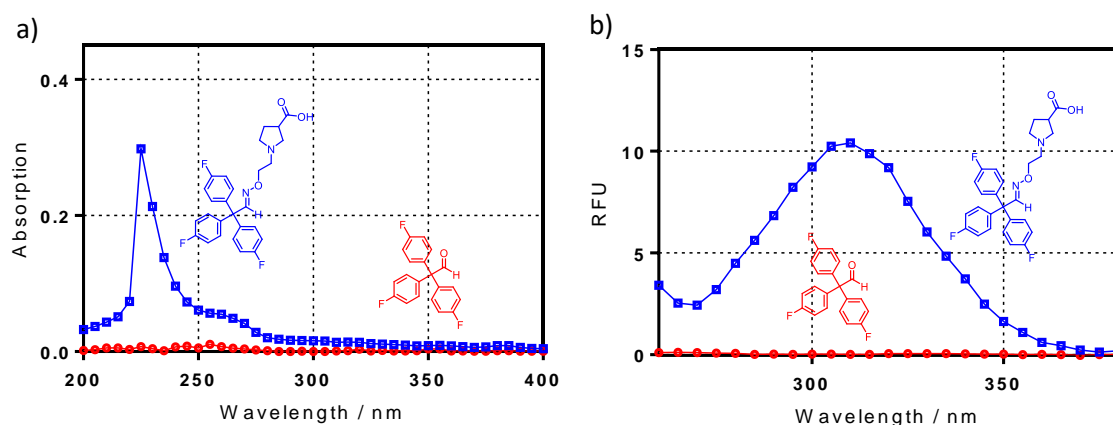


Figure 66: Monitoring of the fluorescence emission of oxime **17k** for possible change of the reaction equilibrium towards the starting materials tritylaldehyde **15k** and hydroxylamine **14** at 37 °C for 4 h after dilution with phosphate buffer (pH 7.1 + 1 % DMSO) to concentration levels of a) 10 μM and b) 1 μM ($\lambda_{\text{ex}} = 310 \text{ nm}$, $\lambda_{\text{em}} = 390 \text{ nm}$).

For the tritylaldehyde **15i** and its oxime derivative **17i** absorption (Figure 67a), excitation (Figure 67b) and emission spectra (Figure 67c) were recorded to obtain maximum wavelength of $\lambda = 310 \text{ nm}$ for excitation and $\lambda = 390 \text{ nm}$ for emission of oxime **17i** with contribution of the aldehyde **15k** of 0.3 % to the total emission. By applying concentration levels from 20 μM to 100 nM linearity was examined (Figure 68) and measurements with concentrations of 10 μM and 1 μM confirmed the stability of the oxime **5i** during the incubation time of 4 h, respectively (Figure 69).



Further Experiments

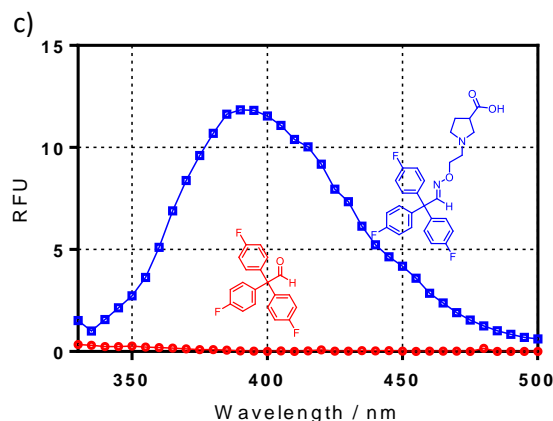


Figure 67: a) UV spectra (absorption versus wavelength, nm), b) excitation spectra [RFU versus wavelength, nm ($\lambda_{\text{ex}} = 260\text{--}380$ nm, $\lambda_{\text{em}} = 400$ nm)] and c) fluorescence spectra [RFU versus wavelength, nm ($\lambda_{\text{ex}} = 310$ nm, $\lambda_{\text{em}} = 330\text{--}500$ nm)]. Each spectrum obtained by measurements of tritylaldehyde **15i** (10 μM , red) and oxime **17i** (10 μM , blue). Spectra were recorded in phosphate buffer (pH 7.1) with 1 % DMSO at 37 $^{\circ}\text{C}$ and were corrected by subtraction of the spectrum of the pure solvent as blank.

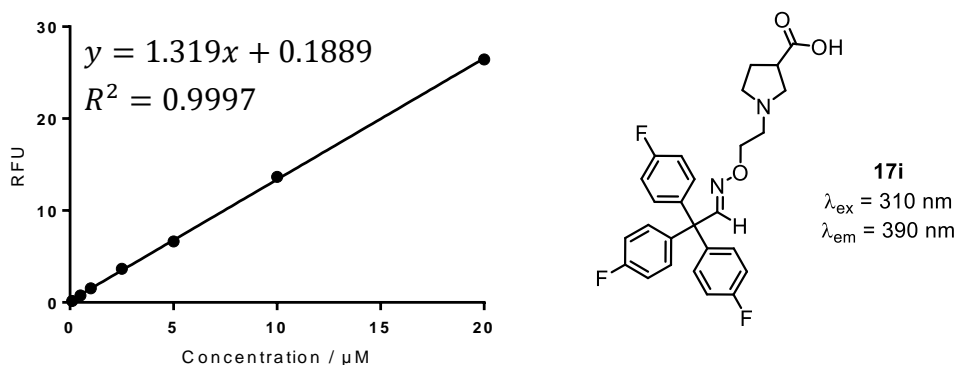


Figure 68: Determination of the linear range [RFU versus concentration, μM ($R^2 = 0.9997$)] in regard to oxime **17i** in different concentration levels (20 μM , 10 μM , 5 μM , 2.5 μM , 1 μM , 0.5 μM , 0.1 μM) in phosphate buffer (pH 7.1) with 1 % DMSO at 37 $^{\circ}\text{C}$ ($\lambda_{\text{ex}} = 310$ nm, $\lambda_{\text{em}} = 390$ nm).

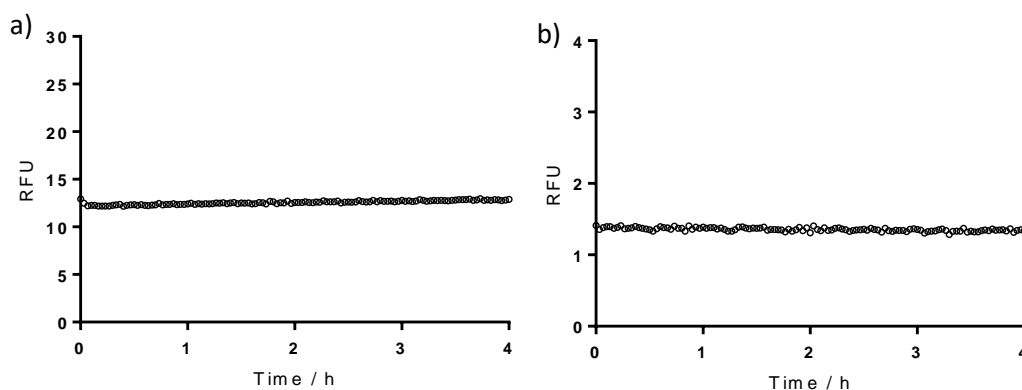


Figure 69: Monitoring of the fluorescence emission of oxime **7i** for possible change of the reaction equilibrium towards the starting materials tritylaldehyde **15i** and hydroxylamine **14** at 37 $^{\circ}\text{C}$ for 4 h after dilution with phosphate buffer (pH 7.1 + 1 % DMSO) to concentration levels of a) 10 μM and b) 1 μM ($\lambda_{\text{ex}} = 310$ nm, $\lambda_{\text{em}} = 390$ nm).

Further Experiments

By employing methoxy-substituted tritylaldehyde **15I** and its corresponding oxime derivative **17I**, maxima of excitation and emission of $\lambda = 310$ nm (Figure 70b) and $\lambda = 390$ nm (Figure 70c) were found with a contribution of 1.5 % of **15I** to the fluorescence signal. Using these conditions linearity was determined within concentrations of 20 μM and 100 nM (Figure 71) and subsequently, stability was confirmed utilizing two concentration levels of 10 μM and 1 μM , respectively (Figure 72).

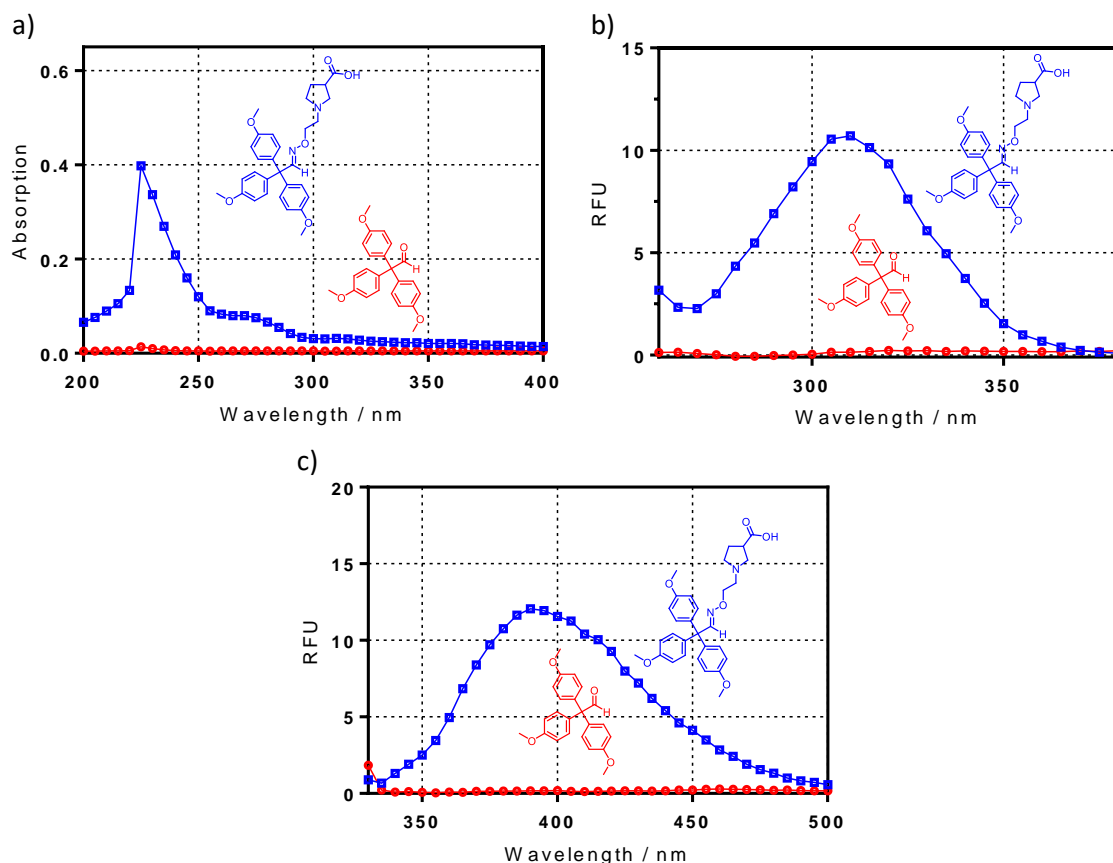
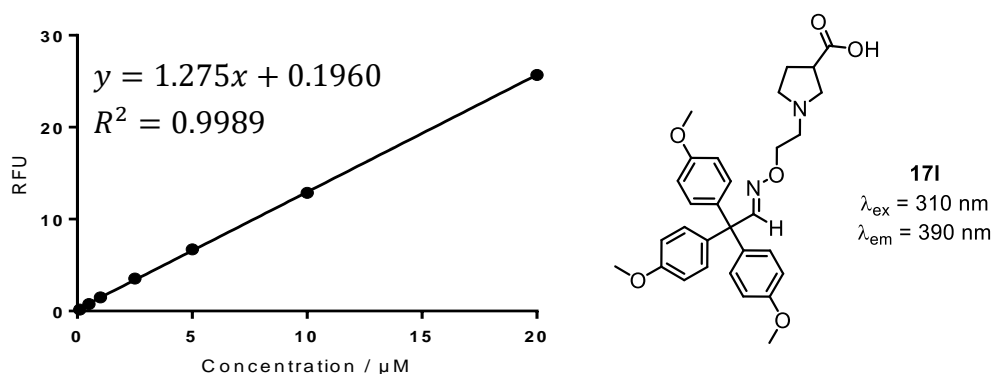


Figure 70: a) UV spectra (absorption versus wavelength, nm), b) excitation spectra [RFU versus wavelength, nm ($\lambda_{\text{ex}} = 260\text{--}380$ nm, $\lambda_{\text{em}} = 400$ nm)] and c) fluorescence spectra [RFU versus wavelength, nm ($\lambda_{\text{ex}} = 310$ nm, $\lambda_{\text{em}} = 330\text{--}500$ nm)]. Each spectrum obtained by measurements of tritylaldehyde **15I** (10 μM , red) and oxime **17I** (10 μM , blue). Spectra were recorded in phosphate buffer (pH 7.1) with 1 % DMSO at 37 $^{\circ}\text{C}$ and were corrected by subtraction of the spectrum of the pure solvent as blank.



Further Experiments

Figure 71: Determination of the linear range [RFU versus concentration, μM ($R^2 = 0.9989$)] in regard to oxime **17I** in different concentration levels (20 μM , 10 μM , 5 μM , 2.5 μM , 1 μM , 0.5 μM , 0.1 μM) in phosphate buffer (pH 7.1) with 1 % DMSO at 37 °C ($\lambda_{\text{ex}} = 310 \text{ nm}$, $\lambda_{\text{em}} = 390 \text{ nm}$).

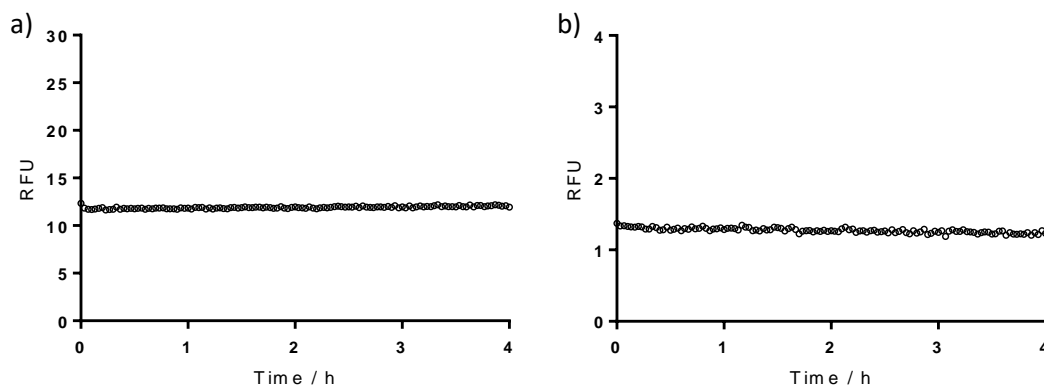


Figure 72: Monitoring of the fluorescence emission of oxime **17I** for possible change of the reaction equilibrium towards the starting materials tritylaldehyde **15I** and hydroxylamine **14** at 37 °C for 4 h after dilution with phosphate buffer (pH 7.1 + 1 % DMSO) to concentration levels of a) 10 μM and b) 1 μM ($\lambda_{\text{ex}} = 310 \text{ nm}$, $\lambda_{\text{em}} = 390 \text{ nm}$).

5 Summary of the Thesis

Neurological disorders like epilepsy or Alzheimer's disease are assumed to be caused by a distorted balance between inhibitory and excitatory neurotransmission. One possibility to treat the mentioned diseases is to block the GABA transporters (GATs) responsible for the reuptake of GABA – the most abundant inhibitory neurotransmitter in the mammalian central nervous system – to enhance the concentration of GABA in the synaptic cleft.

Four different subtypes of GATs are known named mGAT1-4 when cloned from mice but only mGAT1 and mGAT4 are involved in the GABAergic neurotransmission whereby mGAT1 is mainly expressed in neurons and mGAT4 in glial cells.

Many cyclic amino acids like nipecotic acid or guvacine are known potent inhibitors for mGAT1 with affinities in the low micromolare range. Their application as therapeutics is limited due to their inability to cross the blood brain barrier. N-Substitution of the amino acids with lipophilic residues via an alkyl chain possessing various functionalities enhanced not only their lipophilicity but also their selectivity for mGAT1 with significantly increased affinity. One important example is tiagabine which is the (*R*)-enantiomer of the nipecotic acid derivative and is known to be more potent than the (*S*)-enantiomer by more than half a log unit.

Hence, it is important to determine the enantiomeric purity of nipecotic acid when used as starting material for the synthesis of novel enantiopure GAT inhibitors to warrant the validity of the data determined in pharmacological studies. Therefore, a reliable HPLC method for the determination of the enantiopurity of nipecotic acid was developed and validated. To gain high selectivity for the detection of nipecotic acid in order to determine small impurities of the other enantiomer in highly enantiopure samples, derivatization with a 7-nitrobenzo[c][1,2,5]oxadiazole unit prior to chromatography was chosen. The optimized HPLC method was validated regarding specificity, linearity, accuracy, precision and lower limit of quantification for both enantiomers. The highest possible enantiomeric excess is determined to be 99.87% ee for the (*R*)-enantiomer and 99.86% ee for the (*S*)-enantiomer. Additional spiking experiments of enantiopure samples with small amounts of racemic nipecotic acid revealed that even slight changes in the ee values can be detected. Hence, this HPLC method is well suited to determine the ee values of nipecotic acid very precisely in even high enantiopure samples.

Over the years, numerous potent inhibitors for mGAT1 derived from amino acids like nipecotic acid have been synthesized carrying different aromatic residues with diverse substituents attached through linkers of various length. The majority of published studies deal with structure-activity-relationships (SARs) regarding different nipecotic acid and guvacine derivatives towards the target mGAT1 but when looking for other amino acid motifs e.g. like 2-(pyrrolidin-3-yl)acetic acid only scattered publications are available.

Summary of the Thesis

In this study this lack of information was reduced by providing information about SARs of the amino acids 2-(pyrrolidin-3-yl)acetic acid and pyrrolidine-3-carboxylic by identifying new potent and selective inhibitors of mGAT1.

To this end, both 5-membered cyclic amino acids were applied in the combinatorial screening concept which is based on the generation of oxime libraries by the reaction of hydroxylamine derivatives with different sets of aldehydes and the subsequent screening of these libraries by means of competitive LC-MS/MS binding assays. Within this assay NO711 was used as a native MS-marker which allows the indirect determination of the binding affinity of the applied library.

First, both hydroxylamine derivatives were synthesized with good overall yields. The oxime library formation was performed in the absence of the target mGAT1 by reaction of an excess of the above mentioned hydroxylamines with 28 sub-libraries containing eight different aldehydes. For either 2-(pyrrolidin-3-yl)acetic acid and pyrrolidine-3-carboxylic acid derived oximes the full conversion from the aldehydes to the corresponding oximes were exemplarily verified by the means of ^1H NMR experiments. All freshly prepared oxime libraries were diluted to concentrations suitable for MS Binding Assays, for which concentrations the stability was again confirmed using fluorescence measurements. After incubation of the target with the marker NO711 the libraries were subsequently screened. Control experiments of either the pure aldehyde libraries and the hydroxylamine derivative revealed no significant impact on the marker binding.

The libraries which were able to reduce the specific binding of the marker below 20 % were selected for further characterization in deconvolution experiments. In this set of experiments all single oximes of the chosen libraries were generated and tested again under the conditions used for library screening in order to identify the oximes responsible for the affinity of the library. The most affine oximes were then resynthesized in order to fully characterize them regarding their pK_i values in full-scale competitive MS Binding Assays and of their inhibitory affinities ($p\text{IC}_{50}$ values) in $[^3\text{H}]\text{GABA}$ uptake assays¹⁸ at all four murine GABA transporters.

For hydroxylamine delineated from 2-(pyrrolidin-3-yl)acetic acid in the library screening three different concentrations were tested (1 μM , 100 nM and 10 nM), whereby at 100 nM four libraries reduced marker binding under 20 %. Out of the 32 oximes which were individually generated and screened at a concentration of 100 nM eight compounds were able to decrease the marker binding under 50 % and were therefore selected to be resynthesized. All compounds contained a 1,1'-biphenyl residue and yielded pK_i values from 6.97 to 7.87 with high subtype selectivity in favor of mGAT1. The oxime with the highest affinity carries a 2',4'-dichlorobiphenyl moiety.

In case of the hydroxylamine derivatives derived from pyrrolidine-3-carboxylic acid only one concentration level of 1 μM was applied for the library screening and three out of 28 libraries were found to be able to reduce marker binding below 20 %. Deconvolution experiments with

Summary of the Thesis

these three libraries revealed only one compound reaching the limit of 50 % marker binding. But in order to identify a set of potent compounds, the most affine oximes of each of the three most active libraries were chosen for resynthesis. Again all hits possessed an 1,1'-biphenyl residue but in fact showed lower pK_i values from 6.41 to 6.16 compared to oximes with a 2-(pyrrolidin-3-yl)acetic acid motif. The compounds with 2',4'-dichloro and 2'-methoxy-4'-fluoro substitution yielded the highest pK_i values.

A set of different highly affine oximes were identified with the highest pK_i values described so far for either 2-(pyrrolidin-3-yl)acetic acid and pyrrolidine-3-carboxylic acid substructures and again the application of the library screening concept by the means of MS Binding Assays as a read-out tool was successfully proven for the process of drug discovery.

6 List of Abbreviations

°C	degrees Celsius
$\tilde{\nu}$	wave number
δ	chemical shift
calcd	calculated
CNS	central nervous system
CSP	chiral stationary phase
d	doublet (NMR)
DMSO	dimethyl sulfoxide
ee	enantiomeric excess
e. g.	<i>exempli gratia</i> (for example)
equiv.	equivalent
EI	electron ionization
ESI	electrospray ionization
g	gram
GABA	γ -aminobutyric acid
GAT	γ -aminobutyric acid transporter
h	hour
HEK cell	human embryonic kidney cell
HPLC	high performance liquid chromatography
HRMS	high resolution mass spectrometry
HUGO	Human Genome Organization
Hz	Hertz
IC ₅₀	half maximal inhibitory concentration
IR	infrared spectrometry
J	coupling constant
K_i	inhibitory constant
LC	liquid chromatography
LC-MS	liquid chromatography-mass spectrometry
LLOQ	lower limit of quantification
LeuT _{Aa}	<i>Aquifex aeolicus</i> leucine transporter
M	molar
MeOH	Methanol
mGAT1	murine γ -aminobutyric acid transporter subtype 1
min	minute
mp	melting point

List of Abbreviations

MS	mass spectrometry
MS/MS	tandem mass spectrometry
nm	nanometer
NMR	nuclear magnetic resonance
NSB	nonspecific binding
Ppm	part per million
q	quartet (NMR)
qNMR	quantitative nuclear magnetic resonance
R _f	retardation factor
RFU	relative fluorescence unit
rt	room temperature
s	singlet (NMR)
SAR	structure-activity-relationship
SB	specific binding
SD	standard deviation
SEM	standard error of mean
SLC6	solute carrier 6
t	triplet (NMR)
T	temperature
t _R	retention time
TB	total binding
THF	tetrahydrofuran
WHO	World Health Organization

7 References

- ¹ J. Aarli, D. Tarun, A. Janca, A. Muscetta; Neurological disorders: public health challenges. Geneva. World Health Organization, **2006**.
- ² GBD 2015 Neurological Disorder Collaborator Group, *Lancet Neurol.* **2017**, 16, 877–897.
- ³ Fact sheet epilepsy, World Health Organization, 2018. <http://www.who.int/en/news-room/fact-sheets/detail/epilepsy>
- ⁴ R. S. Fisher et al. *Epilepsia* **2014**, 55, 475–482.
- ⁵ M. J. Brodie, F. Besag, J. B. Steinhoff, *Pharmacol. Rev.* **2016**, 68, 563–602.
- ⁶ A. V. Kalueff, D. Nutt, *J. Depress. Anxiety* **2007**, 24, 495–517.
- ⁷ D. F. Owens, A. E. Kriegstein, *Nature Rev. Neurosci.* **2002**, 3, 715–727.
- ⁸ A. C. Forster, J. A. Kemp, *Curr Opin Pharmacol* **2006**, 6, 7–17.
- ⁹ N. G. Bowery, T. G. Smart, *Br. J. Psychiatry* **2006**, 147, S109–S119.
- ¹⁰ A. Schousboe, A. Sarup, O. M. Larsson, H. S. White, *Biochem. Pharmacol.* **2004**, 68, 1557–1563.
- ¹¹ D. M. Treiman, *Epilepsia* **2001**, 42 (Suppl. 3), 8–12.
- ¹² a) K. L. Lanctôt, N. Herrmann, P. Mazzotta, L. R. Khan, N. Ingber, *Can. J. Psychiatry* **2004**, 49, 439–453. b) R. A. Rissmann, A. L. De Blas, D. M. Armstrong, *J. Neurochem.* **2007**, 103, 1285–1292.
- ¹³ D. J. Nutt, A. L. Malizia, *Br. J. Psychiatry* **2001**, 179, 390–396.
- ¹⁴ E. Ben-Menachem, *Acta Neurol. Scand.* **2011**, 124 (Suppl. 192), 5–15.
- ¹⁵ a) E. B. Nielson, P. D. Suzdak, K. E. Andersen, L. J. Knutsen, U. Sonnewald, C. Braestrup, *Eur. J. Pharmacol.* **1991**, 196, 257 – 266. b) B. S. Meldrum, A. G. Chapman, *Epilepsia* **1999**, 40, S2–S6.
- ¹⁶ L. He, K. Vasiliou, D. W. Nebert, *Hum. Genomics* **2009**, 3, 195–206.
- ¹⁷ A. S. Kristensen, J. Andersen, T. N. Jorgensen, L. Sorensen, J. Eriksen, C. J. Loland, K. Stromgaard, U. Gether, *Pharmacol. Rev.* **2011**, 63, 585–640.
- ¹⁸ S. Bröer, U. Gether, *Br. J. Pharmacol.* **2012**, 167, 256–278.
- ¹⁹ G. Rudnick, J. Clark, *Biochim. Biophys. Acta* **1993**, 1144, 249–263.
- ²⁰ K. K. Madsen, P. C. Rasmus, O. M. Larsson, P. Krogsgaard-Larsen, A. Schousboe, H. S. White, *J. Neurochem.* **2009**, 109, 139–144.
- ²¹ K. K. Madsen, H. S. White, A. Schousboe, *Pharmacol Ther.* **2010**, 125, 394–401.
- ²² Y. Zhou, S. Holmseth, C. Guo, B. Hassel, G. Höfner, H. S. Huitfeldt, K. T. Wanner, N. C. Danbolt, *J. Biol. Chem.* **2012**, 287, 35733–35746.
- ²³ Y. Zhou, S. Holmseth, R. Hua, A. C. Lehre, A. M. Olofsson, I. Poblete-Naredo, S. A. Kempson, N. C. Danbolt, *Am. J. Physiol. Renal. Physiol.* **2012**, 302, F316–F328.
- ²⁴ J. Guastella, N. Nelson, H. Nelson, L. Czyzyk, S. Keynan, M. C. Miedel, N. Davidson, H. A. Lester, B. I. Kanner, *Science*, **1990**, 249, 1303–1306.
- ²⁵ R. D. Blakely, H. E. Berson, R. T. Freneau, M. G. Caron, M. M. Peek, H. K. Prince, C. C. Bradley, *Nature* **1991**, 354, 66–70.
- ²⁶ J. E. Kilty, D. Lorang, S. G. Amara, *Science* **1991**, 254, 578–579.
- ²⁷ T. Pacholczyk, R. D. Blakely, S. G. Amara, *Nature* **1991**, 350, 350–354.
- ²⁸ J. G. Chen, S. Liu-Chen, G. Rudnick, *J. Biol. Chem.* **1998**, 273, 12675–12681.
- ²⁹ A. Yamashita, S. K. Singh, T. Kawate, Y. Jin, E. Gouaux, *Nature* **2005**, 437, 215–223.

References

- ³⁰ T. Bauming, L. Shi, J. A. Javitch, H. Weinstein, *Mol. Pharm.* **2006**, *70*, 1630–1642.
- ³¹ a) O. Jardetzky, *Nature* **1966**, *211*, 969–970. b) H. Krishnamurthy, C. L. Piscitelli, E. Gouaux, *Nature* **2009**, *459*, 347–355.
- ³² E. Gouaux, *Phil. Trans. R. Soc. B* **2009**, *364*, 149–154.
- ³³ S. K. Singh, C. L. Piscitelli, A. Yamashita, E. Gouaux, *Science* **2008**, *322*, 1655–1661.
- ³⁴ H. Krishnamurthy, E. Gouaux, *Nature* **2012**, *481*, 469–474.
- ³⁵ L. Shi, M. Quick, Y. Zhao, H. Weinstein, J. A. Javitch, *Mol. Cell* **2008**, *30*, 667–677.
- ³⁶ A. Nyola, N. K. Karpowich, J. Zhen, J. Marden, M. E. Reith, D.-N. Wang, *Curr. Opin. Struct. Biol.* **2010**, *20*, 415–422.
- ³⁷ S. K. Singh, A. Yamashita, E. Gouaux, *Nature* **2007**, *448*, 952–956.
- ³⁸ H. Wang, J. Elferich, E. Gouaux, *Nat. Struct. Mol. Biol.* **2012**, *19*, 212–219.
- ³⁹ A. Penmatsa, K. H. Wang, E. Gouaux, *Nature* **2013**, *503*, 85–90.
- ⁴⁰ A. Penmatsa, K. H. Wang, E. Gouaux, *Nat. Struct. Mol. Biol.* **2015**, *22*, 15–18.
- ⁴¹ J. A. Coleman, E. M. Green, E. Gouaux, *Nature* **2016**, *532*, 334–339.
- ⁴² P. Krogsgaard-Larsen, E. Falch, O. M. Larsson, A. Schousboe, *Epilepsy Res.* **1987**, *1*, 77–93.
- ⁴³ P. Krogsgaard-Larsen, G. A. R. Johnston, *J. Neurochem.* **1975**, *25*, 797–802.
- ⁴⁴ O. M. Larsson, P. Thorbek, P. Krogsgaard-Larsen, A. Schousboe, *J. Neurochem.* **1981**, *37*, 1509–1516.
- ⁴⁵ P. Krogsgaard-Larsen, *Mol. Cell. Biochem.* **1980**, *31*, 105–121.
- ⁴⁶ T. Wein, K. T. Wanner, *J. Mol. Model* **2010**, *16*, 155–161.
- ⁴⁷ S. K. Huber, G. Höfner, K. T. Wanner, *ChemMedChem* **2018**, *13*, 2488–2503.
- ⁴⁸ T. Hellenbrand, G. Höfner, T. Wein, K. T. Wanner, *Bioorg. Med. Chem.* **2016**, *24*, 2072–2096.
- ⁴⁹ T. Wein, M. Petrera, L. Allmendinger, G. Höfner, J. Pabel, K. T. Wanner, *ChemMedChem* **2016**, *11*, 509–518.
- ⁵⁰ S. K. Huber, G. Höfner, K. T. Wanner, *Bioorg. Med. Chem.* **2018**, to be submitted.
- ⁵¹ A. Kragler, G. Höfner, K. T. Wanner, *Eur. J. Med. Chem.* **2008**, *43*, 2404–2411.
- ⁵² F. T. Kern, K. T. Wanner, *ChemMedChem* **2015**, *10*, 396–410.
- ⁵³ F. E. Ali, W. E. Bondinell, P. A. Dandridge, J. S. Frazee, E. Garvey, G. R. Girard, C. Kaiser, T. W. Ku, J. J. Lafferty, G. I. Moonsammy, H. Oh, J. A. Rush, S. E. Setler, O. D. Stringer, J. W. Venslavsky, B. W. Volpe, L. M. Yunger, C. L. Zirkle, *J. Med. Chem.* **1985**, *28*, 653–660.
- ⁵⁴ M. A. Cooper, *Nat. Rev. Drug Discov.* **2002**, *1*, 515–528.
- ⁵⁵ Z. Zhu, J. Cuzzo, *J. Biomol. Screen.* **2009**, *14*, 1157–1164.
- ⁵⁶ K. T. Wanner, G. Höfner, *Vol. 36*, Wiley-VCH, Weinheim, Germany, **2007**.
- ⁵⁷ R. J. Lefkowitz, J. Roth, I. Pastan, *Science* **1970**, *170*, 633–635.
- ⁵⁸ a) C. Zepperitz, G. Höfner, K. T. Wanner, *ChemMedChem* **2006**, *1*, 208–217. b) M. Hess, G. Höfner, K. T. Wanner, *ChemMedChem* **2011**, *6*, 1900–1908. c) S. H. Grimm, G. Höfner, K. T. Wanner, *ChemMedChem* **2015**, *10*, 1027–1039. d) P. Neiens, G. Höfner, K. T. Wanner, *ChemMedChem* **2015**, *10*, 1924–1931. e) M. Schuller, G. Höfner, K. T. Wanner, *ChemMedChem* **2017**, *12*, 1585–1594.
- ⁵⁹ Y.-C. Cheng, W. H. Prusoff, *Biochem. Pharmacol.* **1973**, *22*, 3099–3108.
- ⁶⁰ E. Hulme, *Receptor ligand interactions – a practical approach*, Oxford University Press, New York, **1992**.

References

- ⁶¹ M. Sindelar, K. T. Wanner, *ChemMedChem* **2012**, 7, 1678–1690.
- ⁶² a) H. Brunner, M. Schönherr, M. Zabel, *Tetrahedron: Asymmetry* **2001**, 12, 2671–2675. b) J. Kalia, R. T. Raines, *Angew. Chem. Int. Ed.* 2008, 47, 7523–7526.
- ⁶³ a) T. Miyazawa, H. Iwanaga, T. Yamada, S. Kuwata, *Analytical Letters* **1993**, 26 (2), 367–378. b) A. M. Rustum, G. Menon, S. Patel, *Journal of Pharmaceutical and Biomedical Analysis* **1998**, 17 (8), 1439–1447. c) M. Pawlowska, S. Chen, D. W. Armstrong, *Journal of Chromatography A* **1993**, 641 (2), 257–265. d) S. Chen, *Biomedical Chromatography* **2006**, 20 (8), 718–728. e) N. T. McGachy, N. Grinberg, N. Variankaval, *Journal of Chromatography A* **2005**, 1064 (2), 193–204. f) T. Miyazawa, H. Minowa, K. Imagawa, T. Yamada, *Chroma* **2004**, 60 (1-2), 45-50. g) R. Pell, S. Sić, W. Lindner, *Journal of Chromatography A* **2012**, 1269, 287–296.
- ⁶⁴ A. M. Rustum, *Journal of Chromatography A* **1995**, 696 (1), 75–81.
- ⁶⁵ a) K. Imai, Y. Watanabe, *Analytica Chimica Acta* **1981**, 130 (2), 377-383. b) C. Aoyama, T. Santa, M. Tsunoda, T. Fukushima, C. Kitada, K. Imai, *Biomedical Chromatography* **2004**, 18 (9), 630–636.
- ⁶⁶ H. Günther, *NMR Spectroscopy – Basic Principles, Concepts, and Applications in Chemistry*, Wiley-VCH, Weinheim, Germany, **2013**.